# TAL TECH

**DOCTORAL THESIS**

# Narrowband Internet of Things (NB-IoT): from Radio Network Coverage to Device Energy Consumption Modeling and Energy-Efficient Application

Sikandar Muhammad Zulqarnain Khan

# Narrowband Internet of Things (NB-IoT): from Radio Network Coverage to Device Energy Consumption Modeling and Energy-Efficient Application

SIKANDAR MUHAMMAD ZULQARNAIN  KHAN

**TAL
TECH**
PRESS

TALLINN UNIVERSITY OF TECHNOLOGY
School of Information Technologies
Thomas Johann Seebeck Department of Electronics

**The dissertation was accepted for the defence of the degree of Doctor of Philosophy (Information and Communication Technology) on 28 February 2022**

**Supervisor:** Professor Yannick Le Moullec
Thomas Johann Seebeck Department of Electronics, School of Information Technologies
Tallinn University of Technology
Tallinn, Estonia

**Co-supervisor:** Professor Muhammad Mahtab Alam
Thomas Johann Seebeck Department of Electronics, School of Information Technologies
Tallinn University of Technology
Tallinn, Estonia

**Opponents:** Professor Luca Reggiani
Politecnico di Milano
Milano, Italy

Professor Olivier Berder
Université de Rennes 1/Institut de Recherche en Informatique et Systèmes Aléatoires (IRISA)
Lannion, France

**Defence of the thesis:** 31th March, 2022, Tallinn

**Declaration:**
*Hereby I declare that this doctoral thesis, my original investigation and achievement, submitted for the doctoral degree at Tallinn University of Technology, has not been submitted for any academic degree elsewhere.*

SIKANDAR MUHAMMAD ZULQARNAIN KHAN

_____
signature

# Kitsaribaline asjade internet (NB-IoT): raadiovõrgu katvusest seadme energiatarbe modelleerimise ja energiasäästliku rakenduseni

SIKANDAR MUHAMMAD ZULQARNAIN  KHAN

# Contents

## List of Publications

The present Ph.D. thesis is based on the following publications that are referred to in the text by Roman numbers.

I   Sikandar Zulqarnain Khan, Hassan Malik, Jeffrey Leonel Redondo Sarmiento, Muhammad Mahtab Alam, and Yannick Le Moullec. Dorm: Narrowband iot development platform and indoor deployment coverage analysis. *Procedia Computer Science*, 151:1084–1091, 2019

II   Hassan Malik, Sikandar Zulqarnain Khan, Jeffrey Leonel Redondo Sarmiento, Alar Kuusik, Muhammad Mahtab Alam, Yannick Le Moullec, and Sven Pärand. Nb-iot network field trial: Indoor, outdoor and underground coverage campaign. In *2019 15th International Wireless Communications Mobile Computing Conference (IWCMC)*, pages 537–542, 2019

III   Nishant Poddar, Sikandar Zulqarnain Khan, Jakob Mass, and Satish Narayana Srirama. Coverage analysis of nb-iot and sigfox: Two estonian university campuses as a case study. In *2020 International Wireless Communications and Mobile Computing (IWCMC)*, pages 1491–1497. IEEE, 2020

IV   Sikandar M. Zulqarnain Khan, Muhammad Mahtab Alam, Yannick Le Moullec, Alar Kuusik, Sven Pärand, and Christos Verikoukis. An empirical modeling for the baseline energy consumption of an nb-iot radio transceiver. *IEEE Internet of Things Journal*, 8(19):14756–14772, 2021 [1]

V   Sikandar Zulqarnain Khan, Yannick Le Moullec, and Muhammad Mahtab Alam. An NB-IoT-Based Edge-of-Things Framework for Energy-Efficient Image Transfer. *MDPI Sensors*, 17(21):5929–5949, 2021

---

[1]This publication has been selected as one of the five "Research Articles" of the year 2021 by the School of Information Technologies, TalTech, and is listed in the School's book of honour. https://taltech.ee/en/book-honour

# Author's Contributions to the Publications

I  In Paper I, I was the first author. I developed the DORM (integrateD cOmpact naRrow-band platforM) node by combining a Commercial-off-The-Shelf (CoTS) NB-IoT radio transceiver with a low-cost, low-power processing unit and interfaced it with an IoT backend cloud server i.e., Cumulocity platform. Deploying up to 12 of these DORM nodes across the TalTech Campus, I carried out an on-field investigation of the NB-IoT network coverage at different elevation levels of Thomas Johann Seebeck Department Of Electronics. I collected all the data from these deployed DORM nodes over the Cumulocity server and analysed the NB-IoT test network coverage performance accordingly. Based on my results, I prepared the graphs and figures accordingly and prepared the first draft of this manuscript. I revised this manuscript accordingly as per my supervisors' feedback.

II  In Papers II and III, I was the second author. The first author was an MSc student whose MS thesis work I co-supervised. I briefed all the co-authors on the design, development and deployment of DORM node(s) for performing the coverage analysis of NB-IoT test network across the TalTech campus. I made the deployment map and was part of the deployment team to perform the coverage experiments in an indoor, outdoor and deep indoor environments. I helped in analysing the collected data from the deployed nodes and I also helped in the preparation of associated graphs and other results accordingly. I also contributed in refining the initial manuscript and proof-reading it from time-to-time.

III  In Paper IV, I was the first author. I prepared the hardware and software experimental setup and carried out the detailed power consumption analyses of the various states of an NB-IoT radio transceiver. Based on these analyses, I proposed an empirical baseline energy consumption model for the Radio Resource Control (RRC) communication protocol between an NB-IoT radio transceiver and a cellular base-station (BS). I conducted all the experiments using two Commercial-off-The-Shelf (CoTS) NB-IoT radios that were connected to the NB-IoT test works as provided by the two Mobile Network Operators (MNOs) in Estonia. Using comprehensive analyses of the power profile traces of these operating radios, I showed that the proposed model accurately depicts the energy consumption profile of an NB-IoT radio transceiver operating at different coverage class levels. Based on my results from these experiments, I wrote this manuscript where in I prepared all the figures, graphs and tables. I revised this manuscript accordingly as per my supervisors' feedback from time to time.

IV  In Paper V, I was the first author. I prepared the hardware setup for developing an NB-IoT based Edge-of-Things Framework that could run ML algorithms over the edge to curb the unnecessary data from being transmitted over the NB-IoT network. I also designed and programmed the various nodes of this framework that are deployed and functioning at the three hierarchical layers of this framework. These include i) Detection and Vision Node (DVN) at the perception layer, ii) Smart Transmit Node (STN) at the gateway layer and iii) Server node (SN) at the cloud layer. Integrating all these layers into a single framework through various communication protocols such as BT/BLE, NB-IoT, and MQTT; I carried out on-field experimental trials to test the efficiency of this framework and collected empirical results. Based on a comprehensive analysis of the computation and communication budget of the gateway node, I wrote this manuscript and prepared the figures, graphs and tables accordingly. I refined this manuscript as per my supervisors' feedback.

## Other Publications

In addition to the previous publications, the author also contributed towards designing an IoT node that incorporates transient computing, approximate computing and energy/data predictions to deal with the intermittent nature of energy harvesting sources and at the same time to reduce the energy consumption of the node by minimizing its total number of CC2500 radio link transmissions. This article was published in IEEE CCNC conference 2020, USA.

I Sikandar Zulqarnain Khan, Rashiduddin Kakar, Muhammad Mahtab Alam, Yannick Le Moullec, and Haris Pervaiz. A green iot node incorporating transient computing, approximate computing and energy/data prediction. In *2020 IEEE 17th Annual Consumer Communications Networking Conference (CCNC)*, pages 1–6, 2020

# Abbreviations

| | |
|---|---|
| 1G | First Generation Cellular Network |
| 2G | Second Generation Cellular Network |
| 3G | Third Generation Cellular Network |
| 3GPP | Third Generation Partnership Project |
| 4G | Fourth Generation Cellular Network |
| 5G | Fifth Generation Cellular Network |
| 6LoWPAN | IPv6 over Low Power Wireless Personal Area Networks |
| AES | Advanced Encryption Standard |
| BS | Base Station |
| BT | Bluetooth |
| BLE | Bluetooth Low Energy |
| BPSK | Binary Phase-shift Keying |
| CDRX | Connected DRX |
| CDM | Code Division Multiplexing |
| CoTS | Commercial off The Shelf |
| CPU | Central Processing Unit |
| CSS | Chirp Spread Spectrum |
| CRC | Cyclic Redundancy Check |
| dB | Decibel |
| dBm | Decibel milliwatt |
| DCI | Downlink Control Information |
| DDN | Downlink Data Notification |
| DMRS | Demodulation Reference Signal |
| DL | Downlink |
| DRX | Discontinuous Reception |
| DVN | Detection and Vision Node |
| DUT | Device Under Test |
| eDRX | Extended Discontinuous Reception |
| eNB | evolved NodeB |
| EDGE | Enhanced Data GSM Evolution |
| ECL | Enhanced Coverage Level |
| FSK | Frequency Shift Keying |
| GPRS | General Packet Radio Service |
| GSM | Global System for Mobile Communications |
| HARQ | Hybrid Automatic Repeat Request |
| HTTPs | Hyper Text Transfer Protocol |
| HAT | Hardware Attached on Top |
| HD-FDD | Half-Duplex Frequency Division Duplex |
| IoT | Internet of Things |
| ISM | Industrial, Scientific and Medical |
| IMS | IP Multimedia Services |
| IP | Internet Protocol |
| I2C/IIC | Inter-Integrated Circuit |
| kHz | Kilohertz |
| Kbps | Kilobits per second |
| LEDs | Light Emitting Diodes |
| LTE | Long Term Evolution |
| LTE-M | Long Term Evolution for Machines |

| | |
|---|---|
| LPWAN | Low Power Wide Area Networks |
| LoRaWAN | Long Range Wide Area Network |
| LPM | Low Power Mode |
| M2M | Machine to Machine Communication |
| MNO | Mobile Network Operator |
| MQTT | Message Queuing Telemetry Transport |
| MCU | Micro Controller Unit |
| MCL | Maximum Coupling Loss |
| ML | Machine Learning |
| MIMO | Multiple Inputs Multiple Outputs |
| MTC | Machine Type Communication |
| MME | Mobile Mobility Entity |
| MO | Mobile Originated |
| MT | Mobile Terminated |
| MBMS | Multimedia Broadcast Multi-cast Services |
| mA | Milliampere |
| MHz | Megahertz |
| NFC | Near Field Communication |
| NB-IoT | Narrow Band Internet of Things |
| NB-CIoT | Narrowband Cellular IoT |
| NPRACH | Narrowband Physical Random Access Channel |
| NPDSCH | Narrowband Physical Downlink Shared Channel |
| NPUSCH | Narrowband Physical Uplink Shared Channel |
| NPDCCH | Physical Downlink Control Channel |
| NPBCH | Narrowband Physical Broadcast Channel |
| NPSS | Narrowband Primary Synchronization Signal |
| NRS | Narrowband Reference Signal |
| NSSS | Narrowband Secondary Synchronization Signal |
| OFDM | Orthogonal Frequency Division Multiplexing |
| OTDOA | Observed Time Difference Of Arrival |
| OS | Operating System |
| PA | Power Analyzer |
| PO | Paging Occasion |
| PRNTI | Paging Radio Network Temporary Identity |
| PRB | Physical Resource Block |
| RRM | Radio Resource Management |
| PRS | Positioning Reference Signals |
| PSM | Power Saving Mode |
| PTW | Paging Time Window |
| QoS | Quality of Services |
| QPSK | Quadrature Phase Shift Keying |
| QXGA | Quarter Video Graphics Array |
| RAT | Random Access Technology |
| RACH | Random Access Channel |
| RF | Radio Frequency |
| RU | Radio Unit |

| | |
|---|---|
| RSTD | Reference Signal Time Difference |
| RSSI | Received Signal Strength Indicator |
| RSRP | Reference Signal Received Power |
| RSRQ | Reference Signals Received Quality |
| RFID | Radio Frequency Identification |
| RPi | Raspberry Pi |
| RGB | Red Green Blue |
| SA | Sensitivity Analysis |
| STN | Smart Transmit Node |
| SN | Server Node |
| SMS | Short Messaging Services |
| SNR | Signal to Noise Ratio |
| SINR | Signal to Interference plus Noise Ratio |
| SVGA | Super Video Graphics Array |
| SC-PTM | Single Cell Point-To-Multipoint |
| SC-MTCH | Single-Cell MBMS Traffic CHannel |
| SR | Scheduling Request |
| SPS | Semi-Persistent Scheduling |
| SGW | Serving Gate Way |
| TAU | Timer Area Update |
| TBS | Transfer Block Size |
| TDD | Time Division Duplex |
| ToA | Time of Arrival |
| TR | Technical Report |
| TCP/IP | Transmission Control Protocol and Internet Protocol |
| UMTS | Universal Mobile Telecommunications System |
| UE | User Equipment |
| UL | Uplink |
| UDP | User Datagram Protocol |
| USB | Universal Serial Bus |
| UART | Universal Asynchronous Receiver Transmitter |
| UXGA | Ultra Extended Graphics Array |
| VoIP | Voice over IP |
| VoLTE | Voice over Long Term Evolution |
| VSAT | Very Small Aperture Terminal |
| VGA | Video Graphics Array |
| W | Watt |
| Wh | Watt-Hour |
| WAN | Wide Area Network |
| WU | WakeUp |
| YOLO | You Only Look Once |
| YOLO-v3 | You Only Look Once-Version 3 |

# 1 Introduction

Internet of Things (IoT) is a notion that connects the cyber-physical world (things) to the Internet [7]. It is believed that this radical evolution of connectivity would form a notable segment of the 5G network wherein the interconnected objects would harvest information from the environment through sensors, and send it to the cloud through radios for further analysis and decision making. IoT is expected to integrate a multitude of heterogeneous sensor nodes that are low-cost, low-power, and could support long-range and low-rate transmissions. IoT sensor nodes are also expected to function independently, without human involvement, in span of years.

The short-range radio technologies (e.g., Wifi, ZigBee, BT/BLE) are not adequate for IoT applications as they cannot fulfill the long range transmission needs of IoT. The cellular communication technologies (e.g., 2G, 3G, and 4G) offer large coverage, yet they consume excessive device energy and hence are not suitable for IoT applications. This is why to overcome the low-power device consumption and long-range communication needs of IoT, a new set of wireless communication technologies have emerged; they fall in the category of Low Power Wide Area Networks (LPWANs) [8]. It is thanks to the emergence of LPWAN technologies that myriads of IoT applications in the fields of smart cities [9], smart homes [10], smart cars [11], smart farming [12], smart metering [13], environmental monitoring [14], [15], etc. are coming into play.

Low Power Wide Area Networks (LPWANs) allow a communication range of up to 40 km in rural zones and up to 10 km in urban zones [16]. LPWANs offer low device energy consumption with device lifetime of up-to 10 years or more [17]. LPWANs also have low development cost with an average device price as low as $5 and a low operating cost with an average operating cost as low as $1 per device per year [18]. Thus, the basic motivation behind LPWAN technologies is to transmit short-length messages over long ranges with low power consumption. The positioning of LPWAN technologies in terms of its range and data rate in comparison to the existing short-range and cellular communication technologies is depicted in Figure 1.
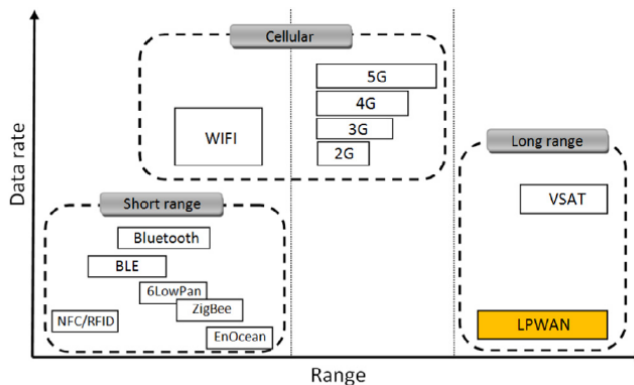


*Figure 1: Data rate vs. range capacity of radio communication technologies: LPWAN positioning. Source: [19]*

Since IoT is expected to work in a multitude of environments, a variety of LPWAN technologies have already emerged in the licensed and unlicensed frequency spectra to account for the diverse application needs. A brief history of the cellular technologies and the motivation for LPWANs is discussed in the section that follows.

## 1.1 Brief history of cellular technologies with LPWAN background

The era of cellular technology started when Global System for Mobile Communications (GSM) was first deployed in 1991, providing calls and Short Messaging Services (SMS) as circuit switched data. This was termed as the 1st Generation (1G) analog cellular technology [20] and was based on circuit-switching networks. In 2000, the 2nd Generation (2G) of cellular technology was developed as a replacement for 1G analog cellular networks and expanded over time to include data communications by packet data transport via General Packet Radio Service (GPRS), and Enhanced Data Rates for GSM Evolution (EDGE). It added internet as packet switched data and was therefore termed as 2G/GPRS [21] cellular digital technology. Subsequently, the 3GPP developed the third-generation (3G) UMTS standards that combined aspects of the 2G network with new technologies and protocols to deliver significantly faster data rates [22]. Further improvements in data rates, capacity and low latency led to the development of fourth-generation (4G) LTE and LTE Advanced [23] and the fifth-generation 5G standards [24]. Figure 2 shows how these technologies transitioned into the LTE standards of today.
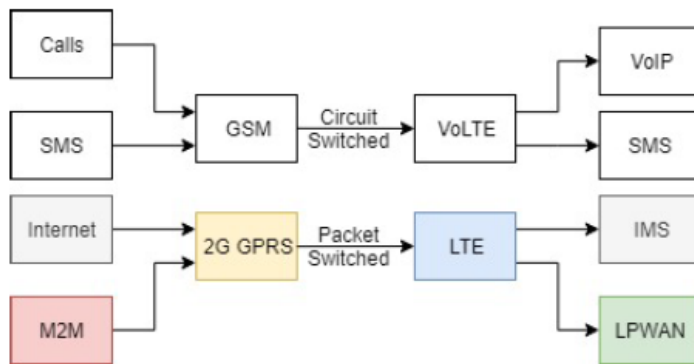


Figure 2: A simplified representation of the transition from 2G to LTE with regard to technologies that keep people and 'things' in contact. Red-orange-blue-green boxes indicates the path that M2M took through the packet-switched cellular network, linking it to LPWANs. Grey boxes indicate the path for internet-based communications and white boxes indicate the path for circuit-switched network.

As indicated in Figure 2, LPWAN (green box) emerged as the direct outcome of Machine-to-machine (M2M) communication (red box) which is defined as the exchange of information between machines, both wired and wireless, without any human intervention. Cellular M2M emerged in 1995 with Siemens creating a GSM module for machines to use wireless networks. Thus 2G/GPRS served as a gateway for M2M communications for many years, but due to its high power usage it was not sustainable for applications that required battery longevity of a few years or more. To fill this gap, the cellular LPWANs emerged both in the unlicensed spectrum such as LoRaWAN and SigFox and the licensed spectrum such as NB-IoT and Cat-M. Howvewr, each LPWAN technology has its own unique benefits and it is yet hard to decide the sole winner when it comes to connecting 'things' to the internet i.e., IoT. A brief comparison of the most prevalent available LPWAN technologies is made in the section to follow.

Table 1: Overview of LPWAN technologies: Sigfox, LoRa, and NB-IoT.

| Overview of LPWAN technologies: Sigfox, LoRa, and NB-IoT. | | | |
|---|---|---|---|
| **Characteristic** | **Sigfox** | **LoraWAN** | **NB-IoT** |
| *Modulation* | BPSK | CSS | QPSK |
| *Frequency* | Unlicensed ISM bands (868 MHz in Europe, 915MHz in North America, and 433 MHz in Asia) | Unlicensed ISM bands (868 MHz in Europe, 915MHz in North America, and 433 MHz in Asia) | Licensed LTE frequency bands |
| *Bandwith* | 192 kHz | 250 kHz and 125 kHz | 180 kHz |
| *Maximum data rate* | 100 bps | 50 kbps | 200 kbps |
| *Maximum messages/day* | 140 (UL), 4 (DL) | Unlimited | Unlimited |
| *Maximum payload length* | 12 bytes (UL), 8 bytes (DL) | 243 bytes | 1600 bytes |
| *Range* | 10 km (urban), 40 km (rural) | 5 km (urban), 20 km (rural) | 1 km (urban), 10 km (rural) |
| *Interference immunity* | Very High | Very High | Low |
| *Encryption* | Not supported | Yes (AES 128b) | Yes (LTE encryption) |
| *Localization* | Yes (RSSI) | Yes (TDOA) | No (under specification) |
| *Allows private network* | No | Yes | No |
| *Standardization* | Sigfox company | LoRa-Alliance | 3GPP |

## 1.2 Available LPWAN technologies and their technical differences

Among the currently available LPWAN technologies, Sigfox, LoRaWAN, and NB-IoT are the most prevalent ones as they dominate the IoT market. Their technical differences are summarized in Table 1 [25].

Sigfox provides promising results in terms of long range, low power and low cost communications and has been deployed in more than 72 countries[2] around the globe. A typical Sigfox device powered by a 2400 mAh battery can achieve a theoretical lifetime of 2.5 years while sending one message every 10 min at 100 bits/s [26].

LoRaWAN was standardized by the LoRa-Alliance in 2015 and is currently deployed across 162 countries [3]. LoRa is the physical layer used in LoRaWAN and features low power operation i.e., around 10 years of battery lifetime, low data rate i.e., 27 kbps with spreading factor 7 and 500 kHz channel or 50 kbps with FSK and long communication range i.e., 2-5 km in urban areas and 15 km in suburban areas [27].

NB-IoT was standardized by the Third Generation Partnership Project (3GPP) [4] in 2016 allowing long-range communications at low data rates i.e., 250 kbps for multi-tone downlink communication and 20 kbps for single-tone uplink communications [19]. The device complexity of NB-IoT nodes is reduced as compared to other unlicensed LPWAN technologies i.e., LoRA and Sigfox, to support ultra low-power IoT applications. The NB-IoT nodes feature battery saving modes such as PSM and eDRX to achieve higher energy efficiency and longer battery life of more than 10 years.

Considering the market capture, LoRa and NB-IoT account for almost 85.5% of all LPWAN connections by 2023 [28]. LoRa uses the unlicensed spectrum just like Sigfox, allowing almost anyone to set up their own network, whereas NB-IoT uses the licensed spectrum and is available only through established mobile network operators.

## 1.3 Why NB-IoT?

NB-IoT, an LTE-based 3GPP standardized LPWAN technology, shows performance benefits over its competitor LPWAN technologies in terms of uplink/downlink throughput, payload, and range, as indicated in Table 1, yet current research shows that variations in en-

---

[2]https://www.sigfox.com/en/coverage

[3]https://lora-alliance.org/

[4]https://www.3gpp.org/news-events/1785-nb_iot_complete/

ergy consumption leaves battery longevity in question. According to 3GPP specifications, the highlights include:

- Licensed spectrum;

- An estimated 10 years of device battery-lifetime;

- Less than 10 seconds of transmission acknowledgement;

- + 20 dB improvement over 2G/GPRS via its enhanced coverage levels (ECL).

Also, since NB-IoT is based on the existing LTE technology, its integration into the existing LTE infrastructure is easier as compared to establishing an entirely separate setup as required by Sigfox and LoRaWAN. And although NB-IoT retains the complexities of the legacy LTE technology i.e., the vast array of sub-protocols and communication overheads, it still claims low power, low bandwidth, and long range benefits that match the requirements for many battery-powered IoT applications. Nevertheless, it would be significant to further investigate the challenges that the NB-IoT technology currently faces, both from the user equipment (UE) and network vendors perspective, so as to solidify the robustness of the aforementioned claims to make NB-IoT one of the most suitable and popular choices for low power wide area implementations.

## 1.4 Challenges in NB-IoT

NB-IoT is an LTE based cellular IoT technology with an allocated bandwidth of 180 kHz only. It is meant to support massive device connectivity with requirements for low-power, low-cost and delay tolerant IoT applications. The limited bandwidth of NB-IoT allows its deployment in three possible deployments i.e., stand-alone, in-band and guard-band. In stand-alone mode, it operates as a dedicated carrier of 200 kHz on a GSM channel. However, for the in-band and guard-band deployments, it operates as one physical resource block (PRB) of the LTE communications. Considering its scarce bandwidth, frequency sharing with existing LTE, and a demand for supporting a gigantic network of low-cost and low-power devices, NB-IoT faces many challenges. The most prominent among these follows as under:

- Utilization of the meagre spectrum of NB-IoT requires an efficient radio resource management (RRM) that can guarantee a reliable and sustainable connectivity to the myriad of IoT devices [29]. The allocation of radio resource to these massive IoT devices becomes even more challenging considering the co-existence of NB-IoT within the future 5G Heterogenous networks (HetNets) that are supposed to face huge inter-cell interference and asymmetric traffic between the uplink and downlink communications [29, 30, 31, 32].

- NB-IoT incorporates the 3GPP Enhanced Coverage (EC) feature to repeat its transmissions and extend its coverage to otherwise inaccessible areas such as deep indoor parking garages and underground pits [33, 34]. This allows NB-IoT to operate in three different coverage levels i.e. EC0 (Normal) for 0dB, EC1 (Robust) for 10dB, and EC2 (Extreme) for 20dB, respectively [33]. These coverage levels are defined by, for example, dedicated settings for channel repetitions applicable to each level. The CE level is selected by the NB-IoT UE according to the network-defined thresholds, based on the received signal conditions in the downlink e.g., Reference Signal Received Power (RSRP). Accordingly, the number of repetitions for downlink (i.e.,

NPDCCH and NPDSCH) can range from 1 to 2048, and the number of repetitions for uplink (i.e., NPRACH and NPUSCH) can range from 1 to 128, respectively [35]. Clearly, improving the coverage with retransmissions is not an optimal choice, both from the device and network perspectives [36]. The trade-off is that repeating signal transmissions consumes additional power and contributes to reducing battery life-time significantly [37]. From the network perspective, the channel remains occupied for longer durations and could lead to network congestion and increased latency in the face of huge number of operating devices [38].

- NB-IoT was conceived within a set of specifications particularly suited at supporting a huge number of battery-powered devices that would transmit small chunks of data for supporting delay-tolerant IoT applications [39]. These devices were conceived to be mostly stationary and installed at hardly accessible areas usually with poor coverage (e.g., basements, underground pits, and manholes etc) and/or battery-operated [40, 41, 42]. Since these devices are expected to operate on a single charge/battery without any human intervention, they are expected to work in span of years [43, 44]. To achieve this, NB-IoT has provisions for reducing the energy consumption of the sensor nodes (i.e., low power modes, extended DRX cycles, elongated PSM, etc.) [45, 46]. The challenge is to fully exploit and optimize the utilization of these provisions to realize the targeted 10-year battery lifetime of an NB-IoT device. This demands optimizing the NB-node node both from the hardware and software perspectives so as to utilize its scarcely available energy in an efficient manner.

- A similar and closely related issue is that the existing literature is replete with theoretical models for the energy and power consumption of an NB-IoT node and these models do not provide a real insights into the variability that the device experiences when deployed in real-world NB-IoT networks [39, 4]. That is why when these devices operate in real conditions they do not meet the 3GPP standardized criteria, as opposed to the predictions of most of these models [39, 4].

- Finally, since NB-IoT is expected to accommodate hundreds of thousands of semiconductor based devices, their maintenance and operation comes at the cost of high carbon footprints [47]. Replacing and disposing of millions of their batteries is not only impractical in terms of cost and maintenance, but also a severe threat to the health and resources of our planet. This demand for optimal resource usage, on the one hand, and controlled power levels and greener communications on the other hand, to reduce their overall carbon footprints on the environment [48, 49, 50].

## 1.5 Problem statement and research questions

Powering myriad of sensor nodes for the future IoT technology brings many challenges in terms of sustainability and maintenance. In particular, managing an NB-IoT network from the perspective of individual NB-IoT sensor nodes in terms of their operation and energy behaviour is a crucial challenge. Extending the battery life-time of an NB-IoT node to 10 years, as standardized by 3GPP, demands optimizing it from both the hardware and software perspectives so as to utilize its scarcely available energy in an efficient manner. That is why I, in this PhD thesis, seek to explore, propose and test new methods, models and algorithms for enabling energy-efficient techniques and architectures for the NB-IoT network. My PhD research, in particular, addresses the following research questions (RQs):

1. RQ1: How to design an NB-IoT sensor node from CoTS components that would transmit its collected data to an IoT server over the available NB-IoT network? Scaling it up, how to setup an "NB-IoT testbed" i.e., integrating a multitude of NB-IoT sensor nodes to collect, analyse and investigate their data over the backend IoT server?

2. RQ2: How to utilize the developed "NB-IoT testbed" for analysing the network coverage performance of a real NB-IoT network, particularly, in an indoor, outdoor and deep-indoor (underground) environments?

3. RQ3: What could be the baseline energy consumption model for such an NB-IoT sensor node i.e., what parameters affect the energy consumption profile of an NB-IoT node and how these parameters could be integrated into the baseline energy consumption model of the node to improve its energy efficiency?

4. RQ4: What different architectures are possible for developing an NB-IoT application? i.e., how many hierarchical layers are actually needed and what could be their respective roles for collecting, processing, and transmitting the collected data to the cloud?

5. RQ5: What type of local data processing could be utilized and what could be the associated benefits? i.e., what could be the trade-offs in terms of computation and communication energy and/or latency between local computing and transmissions?

6. RQ6: How to demonstrate and validate the above approaches in a real NB-IoT network?

## 1.6 Thesis contributions

In order to address the aforementioned research questions in the context of NB-IoT, this thesis makes the following contributions (Cs).

1. C1: I developed the DORM (integrateD cOmpact naRrowband platforM) NB-IoT node to conduct real-life investigation of an NB-IoT node operating under a real NB-IoT network. Replicating 50 of such DORM nodes and connecting them to a single IoT back-end server, I developed the "TalTech NB-IoT testbed" to carry out a comprehensive empirical analysis of the NB-IoT network coverage performance in indoor, outdoor and deep indoor environments.

2. C2: I conducted a thorough investigation of the Radio Resource Control (RRC) communication protocol that an NB-IoT radio transceiver follows to communicate with a 5G base-station that supports an NB-IoT network. Based on a comprehensive power consumption analysis of the various states of an NB-IoT radio transceiver, I proposed an analytical energy consumption model for a 3GPP compliant NB-IoT radio transceiver.

3. C3: I developed an NB-IoT based Edge-of-things framework, wherein the Machine Learning (ML) algorithms running at the edge reduces the number of NB-IoT radio transmissions for transmitting visual data over the NB-IoT network. This contributes to significant gains in terms of NB-IoT radio energy savings and also contributes towards an increased responsiveness of the NB-IoT network, thanks to the decreased usage of the NB-IoT radio.

## 1.7 Thesis organization

The rest of this thesis is structured as follows:

- Chapter 2: This chapter highlights the birth of NB-IoT as a 3GPP standardized random access technology (RAT) with an objective to penetrate the IoT market targeting the low-power, low-cost, low-complexity, low-throughput and delay-tolerant IoT applications. This chapter presents the NB-IoT background, the NB-IoT standard features that were included as part of its initial release i.e., Release13 and the enhancements that were further incorporated as part of its new releases i.e., Releases 14 to Releases 17. This chapter also highlights the design objectives of NB-IoT with an emphasis on the added features that were incorporated to achieve those design objectives. Finally, this chapter positions this PhD thesis, in particular, to the the research areas that this thesis contributes to.

- Chapter 3: This chapter details the development of the "Taltech NB-IoT testbed" by incorporating 50 NB-IoT DORM nodes to a single IoT back-end server that is available over the cloud (internet). These DORM nodes are connected to the Base-Station (BS) through the available NB-IoT network where the BS is further connected to the server on the internet though the core network. Using the "Taltech NB-IoT testbed", a comprehensive coverage analysis of the NB-IoT test network in indoor, outdoor and underground scenarios was carried across the TalTech campus. Some of the results included in this chapter are extracted from three published conference papers.

- Chapter 4: Based on a detailed empirical analysis of the various states of an NB-IoT radio transceiver while operating under real and deployed NB-IoT network where it communicates with the BS through an RRC protocol, this chapter presents an empirical modelling for the baseline energy consumption of an NB-IoT radio transceiver. This work has been published in a high impact Q1 journal paper i.e., IEEE Internet of Things Journal, IF = 9.936.

- Chapter 5: Finally, this chapter presents a three-tiered energy-efficient "Visual NB-IoT testbed" that could smart transmit visual images from visual sensor nodes over the NB-IoT network. The developed "Visual NB-IoT testbed" involves running Machine Learning algorithms at the edge to help reduce the number of NB-IoT radio transmissions at the gateway layer that are required for transmitting an image data over the NB-IoT network. The obtained results indicate that this smart NB-IoT architecture achieves significant gains in terms of the NB-IoT radio energy savings and also pays towards an increased responsiveness of the network, thanks to the decreased usage of the NB-IoT radio. Detailed results have been published in a high impact Q1 journal paper i.e., MDPI Sensor, IF = 3.576.

- Chapter 6: This chapter summarizes the thesis, draw conclusions, and suggests possible future directions.

# 2  NB-IoT Design Challenges, Evolution and State-of-the-Art

Realizing the need for and potential of the new and rapidly growing IoT market, 3GPP started a feasibility study in the beginning of 2014 on cellular system support for ultra-low complexity and low throughput IoT solutions referred to as cellular IoT. In May 2014, Huawei and Vodafone proposed to 3GPP the Narrow Band Machine to Machine (NB-M2M) as a study item to address the IoT market needs. Additional telecom industrial players got interested and later the same year Qualcomm proposed Narrow Band Orthogonal Frequency Division Multiplexing (NB-OFDM). In May 2015, 3GPP merged the two proposals (i.e., NB-M2M and NB-OFDM) and formed the Narrow Band Cellular IoT (NB-CIoT). Eight months later, Ericsson proposed the Narrow Band Long-Term Evolution i.e., NB-LTE. In September 2015, 3GPP included all these proposals as a work item for Release 13. The key difference between NB-CIoT and NB-LTE was the number of the reused legacy LTE network resources to support inter-operability. In June 2016, NB-IoT was recognized as a new clean slate Radio Access Technology (RAT). Only improvement changes could further be allowed and implemented thereafter. Thus, the first version of the NB-IoT standard was released in July 2016, as part of 3GPP Release 13 in technical report (TR) 45.820 [51] providing a support for massive numbers of low-power, low-cost, and low complexity IoT devices with an optimized network architecture.

## 2.1  NB-IoT design challenges

This section highlights the NB-IoT design challenges that were incorporated as significant deviations from the legacy LTE specifications. Some of these design challenges are underlining, to various extents, the research questions as laid down Section 1.5 that have been addressed by this PhD thesis.

- Super Coverage: In 3GPP standardization for NB-IoT, reduced network bandwidth and re-transmissions are employed as the two basic features to achieve the coverage enhancement for NB-IoT.

  Firstly, using reduced system bandwidth elevates the UE transmit power spectral density (PSD). For example, the NB-IoT bandwidth for the uplink can only be 3.75 kHz, whereas that for GPRS is 200 kHz. So, their PSD ratio reaches to around 5.33 and this ratio when converted into dB, i.e., $10 \times \log(5.3)$, equals nearly 7 dB implying that the reduced bandwidth of NB-IoT adds up to 7 dB gains to its coverage enhancement [52].

  Secondly, NB-IoT utilizes repeat transmissions to achieve its super coverage. For example, NB-IoT employs Hybrid Automatic Re-transmission Request (HARQ) type-II scheme where each re-transmission is incrementally soft combined at the receiver to improve error correction [53]. NB-IoT also increases the maximum repetition number by a large margin as compared to legacy LTE. These repetitions reaches upto a maximum number of 128 in the uplink. According to the channel estimator, a repetition of a factor of 2 results in less than 3 dB improvement in coverage performance [54], and thus a repetition of 128 achieves a coverage gain of about 13 dB in practice. Thus a coverage enhancement gain of 20 dB is achieved as compared to the standard GPRS.

  The downside is that the reduced bandwidth degrades the data rate, and the large number of re-transmissions increases the latency and power consumption of the node.

- Low Power: The ultra long battery life of NB-IoT is mainly achieved through the introduction of two features i.e., PSM, and eDRX. During the PSM, the radio frequency (RF) unit of the UE is completely shut off, causing the downlink to be inaccessible. If some downlink data arrive for this UE, it is cached at the network such that when the UE itself has mobile originated (MO) messages and goes to its CONNECT state, it ultimately receives its cached data. For NB-IoT, the the maximum PSM is upto 310 hours. The only drawback is the no-response time for the mobile terminated (MT) messages for as long as the UE is in PSM state. And to mitigate the no-response problem for the MT messages caused by PSM, the 3GPP introduced eDRX, in Release 13, as a supplement for the PSM low power solution. eDRX is an evolution of the DRX technique that works at the IDLE or CONNECT states with an objective to increase the paging monitoring interval of the UE and to avoid its unnecessary power consumption. Albeit, inferior to PSM in energy savings due to frequent paging occasion (PO) monitoring, eDRX can effectively improves the downlink accessibility. According to TR 45.820 [51], if both PSM and eDRX are employed and the UE transmits a packet message of 200 bytes once a day, the life-time of a 5 Wh battery is estimated at 12.8 years. However, it is worth clarifying that this prediction is only simulation-based and when it comes to the battery life-time estimation in real scenarios, it is rather more complicated since there are many factors that needs to be considered.

- Low Cost: This objective is eventually achieved by decreasing the system performance and simplifying the protocol volume. Decreasing system performance include three aspects. Firstly, NB-IoT uses only one transceiver that is shared both by the uplink and the downlink, in contrast to the legacy LTE design that includes two transceivers that correspond to two different links respectively. NB-IoT, thus supports only HD-FDD (Half-Duplex Frequency Division Duplex) transmission mode allowing the uplink and the downlink to operate alternatively in different frequency bands, but not simultaneously. Reserving only one transceiver also lowers the power consumption of the RF unit. Secondly, NB-IoT supports low data rate applications that demands lower sampling rates and the smaller transfer block size (TBS). Besides, despite the regulation for supporting a maximum of two antennas for NB-IoT in Release 13, the mainstream NB-IoT chip vendors tend to include only one antenna. All these features make NB-IoT chips cost effective as compared to its competitors IoT technologies [52].

- Massive Connection: The supported connection number of 52547 for NB-IoT per cell site sector is calculated based on the assumption of TR 36.888 [55]. The massive connectivity objective of NB-IoT is achieved based on the following three key factors. Firstly, the data transmission characteristic of the MTC (Machine Type Communication) application plays an essential role for massive connectivity where each user transmits only a small amount of data at low frequency, and they are insensitive to the transmission delay. Therefore, although the 50K+ users can camp on the same cell simultaneously, the majority of them are in the sleep state. Secondly, NB-IoT system exploits subcarrier (or tone) level uplink transmission scheme, which is one key difference from the legacy LTE where the downlink transmission scheme is similar to LTE except for some restrictions. This way, although the NB-IoT only has 180 kHz bandwidth, it can still simultaneously serve multiple UEs. Thirdly, NB-IoT simplifies signaling overhead, which can also improve the spectrum efficiency. Having less signaling signals is helpful to release the resources as early as possible so that the eNB can accommodate more UEs.

## 2.2 NB-IoT evolution

NB-IoT has been evolving ever since its birth in 2016 so as to incorporate more and more features to meet the ever-increasing demands of IoT market. In what follows, we start by providing an overview of the NB-IoT basic standard as part of its first release i.e., Release 13 in 2016. We then briefly highlight the improvements that were made as NB-IoT evolved in time with its onward releases until its freeze version in Release 17.

### 2.2.1 NB-IoT Initial Release 13 (June 2016):

Figure 3 summarizes some of basic features of NB-IOT technology as part of its initial Release 13 in 2016. Other features include the following.

- Mode of Operation: NB-IoT can operate in three different modes i.e., standalone, in-band, and guard-band. For the in-band and guard-band modes, NB-IoT occupies only one PRB of 180 KHz in the LTE spectrum. It can also be allocated a standalone band of 200 KHz bandwidth in the GSM spectrum. These flexible deployment enable its fast integration and coexistence with the legacy LTE and GSM technologies.

- Complexity and Cost Reduction Techniques: NB-IoT includes relaxed base-band processing, low memory storage, and reduced radio-frequency (RF) components to achieve the low complexity and low-cost objective [52]. Also, NB-IoT uses the restricted BPSK and QPSK modulation schemes with only one antenna support both in uplink and downlink transmission with the same objective.

- Power Reduction: NB-IoT includes Power Saving Mode (PSM) and extended Discontinuous Reception (eDRx) to help achieve the UE's battery life time of 10 years. In PSM, the NB-IoT device sleeps completely where it is not reachable by the BS signaling. However, it remains registered with the network and can be in the PSM for up-to 413 days. In eDRX, the device is in an inactive mode from up-to a few minutes to a few hours. In both cases, the partial or complete inability to receiving
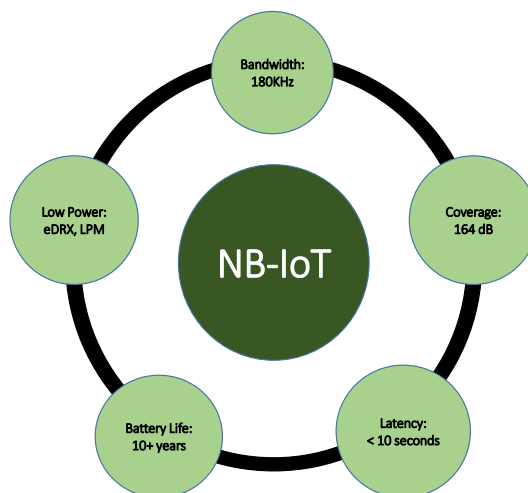


*Figure 3: A simplified representation of the basic features of NB-IoT technology as part of its first release i.e., Release 13 in June 2016. These features include lower bandwidth, low-power consumption, longer device lifetime, extended network coverage, and higher latency.*

and sending different signals enhance the battery life longevity; however, choosing either PSM, eDRX, or both, depends on the corresponding use-case requirements.

- Coverage Enhancement: NB-IoT delivers an additional 20 dB of coverage over the legacy LTE system. This corresponds to 164 dB of MCL. To enhance its coverage, NB-IoT uses up to 128 and 2048 re-transmissions in the uplink and downlink, respectively. This, on the one hand, enhances the coverage of NB-IoT, but on the other hand also increases the latency in the transmission (as well as increases energy consumption). That is why NB-IoT is suitable for latency insensitive applications that can tolerate up to 10 seconds of transmission delay.

### 2.2.2 NB-IoT enhancements (Release 14- Release 17)

The enhancements features in NB-IoT Release 14 (June 2017) included positioning update, multi-cast services, and a new UE output power class in which the NB-IoT system throughput, mobility, service continuity and non-anchor carrier operation were improved [56, 57].

NB-IoT Release 15 (June 2019) introduced improvements such as Latency Reduction, Semi-Persistent Scheduling (SPS), Small Cell Support and Long Range, Enhanced User Equipment Measurements and Time Division Duplex (TDD) Support to further improve the QoS of NB-IoT applications [58, 59].

The introduced improvements in NB-IoT Release 16 (July 2020) are related to enhancements of the previous features i.e., improved DL/UL transmission efficiency, UE power consumption, scheduling enhancement, network management enhancement, mobility enhancements, and coexistence with NR and incorporated features such as Grant-Free Access, Simultaneous Multi-User Transmission, Enhanced Group Message Mechanism, and Inter-RAT Idle-Mode Mobility [60, 61].

Finally, the planned features for Release 17 (standard freeze now in production) are to increase the peak data rate introducing the support for a higher modulation (i.e., 16 QAM) in downlink and also in uplink communications, reduction of the RRC re-establishment time to another cell defining specific signaling for neighbor cell measurements and the corresponding measurement triggering before radio link failure, and a support for NB-IoT carrier selection depending on the coverage level and specific carrier configurations [62].

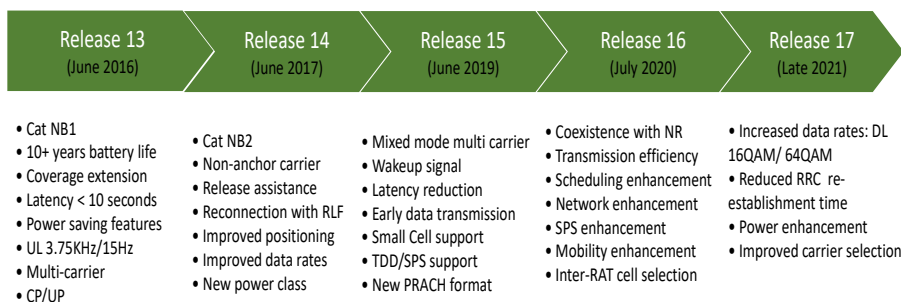| Release 13 (June 2016) | Release 14 (June 2017) | Release 15 (June 2019) | Release 16 (July 2020) | Release 17 (Late 2021) |
|---|---|---|---|---|
| • Cat NB1 <br> • 10+ years battery life <br> • Coverage extension <br> • Latency < 10 seconds <br> • Power saving features <br> • UL 3.75KHz/15Hz <br> • Multi-carrier <br> • CP/UP | • Cat NB2 <br> • Non-anchor carrier <br> • Release assistance <br> • Reconnection with RLF <br> • Improved positioning <br> • Improved data rates <br> • New power class | • Mixed mode multi carrier <br> • Wakeup signal <br> • Latency reduction <br> • Early data transmission <br> • Small Cell support <br> • TDD/SPS support <br> • New PRACH format | • Coexistence with NR <br> • Transmission efficiency <br> • Scheduling enhancement <br> • Network enhancement <br> • SPS enhancement <br> • Mobility enhancement <br> • Inter-RAT cell selection | • Increased data rates: DL 16QAM/ 64QAM <br> • Reduced RRC re-establishment time <br> • Power enhancement <br> • Improved carrier selection |

*Figure 4: A simplified representation of the evolution of NB-IoT through time i.e., with each new release old features were enhanced and/or new features were added in the NB-IoT technology to meet the increasing demands of IoT applications.*

## 2.3 NB-IoT State-of-the-Art and positioning of this PhD thesis

Although the aforementioned features in the previous section paved a prospective way towards meeting the NB-IoT design challenges, these features only provided simulation based feasibility for meeting the NB-IoT design objectives. However, when it comes to the practical implementation of NB-IoT technology, it is expected to encounter unprecedented issues which demands a pragmatic investigation of the NB-IoT technology from the implementation perspectives. With such a motive, this section highlights the positioning of this PhD thesis vis-à-vis the corresponding state-of-the-art (SoA) NB-IoT research areas as summarized in Figure 5. In what follows, these particular research areas are discussed with respect to their shortcoming in the existing SoA and how this thesis contributed towards filling these gaps.
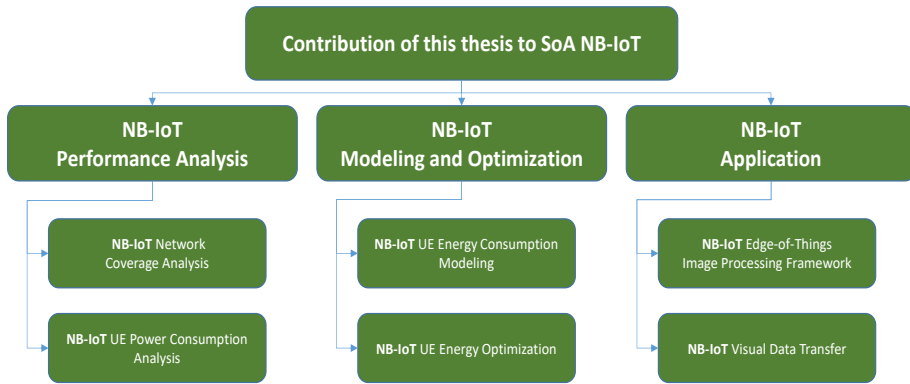


*Figure 5: Contribution of this thesis to the particular research areas of NB-IoT.*

### 2.3.1 NB-IoT Network Coverage analysis:

Majority of the existing SoA related to the NB-IoT coverage is modeling and simulation based. Modeling-based methodology usually starts with setting up the simulation environments, and then the network performance is studied for different parameters under given link budgets. The objective is to generate precise modeling for each parameter according to the protocol characteristics. In general, the simulation parameters are composed of carrier frequency, system bandwidth, transmit power for eNB and UE, propagation model, power consumption model for UE, Doppler spread, antenna configuration, noise figure for uplink and downlink, etc. The performance metrics are either duration time for control channels at a given Block Error Rate (BLER) and target Signal to Noise Ratio (SNR), or data rate for shared channels at different configurations. For example the work in [54] illustrates the evaluation of the coverage performance of NB-IoT i.e., channel performance evaluation results for both downlink and uplink under some specific SNR and BLER. Regretfully, most of similar simulation based works such as [63, 64, 65, 66] differ a lot in their results to great extents and could not be entirely trusted for real-life deployments. Furthermore, most of these works are done by taking only one single device into account, but lack the entire system perspective. It would be more significant to study the overall network performance assuming around 50K+ devices within one cell in the manner of stochastic geometry. This is still an unresolved research issue.

In addition to the modeling-based campaign, some other works aim at developing the

toolkit and simulator for NB-IoT. For example, Miao et al. [63] exploit OPNET simulation platform to build a NB-IoT system model, which consists of UE, eNB, core network, cloud platform and vertical industry center. Based on this platform, it is verified that the NB-IoT network indeed outperforms the LTE network with different channel width in terms of coverage range, channel utilization and queuing delay. Similarly, Troha et al. [67] develop a downlink simulator for NB-IoT network using Matlab. They make detailed implementations for both eNB-side and UE-side functions, including all physical channels and signals, resource scheduling and equalization. With this simulator, they evaluate the relationship of BLER, SNR and repetition times on different channels. Although these outstanding works provide good starting points to explore the NB-IoT performance, their simulators are not universal enough to be extensively used. In contrast, the well-known network simulator ns-3 is more popular [68], however, there is no available NB-IoT module that can be integrated into it so far. It can be viewed as another potential research direction.

There are still some works devoted to making field tests based on SDR platform. These experiments show that the NB-IoT coverage improvement is limited by the channel estimation quality and coherence time of the channel [69]. Lauridsen et al. [70] focus on what kind of coverage and capacity can be achieved in a realistic scenario. They employ the commercially deployed LTE sites' configuration and location in a rural area, and calibrate the simulation using drive test measurements. Their tests reveal that NB-IoT can provide better coverage performance than LTE-M, but the costs are the lower number of supported devices per sector and higher device power consumption as compared to LTE-M. In spite of these findings, they claim that the NB-IoT still can support 25K devices and device battery life of above 5 years. To this end, the existing literature demands performance reports based on real field deployments both for the coverage analysis and network reliability of NB-IoT. This shall also highlight the energy measurements of UE in real environments and the related latency issues of the various transmission protocols when put in real test.

**In contrast to the existing SoA, this thesis starts with the design of an NB-IoT node from CoTS components and then setting up a complete NB-IoT testbed where these nodes are deployed in real environments to perform the practical on-field coverage analysis of real NB-IoT network various scenarios.**

### 2.3.2 NB-IoT UE Power Consumption Analysis and Energy Consumption Modeling:

To the best of our knowledge, only a few works have evaluated NB-IoT technology in terms of its UE's power consumption analysis and battery life-time estimations; providing analytical and simulation based results only where the few practical works are mostly very limited in scope.

Regarding the analytical works, the authors in [71] have developed an analytical model for the DRX power savings in an LTE system where the work in [72] proposed a mathematical model for the optimum length of an eDRX cycle that can help mitigate the signaling cost in an LTE network. Similarly, the authors in [73] and [74] have tried to estimate the NB-IoT device battery life-time by using some simplified energy consumption equations. The authors in [75] and [76] have proposed an NB-IoT UE energy consumption analytical model that is based on Markov chain where the work in [77] presents an analytical model for evaluating the latency and maximum number of devices in the network.

Second, regarding simulation based works, the authors in [72], and [73]; who proposed their own mathematical models used ns-2 and Matlab-based simulators to validate their models. The authors in [76] and [77] followed suit by validating their models in ns-3 simulator. The authors in [78] extended the analytical model of [76] so as to incorporate the

NB-IoT specific features for evaluating the NB-IoT device battery lifetime in different coverage levels. The work in [74] has presented an ns-3 based design to evaluate the NB-IoT UE's energy consumption and latency where the work in [79] has presented an ns-3 based design to evaluate the LTE UE energy consumption.

Third, regarding the power consumption analysis of the NB-IoT UE from the practical perspective, the existing literature is very limited in scope. For example, the work in [69] provides power consumption measurements of the NB-IoT end-device, but the provided measurements refer to the NB-IoT node as a whole where the individual power consumption details of each component of the node are missing. The work in [80] focuses on the latency issues of NB-IoT while making use of a commercial NB-IoT network in Belgium. Although this work provides empirical results for analyzing the network performance in terms of setup times, throughput and latency, it does not refer to the power consumption details of the UE. The work in [39] provides empirical measurements for the energy consumption and transmission delays for the two CoTS NB-IoT platforms i.e., Ublox SARA-N211 and Quectel BC68 while operating in a commercially deployed Vodafone network in Barcelona, Spain. However, their provided current traces are very superficial in nature where the underneath consumption details of the various RRC states are obscured. Also, the provided current graphs do not actually portray the undermentioned titles especially for the values of their acclaimed timers. The authors in [43] claim to present the first publicly available empirical power consumption measurements for the NB-IoT devices so as to provide a power consumption model for IoT battery lifetime estimation. However, they provide no details of their used devices and their measurement setup is emulated using a Keysight UXM, which is a standard-compliant NB-IoT BS emulator; so their results could not be fully trusted for a real commercially operating NB-IoT BS. Since, their analysis is based on an emulated NB-IoT network so their results could not be trusted for a commercially operating NB-IoT BSs. Moreover, the power consumption details are way too generic, lacking detailed power-consumption profiling of the internal states of the NB-IoT radio module. Similarly, the work in [81] proposes a Dual-RAT LPWAN node supporting NB-IoT and LoRaWAN where the node is composed of an STM32 based microcontroller attached to a LoRaWAN radio module (built around RN2483 transceiver from Microchip) and NB-IoT radio module (built around Cat NB1 Ublox N211 chipset) with the necessary power regulator circuitry. Here too the power consumption details of the whole node is given where the individual power graphs from each radio state with their details are completely ignored. Similarly, the work in [75] claims to provide experimental validation of NB-IoT UE energy consumption but just as the rest of the works, they fail to touch the minute energy consumption details of their device.

Considering the above discussion, it is evident that most of the existing works present only a superficial analysis of the NB-IoT UE's power consumption, providing mostly the aggregated power consumption details of the node as a whole where the individual power consumption details of each component remain obscured. That is why the detailed energy-consumption profiling of the various states of the CoTS NB-IoT radio and its underneath activities remain unexplored to date. Secondly, most of the existing analysis are based on emulated NB-IoT networks i.e., where the BS is emulated and so the results of these works could not be trusted for the commercially operating NB-IoT BS. Similarly, the detailed energy profiling of the commercially available (CoTS) NB-IoT devices in practical use-cases under commercial networks are yet to be explored.

**To fill this gap, this PhD thesis provides detailed power consumption analysis of the various RRC states (Connected, Idle, PSM) of the NB-IoT radio with minute power consumption details of the underneath activities i.e., C-DRX cycles, I-eDRX cycles, PTW, DRX**

**Cylce, PO and PSM which to date haven't been analyzed to that granularity. Furthermore, this PhD thesis also provides an analytical energy consumption model for an NB-IoT radio that truly depicts the practical energy consumption of any CoTS NB-IoT radio. On top of that, a detailed sensitivity analysis (SA) of the presented model gives a comprehensive understanding of of power consumption parameters and timings parameters of any generic NB-IoT radio.**

### 2.3.3 NB-IoT Edge-of-Things based Machine Learning Framework:

NB-IoT is specifically designed for low-end MTC applications, but as time goes on, NB-IoT is possibly expected to sustain richer scenarios with better performance as compared to its current usage in terms of its capacity, power and latency. These objectives are difficult to accomplish purely depending on the NB-IoT itself. Thus, it could be combined with other SoA technologies such as AI [82], Blockchain [83], NOMA [84], SIC [85] and D2D [86] to meet the ever-growing demands of IoT.

The last few years have witnessed a regain in AI popularity, in particular to Machine Learning (ML) and deep learning (DL) areas. Of special interest are the recent and ongoing developments related to "Edge AI", i.e. executing ML/DL models and algorithms on embedded edge devices located at the outer edge of a network. According to [87], "The edge AI hardware market is projected to grow from 920 million units in 2021 to 2,080 million units by 2026; it is expected to grow at a CAGR of 17.7% from 2021 to 2026". Among the various reasons for this commercial growth, it is worth mentioning the increasing need for local processing at the edge instead of in the cloud (for latency, privacy, etc. reasons), the emergence of commercially-available edge AI hardware accelerators, and the increasing availability of LPWANs including NB-IoT.

**Towards this direction, this PhD thesis combines NB-IoT with ML algorithms i.e., "NB-IoT Edge-of-Things Framework", wherein ML algorithms running at the edge processes an image only to obtain the useful information out of it and discards the unnecessary data. This in turn reduces the communication budget of each individual NB-IoT radio and thus relaxes the channel occupancy, minimizes the network load and reduces the transmission latency. Using our proposed "NB-IoT Edge-of-Things Framework" for visual data transfer application, we showed practically that ML can play a pivotal role towards revolutionizing the future IoT technology where the inference performed at the edge could prevent sending huge amount of data over the core IoT networks and this could significantly save in terms of power, energy and latency of the overall IoT infrastructure.**

### 2.3.4 NB-IoT Visual Data Transfer Application:

LPWANs were not designed as a suitable choice for visual data transfer, nevertheless there have been several attempts to use LPWANs for image data transfer. For example, C. Pham in 2016 (a year after the introduction of the LoRaWAN framework) used a LoRa network for the first time for image data transfer in a visual surveillance application [88]. He successfully transmitted an image of about 2.4 Kb up to 1.8 km using LoRa. Jebril et al. [89] proposed an approach for mangrove forest monitoring in Malaysia, wherein they transferred image sensor data over the LoRa physical layer (PHY) in a node-to-node network model. In their work, they also proposed a novel scheme for overcoming the bandwidth limitations of LoRa. Chen et. al. [90] suggested a light trustworthy communication protocol called MPLR for image dispatching in LoRa to facilitate image monitoring in an agricultural IoT platform. Ji et al [91] proposed a method for farming application wherein an image is transmitted into tiny of grid of patches such that any grid patch is only dispatched when a change in it is noticed. They showed that this approach reserves a lot of link bud-

get during the surveillance of static agriculture sites and provide better performance. Wei et. al [92] proposed a methodology for transmission of JPEG compressed image data in a multiplexing mode with different spreading factors to reduce the transmission time of image data by keeping the quality of the images at the receiver side to high PSNR values. Other similar works that use LoRA for image transmission include [93], [94], [95].

**However, to the best of our knowledge, NB-IoT has never been used for visual application and this PhD thesis presents the first NB-IoT based framework for visual data transfer**.

From the perspective of utilizing edge computing for increasing the efficiency of IoT, several works have proposed and evaluated ML techniques for higher energy efficiency, bandwidth saving, lower latency, and collaborative intelligence of the network [96], [97], [98], [99], [100], [101] and [102]. However, most of these works provide analytical models with simulation-based results that cannot be entirely relied upon for the real deployed networks because simulation-based validations do not accurately portray the empirical measurements of real-life systems. Other works such as[103], [104], [105], and [106] proposed deep learning for image recognition and classifications in IoT-based architectures. However, the focus of most of these works is mostly the obtained accuracy and precision of the models used for sending the final inferences to the cloud rather than original images. These works also lack the details on the amount of energy that is being consumed for ML computations with respect to the energy gains in terms of the device and network perspective. Nevertheless, some works proposed and utilized ML for increasing the energy efficiency of IoT nodes. For example the work in [107] uses a ML technique to determine whether to offload the classification of the current input data to the higher processing gateway layer or to perform it locally on the node and thereby achieve energy savings. However, they used the CC1350 IoT platform (a short range radio device) and lack details on larger family of networks such as LPWAN technologies. The work in [108] presented a hierarchical inference model to cut down the amount of data that is to be transmitted and produced interesting energy-related results. However, they made use of BLE and Zig-Bee transmission protocols, lacking any correlation with LPWAN technologies. Though the work in [109] presented a real-time context-aware and collaborative intelligence among nodes in large-area IoT testbed, they showcased their results using LoRa and BLE only. Other works that consider the use of ML for energy efficiency in LoRa networks include [110], [111] and [112].

**In contrast to these works, this PhD thesis showcases a practical edge-of-things computing based framework for dispatching optimized images over an NB-IoT test network wherein computations at the edge help reduce the number of NB-IoT radio transmissions over the core network. This thesis also shows how the reductions in the communication budget of the radio can in turn contribute to relaxing the channel occupancy, minimizing the network load and reducing the transmission latency**.

# 3 Development of an NB-IoT Testbed and Coverage Analysis of an NB-IoT Network

This chapter covers the development of DORM (integrateD cOmpact naRrowband platforM) NB-IoT node from CoTS low-cost and low-power components with the development of "TalTech NB-IoT testbed" that encompasses 50 DORM nodes with their NB-IoT connection setup to Telia's 5G BaseStation (BS). The BS is further connected to an IoT back-end server at the cloud (internet). A simplified representation of "Taltech NB-IoT testbed" setup is shown in Figure 6. Using this setup, the coverage analysis of NB-IoT test network across Taltech campus is performed in an indoor, outdoor and deep indoor environments with the obtained results published in [1], [2], and [3].
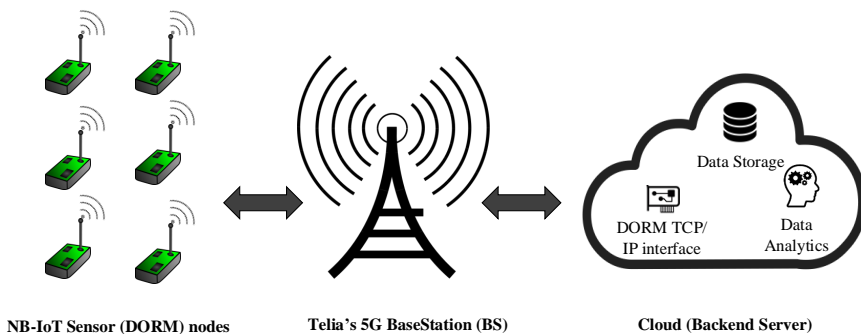


*Figure 6: A simplified representation of TalTech NB-IoT testbed architecture incorporating NB-IoT sensor (DORM) nodes, a 5G BaseStation supporing NB-IoT network, and an IoT backend server that is available on the cloud (internet). An application running over the server collects and analyses the collected data from the DORM nodes.*

This chapter is based on the following publications:

- Sikandar Zulqarnain Khan, Hassan Malik, Jeffrey Leonel Redondo Sarmiento, Muhammad Mahtab Alam, and Yannick Le Moullec. Dorm: Narrowband iot development platform and indoor deployment coverage analysis. *Procedia Computer Science*, 151:1084–1091, 2019, [1].

- Hassan Malik, Sikandar Zulqarnain Khan, Jeffrey Leonel Redondo Sarmiento, Alar Kuusik, Muhammad Mahtab Alam, Yannick Le Moullec, and Sven Pärand. Nb-iot network field trial: Indoor, outdoor and underground coverage campaign. In *2019 15th International Wireless Communications Mobile Computing Conference (IWCMC)*, pages 537–542, 2019, [2].

- Nishant Poddar, Sikandar Zulqarnain Khan, Jakob Mass, and Satish Narayana Srirama. Coverage analysis of nb-iot and sigfox: Two estonian university campuses as a case study. In *2020 International Wireless Communications and Mobile Computing (IWCMC)*, pages 1491–1497. IEEE, 2020, [3].

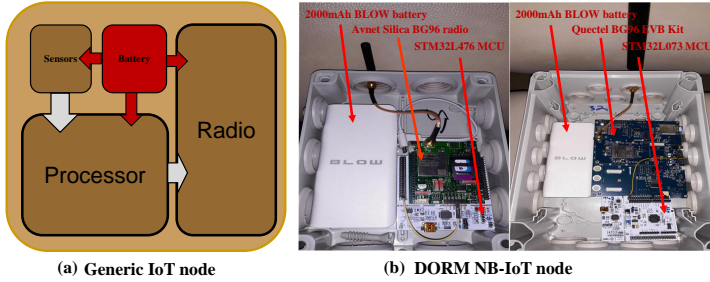**(a) Generic IoT node**          **(b) DORM NB-IoT node**

*Figure 7: (a) A simplified representation of an IoT node incorporating a radio, a processor, sensors and a battery. (b) DORM NB-IoT node incorporating an NB-IoT radio, a micro-processing unit, embedded sensors and a DC power supply.*

## 3.1 Development of DORM node

The device complexity of an NB-IoT node is reduced as compared to other unlicensed LPWAN technologies such as LoRA, Sigfox, and Telensa etc., so as to address the ultra low-power IoT applications [1]. A typical IoT node, as shown in Figure 7 (a) includes a generic processing unit that along with its processing capability supports a variety of interfaces for integrating a multitude of sensors for monitoring the environment, a radio that provides an IoT network connectivity to the node and a DC power supply to provide power to all the components of the node. The node collects data from its surroundings through the attached/embedded sensors, processes it accordingly using its CPU and send the processed data in proper format to the attached radio for possible transmission over the air through the available IoT network. The DORM (integrateD cOmpact naRrowband platforM) nodes, as shown in Figure 7(b) combines an ultra-low-power processor with an NB-IoT radio and is powered by a DC battery as represented in Figure 7(a). The first variant of DORM node integrates an STM32L476RG (Cortex M4) MCU board[5] as its processing unit with an Avnet Silica NB-IoT shield[6] as its radio and is powered by an external 2000mAh BP15 BLOW battery[7]. The second variant of DORM node integrates STM32L073RZ (Cortex M0+) MCU board[8] as its processing unit with a Quectel GSM/NB-IoT EVB Kit[9] as its radio and is powered by the same BP15 BLOW battery The STM32-based Nucleo boards are used as the processing units as these CPUs are highly affordable and can support a variety of hardware add-ons to seamlessly work with a wide range of sensors. The Quectel BG96 radio chipset features ultra-low power consumption and supports LTE Cat NB1 and LTE Cat M communication protocols along with a set of industry-standard interfaces (such as USB/UART/I2C/Status Indicator) and are suitable for a wide range of IoT applications. Furthermore, the whole DORM node setup is packaged in a dust-proof and water-proof IP65 plastic junction boxes for possible deployment in an indoor, outdoor and underground environments capable of sustaining all kind of harsh weather conditions. The two variants of our DORM nodes placed in the IP65 plastic junction boxes are shown in Figure 8.

---

[5] https://os.mbed.com/platforms/ST-Nucleo-L476RG/
[6] https://www.avnet.com/wps/portal/silica/products/new-products/npi/2018/avnet-nb-iot-shield-sensor/
[7] https://botland.store/447-powerbank-mobile-batteries
[8] https://os.mbed.com/platforms/ST-Nucleo-L073RZ/
[9] https://www.quectel.com/product/umts-lte-evb-kit

To achieve higher energy efficiency, the processing units of these DORM nodes feature low power modes (LPMs) to help reduce its power consumption. The NB-IoT radio also features power saving modes i.e., eDRX and PSM as standardized by 3GPP so as to save its communication budget especially when the radio is not communicating with the Base-Station (BS). All these features are provided to achieve the 3GPP standardized 10 years battery life-time of an NB-IoT node [113, 43].
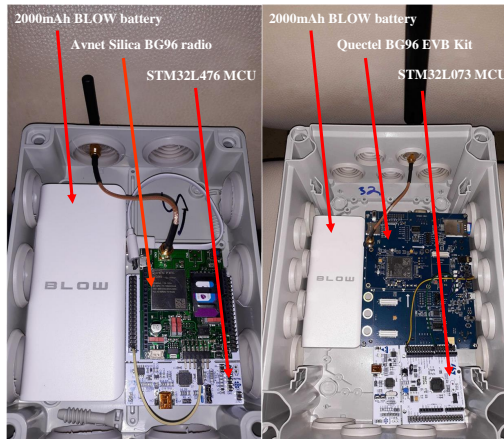


*Figure 8: Two variants of DORM nodes incorporating a processing unit i.e., STM32L476RG MCU or STM32L073RZ MCU, an NB-IoT radio i.e., Avnet Silica NB-IoT shield or Quectel GSM/NB-IoT EVB Kit, and an external DC power supply i.e., 20000 mAh BP15 BLOW battery placed with in the IP65 plastic junction boxes to survive in the extreme weather conditions of moist, rain, snow, and wind etc.*

## 3.2 Development of TalTech NB-IoT testbed

A generic IoT system [114, 115, 116] is comprised of a number of layers to facilitate functionalities such as sensing and monitoring of the environment, transmission of the sensed data over the air (network), and finally collection of the transmitted data at some central point (server) for further analysis and investigation [116]. The server may also offer functionalities such as data management, data storage, data backup and decision making as per the application's requirements [116]. The "TalTech NBIoT testbed" achieves these functionality through following three layers:

- Sensing/Perception Layer: DORM nodes are deployed at the sensing layer for sensing and monitoring the environment.

- Network Layer: Telia's commercial 5G Base-station that is installed within the premises of TalTech campus provides 5G network supporting Cat-NB1 (NB-IoT) and CatM networks.

- Cloud Layer: Cumulocity server is running at the cloud layer (internet) that gathers all the data from the deployed DORM nodes through the network layer and supports data collection, data management and data analysis as per users' application requirements.
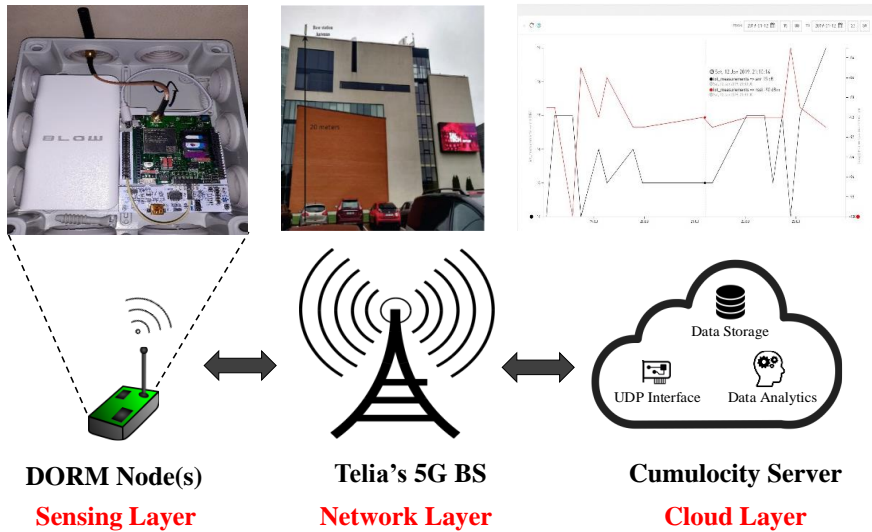
*Figure 9: TalTechNB-IoT testbed incorporating DORM nodes at the Sensing Layer, Telia's 5G BS at the Network Layer and a Cumulocity back-end server at the Cloud layer.*

The DORM nodes are deployed at the sensing layer of the "TalTech NB-IoT testbed" that are meant to sense the environment and send their sensed data to the BS through utilizing the NB-IoT network. The NB-IoT network is provided by Telia's 5G BS that is installed within the premises of TalTech Campus as shown in Figure 9(b). The DORM nodes monitor their surroundings through embedded/attached sensors and send their sensed data to the STM32 MCU through appropriate interfaces. The STM32 encapsulate this data into proper UDP format packets and send it to the BG96 module through the UART interface. The STM32 MCUs of the DORM nodes are programmed using C/C++ while the BG96 modules are configured using its AT commands as provided by its vendor [117]. Using the appropriate AT commands for BG96 radio as provided in [117], the module first establishes a secure NB-IoT connection with the BS and then sends the encapsulated data (coming from STM32) to the BS through the available NB-IoT network. The BS further forwards the received data from the deployed DORM nodes to the cloud where an IoT back-end server i.e., Cumulocity platform[10] collects all the data from these nodes for further analyses and investigation. The Cumulocity platform supports various data transmission protocols i.e., UDP, TCP/IP, HTTP, HTTPs, and MQTT where for the initial setup, the simplest UDP protocol was used for data exchange between the DORM nodes and the cloud. The Cumulocity server also features securely storing the incoming data from the DORM nodes with traces of all the previously sent data from each individual node with details of device ID, device location and data reception time. Figure 9 shows the different layers of TalTech NB-IoT testbed: (a) Sensing layer where DORM nodes are deployed, (b) Network layer where Telia's 5GF BS is at work and (c) Cloud layer where Cumulocity server platform collected all the data for futrher analysis.

---

[10]https://iot.ttu.ee/cumulocity-iot-platvorm-liidab-koik-seadmed-uhtsesse-susteemi/

| Floor Number (Elevation from the ground) | Observation point at 300 meters from the BS | | | | | |
|---|---|---|---|---|---|---|
| | Morning (08:00-13:59) | | | Evening (18:00-23:59) | | |
| | Avg. SNR (dB) | Avg. RSSI (dBm) | Signal Strength | Avg. SNR (dB) | Avg. RSSI (dBm) | Signal Strength |
| 5$^{th}$ Floor (15 m) | 18.11 | -65.75 | Good | 19.13 | -64.93 | Good |
| 4$^{th}$ Floor (12 m) | 18.68 | -67.50 | Good | 19.74 | -66.61 | Good |
| 3$^{rd}$ Floor (9 m) | 21.12 | -68.04 | Good | 21.33 | -67.71 | Good |
| 2$^{nd}$ Floor (3 m) | 21.28 | -69.48 | Good | 21.75 | -68.92 | Good |
| 1$^{st}$ Floor (0 m) | 23.58 | -70.20 | Good | 23.74 | -69.70 | Good |

*Figure 10: Average SNR and RSSI values obtained at 300m from the BS for different elevation levels. Source [1].*

## 3.3 Coverage Analysis of the NB-IoT network using TalTech NB-IoT testbed

Deploying 50 of such DORM nodes across the TalTech campus, a comprehensive real-life investigation of the NB-IoT test network was carried out to perform the coverage analysis of NB-IoT network in an indoor, outdoor and deep indoor (underground) environments. The obtained results in Figure 10 presents empirical measurements of the NB-IoT network coverage at different elevation levels at an observation point that was 300m away from the BS as shown in Figure 11. These results showed an average SNR values in the range of 18 dB to 23 dB and an average RSSI values in the range -65 dBm to -70 dBm, respectively. These results concluded that the NB-IoT network provides an excellent connectivity in indoor environments and can satisfy the IoT application requirements at different elevation levels. Nevertheless, small variations in the SNR and RSSI values were observed at different elevation levels possibly due to positioning and placement of the measuring nodes, proximity of the antenna with respect to base-station, building structure and its construction material. Our obtained results as shown in Figure 12 presented a preliminary inves-
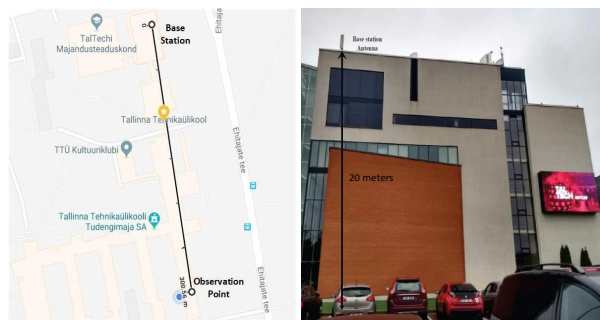


*Figure 11: Observation point is 300m away from the installed Telia's BS as shown by Google Maps (left) whereas the BS is 20m above the ground (right). Source [1].*

tigation of the coverage of NB-IoT in an outdoor, indoor, and deep indoor (underground) scenarios with empirical measurements under real NB-IoT network. All these measurements were conducted on Tallinn University of Technology (TalTech) campus and nearby residential areas within a range of 700 m. The obtained results indicated that NB-IoT is

able to provide good connectivity to meet the IoT application requirements in outdoor and indoor environments. However, for an underground scenario with the beam enabled for 700 m, it was only possible to provide connectivity to the devices up to 400 m. Furthermore, it was also observed that NB-IoT is able to provide connectivity to devices with a received signal strength indicator (RSSI) as low as 105 dBm as compared to 95 dBm as in long-term evolution (LTE). This revealed a better network performance of NB-IoT network over the existing LTE network, possibly due to the increased number of its repetitive transmissions.
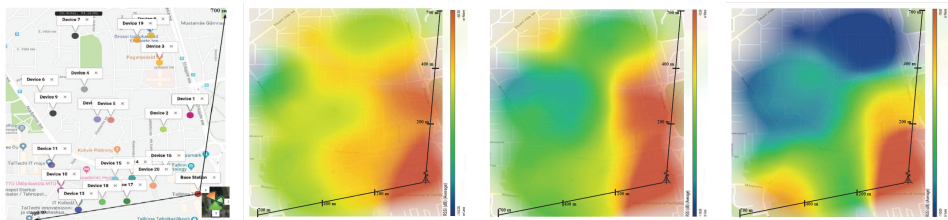


(a) Coverage area under study. The bottom right corner presents the available Telia's 5G BS ( beam 2 is used for coverage analysis).

(b) Coverage analysis of Telia's NB-IoT test network across TalTech campus in terms of its RSSI factor in an outdoor scenario.

(c) Coverage analysis of Telia's NB-IoT test network in terms of its RSSI factor in an indoor scenario

(d) Coverage analysis of Telia's NB-IoT test network in terms of its RSSI factor in an underground scenario

Figure 12: Coverage Analysis of NB-IoT network in an outdoor (b), indoor (c), and underground scenarios (d) within the covered area as shown in (a). Source [2].

## 3.4 Comparison of the coverage analysis of NB-IoT and Sigfox networks

A side-by-side comparison of the coverage analysis of the NB-IoT and Sigfox networks was conducted across TalTech and University of Tartu campuses. The NB-IoT coverage was investigated using three parameters i.e., RSSI, RSRP, and RSRQ such that in situations where RSSI values were not available (RSSI is not sufficient for evaluating the LTE-based technologies including NB-IoT); the coverage analysis was conducted based on RSRP and RSRQ. For analysing the Sigfox coverage, the RSSI factor was used only. Since Sigfox is a Non-LTE technology and its coverage could sufficiently be analysed by the RSSI factor only. Both of these LPWAN technologies were evaluated in an indoor, outdoor and deep-indoor environments so as to provide an understanding of their coverage levels in various propagation and penetration conditions.

### 3.4.1 Deployment setup for analysing NB-IoT and Sigfox networks

There are 4 LPWAN service providers in Estonia i.e. Telia Eesti AS[11] , Elisa Eesti AS[12], Connected Baltics OÜ[13], and Levikom Eesti OÜ[14]. Telia and Elisa provide NB-IoT networks and cover around 90% of the whole territory of Estonia as indicated by the large shaded ellipsoid in Figure 13. Connected Baltics is the exclusive Sigfox operator in Estonia and covers the major cities of Tallinn, Tartu, Pärnu and Narva as indicated by small heated circles (red, blue and green) in Figure 13. LEVIKOM provides LoRaWAN services but there are no details on their coverage across Estonia and thus their coverage is not shown in Figure 13.

---

[11]https://www.telia.ee/en

[12]https://www.elisa.ee/en

[13]https://www.connectedbaltics.com/coverage/
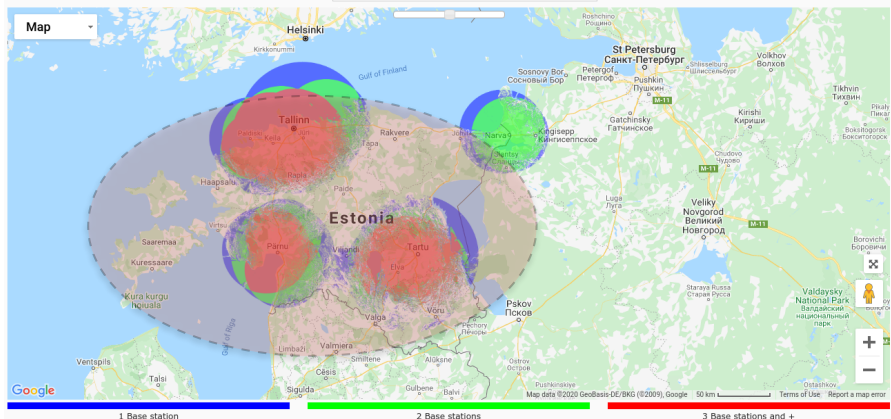
[14]https://www.levikom.ee/iot/

*Figure 13: Sigfox (red, blue, green smaller circles) and NB-IoT (large shaded ellipsoid) coverage in Estonia. Source [3]*

The NB-IoT DORM nodes [1] were deployed at various locations inside and outside the buildings of TalTech and Tartu University campuses as shown in Figure 14. These DORM nodes were programmed to transmit data packets every 30 minutes that included RSSI, RSRP, and RSRQ values. The transmitted data packets were received at the freely-available Ubidots[15] cloud platform for further analysis and investigation.

For the coverage analysis of Sigfox, the proprietary Sigfox Airwits[16] devices were used for collecting the Sigfox network information both in TalTech and Tartu University campuses. The Sigfox devices were programmed to transmit data every 30 minutes containing the RSSI values along with time stamps. The deployed Sigfox nodes could be seen as small boxes on top of the NB-IoT DORM nodes (bigger boxes) in Figure 14.



*(a) Outdoor*                    *(b) Indoor*                    *(c) Deep-Indoor*
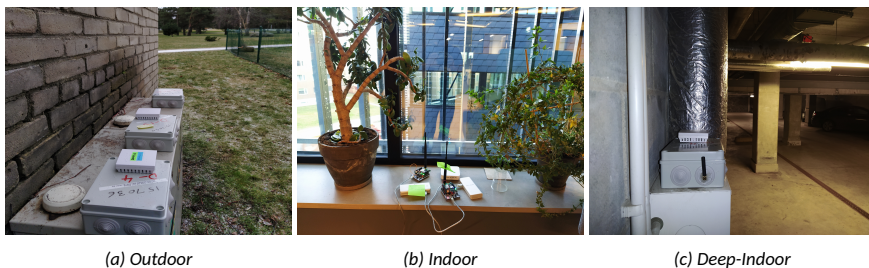
*Figure 14: Examples of deployment scenarios (a) outdoor, (b) indoor, and (c) deep-indoor. Source [3]*

### 3.4.2 Empirical coverage analysis of NB-IoT and Sigfox networks

The network coverage is affected by many factors such as path loss, fading, reflection, refraction, building structure, distance from the BS and Fresnel zone etc [118, 119].

The Sigfox network coverage was analysed based on the RSSI values only where the NB-IoT network coverage was analysed based on the values of RSSI, RSRP and RSRQ of

---

[15]https://ubidots.com/

[16]https://partners.sigfox.com/products/connected-airwits

the received radio signal. The corresponding RSSI reference values for Sigfox network are summarized in Table 2(b) where the corresponding RSSI values that differ for an NB-IoT network are detailed in Table 2(a). The obtained RSRP and RSRQ values for an NB-IoT network were further classified into four distinct link quality levels i.e., POOR, FAIR, GOOD and EXCELLENT as summarized in Table 3. Furthermore, the results have been categorised

| > -65 dBm | EXCELLENT |
|---|---|
| -65 to -75 dBm | GOOD |
| -75 to -85 dBm | FAIR |
| < -85 | POOR |

| > -122 dBm | EXCELLENT |
|---|---|
| -122 to -135 dBm | GOOD (with 3 BS) |
| -122 to -135 dBm | Average (with 2 BS) |
| < -135 dBm | POOR |

*(a) RSSI reference values for NB-IoT network[119, 120]*    *(b) RSSI reference values for Sigfox network[121]*

*Table 2: RSSI Reference values for NB-IoT and Sigfox networks*

| > 84 dBm | EXCELLENT |
|---|---|
| 85 to 102 dBm | GOOD |
| 103 to 111 dBm | FAIR |
| < -112 | POOR |

| >5 dB | EXCELLENT |
|---|---|
| -5 to -8 dB | GOOD |
| -8 to -11 dB | FAIR |
| < -11 dB | POOR |

*(a) RSRP*    *(b) RSRQ*

*Table 3: Reference values of NB-IoT as per 3GPP standards [119, 120]*

in three subsections based on three deployment scenarios i.e, outdoor, indoor and deep-indoor.

- Outdoor coverage analysis: Our coverage results obtained at the $University\ of\ Tartu$ indicate that NB-IoT $operator\ B$ offers slightly better outdoor coverage performance than NB-IoT $operator\ A$ with average RSSI values of -77 dBm at location A and -69 dBm at location B for $operator\ B$'s NB-IoT network, compared to average RSSI values of -90 dBm at location A and -87 dBm at location B for $operator\ A$'s NB-IoT network. For Sigfox network coverage, the average RSSI values were -114 dBm at location A and -103 dBm at location B, reflecting an excellent Sigfox coverage as per [121]. Across the $Taltech$ campus, NB-IoT $operator\ A$ offered better outdoor coverage performance with an average RSSI value of -64 dBm whereas NB-IoT $operator\ B$ had a fair network coverage with an average RSSI value of -87 dBm. The RSRP and RSRQ values revealed the same patterns with average RSRP values of -64 dBm for $operator\ A$'s NB-IoT network and -97 dBm for $operator\ B$'s NB-IoT network. The Sigfox network provided a good RSSI strength of -101 dBm reflecting excellent coverage as per Table 2. For more details on these measurements and their analysis, please refer to Figure 5, 6, 7 in [3].

- Indoor coverage analysis: In case of indoor environments at the $University\ of\ Tartu$, the average RSRP and RSRQ values for the NB-IoT network were -128 dBm and -14 dB, respectively, indicating a poor NB-IoT network coverage as per Table 3. However, interestingly, even with a weaker network coverage there were no packet losses, which reflects the strength of NB-IoT network in particular possibly thanks to the re-transmissions mechanism of NB-IoT (NB-IoT allows up to 128 re-transmissions in the uplink). Furthermore, fluctuations in the RSSI values for the NB-IoT network

were observed, this is possibly due to an increased human activity inside the buildings and also possibly their mobile usage. However, this pattern was not observed for the Sigfox network, indicating that Sigfox is unaffected by the LTE interferences [122]. For more details on these results, please refer to Figure 8, 9 in [3].

- Deep-indoor coverage analysis: It is interesting to note that the NB-IoT network from $operator\ A$ had a network outage in deep-indoor/underground environments at the $University\ of\ Tartu$ whereas the NB-IoT network from $operator\ B$ faced maximum packet losses of 61% at the same location. However, the Sigfox network showed only 9% packet losses at this location. Furthermore, no network outage or higher packet loss was observed for the NB-IoT network inside the $TalTech$ campus in deep-indoor/underground environments, indicating a good network connectivity for both $operator\ A$ and $operator\ B$ at the time of writing this thesis. For more details on these measurements and their analysis, please refer to Figure 10, 11 in [3].

# 4  An Empirical Baseline Energy Consumption Model for an NB-IoT Radio Transceiver

This chapter covers a thorough investigation of the energy consumption profiling of the Radio Resource Control (RRC) communication protocol between an NB-IoT radio transceiver and a cellular base-station (BS) at Tallinn University of Technology (TalTech) campus, Estonia. Based on the comprehensive analyses of the energy profile traces from the widely used BG96 radio operating in various states of RRC protocol, a baseline energy consump-tion model for an NB-IoT radio transceiver was proposed. our results indicate that the proposed model accurately depicts the baseline energy consumption of an NB-IoT radio transceiver while operating at different coverage class levels under real NB-IoT networks. The evaluation errors for our proposed model varied between 0.33% and 15.38%. This chapter is based on the following publication:

- Sikandar M. Zulqarnain Khan, Muhammad Mahtab Alam, Yannick Le Moullec, Alar Kuusik, Sven Pärand, and Christos Verikoukis. An empirical modeling for the baseline energy consumption of an nb-iot radio transceiver. *IEEE Internet of Things Journal*, 8(19):14756–14772, 2021, [4].

## 4.1  Overview of Radio Resource Control (RRC) Communication Protocol between an NB-IoT radio and a cellular Base-Station (BS)

The RRC is a communication protocol between an end device/UE and the base-station (also termed evolved Node-B (eNB)) through which network services such as connection establishment, connection maintenance, data exchange, sleep and notification patterns, security and Quality of Service (QoS), etc. take place. The RRC protocol model has only two complementary states , i.e. 1) RRC_Connected and 2) RRC_Idle, as shown in the RRC protocol reference model in Figure 15; the radio alternates between these two states during its operation.

As shown in Figure 15, the UE, on power up (or cold start), requests a network connection from the BS which upon acknowledgement is granted network resources and it thus enters into the RRC_Connected state. The connection establishment takes place in the "Attach" procedure and is always initiated by the UE. Once connected, the exchange of (uplink(Tx)/downlink(Rx)) data between the UE and the network takes place in the allocated transmission and reception slots that have been previously allocated to the UE during the "Attach" procedure. After a secure exchange of data, the UE listens to the broadcast information from the eNB for a certain period of time that is termed as "Active waiting" and whose period is set by the network operator. If any data arrives during this period, the RRC connection is resumed for the exchange of data between the UE and the network such that active waiting period restarts at the end of the data exchange. However, if no data arrives during active waiting, the eNB releases the connection and the UE switches to the RRC_Idle state, thereby saving all the context of the network in local memory.

Transiting into RRC_Idle state, the UE may enter either into eDRX or into PSM as per its configuration. The UE can also alternate between these two states, with eDRX first and PSM next, incase if both states are enabled. In the eDRX mode, the UE listens to the broadcast information from the eNB in cyclic patterns known as eDRX cycles; hence this phase is termed as eDRX mode. When the eDRX mode expires, or when it is forced to expire, the UE switches to the PSM mode during which it turns off its radio and is therefore not reachable by the network. This mechanism facilitates the device to enter deeper
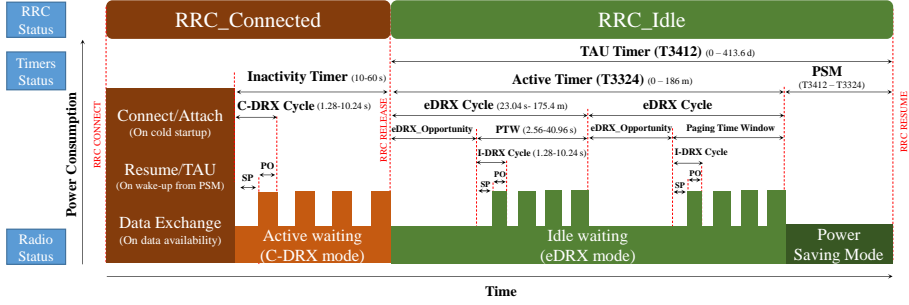
*Figure 15: RRC protocol reference model for the NB-IoT radio. It is composed of two complementary states , i.e. RRC_Connected and RRC_Idle and exploits Active waiting, Idle waiting and Power Saving Mode (PSM) after establishing a connection with the network. From top to bottom: (top) RRC connection status, (middle) timers with their minimum and maximum limits, and (bottom) radio status with associated power consumption, as depicted schematically.*

hardware sleep modes and thus contribute towards maximum power savings of the UE's battery, but at the cost of increased latency.

To summarize, the NB-IoT radio goes through the following states as it operates under the RRC protocol , i.e. (i) Attach – registration to the network on a cold start or power up, (ii) Data Exchange (Tx/Rx) – transmission and reception of data to/from the network, (iii) Active Waiting (C-DRX mode) - continuous listen to the broadcast information from the eNB for a period as permitted by the network operator and as configured by the UE, (iv) Idle Waiting (eDRX mode) – partly listens to the broadcast information from eNB for a period as permitted by the operator and as configured by the UE, (vi) Power Saving Mode (PSM) - shut-down of the radio activity for a period as requested by the UE and that as acknowledged by the network, and (viii) Tracking Area Update (TAU) - resuming the connection with eNB on wake up from PSM. All these radio states are shown in the RRC reference model in Figure 15.

## 4.2 Derivation of energy consumption model for an NB-IoT radio transceiver

The following pages present the NB-IoT radio transceiver energy consumption model that has been derived in this PhD thesis.

As depicted in the RRC protocol reference model in Figure 15, it has only two states, i.e., 1) RRC_Connected and 2) RRC_Idle. Thus the total energy consumed by an NB-IoT radio while communicating with the BS through an RRC protocol can be given as:

$$E_{TOTAL} = E_{RRC\_CONNECTED} + E_{RRC\_IDLE} \tag{1}$$

In the RRC_Connected state, the radio goes through the four following states, i.e. Attach, Data Exchange (Tx/Rx), Active waiting (C-DRX) and TAU. The Attach procedure occurs only after a cold start whereas the TAU procedure occurs each time the radio wakes up from PSM. Exchange of data between the radio and the BS takes place during the (Tx/Rx) state and its duration depends on the amount of data that is to be exchanged between the radio and the BS. After data exchange, the radio enters into an Active waiting state, also called the C-DRX mode where its duration is defined by the Inactivity Timer as set by the operator. Thus, the total energy consumed during the RRC_Connected state can be

written as:

$$E_{RRC\_CONNECTED} = E_{ATTACH} + E_{Tx/Rx}$$
$$+ E_{C-DRX} + E_{TAU} \qquad (2)$$

As the Inactivity Timer (C-DRX mode) finishes, the RRC connection is released and the radio goes into the RRC_Idle state where the radio first enters into Idle waiting state or eDRX mode, followed by PSM. Thus, the total energy consumed during the RRC_Idle state can be written as:

$$E_{RRC\_IDLE} = E_{eDRX} + E_{PSM} \qquad (3)$$

Since $Energy = Power \times Time$, the average energy consumption during the RRC_Connected state can be written as:

$$E_{RRC\_CONNECTED} =$$
$$\left\{ P_{ATTACH(avg)} \times T_{ATTACH} \right\} + \left\{ (P_{Tx(avg)} \times T_{Tx}) \right.$$
$$\left. + (P_{Rx(avg)} \times T_{Rx}) \right\} + \left\{ P_{C-DRX(avg)} \right.$$
$$\left. \times T_{InactivityTimer} \right\} + \left\{ P_{TAU(avg)} \times T_{TAU} \right\} \qquad (4)$$

Since the $ActiveWaiting$ (C-DRX mode) period is a series of repeated C-DRX cycles, the above equation can be re-written as:

$$E_{RRC\_CONNECTED} = \left\{ P_{ATTACH(avg)} \times T_{ATTACH} \right\} +$$
$$\left\{ (P_{Tx(avg)} \times T_{Tx}) + (P_{Rx(avg)} \times T_{Rx}) \right\} + \left\{ P_{C-DRX(avg)} \right.$$
$$\left. \times (T_{CDRX\_Cycle} \times N_{CDRX\_Cycles}) \right\} + \left\{ P_{TAU(avg)} \times T_{TAU} \right\} \qquad (5)$$

where $T_{CDRX\_Cycle}$ is the time period of each C-DRX cycle, and $N_{CDRX\_Cycle}$ is the total number of C-DRX cycles that occur during the $ActiveWaiting$ period.

Similarly, the average energy consumption of the radio during the RRC_Idle state is:

$$E_{RRC\_IDLE} = E_{eDRX} + E_{PSM} \qquad (6)$$

and can be re-written as:

$$E_{RRC\_IDLE} =$$
$$\left\{ P_{eDRX(avg)} \times T_{eDRX} \right\} + \left\{ (P_{PSM(avg)} \times T_{PSM} \right\} \qquad (7)$$

The duration of the entire Idle state of the radio, and its eDRX and PSM durations, can be set by the values of 3GPP specified timers, such that:

$$T_{RRC\_IDLE} = T_{3412} \qquad (8)$$

$$T_{eDRX} = T_{3324} \qquad (9)$$

$$T_{PSM} = T_{3412} - T_{3324} \qquad (10)$$

Thus, the average energy consumption of the radio during the RRC_Idle state can be re-written as:

$$E_{RRC\_IDLE} = \left\{ P_{eDRX(avg)} \times T_{3324} \right\}$$
$$+ \left\{ P_{PSM(avg)} \times (T_{3412} - T_{3324}) \right\} \qquad (11)$$

Since, the *eDRX* mode is composed of repeated *eDRX* cycles, thus:

$$E_{RRC\_IDLE} = \{P_{eDRX(avg)} \times (T_{eDRX\_Cycle} \times N_{eDRX\_Cycles})\}$$
$$+ \{(P_{PSM(avg)} \times (T_{3412} - T_{3324}))\} \tag{12}$$

where $T_{eDRX\_Cycle}$ is the time period of each eDRX cycle and $N_{eDRX\_Cycles}$ is the total number of eDRX cycles that occur during the *IdleWaiting* period.

Since each *eDRX cycle* is composed of a *PTW* (active phase of an *eDRX cycle*) and *eDRX_opportunity* (inactive phase of an *eDRX cycle*), the above equation can be expanded to:

$$E_{RRC\_IDLE} = \{P_{eDRX(avg)} \times (T_{eDRX\_PTW} +$$
$$T_{eDRX\_OPP}) \times N_{eDRX\_Cycles}\} + \{(P_{PSM(avg)} \times$$
$$(T_{3412} - T_{3324})\} \tag{13}$$

Moreover, since the power consumption of *PTW* and *eDRX_opportunity* during each *eDRX cycle* is different, the above equation can be written as:

$$E_{RRC\_IDLE} = \{(P_{eDRX\_PTW(avg)} \times T_{eDRX\_PTW})$$
$$+ (P_{eDRX\_OPP(avg)} T_{eDRX\_OPP}) \times N_{eDRX\_Cycles}\}$$
$$+ \{(P_{PSM(avg)} \times (T_{3412} - T_{3324}))\} \tag{14}$$

As *PTW* is a repeated sequence of $I-DRX$ cycles, the above becomes:

$$E_{RRC\_IDLE} = \{(P_{eDRX\_PTW(avg)} \times (T_{I-DRX\_Cycle}$$
$$\times N_{I-DRX\_Cycles})$$
$$+ (P_{eDRX\_OPP(avg)} T_{eDRX\_OPP})$$
$$\times N_{eDRX\_Cycles}\}$$
$$+ \{(P_{PSM(avg)} \times (T_{3412} - T_{3324}))\} \tag{15}$$

where $T_{I-DRX\_Cycle}$ is the time period of each $I-DRX$ cycle and $N_{I-DRX\_Cycles}$ is the total number of $I-DRX$ cycles occurring during the *PTW* of each *eDRX cycle*.

Next, since each $I-DRX$ cycle has an on phase (i.e. PO) during which the NPDSCCH signal is monitored and an off phase with no activity, the above equation can be expanded to:

$$E_{RRC\_IDLE} = \{(P_{I-DRX\_on(avg)} \times T_{I-DRX\_on}) +$$
$$(P_{I-DRX\_off(avg)} \times T_{I-DRX\_off}) \times N_{I-DRX\_Cycles})$$
$$+ (P_{eDRX\_OPP(avg)} \times T_{eDRX\_OPP}) \times N_{eDRX\_Cycles}\}$$
$$+ \{(P_{PSM(avg)} \times (T_{3412} - T_{3324}))\} \tag{16}$$

Finally, given that

$$E_{TOTAL} = E_{RRC\_CONNECTED} + E_{RRC\_RELEASED} \tag{17}$$

we obtain:

$$E_{TOTAL} = \left\{ \left\{ P_{ATTACH(avg)} \times T_{ATTACH} \right\} + \left\{ (P_{Tx(avg)} \times T_{Tx}) \right. \right.$$
$$+ (P_{Rx(avg)} \times T_{Rx}) \right\} + \left\{ P_{C-DRX(avg)} \times (T_{CDRX\_Cycle} \right.$$
$$\times N_{CDRX\_Cycles}) \right\} + \left\{ P_{TAU(avg)} \times T_{TAU} \right\} \right\} +$$
$$\left\{ \left\{ \left\{ (P_{I-DRX_{on(avg)}} \times T_{I-DRX_{on}}) + (P_{I-DRX_{off(avg)}} T_{I-DRX_{off}}) \right. \right. \right.$$
$$\times N_{I-DRX\_Cycles} \right\} + \left\{ (P_{eDRX\_OPP(avg)} \times T_{eDRX\_OPP}) \right\}$$
$$\times N_{eDRX\_Cycles} \right\} + \left\{ P_{PSM(avg)} \times (T_{3412} - T_{3324}) \right\} \right\} \tag{18}$$

For simplicity, the above equation can be rearranged in terms of the 3GPP specified timers such that each row in the following equation represents the energy consumption of each separate state of the radio, i.e. Attach, Data Exchange (Transmit (Tx) and Receive (Rx)) , Active waiting (C-DRX mode), Idle waiting (eDRX mode), deep sleep mode (PSM) and Resume (TAU), i.e.

$$E_{TOTAL} =$$
$$\begin{pmatrix} \left\{ P_{ATTACH(avg)} \times T_{ATTACH} \right\} + \\ \left\{ (P_{Tx(avg)} \times T_{Tx}) + (P_{Rx(avg)} \times T_{Rx}) \right\} + \\ \left\{ P_{C-DRX(avg)} \times (T_{InactivityTimer}) \right\} + \\ \left\{ P_{TAU(avg)} \times T_{TAU} \right\} \end{pmatrix}$$
$$+ \begin{pmatrix} \left\{ (P_{eDRX(avg)} \times T_{3324}) \right\} + \\ \left\{ P_{PSM(avg)} \times (T_{3412} - T_{3324}) \right\} \end{pmatrix} \tag{19}$$

This section has presented the proposed NB-IoT UE energy consumption model. The next sections detail the corresponding results and corresponding evaluations.

## 4.3 Preparing the testbed for measuring the power consumption of an NB-IoT radio transceiver while communicating with the BS through an RRC protocol

Two CoTS NB-IoT radio modules, i.e. Avnet Silica NB-IoT shield[17] and Quectel UMTS LTE EVB Kit[18] that are based on 3GPP Rel-13 compliant Quectel BG96 LPWAN chipset[19] are used for analysing the power consumption measurements operating through an RRC communication protocol with the BS and connected to the two publicly available NB-IoT test networks in Tallinn. These NB-IoT test networks are operated by the two famous Mobile Network Operatros (MNOs) in Estonia and are referred to as Operator 1 and Operator 2 in this thesis. A Keysight Technologies N6705C DC Power Analyzer[20] (PA) is used for collecting the power traces during these measurement campaigns. The test-bed setup that is composed of an Avnet BG96 shield as our DUT1 and Quectel EVB Kit as our DUT2, along with

---

[17] https://www.avnet.com/wps/portal/silica/products/new-products/npi/2018/avnet-nb-iot-shield-sensor/

[18] https://www.quectel.com/product/umts-lte-evb-kit

[19] https://www.quectel.com/product/lpwa-bg96-cat-m1-nb1-egprs

[20] https://www.keysight.com/zz/en/product/N6705C/dc-power-analyzer-modular-600-w-4-slots.html
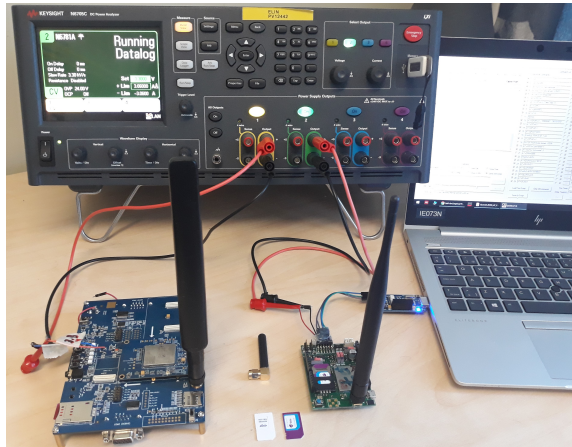
*Figure 16: Testbed Setup with Quectel BG96 and Avnet Silica BG96 NB-IoT radio modules, Keysight N6705C DC Power Analyzer, and SIM cards from Operator 1 and Operator 2.*

the Keysight's PA is shown in Figure 16. A constant voltage of 3.3 V is supplied to DUT1 and a constant voltage of 3.8 V is applied to DUT2 from the PA. SIM cards for both the networks under test are also visible in our setup, as shown in Figure 16. The required AT commands as needed for configuring the BG96 chipset are sent from the QCOM software running on the PC through the USB-PMOD interface for DUT1 and through the USB interface for DUT2. Necessary modifications were made to both of the DUTs to make precise power consumption measurements from the PA and this include flashing the chipsets of both the DUTs with the latest firmware, disabling all the functional LEDs as per the schematics[21] and developing proper interfaces for these boards so that the power from the PA does no get disrupted from the attached PC that is required to send the associated AT commands for configuring these DUTs accordingly.

The details of the two MNOs' NB-IoT test networks that have been considered for carrying out these experiments are summarized in Table 4. For the measurement campaign, the NB-IoT devices (DUT1 and DUT2) were placed at different locations inside Thomas Johann Seebeck Department of Electronics building and students' dormitory building that are located on TalTech campus. For triggering the different coverage levels, the devices were deployed on the second basement (B2) floor of Thomas Johann Seebeck Department of Electronics building where the received signal strength is lower than on the upper floors. On each test location, the current value of the CE level was queried using the adequate AT commands and when the required CE levels were achieved, i.e. CE Level 0 and CE Level 1, the measurements were made accordingly. Small differences between the two operators in terms of their SNR, SINR, RSSI, RSRP, and RSRQ for the same CE levels could be observed from their respective values as given in Table I. However, to smooth out the minor variations of the individual results for SNR, SINR, RSSI, RSRP, and RSRQ; their experiments were repeated in the order of 100 times on each test location and the obtained results were averaged into their final values, under their respective CE levels, as summarized in Table 4. Table 5 summarizes the network parameters that are operator specific and/or UE configurable with a short description of their control and possible values.

During our measurement campaign, the NB-IoT devices were placed at different lo-

---

[21]https://github.com/Avnet-Silica-team/NBIoTBG96-HW/blob/master/ BAENBIOTBG96SHIELD_RSR1157C-SCHEMA.pdf/

Table 4: Details of the publicly available NB-IoT networks that have been used during our measurement campaigns on test location

| Details | Operator 1 | Operator 2 |
|---|---|---|
| Operator numeric code | 24801 | 24802 |
| Selected Access Technology | CAT-NB1 | CAT-NB1 |
| Selected Band | LTE BAND 20 | LTE BAND 20 |
| Selected Channel ID | 6254 | 6152 |
| CE level (at test locations) | 0 , 1 | 0 , 1 |
| SNR {0(bad) to 31(good)}(dB) | 28 , 6  (avg) | 21 , 5  (avg) |
| SINR{0(bad) to 250 (good)}(dB) | 185, 178 (avg) | 153, 142 (avg) |
| RSSI{-110(bad) to -60(good)}(dBm) | -67, -101 (avg) | -72, -110 (avg) |
| RSRP{-140(bad) to -44(good)}(dBm) | -67, -111 (avg) | -74, -117 (avg) |
| RSRQ{-19.5(bad) to -3(good)}(dB) | -3 , -9  (avg) | -3 , -10  (avg) |

Table 5: Operator specific and UE configurable parameters

| Network Params | Symbol | Value |
|---|---|---|
| Attach | T_ATTACH | Network_conditions |
| Inactivity Timer | InactivityTimer | Operator_defined |
| C-DRX Cycle | CDRX_Cycle | Operator_defined |
| RRC_Idle | RRC_Idle | UE defined = T3412 Timer value |
| Active Timer | T3324 Timer | UE defined = T3324 Timer value |
| eDRX Cycle | eDRX_Cycle | Network defined; UE configurable |
| PagingTimeWindow | PTW | Network defined; UE configurable |
| eDRX_Opportuity | eDRX_Opp | (eDRX_Cycle - PTW) |
| I-DRX Cycle | I-DRX_Cyc | Operator_defined |
| PowerSavingMode | PSM | UE defined = (T3412-T3324) value |

cations inside Thomas Johann Seebeck Department of Electronics building and students' dormitory building that are located on TalTech campus. For triggering the different coverage levels, the devices were deployed on the second basement (B2) floor of Thomas Johann Seebeck Department of Electronics building where the received signal strength is lower than on the upper floors. On each test location, the current value of the CE level was queried using the adequate AT commands and when the required CE levels were achieved, i.e. CE Level 0 and CE Level 1, the measurements were made accordingly. Small differences between the two operators in terms of their SNR, SINR, RSSI, RSRP, and RSRQ for the same CE levels could be observed from their respective values as given in Table 4. However, to smooth out the minor variations of the individual results for SNR, SINR, RSSI, RSRP, and RSRQ; their experiments were repeated in the order of 100 times on each test location and the obtained results were averaged into their final values, under their respective CE levels, as summarized in Table 4. Table 5 summarizes the network parameters that are operator specific and/or UE configurable with a short description of their control and possible values.

## 4.4 Obtained empirical results for the power consumption measurements of an NB-IoT radio transceiver under real network

Various timings for the different states of the NB-IoT radio were tried and tested for different power saving schemes. These measurements were recorded as data log files and are displayed in the Marker view of PA for the rest of this thesis. For all the power measurements and energy calculations for rest of the waveforms/traces in this thesis, the average power consumption and average timings between the m1 and m2 markers were taken into account. These markers are set to various positions on the respective power traces of the BG96 radio transceiver, so as to obtain the adequate power consumption and timings details for the various states of its RRC operation.

### 4.4.1 Testing the power cycle (a repeated sequence of C-DRX, eDRX, and PSM) of the Avnet BG96 radio under Operator1 network

In these set of experiments, we evaluated the fine-grain energy consumption of the BG96 radio in a power cycle consisting of C-DRX mode, eDRX-Mode, and PSM with the T3324 timer set to 4 min and T3412 timer set to 1 h; the results are shown in Figure 17. Furthermore, it was observed that the radio automatically woke up from its PSM to re-attach with the network and repeat its power cycle with its previous settings. The power traces for the C-DRX, eDRX and PSM states during these experiments are shown in Figures 17a, 17b, and 17c, respectively.

To observe the power consumption of BG96 radio in different coverage class levels (CEL), a 10 bytes of data was transmitted from the BG96 radio on Operator1 network using UDP protocol at CEL0 and CEL1 as shown in Figure 18a, 18b. It was observed that the radio consumed 0.000372 Wh to transmit data at CEL = 0 whereas it consumed 0.000816 Wh to transmit the same data at CEL = 1, i.e. an increase of 124.09%.
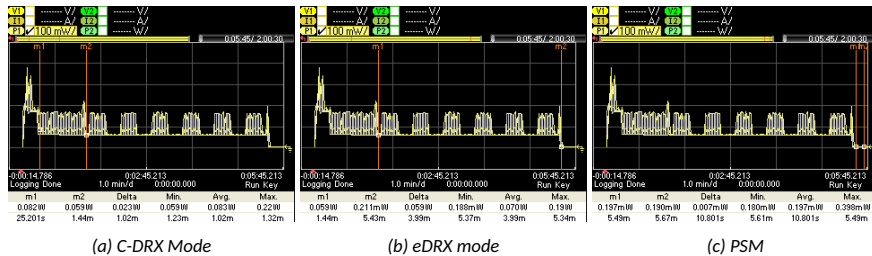


(a) C-DRX Mode  (b) eDRX mode  (c) PSM

Figure 17: Power cycle with BG96/Avnet shield under Operator1 network: (a) C-DRX mode runs for 1.0 min (UE configured), (b) eDRX mode runs for 4 min (UE-configured), and (c) PSM runs for 60 min (UE-configured), not shown in full for readability.

### 4.4.2 Testing the power cycle (a repeated sequence of C-DRX, eDRX, and PSM) of the Avnet BG96 radio under Operator2 network

All the above experiments were repeated with the Avnet BG96 shield under similar conditions but this time with Operator 2's network. The obtained results from these tests are summarized in Figure 19. During these tests, it was observed that Operator 2's network had more restrictions on their network parameters as compared to Operator 1, i.e. the UE/radio had little provisions to configure the network parameters. For example, the C-DRX mode was fixed to 34 s (during all our tests) whereas the eDRX mode and PSM could

<div align="center">

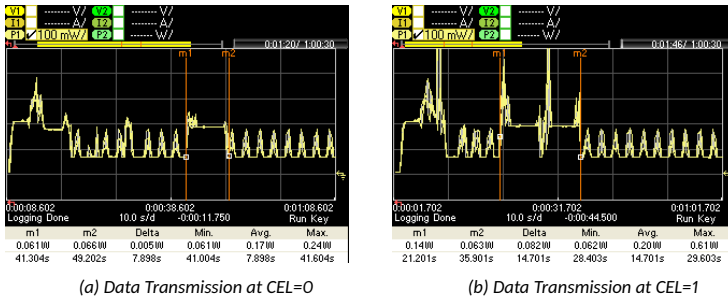| (a) Data Transmission at CEL=0 | (b) Data Transmission at CEL=1 |
|---|---|

</div>

*Figure 18: Transmitting 10 bytes of data using UDP protocol on Operator1 network. (a) Data Transmission at CEL=0 consumes 0.17 W for 7.898 s (0.000372 Wh), (b) Data Transmission at CEL=1 consumes 0.20 W for 14.701 s (0.000816 Wh), i.e. an increase of 119.35%.*



<div align="center">

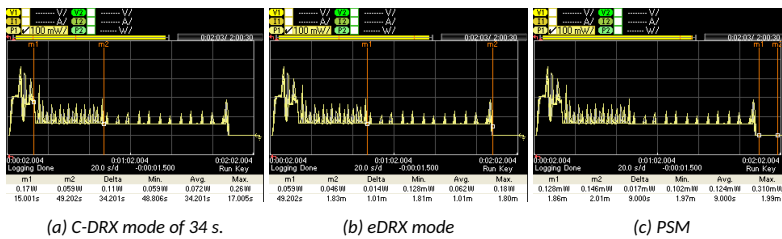| (a) C-DRX mode of 34 s. | (b) eDRX mode | (c) PSM |
|---|---|---|

</div>

*Figure 19: Power cycle of the Avnet BG96 shield under Operator2 network: (a) C-DRX mode runs for 34.2 s, (b) eDRX mode runs for 1.0 min (UE configured), and (c) PSM runs for 1.0 h (UE configured), not shown in full for readability.*



<div align="center">

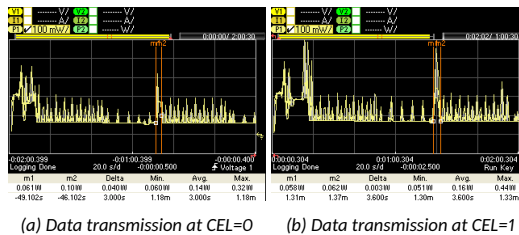| (a) Data transmission at CEL=0 | (b) Data transmission at CEL=1 |
|---|---|

</div>

*Figure 20: Transmitting 10 byte of data using UDP protocol on Operator2 network. (a) Data Transmission at CEL=0 consumes 0.14 W for 3 s (0.00011 Wh), (b) Data Transmission at CEL=1 consumes 0.16 W for 3.6 s (0.00016 Wh), i.e. an increase of 45.45%.*

be configured by the UE as desired. However, the eDRX cycle and its underneath PTW in the C-DRX mode could not be configured (contrary to the case with Operator 1). It was also noted that the radio took 12.6 s on average to get connected to Operator 2's network, as compared to an average of 18 s on Operator 1's network.

### 4.4.3 Verifying our results for Operator1 and Operator2 networks with Quectel BG96 EVB Kit

All the above experiments were repeated for both the operators on the same location and under similar conditions using the Quectel BG96 EVB kit. Since similar power graphs for C-DRX, eDRX, and PSM modes of the BG96 radio were obtained from the PA, these graphs

are not included in the paper for conciseness. A side-by-side comparison of the current and power consumption of the two boards i.e., Avnet BG96 shield and Quectel BG96 EVB kit , for both the networks i.e, Operator 1 and Operator 2, are summarized in Tables 6 and Tables 7.

Table 6: Side by side comparison of the average power measurements of Avnet BG96 shield and Quectel BG96 EVB Kit under Operator1 and Operator2 networks

| Power Consumption of the Avnet BG96 shield and Quectel BG96 EVB Kit | | | | |
|---|---|---|---|---|
| Avnet \ Quectel | Attach (mW) | CDRX (mW) | eDRX (mW) | PSM (mW) |
| Operator 1 | 200 / 180.0 | 100 / 82.0 | 77.0 / 71.0 | 0.20 / 0.19 |
| Operator 2 | 190 / 190.0 | 86.0 / 72.0 | 63.0 / 63.0 | 0.19 / 0.12 |

Table 7: Side by side comparison of the average current measurements of Avnet BG96 shield and Quectel BG96 EVB Kit under Operator1 and Operator2 networks

| Current consumption of the Avnet BG96 shield and Quectel BG96 EVB Kit | | | | |
|---|---|---|---|---|
| Avnet \ Quectel | Attach (mA) | CDRX (mA) | eDRX (mA) | PSM (mA) |
| Operator 1 | 51.8 / 56.8 | 26.1 / 25.1 | 20.22 / 21.8 | 0.05 / 0.05 |
| Operator 2 | 59.3 / 40.1 | 25.3 / 21.3 | 19.2 / 19.2 | 0.05 / 0.03 |

## 4.5  Evaluation of the proposed NB-IoT radio energy consumption model

Three sets of experiments were conducted where the base cycle lasted from 12.3 min to 1.2 h and was repeated 2 to 10 times during the observation window. Doing so forces the NB-IoT radio in various operational conditions and allows characterizing the average differences between the energy consumption predicted by the model and the real-life values.

The first evaluation test was executed with an Avnet BG96 shield board operating on Operator1 network. The test consisted of a base power cycle of 30 min as captured between m1 and m2 (29.55 min shown) in Figure 21a and repeated twice in an observation window of 1 h (59.53 min shown) between m1 and m2, as shown in Figure 21b. As can be seen in Figure 21a, the base power cycle includes an attach procedure of 18 s, and C-DRX, e-DRX and PSM states of a bit less than 10 min each where the average power consumption for the base power cycle is 0.052 W. And as can be seen in Figure 21b, it is repeated twice over a period of 60 min captured between m1 and m2 (59.53 min shown) where the average power consumption is found to be 0.052 W. The energy consumed per each power cycle as per the NB-IoT UE energy consumption model of Equation (19) derived in Section 4.2 is 0.022 Wh, whereas that measured with the PA is 0.026 Wh. The energy consumed for the entire observation window as per Equation (19) derived in Section 4.2 is 0.044 Wh, whereas that measured with the PA is 0.052 Wh, i.e. an error of 15.38%, as indicated in Table 8.
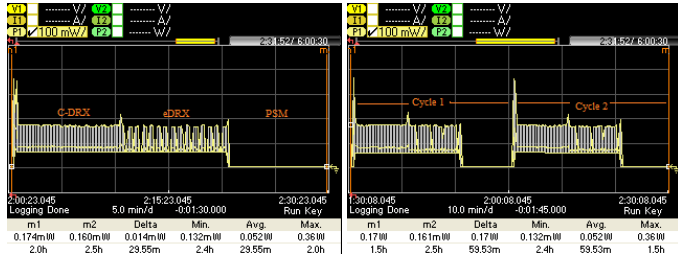
(a) A power cycle of 30 min ("29.55m" displayed between m1 and m2 markers) that includes an Attach procedure of 18 s, C-DRX, e-DRX and PSM of a bit less than 10 min each.

(b) The power cycle of (a) is repeated for 2 times in an observation window of 60 min ("59.53m" displayed between m1 and m2 markers).

Figure 21: Power traces of the first evaluation test with the Avnet BG96 shield operating on Operator1 network.
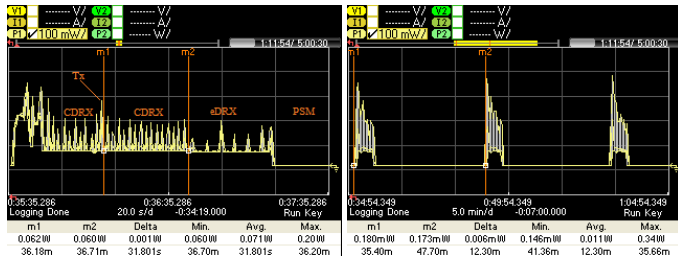


(a) A power cycle of 12.3 min that includes an Attach procedure of 12.1 s, C-DRX mode of 20 s, Tx (10 bytes data over UDP) of 3 s, repeated C-DRX of 32 s ("31.801s" displayed between m1 and m2 markers), eDRX of 34 s and PSM of a bit more than 10 min (not shown in full for readability).

(b) The power cycle of (a) 12.3 min ("12.30m" displayed between m1 and m2 markers) is repeated 3 times (The last PSM phase is not shown in full for readability)).

Figure 22: Power traces of the second evaluation test with Avnet BG96 shield on Operator2 network
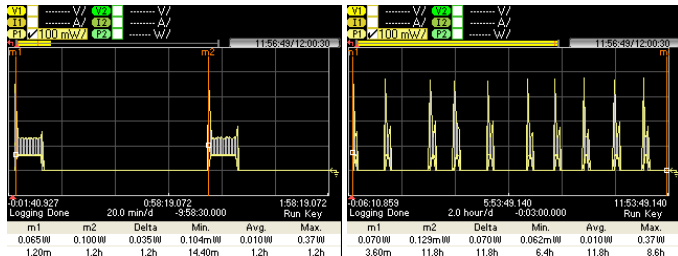


(a) A power cycle of 1.2 h ("1.2h" between m1 and m2 markers) including an Attach procedure of 12.1 s, C-DRX of 32 s, e-DRX of 10 min and PSM of 64 min.

(b) The power cycle of (a) is repeated 10 times in an observation window of 11.8 h ("11.8h" between m1 and m2 markers). (Note that some of the PSM durations are shorter than others).

Figure 23: Power traces of the third evaluation test with Avnet BG96 shield under Operator2 network.

48

*Table 8: NB-IoT radio energy consumption error: proposed model (Equation (19) derived in Section 4.2) vs. real-life evaluation tests*

| Test setup | Energy as per model (Eq. (19)) | Energy as per PA | Error |
|---|---|---|---|
| Avnet BG96 shield, Operator1 | 0.052 Wh | 0.044 Wh | 15.38% |
| Avnet BG96 shield, Operator2 | 0.0024 Wh | 0.0022 Wh | 9.09% |
| Avnet BG96 shield, Operator2 | 0.01204 Wh | 0.01200 Wh | 0.33% |

The second evaluation test was also conducted with an Avnet BG96 shield, but this time operating on Operator2 network. The test consisted of the base power cycle shown in Figure 22a (m1 and m2 in this figure are used to record the repeated C-DRX cycle of the radio after a data transmission (Tx)); this power cycle is repeated 3 times as shown in Figure 22b. The base power cycle lasts 12.3 min and includes an Attach procedure of 12.1 s, C-DRX mode of 20 s, Tx through UDP protocol of 3 s, repeated C-DRX of 32 s, eDRX of 34 s, and PSM of a bit more than 10 m. The base power cycle consumes on average 0.011 W during the 12.3 min duration, i.e. an average energy consumption of 0.0022 Wh. As indicated in Table 8, the energy consumed per power cycle as per Equation (19) derived in Section 4.2 is 0.0024 Wh, i.e. an error of 9.09%.

Like the second one, the third evaluation test was conducted with the Avnet BG96 shield operating under Operator2 network, but this time for a longer duration. The base cycle lasts 1.2 h including an Attach procedure of 12 s, CDRX of 32 s, e-DRX of 10 min and PSM of 64 min, as shown in Figure 23a. This power cycle of 1.2 h has an average power consumption of 0.010 W. It is then repeated 10 times in an observation window of 11.8 h, as shown in Figure 23b (note that some of the PSM durations are shorter than others). In this case, the energy consumed per power cycle measured with the PA is 0.01200 Wh, whereas as per Equation (19) derived in Section 4.2 it is found to be 0.01204 Wh, i.e. an error of 0.33% only, as indicated in Table 8.

The error of the proposed model ranges from as low as 0.33% for longer durations (e.g. when the radio has to activate after several hours or more), and reaches up to approximately 15.38% for shorter durations (e.g. when the radio has to activate after several minutes to hours). Since the majority of NB-IoT applications are intended for longer duration scenarios, the error will lie on the smaller end; as also indicated by the sensitivity analysis of the model.

## 4.6  Sensitivity Analysis of the proposed NB-IoT energy consumption model

The sensitivity analysis (SA) was carried out on both the power consumption parameters and timings parameters of the proposed model. The SA of the power consumption parameters i.e., $P_{ATTACH}$, $P_{TX}$, $P_{RX}$, $P_{CDRX}$, $P_{eDRX}$, $P_{PSM}$, and $P_{TAU}$ of our proposed model indicates that they are technology-dependent and may vary for various chipsets. For example, typical values for the power consumption parameters of the BC95 chipset (an advanced IoT chipset from Quectel) are slightly lower than those for the BG96 chipset from the same vendor. Similarly, the values for these power parameters may also differ slightly from ven-

dor to vendor. That is why these power parameters affect the overall energy consumption of the radio but only to a smaller extent. And since we have used BG96 chipset based modules for all our experiments in this work, we thus decided to use the values for the power consumption parameters of BG96 chipset; with a possible impact on the overall energy consumption of the radio in a descending order as shown in table 9.

Table 9: Sensitivity Analysis of the power consumption parameters of BG96 radio

| BG96 Power Parameters | | | | | | |
|---|---|---|---|---|---|---|
| $P_{TAU}$ | $P_{ATTACH}$ | $P_{TX}$ | $P_{RX}$ | $P_{CDRX}$ | $P_{eDRX}$ | $P_{PSM}$ |
| 0.18W | 0.18W | 0.17W | 0.16W | 0.083W | 0.070W | 0.0002W |

On the other hand, the timing parameters of the proposed model i.e., $T_{ATTACH}$, $T_{TX}$, $T_{RX}$, $T_{CDRX}$, $T_{eDRX}$, $T_{PSM}$, and $T_{TAU}$ have their minimum and maximum values are given in Table 10 (as standardized by 3GPP).

Table 10: Sensitivity Analysis of the timings parameters of NB-IoT radio

| Minimum and Maximum values for the Timing Parameters | | | | |
|---|---|---|---|---|
| $T_{TAU}/T_{ATTACH}$ | $T_{TX}/T_{RX}$ | $T_{CDRX}$ | $T_{eDRX}$ | $T_{PSM}$ |
| 18.6s - # of attempts | 0s–# of transmissions | 10s–60s | 0s–186m | 0s–413d |

The sensitivity analysis of these timing parameters indicate that they have an impact on the total energy consumption of the radio, in a descending order, as explained below:

- First, $T_{ATTACH}$ has the most impact on the overall energy consumption of the radio, especially when the radio wakes-up frequently (e.g. in patterns of a few minutes). However, in less frequent scenarios (e.g. once per day or weeks); its impact is negligible. Furthermore, the TAU procedure has almost the same effect as that of the ATTACH procedure (especially from the practical perspective).

- Secondly, the active waiting period i.e., $T_{CDRX}$ and the idle waiting period i.e., $T_{eDRX}$ have almost an equal impact on the total energy consumption of the radio. However, since the Inactivity timer is limited by the operator (usually set to lower than 60 s), its impact on the total energy consumption is lower as compared to $T_{CDRX}$ of relatively longer durations.

- Similarly, the impact of the payload size both in ($T_{TX}$, $T_{RX}$) is not significant on the total energy consumption of the radio while the radio is operating in good coverage. However, as the coverage worsens, its impact adds up as a function of the number of repetitions that an NB-IoT radio has to perform in that coverage level.

- Finally, the effect of PSM and its benefits in terms of the total energy consumption of the radio becomes substantial only when enabled for longer durations.

# 5  Edge-of-Things based Visual NB-IoT Framework

This chapter covers a thorough investigation of an NB-IoT based Edge-of-Things Framework that runs ML algorithms on the edge to curb the unnecessary data from being transmitted over the NB-IoT network. This significantly reduces the burden of an NB-IoT radio which in-turn reduces its energy consumption, minimizes the transmission time of the data and relaxes the channel occupancy from the network perspective. Our on-field experimental results indicate up to 93% reductions in the number of NB-IoT radio transmissions, up to 90.5% reductions in the NB-IoT radio energy consumption and up to 90% reductions in the data transmission time. This chapter is based on the following publication:

- Sikandar Zulqarnain Khan, Yannick Le Moullec, and Muhammad Mahtab Alam. An NB-IoT-Based Edge-of-Things Framework for Energy-Efficient Image Transfer. *MDPI Sensors*, 17(21):5929–5949, 2021, [5].

## 5.1  Hardware Architecture of our proposed Visual NB-IoT Framework

The "TalTech Edge-of-Things based Visual NB-IoT Framework" is shown in Figure 24. It is composed of the following nodes operating at its three hierarchical layers :

4.1.1 - Detection and Vision Node (DVN) at the Perception Layer,
4.1.2 - Smart Transmit Node (STN) at the Gateway Layer,
4.1.3 - Server node (SN) at the Cloud Layer.

The Detection and Vision Nodes (DVNs) are deployed at the perception layer to collect images of their surroundings. These images are transmitted to the Smart Transmit Node (STN) at the gateway layer, The STN processes the collected visual data from DVNs to offload the unnecessary data from being transmitted over the air. An application running over the Server Node (SN) at the cloud layer utilizes these images as required. The application, used as an example, monitors a parking lot in terms of authorized vehicles. The collected images at the entrance of the parking lot contain detailed information of the entering vehicles such as their type, color and more specifically their license plate numbers. These images are compared against a database of authorized vehicles such that when an unknown vehicle is detected, the security services are notified with the visual description of the front of the vehicle. However, there could be a number of use-cases where image transmission would be required by applications such as [123], [124], and [103], etc.
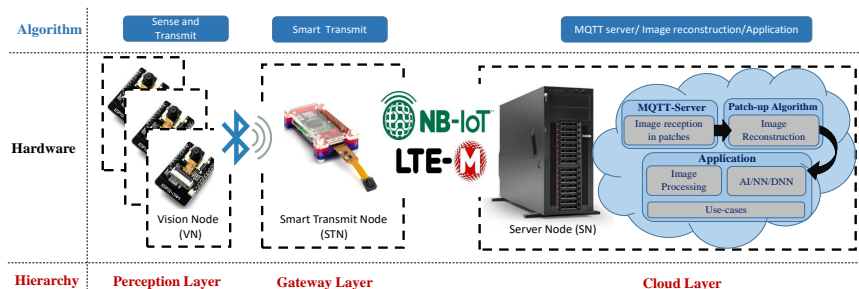


*Figure 24: Proposed three-layers hierarchical model for energy-efficient image transfer via NB-IoT*

### 5.1.1 Detection and Vision Node (DVN) at Perception Layer

An ESP32-CAM module[22] is integrated with an HC-SR501 Passive Infra Red (PIR) sensor[23] into a Detection and Vision Node (DVN) as shown in Figure 25a. This DVN is mounted over the automatic gate barrier of Tallinn University of Technology (TalTech)'s main entrance as shown in Figure 25b. As any vehicle enters into DVN's sensitivity field, the PIR sensor detects its presence and wakes up the ESP-32 CAM module from its deep sleep mode. The ESP32-CAM module captures an image of the entering vehicle and sends it to the STN (gateway) through its Bluetooth connectivity. As the image transmission ends, the DVN enters into its deep sleep mode once again.
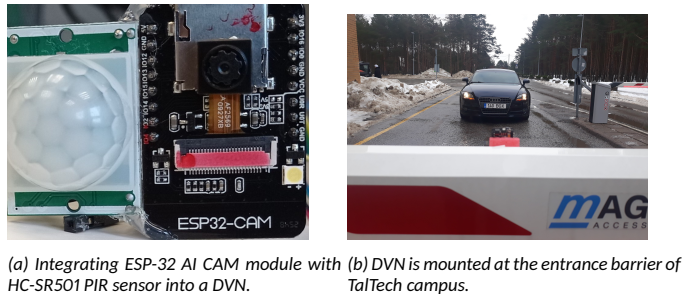


(a) Integrating ESP-32 AI CAM module with HC-SR501 PIR sensor into a DVN.    (b) DVN is mounted at the entrance barrier of TalTech campus.

Figure 25: Detection and Vision Node at the perception layer.

### 5.1.2 Smart Transmit Node (STN) at Gateway Layer

A RaspberryPi (RPi) 3B module[24] is attached to a Sixfab's cellular IoT HAT[25] into a Smart Transmit Node (STN) as shown in Figure 26. This STN is deployed at the gateway layer of our proposed Visual NB-IoT Framework as depicted in Figures 24. The STN receives images from the DVN through its Bluetooth connectivity, processes it locally and smart transmits these images to the Server Node (SN) at the cloud layer through an NB-IoT connectivity. The RPi 3B is preferred over its latest counterparts i.e., RPi 3B+ and RPi 4B for it has lower power consumption [125] and sufficient computational capability to safely run our required ML algorithms. The attached Sixfab 's cellular IoT HAT is an add-on for RPi that is based on Quectel's BG96 LPWAN chipset[26] adding Cat NB1 (NB-IoT)/Cat M features to the RPi module.

### 5.1.3 Server Node (SN) at Cloud Layer

Our physical server is based on an Intel Core-i7 platform that operates at 2.2 GHz, and is equipped with 8GB SRAM, 512GB HDD and runs Windows 10 as its Operating System (OS). Python (version 3.8) with all the required libraries runs on top of Windows 10. A python-based HBMQTT broker (an open source MQTT broker and client implementation) is accessible to all its clients, both physical and virtual, through an internet connection via a dedicated IP address and a port.
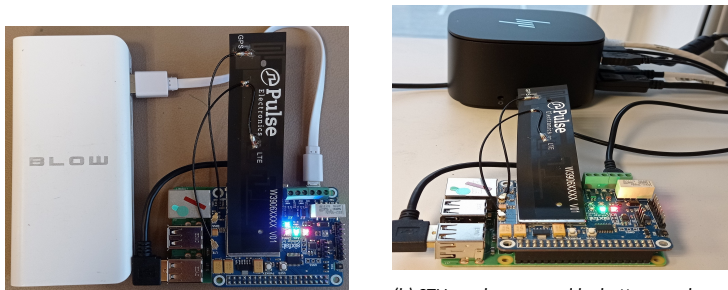
---

[22] http://www.ai-thinker.com/pro_view-24.html

[23] https://components101.com/sensors/hc-sr501-pir-sensor

[24] https://www.raspberrypi.com/products/raspberry-pi-3-model-b/

[25] https://sixfab.com/

[26] https://www.quectel.com/product/lpwa-bg96-cat-m1-nb1-egprs

(b) STN can be powered by battery as shown in (a)

(a) Integrating RPi 3B with Cellular IoT HAT into STN. or DC power supply as shown in (b).

*Figure 26: Smart Transmit Node (STN) deployed at the gateway layer.*

## 5.2  Algorithmic Structure of Our Proposed Visual NB-IoT Framework

The algorithms running across the various nodes of our three-layers hierarchical model include:

    4.2.1 - Sense & Transmit algorithm running over DVN,

    4.2.2 - Smart Transmit algorithm running over STN,

    4.2.3 - MQTT broker, Image reconstruction and an Application running over the SN.

### 5.2.1  Sense & Transmit algorithm over the DVN

The algorithm running over the DVN works in a sense-and-transmit fashion as shown in Figure 27 where upon any motion detection from the PIR sensor, the node wakes-up to capture an image of the approaching vehicle and sends it to the STN through a BT connectivity. As the transmission end, the DVN goes back into its deep sleep until triggered again by the PIR motion sensor.
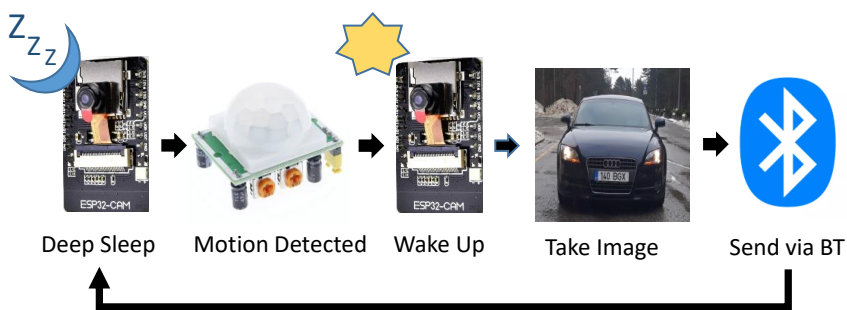


Deep Sleep    Motion Detected    Wake Up    Take Image    Send via BT

*Figure 27: Sense and transmit procedure*

### 5.2.2  Smart Transmit Algorithm running over the STN

The STN runs a series of algorithms in a sequential order as shown in Figure 28. These algorithms are discussed in their order of execution in the subsections to follow.
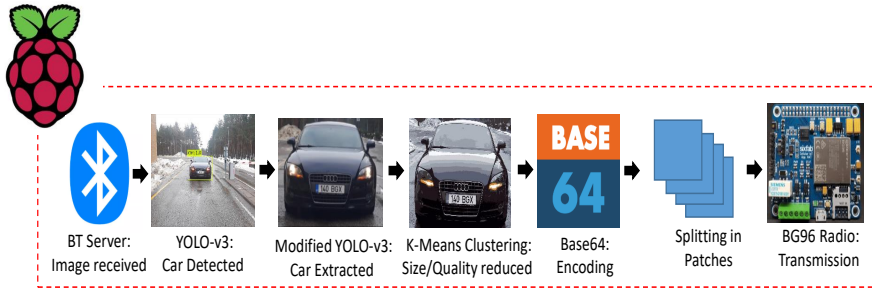
*Figure 28: Smart transmit procedure*

1- Bluetooth Server: A Bluetooth (BT) server [126] runs over the STN such that when VDN detects and capture an image of the vehicle, it initiates a BT connection (acting as a BT client) with the BT server and transmits the captured image to the STN. The STN receives the image and passes it to Tiny-YOLOv3 algorithm for vehicle detection and extraction as discussed below.

2- Tiny-YOLOv3 for vehicle detection and extraction: "You Only Look Once" (YOLO) is a state-of-the-art, real-time object detection algorithm [127], [128]. A lighter version of YOLO-v3 [129] runs on RPi 3B where its modified code extracts the detected vehicle and save it as a separate JPG image file in the memory. This discards the unnecessary information with in the received image that could cost significantly both in terms of the RPi processing and NB-IoT radio transmissions (to be discussed later in the results section). The extraced image from Tiny-YOLOv3 is fed into K-means clustering for size reduction as discussed below.

3- K-MEANS Clustering algorithm: K-Means clustering is exploited for image compression [130] based on the reduction of the number of (k) colors in the image. The number of colors could be set (equall to k) as desired and this leads to significant reductions in the size of an image contributing to reductions in the number of radio transmissions.

4- BASE-64 Encoding of the compressed image: The use of an encoding scheme [131] becomes a necessity especially when transferring image data to web-sockets, so that the image data does not interfere with many of the internet protocols across its way to its destination [132], [133]. In our case, we make use of the Base64 encoding scheme to transmit our image over the internet.

5- Transmission of the encoded image over the air through an MQTT protocol: The encoded image is sent over the air (NB-IoT network) by the BG96 radio utilizing an MQTT protocol [134] [135]. And since the MQTT protocol supports sending a maximum payload of 1548 bytes [136], images of size larger than 1548 bytes cannot be transmitted in a single communication transaction. That is why larger images are broken down into a grid of patches, each of 1500 bytes, such that these patches are dispatched separately with a header indicating its order in the source image. This is shown on the left side of Figure 29. The number of communication transactions that are required to send an image that

is larger than the minimum transaction of ca. 1500 bytes size is given as:

$$\#\_communication\_transactions = \left\lceil \frac{image\_size(kB)}{1.5} \right\rceil \qquad (20)$$
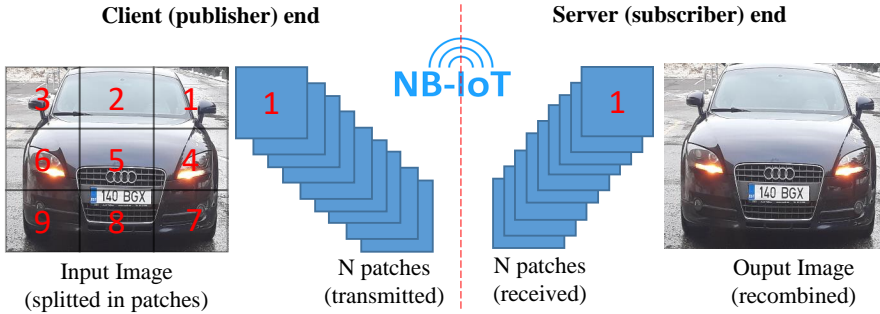


Figure 29: Splitting of an image into patches (at the publisher end) and its reconstruction (at the server end) procedure.

### 5.2.3 MQTT broker, Image reconstruction and an Application running over the SN

A python-based HBMQTT broker [137] runs over the SN that is accessible to any physical/virtual client through an IP address and a port. Since the image from STN is received in a number of patches, a python-based image-reconstruction algorithm combines all the received patches in proper order to re-construct the encoded image back into the format as sent from STN. After reconstruction, the image is decoded back (from base-64 encoded format) into its original JPG format and is saved to hard-drive. The application, used as an example, monitors a parking lot in terms of the authorized vehicles such that when an unknown vehicle is detected, the security services are notified with the visual description of the front of the vehicle. However, there could be a number of use-cases where image transmission would be required by applications such as [123], [124], [103], etc.

## 5.3 On-field Experimental Trials with Energy/Time Consumption Evaluations

The field-deployed DVN is installed at the entrance barrier of Tallinn University of Technology (TalTech) campus and is configured to generate images of an approaching vehicle with different resolutions i.e., i) 1600x1200 full-resolution image, ii) 800x600 medium-resolution image, iii) 640x480, and iv) 320x240 low-resolution images. Examples of the on-field image is shown in Figure 30. Details of images with other resolution are summarized in Table 11.

The DVN after capturing an image of the entering vehicle transmits it to the GN through its Bluetooth connectivity. This image is fed as input to Tiny-YOLOv3 at the GN that extracts the detected vehicle out of it. Though the cropped-out image has a lower resolution as compared to its source image from DVN, its quality in terms of the number of associated colors in the extracted image remains the same. For example, for an input UXGA image (i.e. Figure 30), the corresponding detected and extracted images are shown in Figure

31(a) and (b), respectively. Since the output images from Tiny-YOLOv3 for the rest of images of the images different resolution (as summarized in Table 11) look the same, they are omitted from display. However, their details are summarized in Table 12.



*Figure 30: Resolution type (4:3 aspect ratio): UXGA (1600x1200), Size: 360 kB approx.*

Table 11: Image details with their resolution, aspect ratio, total number of pixels and their sizes in (kB) when stored in JPG format.

| Resolution Type | Resolution (W x H) | Aspect Ratio | No. of pixels | Size (kB) |
|---|---|---|---|---|
| UXGA | 1600 x 1200 | 4:3 | 1920,000 | 357.17 |
| SVGA | 800 x 600 | 4:3 | 480,000 | 118.89 |
| VGA | 640 x 480 | 4:3 | 307,200 | 87.18 |
| QVGA | 320 x 240 | 4:3 | 76,800 | 44.79 |



*(a) Detected Vehicle: Original Image Resolution (1600x1200), Size: 360kB approx.*

*(b) Cropped out vehicle: Cropped image resolution (513 x 355), Size: 66.97 kB approx.*

*Figure 31: Output images from TINY-YOLOv3 algorithm: (a) Detected vehicle and (b) Cropped-out vehicle.*

The cropped-out image from Tiny YOLO-v3 is fed as an input to the K-means clustering algorithm for compression based on the reduction of its number of colors into K number of colors (i.e., K clusters). The output images from K-means clustering algorithm for K = 5, 10, 12, and 20 with an input image of 513x355 resolution are shown in Figure 32(a)(b)(c)(d), respectively. For input images of other resolutions, their details in terms of total number

Table 12: Images with their input/output properties (resolution, size in kB) and percent reduction in size when processed in JPG format before and after the application of TINY-YOLOv3.

| Input image resolution | Detected vehicle resolution | Input image size (kB) | Extracted image size (kB) | Percent reduction in size thanks to cropping |
|---|---|---|---|---|
| 1600 x 1200 | 513 x 355 | 357.17 | 66.97 | 81% |
| 800 x 600 | 260 x 175 | 118.89 | 20.51 | 82% |
| 640 x 480 | 206 x 138 | 87.18 | 14.35 | 83% |
| 320 x 240 | 105 x 67 | 44.79 | 4.60 | 89% |

of colors, sizes and the corresponding output images from K-means clustering algorithm in terms of K number of colors and their resulting size(s) are summarized in Table 13.



(a)Output image from K_Means algorithm for K (colors) = 5, Size: 27.1kB approx.

(b)Output image from K_Means algorithm for K (colors) = 10: Size: 31.6kB approx.

(c)Output image from K_Means algorithm for K (colors) = 12: Size: 32KB approx.

Figure 32: Output of K_Means algorithm for an input image with resolution of 513x355 pixels, total number of pixels = 182115, total number of unique colors = 25512 and an input size = 66.97 kB for (a) K (colors) = 5, (b) K (colors) = 10, and (c) K (colors) = 12.

Table 13: K-means Clustering on images of various resolutions, colors and sizes and the resulting images with K number of colors (clusters) and their output sizes in (kB)

| Images from T-YOLOv3 | Resolution 1 (513 x 355) | | Resolution 2 (260 x 175) | | Resolution3 (206 x 138) | | Resolution 4 (105 x 67) | |
|---|---|---|---|---|---|---|---|---|
| K clusters | color | Size | color | Size | color | Size | color | Size |
| **K = all colors** | 25512 | 66.97 | 14503 | 20.51 | 11340 | 14.35 | 4830 | 4.60 |
| K=20 | 20 | 34.1 | 20 | 11.1 | 20 | 8.0 | 20 | 3.1 |
| **K=12** | 12 | **32.0** | 12 | **10.2** | 12 | **7.2** | 12 | **2.5** |
| K=10 | 10 | 31.6 | 10 | 10.1 | 10 | 7.0 | 10 | 2.3 |
| K=5 | 5 | 27.1 | 5 | 8.2 | 5 | 5.8 | 5 | 2.1 |

**color:** No. of colors in the image, **Size:** given in kB

### 5.3.1 Computation Cost

To assess the energy consumption of the proposed computations i.e., execution of TINY-YOLOv3 followed by the execution of K-means clustering algorithm, the power consumption of RPi 3B and its corresponding execution times for the said algorithms were mea-

sured. It was found that the mean %CPU utilization of RPi was $< 10.0\%$ in idle state i.e., when no code was being executed while its %CPU utilization reaches to a maximum of 93% in stress condition i.e, when the code was being executed. It was observed that the RPi's CPU was never starved out even while processing the highest resolution image on a single core (note: for experimental purpose we disabled all but one of the cores to assess if it can handle the code with only one core). As for the current and power consumption, the Raspberry Pi 3B consumed, on average, a mean current of 260 mA at 5.0 V (which is about 1.3 W) in its idle state and it consumed, on average, a mean current of 350 mA at 5.0 V (which is about 1.75 W) under stress conditions. Table 14 summarizes the energy consumed by Raspberry Pi 3B for processing original images to create their optimized versions.

Table 14: Energy consumed by Raspberry Pi 3B, on average, for processing an original image to create its optimized version

| Average energy consumption of Raspberry Pi 3B for processing an image | | | |
|---|---|---|---|
| Resolution | Computing Power (W) | Execution Time (s) | Energy consumed (Wh) |
| 1600 x 1200 | 1.75 | 22 | 0.0107 |
| 800 x 600 | 1.75 | 18 | 0.0072 |
| 640 x 480 | 1.75 | 13 | 0.0063 |
| 320 x 240 | 1.75 | 6 | 0.0029 |

**W:** Watt, **s:** seconds, **Wh:** Watthour

### 5.3.2 Communication Budget: Original vs. Reduced

Thanks to these local computations (application of ML algorithms on images), the size of source images are significantly reduced as summarized in Table 13. These reductions in sizes contribute greatly towards minimizing the communication budget of an NB-IoT radio, both in terms of the required number of radio transmissions and vice-versa its energy consumption. Table 15 summarizes the total number of NB-IoT radio transmissions that are required to send images in their full resolution and colors (with no local computations) in comparison to sending their optimized versions with reduced resolutions and reduced number of colors. For example, an input image of 1600x1200 resolution require a total of 239 transmissions (3rd column) to be transmitted over the radio, while its optimized version image of 513x355 resolution in 12 colors require only 22 transmissions (6th column) to be transmitted over the radio i.e., 90% reductions in the total number of NB-IoT radio transmissions.

### 5.3.3 Energy Consumed by an NB-IoT (BG96) Radio in Transmissions

To measure the energy consumption of BG96 radio (in NB-IoT mode) for transmitting these images (original Vs. optimized) over the publicly available NB-IoT test network, their associated power graphs were measured using a Keysight Technologies N6705C DC Power Analyzer (PA)[27]. These power graphs are shown in Figures 33, 34, 35, and 36 and display the average power consumption measurements of an NB-IoT (BG96) radio along with the associated transmission periods for the images i.e., (a) when transmitted as original and (b) when transmitted as optimized. For example, Figure 33 shows that the BG96 radio

---

[27]https://www.keysight.com/zz/en/product/N6705C/dc-power-analyzer-modular-600-w-4-slots.html

Table 15: *Reduced number of transmissions for transmitting an optimized image with K=12 colors in contrast to transmitting an original with K=all colors. Size given in kB.*

| Original Image (full resolution, and all colors) | | | Optimized Image (cropped and K= 12 Colors) | | | Red_Tr (%) |
|---|---|---|---|---|---|---|
| Resolution | Size | ReqT | Resolution | Size | ReqT | |
| 1600x1200 | 357.17 | 239 | 513x355 | 32.0 | 22 | -90 |
| 800x600 | 118.90 | 80 | 260x175 | 10.2 | 7 | -91 |
| 640x480 | 87.18 | 58 | 206x138 | 7.2 | 5 | -91.3 |
| 320x240 | 44.7 | 30 | 105x67 | 2.5 | 2 | -93.3 |

$R_{eq}T$: Required number of transmissions, $R_{ed}Tr$: Reduced number of transmissions
$R_{eq}T$: is obtained by deviding the size of an image in kB by 1.5 as given in Eq(1)

consumed 0.0357 Wh of energy in transmitting the original image of 1600x1200 resolution while it consumed only 0.0034 Wh for transmitting its optimized version(with K = 12 colors).
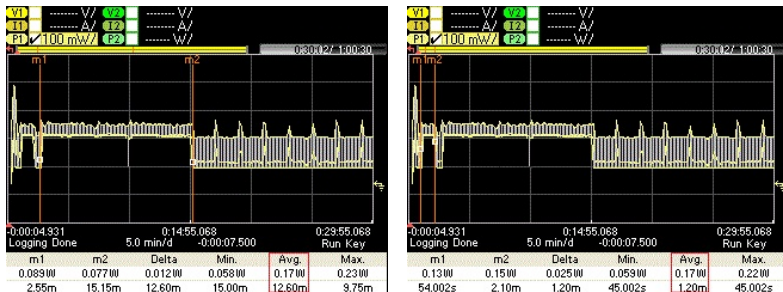


(a) *Power graph of the BG96 NB-IoT module when transmitting an image (1600x1200 pixels, 357.17 kB). 239 transmissions are needed (12.60 m) with an average power of 0.17 W, which translates to an energy consumption of 0.0357 Wh*
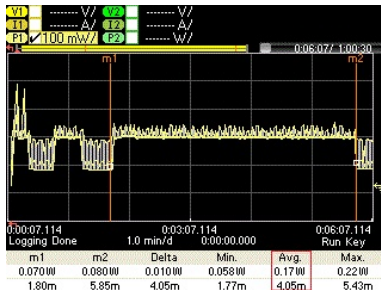
(b) *Power graph of the BG96 NB-IoT module when transmitting an image (513x355 pixels, 32 kB). 22 transmissions are needed (12.60 m) with an average power of 0.17 W, which translates to an energy consumption of 0.0034 Wh*

Figure 33: *Energy consumed for transmitting an original image is (a) 0.0357 Wh and transmitting its optimized version is (b) 0.0034 Wh, i.e. 90.5% energy savings.*

### 5.3.4 Time/Energy Comparisons

Table 16 summarizes the transmission times of sending original images in contrast to the transmission times of sending optimized images from an NB-IoT radio. For example an original image of 1600x1200 resolution takes 12.6 minutes to be transmitted over the radio while its optimized image of 513x355 resolution in 12 colors only take 1.20 minutes to be transmitted over the radio, a 90% in its transmission time as indicted by the third row of Table 16.

Similarly, Table 17 summarizes the energy consumption measurements for BG96 radio for transmitting original images in comparison to transmitting their optimized versions with K = 12 colors. These energy measurement are obtained by multiplying the average transmission time of an image with the average transmission power of the radio i.e, 0.17 W.
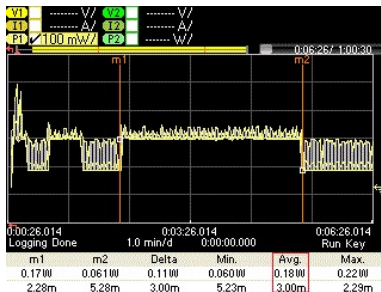
(a) Power graph of the BG96 NB-IoT module when transmitting an image (800x600 pixels, 118.9 kB). 80 transmissions are needed (4.05 m) with an average power of 0.17 W, which translates to an energy consumption of 0.0102 Wh
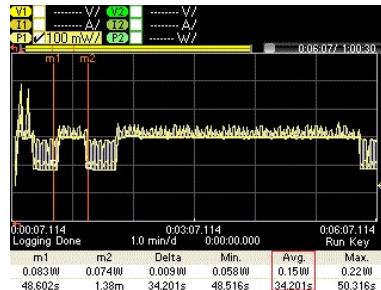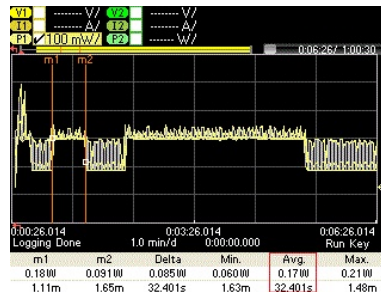
(b) Power graph of the BG96 NB-IoT module when transmitting an image (260x175 pixels, 10.2 kB). 7 transmissions are needed (34.20 s) with an average power of 0.17 W, which translates to an energy consumption of 0.0.0016 Wh

Figure 34: Energy consumed for transmitting an original image is (a) 0.012 Wh and transmitting its optimized image is (b) 0.0016 Wh, i.e. 84.3% energy savings.
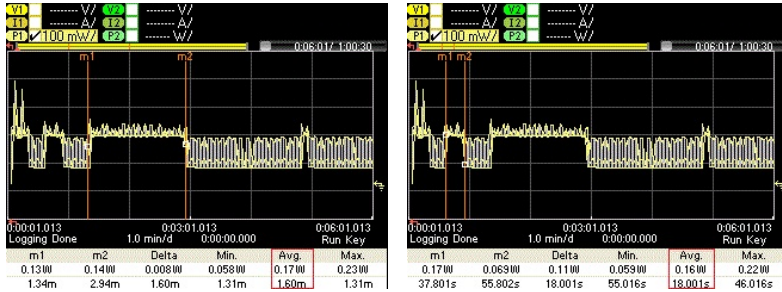


(a) Power graph of the BG96 NB-IoT module when transmitting an image (640x480 pixels, 87.18 kB). 58 transmissions are needed (3.00 m) with an average power of 0.17 W, which translates to an energy consumption of 0.0085 Wh

(b) Power graph of the BG96 NB-IoT module when transmitting an image (206x138 pixels, 7.2 kB). 5 transmissions are needed (32.40 s) with an average power of 0.17 W, which translates to an energy consumption of 0.0015 Wh

Figure 35: Energy consumed for transmitting an original image is (a) 0.0085 Wh and transmitting its optimized version is (b) 0.0015 Wh, i.e. 82.3% energy savings.

Table 18 summarises the overall energy savings per image considering both their computation and communication cost. For example, when an original image of 1600x1200 resolution is transmitted from an NB-IoT radio (without any local computation) it consumes 0.0357 Wh (as indicated by the third row of Table 18). On the other hand, when it is processed locally by the RPi, it consumes 0.0107 Wh in computations (Table 14) and 0.0034 Wh in transmissions (Table 17), i.e. a total of 0.0141 Wh; this is a 0.0216 Wh energy difference, i.e. a total of 60% energy savings per a single image. Since Table 18 shows the energy savings per image, these individual energy savings scale-up as a multiple of the number of images that are processed by the RPi. For example, the RPi processed, on an average, six images of 1600x1200 resolution in an hour i.e., a total of 144 cars entered the campus in 24 hours, and it thus saved on an average 0.20 Wh of energy in 24 hours.

(a) Power graph of the BG96 NB-IoT module when transmitting an image (320x240 pixels, 44.79 kB). 30 transmissions are needed (1.6 m) with an average power of 0.17 W, which translates to an energy consumption of 0.0034 Wh

(b) Power graph of the BG96 NB-IoT module when transmitting an image (105x67 pixels, 2.5 kB). 2 transmissions are needed (18.00 s) with an average power of 0.17 W, which translates to an energy consumption of 0.0008 Wh

Figure 36: Energy consumed for transmitting an Original image is (a) 0.0034 Wh and transmitting its Optimized image is (b) 0.0008 Wh; 76.5% energy savings.

Table 16: Reduced transmission period for transmitting an optimized image with K = 12 colors in contrast to transmitting an original image with K = all colors

| Reduction in the transmission period of NB-IoT radio | | | | | | |
|---|---|---|---|---|---|---|
| Original Image (all colors) | | | Optimized Image (K= 12 colors) | | | Red_TrTime (%) |
| Resolution | Size | TrTime | Resolution | Size | TrTime | |
| 1600x1200 | 357.17 | 12.60 m | 513x355 | 32.0 | 1.20 m | -90 |
| 800x600 | 118.90 | 4.05 m | 260x175 | 10.2 | 34.20 s | -82 |
| 640x480 | 87.18 | 3.0 m | 206x138 | 7.2 | 32.4 s | -82 |
| 320x240 | 44.7 | 1.6 m | 105x67 | 2.5 | 18.0 s | -81 |

**TrTime:** transmission time (m: minutes, s: seconds)
**Red_TrTime:** percent reductions in transmission time

Table 17: Reduced energy consumption for transmitting an optimized image with K = 12 colors in contrast to transmitting an original image with K = all colors

| Reduction in the energy consumption of NB-IoT radio | | | | | |
|---|---|---|---|---|---|
| Original Image (in all colors) | | Optimized Image (in K=12 colors) | | $E_{Red}$(Wh) | $E_{Red}$ (%) |
| Resolution | $E_{con}$(Wh)* | Resolution | $E_{con}$(Wh) | | |
| 1600 x 1200 | 0.0357 | 513x355 | 0.0034 | -0.0323 | -90.5 |
| 800 x 600 | 0.0102 | 260x175 | 0.0016 | -0.0086 | -84.3 |
| 640 x 480 | 0.0085 | 206x138 | 0.0015 | -0.0070 | -82.3 |
| 320 x 240 | 0.0034 | 105x67 | 0.0008 | -0.0026 | -76.5 |

$E_{con}$: Energy consumed, $E_{Red}$: energy reduction, $E_{Red}$(%): energy reduction in percentage
*: $E_{con}$ is obtained by multiplying $P_{Tx}$ with $T_{Tx}$ (For reference see Table 9 and Table 10)

With this rate, it can save, on an average 1.41 Wh of energy in a week and so on. It should also be noted that these energy savings are the outcome from a single STN at the gateway

*Table 18: Overall energy savings in transmitting an optimized image (considering both its computing and communication energy) as compared to transmitting an original image (communication energy only since no computation needed)*

| Energy consumption per Original image Vs Energy consumption per Optimized Image | | | | | |
|---|---|---|---|---|---|
| **Original Image** | | **Optimized Image** | | **E_Savings (Wh) (a-b)** | ES (%) |
| Resolution | $E_{COMM}$(Wh) (a) | Resolution | $E_{COMP}$+$E_{COMM}$(Wh) (b) | | |
| 1600x1200 | 0.0357 | 513x355 | 0.0107 + 0.0034 | 0.0216 | -60.50 |
| 800x600 | 0.0102 | 260x175 | 0.0072+0.0016 | 0.0014 | -13.72 |
| 640x480 | 0.0085 | 206x138 | 0.0063+.0015 | 0.007 | -8.23 |
| 320x240 | 0.0034 | 105x67 | 0.0029+.0008 | 0.002 | -5.88 |

$E_{COMM}$: Communication energy, $E_{COMP}$: Computation energy
**E_Savings**: Total energy savings per image
**ES(%)**: Percent reduction in energy consumption

layer and these savings could further scale-up as a function of the increasing number of smart nodes in the network. As a side-note, since a single 100 W PVC solar panel generates around 400 Wh/24hours, a 15/20 W solar panel could also be utilized to power such a system [103].

# 6 Conclusion

## 6.1 Summary

This PhD thesis dealt with several issues related to the NB-IoT wireless communication technology with a special interest for energy consumption. At the device level, this thesis sought to gain a thorough understanding of the power and energy saving provisions available in the NB-IoT standard and actual devices, as well as to create a model thereof. This new knowledge and model can allow using and optimizing such provisions in view of achieving the expected 10-year battery lifetime of NB-IoT devices. At the network level, the focus was on devising an architecture and application running on top of it to exploit the NB-IoT wireless communication technology in combination with computing devices.

To this end, my PhD thesis addressed the following research questions (stated earlier in Chapter 1, Section 1.5):

1. RQ1: How to design an NB-IoT sensor node from CoTS components that would transmit its collected data to an IoT cloud server over the available NB-IoT network? Scaling it up, how to setup an "NB-IoT testbed" i.e., integrating a multitude of NB-IoT sensor nodes to a single IoT server over the available NB-IoT network to collect the data from all the deployed nodes for further analysis and investigation.

2. RQ2: How to utilize the developed "NB-IoT testbed" for analysing the network coverage performance of a real NB-IoT network, particularly, in an indoor, outdoor and deep-indoor (underground) environments?

3. RQ3: What could be the baseline energy consumption model for an NB-IoT sensor node i.e., what parameters affect the energy consumption profile of an NB-IoT node and how these parameters could be integrated into the baseline energy consumption model of the node to improve its energy efficiency?

4. RQ4: What different architectures are possible for developing an NB-IoT application? i.e., how many hierarchical layers are actually needed and what could be their respective roles for collecting, processing, and transmitting the collected data to the cloud?

5. RQ5: What type of local data processing could be utilized and what could be the associated benefits? i.e., what could be the trade-offs in terms of computation and communication energy and/or latency between local computing and transmissions?

6. RQ6: How to demonstrate and validate the above approaches in a real NB-IoT network?

To contribute to answering these research questions, I opted for an empirical approach to analyze the NB-IoT radio access technology, both from the device and network level.

To recap, I developed the DORM (integrateD cOmpact naRrowband platforM) node from CoTS components with the aim to conduct on-field experimental trials under a real NB-IoT test network, both from the device and network perspectives. Replicating 50 of such DORM nodes and connecting them to an IoT backend server through the available NB-IoT network, I developed the "TalTech NB-IoT testbed". It should be noted here that at the time this PhD thesis started, integrated MCU/NB-IoT radio nodes were not commercially available. Thus, the development of this testbed paved a definite way towards

researching on essential aspects of NB-IoT as stated in RQ2-RQ6 and with explanations as given in what follows.

Contributing towards RQ2, I carried out a comprehensive practical coverage analysis of the NB-IoT network in indoor, outdoor and deep indoor environments, which is in contrast to the existing SoA where the majority of efforts on NB-IoT coverage is replete with modeling and simulation based results as illustrated by the following many references [54, 63, 64, 65, 66, 67, 68, 69, 70]. It should be mentioned here that network coverage of LPWAN technologies is an important performance indicator as it affects the battery-life time of the associated node to a greater extent, particularly in-case of the NB-IoT network. This contribution, on the one hand, highlighted the practical network performance of NB-IoT network in different environments, and it also helped towards analyzing the battery-life time of the individual NB-IoT node from different coverage class levels.

Contributing towards RQ3, I conducted a thorough investigation of the Radio Resource Control (RRC) communication protocol that an NB-IoT radio follows to communicate with a 5G base-station (BS), and based on this I proposed an analytical energy consumption model for a 3GPP compliant NB-IoT radio transciever. This is in contrast to the existing literature on NB-IoT UE energy consumption that mostly provides analytical [71, 72, 73, 74] and simulation based results [76, 77, 79]. Moreover, practical works such as [69, 81, 75] made only a superficial analysis of the NB-IoT UE's power consumption by providing aggregated power consumption details of the node as a whole where the individual power consumption details of each component of the node remain obscured. Towards this direction, this thesis provided a comprehensive power consumption analysis of the various RRC states of an NB-IoT radio with detailed granularity of the involved underneath sub-states i.e., C-DRX cycles, eDRX cycles, PTW, I-DRX cycles, etc. which to date have not been studied empirically to that granularity. Furthermore, based on a comprehensive analysis of the various operating states of the NB-IoT radio, while operating under a real NB-IoT network, this thesis proposed an analytical energy consumption model for a 3GPP compliant NB-IoT radio transceiver. The sensitivity analysis of this model revealed that it truly depicts the energy consumption of any generic CoTS NB-IoT radio transceiver with high accuracy.

Towards RQ4 and RQ5, I furthered the "TalTech NB-IoT testbed" into a three-tiered energy-efficient "NB-IoT Edge-of-Things Framework", wherein ML algorithms running at the edge processes an image to obtain only the useful information out of it where the unnecessary data is discarded. This in turn reduces the communication budget of each individual NB-IoT radio and this contributes towards relaxing the channel occupancy, minimizing the network load and reducing the transmission latency of the network. From the perspective of utilizing edge computing for increasing the efficiency of an IoT network, several works have proposed and evaluated ML techniques for higher energy efficiency, bandwidth saving, lower latency, and collaborative intelligence of the network. However, most of these works provided analytical models with simulation-based results only [96, 97, 98, 99, 100, 101, 102]. Nevertheless, some works have proposed utilizing ML for increasing the energy efficiency of IoT nodes [107, 108, 109, 110, 111, 112]. However, integration of NB-IoT with ML from a practical perspective was still missing in the existing literature. To cover this gap, this PhD thesis practically showcased that ML can play a pivotal role towards revolutionizing the future IoT technology, NB-IoT in particular.

Last but not the least, all the experiments included in this thesis were performed on a real NB-IoT test network, where results were analysed practically on a real setup and this contributed towards addressing RQ6.

## 6.2 Claims

Below is a summary of the claims of novelty that this PhD thesis has made. These claims correspond to the Contributions I-V and relate to papers in Appendix 1-5.

### 6.2.1 Claim 1:

At a time when NB-IoT was still in its infancy, there was hardly any available data on the practical coverage analysis of the NB-IoT network. The author made a comprehensive real-life investigation of the NB-IoT coverage in indoor, outdoor, and underground environments in his contributions in I, II, and III. As explained in Section 6.1 in relation to RQ1-RQ2, such an extensive summary with practical coverage analysis of the NB-IoT network was published for the first time in the literature. Furthermore, starting from the device prototyping towards developing the whole NB-IoT testbed yielded an insight into setting up an IoT platform from CoTS components from practical perspectives. This corresponds to contributions and papers in Appendix 1-3.

### 6.2.2 Claim 2:

The author provided a modelling methodology for profiling the empirical baseline energy consumption of an NB-IoT radio transceiver. The author provided a fine grain analysis of the LTE RRC protocol by mapping its different modes with detailed experimental results in terms of the radio energy consumption in contrast to most existing works that were limited to the aggregated power or energy consumption of the whole NB-IoT UE and/or rely on either simulations or emulated networks. This modelling methodology considered all the states of the RRC protocol standardized by 3GPP and hence is applicable to generic NB-IoT radio chips that are standard compliant. As explained in Section 6.1 in relation to RQ3, this contribution was the first one to propose a detailed and realistic NB-IoT radio transceiver energy consumption model thanks to the detailed analysis and real-life empirical experiments. This corresponds to contributions IV and the paper in Appendix 4.

### 6.2.3 Claim 3:

The author showcased a practical edge-of-things computing based NB-IoT framework for dispatching optimized images over the NB-IoT network, wherein the computations at the edge were used to reduce the number of NB-IoT radio transmissions over the NB-IoT network. These reductions in the communication budget of a single NB-IoT radio contributed to relaxing the channel occupancy, minimizing the network load and reducing the transmission latency from each single radio from the network perspective. Furthermore, an in-depth in-sensor analytics of the communication and computational cost of the gateway (computing) node along with mapping its energy-latency trade-offs were investigated and compiled in Contributions V and paper in Appendix 5. In line with the discussion about RQ4-RQ6 in Section 6.1, these details had never been previously provided in the literature before, particularly for NB-IoT from a practical perspective.

## 6.3 Perspectives

The experiments for analysing the NB-IoT coverage in this thesis were conducted with all our devices connected to an NB-IoT test network wherein the total number of connected NB-IoT devices were limited i.e., in orders of tens. However, commercially operating NB-IoT networks are expected to allow up-to 50K+ devices per cell [52]. Such an immense number of connected NB-IoT devices per cell would contribute to added intra-cell interference and inter-cell interference affecting the QoS of the NB-IoT network including its

coverage. This demands a practical investigation of the massive NB-IoT networks containing thousands of connected devices with their conjoint traffic with other LTE technologies, so as to identify algorithms and techniques such as e.g. [138, 139, 140, 141, 142] that could improve or at least sustain the required QoS of the NB-IoT network.

This PhD thesis provided a modelling methodology for profiling the empirical baseline energy consumption of an NB-IoT radio transceiver by mapping the various states of LTE RRC protocol with their associated energy consumption profiles from an NB-IoT radio transceiver. Since this empirical model includes all the RRC states of the NB-IoT radio as standardized by 3GPP, it is applicable to the standard compliant NB-IoT radio chips. Furthermore, for profiling the power consumption details of an NB-IoT radio, we also showcased how the various CE levels of an NB-IoT radio affect its total energy consumption due to re-transmissions. While we successfully curbed the number of NB-IoT radio transmissions through incorporating ML algorithms on the edge, we could not possibly control the number of NB-IoT radio re-transmissions with our current setup and hardware prototype. Despite the promising benefits of re-transmissions in terms of the NB-IoT coverage enhancements, there are still significant challenges in terms of radio energy consumption and this calls for further investigations to find the optimum number of re-transmission in each CE level that the radio must operate in; see e.g. [143, 144, 145].

Furthermore, to curb the unnecessary data from being transmitted over the radio, we used compute intensive AI algorithms such as YOLO-v3 and K-Means algorithms. It should be mentioned here that most of the existing studies including ours use compute intensive AI algorithms for implementing smart IoT applications. As these algorithms are compute intensive they can only run on powerful machines and are usually time-consuming dragging more power and also low in response. This calls for the design and development of portable or tiny AI algorithms that could run even on the not-so-powerful generic microcontrollers that could be used in the design of IoT nodes for supporting autonomous intelligence with quick and precise responses [146, 147].

Finally, a testbed such as the one presented in this thesis allows collecting large amount of data over time in varying operational conditions (network and computational loads, weather condition, etc.) There is a tremendous opportunity to exploit such large amounts of data to optimize the network performance in terms of latency, throughput, packet loss, network and computational load balancing, and energy consumption, etc. [148, 149]. Indeed, analyzing such data in time and space domains could help in identifying the most suitable configurations for various scenarios. On the device side, this could be used to assess the impact of its own mobility or that of objects/vehicles/humans in its vicinity, e.g. predicting in which coverage class a UE will be in the near future and how this information could be used to decide e.g. when to send data/schedule re-transmissions. Taking this a step further, considering that networks are more and more automated, a data-driven learning approach for predictive dynamic network reconfiguration could be realized. This could be used on the BS side to optimize its operations wherein e.g. the network and computing application parameters are automatically adjusted as a function of the predicted and actual changes taking place in the network and its environment [150]. Another possibility could be data-driven dynamic self-healing systems [151], wherein corrective measures such as load-balancing, routing, etc. are applied based on the predicted and actual status and health (including energy-level) of the NB-IoT nodes with a view to maintain a minimum quality of service (QoS).

# References

[1] Sikandar Zulqarnain Khan, Hassan Malik, Jeffrey Leonel Redondo Sarmiento, Muhammad Mahtab Alam, and Yannick Le Moullec. Dorm: Narrowband iot development platform and indoor deployment coverage analysis. *Procedia Computer Science*, 151:1084–1091, 2019.

[2] Hassan Malik, Sikandar Zulqarnain Khan, Jeffrey Leonel Redondo Sarmiento, Alar Kuusik, Muhammad Mahtab Alam, Yannick Le Moullec, and Sven Pärand. Nb-iot network field trial: Indoor, outdoor and underground coverage campaign. In *2019 15th International Wireless Communications Mobile Computing Conference (IWCMC)*, pages 537–542, 2019.

[3] Nishant Poddar, Sikandar Zulqarnain Khan, Jakob Mass, and Satish Narayana Srirama. Coverage analysis of nb-iot and sigfox: Two estonian university campuses as a case study. In *2020 International Wireless Communications and Mobile Computing (IWCMC)*, pages 1491–1497. IEEE, 2020.

[4] Sikandar M. Zulqarnain Khan, Muhammad Mahtab Alam, Yannick Le Moullec, Alar Kuusik, Sven Pärand, and Christos Verikoukis. An empirical modeling for the baseline energy consumption of an nb-iot radio transceiver. *IEEE Internet of Things Journal*, 8(19):14756–14772, 2021.

[5] Sikandar Zulqarnain Khan, Yannick Le Moullec, and Muhammad Mahtab Alam. An NB-IoT-Based Edge-of-Things Framework for Energy-Efficient Image Transfer. *MDPI Sensors*, 17(21):5929–5949, 2021.

[6] Sikandar Zulqarnain Khan, Rashiduddin Kakar, Muhammad Mahtab Alam, Yannick Le Moullec, and Haris Pervaiz. A green iot node incorporating transient computing, approximate computing and energy/data prediction. In *2020 IEEE 17th Annual Consumer Communications Networking Conference (CCNC)*, pages 1–6, 2020.

[7] Peter Marwedel. *Embedded system design: embedded systems foundations of cyber-physical systems, and the internet of things*. Springer Nature, 2021.

[8] Rapeepat Ratasuk, Nitin Mangalvedhe, and Amitava Ghosh. Overview of lte enhancements for cellular iot. In *2015 IEEE 26th annual international symposium on personal, indoor, and mobile radio communications (PIMRC)*, pages 2293–2297. IEEE, 2015.

[9] Hamidreza Arasteh, Vahid Hosseinnezhad, Vincenzo Loia, Aurelio Tommasetti, Orlando Troisi, Miadreza Shafie-khah, and Pierluigi Siano. Iot-based smart cities: A survey. In *2016 IEEE 16th International Conference on Environment and Electrical Engineering (EEEIC)*, pages 1–6. IEEE, 2016.

[10] Hemant Ghayvat, Subhas Mukhopadhyay, Xiang Gui, and Nagender Suryadevara. Wsn-and iot-based smart homes and their extension to smart buildings. *sensors*, 15(5):10350–10379, 2015.

[11] Fabio Arena, Giovanni Pau, and Alessandro Severino. An overview on the current status and future perspectives of smart cars. *Infrastructures*, 5(7):53, 2020.

[12] Miguel A Zamora-Izquierdo, José Santa, Juan A Martínez, Vicente Martínez, and Antonio F Skarmeta. Smart farming iot platform based on edge and cloud computing. *Biosystems engineering*, 177:4–17, 2019.

[13] Jaime Lloret, Jesus Tomas, Alejandro Canovas, and Lorena Parra. An integrated iot architecture for smart metering. *IEEE Communications Magazine*, 54(12):50–57, 2016.

[14] Sean Dieter Tebje Kelly, Nagender Kumar Suryadevara, and Subhas Chandra Mukhopadhyay. Towards the implementation of iot for environmental condition monitoring in homes. *IEEE sensors journal*, 13(10):3846–3853, 2013.

[15] D Pavithra and Ranjith Balakrishnan. Iot based monitoring and control system for home automation. In *2015 global conference on communication technologies (GCCT)*, pages 169–173. IEEE, 2015.

[16] Marco Centenaro, Lorenzo Vangelista, Andrea Zanella, and Michele Zorzi. Long-range communications in unlicensed bands: The rising stars in the iot and smart city scenarios. *IEEE Wireless Communications*, 23(5):60–67, 2016.

[17] Dhaval Patel and Myounggyu Won. Experimental study on low power wide area networks (LPWAN) for mobile Internet of Things. In *2017 IEEE 85th Vehicular Technology Conference (VTC Spring)*, pages 1–5. IEEE, 2017.

[18] Usman Raza, Parag Kulkarni, and Mahesh Sooriyabandara. Low power wide area networks: An overview. *IEEE Communications Surveys & Tutorials*, 19(2):855–873, 2017.

[19] Kais Mekki, Eddy Bajic, Frederic Chaxel, and Fernand Meyer. A comparative study of lpwan technologies for large-scale iot deployment. *ICT express*, 5(1):1–7, 2019.

[20] Pankaj Sharma. Evolution of mobile wireless communication networks-1g to 5g as well as future prospective of next generation communication network. *International Journal of Computer Science and Mobile Computing*, 2(8):47–53, 2013.

[21] Ajay R Mishra. *Advanced cellular network planning and optimisation: 2G/2.5 G/3G... evolution to 4G*. John Wiley & Sons, 2007.

[22] Michael Steer. Beyond 3g. *IEEE microwave Magazine*, 8(1):76–82, 2007.

[23] Ghassan A Abed, Mahamod Ismail, and Kasmiran Jumari. The evolution to 4g cellular systems: Architecture and key features of lteadvanced networks. *spectrum*, 2, 2012.

[24] Amitabha Ghosh, Andreas Maeder, Matthew Baker, and Devaki Chandramouli. 5g evolution: A view on 5g cellular technology beyond 3gpp release 15. *IEEE access*, 7:127639–127651, 2019.

[25] Mekki, Kais and Bajic, Eddy and Chaxel, Frederic and Meyer, Fernand. Overview of cellular LPWAN technologies for IoT deployment: Sigfox, LoRaWAN, and NB-IoT. In *2018 IEEE International Conference on Pervasive Computing and Communications Workshops (PerCom Workshops)*, pages 197–202. IEEE, 2018.

[26] Carles Gomez, Juan Carlos Veras, Rafael Vidal, Lluís Casals, and Josep Paradells. A sigfox energy consumption model. *Sensors*, 19(3):681, 2019.

[27] Ferran Adelantado, Xavier Vilajosana, Pere Tuset-Peiro, Borja Martinez, Joan Melia-Segui, and Thomas Watteyne. Understanding the limits of lorawan. *IEEE Communications magazine*, 55(9):34–40, 2017.

[28] LoRaWAN vs NB-IoT: A Comparison Between IoT Trend-Setters. https://ubidots.com/blog/lorawan-vs-nb-iot/. Accessed: 2021-04-05.

[29] Hassan Malik, Muhammad Mahtab Alam, Haris Pervaiz, Yannick Le Moullec, Anwer Al-Dulaimi, Sven Parand, and Luca Reggiani. Radio resource management in nb-iot systems: Empowered by interference prediction and flexible duplexing. *IEEE Network*, 34(1):144–151, 2019.

[30] Hassan Malik, Haris Pervaiz, Muhammad Mahtab Alam, Yannick Le Moullec, Alar Kuusik, and Muhammad Ali Imran. Radio resource management scheme in nb-iot systems. *IEEE Access*, 6:15051–15064, 2018.

[31] Songlin Sun, Liang Gong, Bo Rong, and Kejie Lu. An intelligent sdn framework for 5g heterogeneous networks. *IEEE Communications Magazine*, 53(11):142–147, 2015.

[32] Ke Zhang, Yuming Mao, Supeng Leng, Quanxin Zhao, Longjiang Li, Xin Peng, Li Pan, Sabita Maharjan, and Yan Zhang. Energy-efficient offloading for mobile edge computing in 5g heterogeneous networks. *IEEE access*, 4:5896–5907, 2016.

[33] GSM Association et al. Nb-iot deployment guide to basic feature set requirements. *En ligne]. Disponible sur: https://www. gsma. com/iot/wp-content/uploads/2018/04/NB-IoT_Deployment_Guide_v2_5Apr2018. pdf.[Consulté le: 10-mai-2019]*, 2019.

[34] Nokia Networks. 3GPP R1157248: NB IoT Capacity evaluation, Tech.Report,. 2015.

[35] Kamil Staniec, Michał Kucharzak, Zbigniew Jóskiewicz, and Bartłomiej Chowański. Measurement-based investigations of the nb-iot uplink performance at boundary propagation conditions. *Electronics*, 9(11):1947, 2020.

[36] Rubbens Boisguene, Sheng-Chia Tseng, Chih-Wei Huang, and Phone Lin. A survey on nb-iot downlink scheduling: Issues and potential solutions. In *2017 13th International Wireless Communications and Mobile Computing Conference (IWCMC)*, pages 547–551. IEEE, 2017.

[37] TR 45.820. Cellular system support for ultra low complexity and low throughput internet of things. *V2. 1.0*, 2015.

[38] Safiu Abiodun Gbadamosi, Gerhard P Hancke, and Adnan M Abu-Mahfouz. Building upon nb-iot networks: A roadmap towards 5g new radio networks. *IEEE Access*, 8:188641–188672, 2020.

[39] Borja Martinez, Ferran Adelantado, Andrea Bartoli, and Xavier Vilajosana. Exploring the performance boundaries of nb-iot. *IEEE Internet of Things Journal*, 6(3):5702–5712, 2019.

[40] Jeanette Wannstrom. Lte-advanced. *Third Generation Partnership Project (3GPP)*, 2013.

[41] ETSI LTE. Evolved universal terrestrial radio access (e-utra) and evolved universal terrestrial radio access network (e-utran)(3gpp ts 36.300, version 8.11. 0 release 8), december 2009. *ETSI TS*, 136(300):V8, 2011.

[42] Jim Zyren and Wes McCoy. Overview of the 3gpp long term evolution physical layer. *Freescale Semiconductor, Inc., white paper*, 7:2–22, 2007.

[43] Mads Lauridsen, Rasmus Krigslund, Marek Rohr, and Germán Madueno. An empirical nb-iot power consumption model for battery lifetime estimation. In *2018 IEEE 87th Vehicular Technology Conference (VTC Spring)*, pages 1–5. IEEE, 2018.

[44] Pascal Jörke, Robert Falkenberg, and Christian Wietfeld. Power consumption analysis of nb-iot and emtc in challenging smart city environments. In *2018 IEEE Globecom Workshops (GC Wkshps)*, pages 1–6. IEEE, 2018.

[45] Ashish Kumar Sultania, Carmen Delgado, and Jeroen Famaey. Implementation of nb-iot power saving schemes in ns-3. In *Proceedings of the Workshop on Next-Generation Wireless with ns-3*, pages 5–8, 2019.

[46] Ashish Kumar Sultania, Pouria Zand, Chris Blondia, and Jeroen Famaey. Energy modeling and evaluation of nb-iot with psm and edrx. In *IEEE Globecom Workshops (GC Wkshps)*, pages 1–7. IEEE, 2018.

[47] Rakesh Kumar Jha, Sanjeev Jain, et al. A comprehensive survey on green ict with 5g-nb-iot: Towards sustainable planet. *Computer Networks*, page 108433, 2021.

[48] KC Raveendranathan. Future directions: smart sensors for green internet of things (green iot). *Advances in Modern Sensors*, pages 15–1, 2020.

[49] Nitin B Raut and NM Dhanya. A green dynamic internet of things (iot)-battery powered things aspect-survey. In *Soft Computing: Theories and Applications*, pages 153–163. Springer, 2020.

[50] Sakshi Popli, Rakesh Kumar Jha, and Sanjeev Jain. A survey on energy efficient narrowband internet of things (nbiot): architecture, application and challenges. *IEEE Access*, 7:16739–16776, 2018.

[51] Y-P Eric Wang, Xingqin Lin, Ansuman Adhikary, Asbjorn Grovlen, Yutao Sui, Yufei Blankenship, Johan Bergman, and Hazhir S Razaghi. A primer on 3gpp narrowband internet of things. *IEEE communications magazine*, 55(3):117–123, 2017.

[52] Jun Xu, Junmei Yao, Lu Wang, Zhong Ming, Kaishun Wu, and Lei Chen. Narrowband internet of things: Evolutions, technologies, and open issues. *IEEE Internet of Things Journal*, 5(3):1449–1462, 2017.

[53] Antonino Masaracchia, Raffaele Bruno, Andrea Passarella, and Stefano Mangione. Analysis of mac-level throughput in lte systems with link rate adaptation and harq protocols. In *2015 IEEE 16th International Symposium on A World of Wireless, Mobile and Multimedia Networks (WoWMoM)*, pages 1–9. IEEE, 2015.

[54] Ansuman Adhikary, Xingqin Lin, and Y-P Eric Wang. Performance evaluation of nb-iot coverage. In *2016 IEEE 84th Vehicular Technology Conference (VTC-Fall)*, pages 1–5. IEEE, 2016.

[55] 3GPP. Study on provision of low-cost machine-type communications (mtc) user equipments (ues) based on lte. 2013.

[56] Andreas Hoglund, Xingqin Lin, Olof Liberg, Ali Behravan, Emre A. Yavuz, Martin Van Der Zee, Yutao Sui, Tuomas Tirronen, Antti Ratilainen, and David Eriksson. Overview of 3gpp release 14 enhanced nb-iot. *IEEE Network*, 31(6):16–22, 2017.

[57] Rapeepat Ratasuk, Nitin Mangalvedhe, Zhilan Xiong, Michel Robert, and David Bhatoolaul. Enhancements of narrowband iot in 3gpp rel-14 and rel-15. In *2017 IEEE Conference on Standards for Communications and Networking (CSCN)*, pages 60–65. IEEE, 2017.

[58] 3GPP. TS 36.213, 2018. `https://portal.3gpp.org/desktopmodules/Specif ications/SpecificationDetails.aspx?specificationId=2427`. Accessed: 2021-04-05.

[59] Collins Burton Mwakwata, Hassan Malik, Muhammad Mahtab Alam, Yannick Le Moullec, Sven Parand, and Shahid Mumtaz. Narrowband internet of things (nb-iot): From physical (phy) and media access control (mac) layers perspectives. *Sensors*, 19(11):2613, 2019.

[60] Eshita Rastogi, Navrati Saxena, Abhishek Roy, and Dong Ryeol Shin. Narrowband internet of things: A comprehensive study. *Computer Networks*, 173:107209, 2020.

[61] 3GPP. TS 36.300 V16.2.0 (2020-07). `https://www.3gpp.org/ftp//Specs/arc hive/36_series/36.300/36300-g20.zip`. Accessed: 2022-02-28.

[62] 3GPP. TR 21.917. `https://www.3gpp.org/release-17/`. Accessed: 2022-02-28.

[63] Yiming Miao, Wei Li, Daxin Tian, M Shamim Hossain, and Mohammed F Alhamid. Narrowband internet of things: Simulation and modeling. *IEEE Internet of Things Journal*, 5(4):2304–2314, 2017.

[64] Nitin Mangalvedhe, Rapeepat Ratasuk, and Amitava Ghosh. Nb-iot deployment study for low power wide area cellular iot. In *2016 ieee 27th annual international symposium on personal, indoor, and mobile radio communications (pimrc)*, pages 1–6. IEEE, 2016.

[65] Rapeepat Ratasuk, Benny Vejlgaard, Nitin Mangalvedhe, and Amitava Ghosh. Nb-iot system for m2m communication. In *2016 IEEE wireless communications and networking conference*, pages 1–5. IEEE, 2016.

[66] Rapeepat Ratasuk, Nitin Mangalvedhe, Jorma Kaikkonen, and Michel Robert. Data channel design and performance for lte narrowband iot. In *2016 IEEE 84th Vehicular Technology Conference (VTC-Fall)*, pages 1–5. IEEE, 2016.

[67] Piotr Krasowski and Douglas Troha. Wireless system design: Nb-iot downlink simulator, 2017.

[68] Gustavo Carneiro. Ns-3: Network simulator 3. In *UTM Lab Meeting April*, volume 20, pages 4–5, 2010.

[69] Yihenew Dagne Beyene, Riku Jantti, Kalle Ruttik, and Sassan Iraji. On the performance of narrow-band internet of things (nb-iot). In *2017 ieee wireless communications and networking conference (wcnc)*, pages 1–6. IEEE, 2017.

[70] Mads Lauridsen, István Z Kovács, Preben Mogensen, Mads Sorensen, and Steffen Holst. Coverage and capacity analysis of lte-m and nb-iot in a rural area. In *2016 IEEE 84th Vehicular Technology Conference (VTC-Fall)*, pages 1–5. IEEE, 2016.

[71] Li-Ping Tung, Li-Chun Wang, Cheng-Wen Hsueh, and Chung-Ju Chang. Analysis of drx power saving with rrc states transition in lte networks. In *2015 European Conference on Networks and Communications (EuCNC)*, pages 301–305. IEEE, 2015.

[72] Chia-Wei Chang and Jyh-Cheng Chen. Adjustable extended discontinuous reception cycle for idle-state users in lte-a. *IEEE Communications Letters*, 20(11):2288–2291, 2016.

[73] Galini Tsoukaneri, Franscisco Garcia, and Mahesh K Marina. Narrowband iot device energy consumption characterization and optimizations. In *EWSN*, pages 1–12, 2020.

[74] Chun Yeow Yeoh, Abdullah bin Man, Qazi Mamoon Ashraf, and Ahmad Kamsani Samingan. Experimental assessment of battery lifetime for commercial off-the-shelf nb-iot module. In *2018 20th international conference on advanced communication technology (icact)*, pages 223–228. IEEE, 2018.

[75] Pilar Andres-Maldonado, Mads Lauridsen, Pablo Ameigeiras, and Juan M Lopez-Soler. Analytical modeling and experimental validation of nb-iot device energy consumption. *IEEE Internet of Things Journal*, 6(3):5691–5701, 2019.

[76] Pilar Andres-Maldonado, Pablo Ameigeiras, Jonathan Prados-Garzon, Juan J Ramos-Munoz, and Juan M Lopez-Soler. Optimized lte data transmission procedures for iot: Device side energy consumption analysis. In *2017 IEEE International Conference on Communications Workshops (ICC Workshops)*, pages 540–545. IEEE, 2017.

[77] Mohieddine El Soussi, Pouria Zand, Frank Pasveer, and Guido Dolmans. Evaluating the performance of emtc and nb-iot for smart city applications. In *2018 ieee international conference on communications (icc)*, pages 1–7. IEEE, 2018.

[78] Pilar Andres-Maldonado, Pablo Ameigeiras, Jonathan Prados-Garzon, Jorge Navarro-Ortiz, and Juan M Lopez-Soler. Narrowband iot data transmission procedures for massive machine-type communications. *Ieee Network*, 31(6):8–15, 2017.

[79] S Thomas Valerrian Pasca, B Akilesh, Arjun V Anand, and Bheemarjuna Reddy Tamma. A ns-3 module for lte ue energy consumption. In *2016 IEEE International Conference on Advanced Networks and Telecommunications Systems (ANTS)*, pages 1–6. IEEE, 2016.

[80] Subho Shankar Basu, Ashish Kumar Sultania, Jeroen Famaey, and Jeroen Hoebeke. Experimental performance evaluation of nb-iot. In *2019 International Conference on Wireless and Mobile Computing, Networking and Communications (WiMob)*, pages 1–6. IEEE, 2019.

[81] Konstantin Mikhaylov, Martin Stusek, Pavel Masek, Vitaly Petrov, Juha Petajajarvi, Sergey Andreev, Jiri Pokorny, Jiri Hosek, Ari Pouttu, and Yevgeni Koucheryavy. Multi-rat lpwan in smart cities: Trial of lorawan and nb-iot integration. In *2018 IEEE International Conference on Communications (ICC)*, pages 1–6. IEEE, 2018.

[82] Haibin Zhang, Jianpeng Li, Bo Wen, Yijie Xun, and Jiajia Liu. Connecting intelligent things in smart hospitals using nb-iot. *IEEE Internet of Things Journal*, 5(3):1550–1560, 2018.

[83] Mohammad Wazid, Ashok Kumar Das, and Youngho Park. Blockchain-envisioned secure authentication approach in aiot: Applications, challenges, and future research. *Wireless Communications and Mobile Computing*, 2021, 2021.

[84] Ahmed Elhamy Mostafa, Yong Zhou, and Vincent WS Wong. Connectivity maximization for narrowband iot systems with noma. In *2017 IEEE International Conference on Communications (ICC)*, pages 1–6. IEEE, 2017.

[85] Sha Hu, Axel Berg, Xuhong Li, and Fredrik Rusek. Improving the performance of otdoa based positioning in nb-iot systems. In *GLOBECOM 2017-2017 IEEE Global Communications Conference*, pages 1–7. IEEE, 2017.

[86] Leonardo Militano, Antonino Orsino, Giuseppe Araniti, and Antonio Iera. Nb-iot for d2d-enhanced content uploading with social trustworthiness in 5g systems. *Future Internet*, 9(3):31, 2017.

[87] Markets and Markets. Edge ai hardware market with covid-19 impact analysis device, processor (cpu, gpu, and asics), end user, function (training and inference), power (less than 1w, 1-3 w, 3-5 w, 5-10w and more than 10w) and region - global forecast to 2026, August 2021.

[88] Congduc Pham. Low-cost, low-power and long-range image sensor for visual surveillance. In *Proceedings of the 2nd Workshop on Experiences in the Design and Implementation of Smart Objects*, pages 35–40, 2016.

[89] Akram H Jebril, Aduwati Sali, Alyani Ismail, and Mohd Fadlee A Rasid. Overcoming limitations of lora physical layer in image transmission. *Sensors*, 18(10):3257, 2018.

[90] Tonghao Chen, Derek Eager, and Dwight Makaroff. Efficient image transmission using lora technology in agricultural monitoring iot systems. In *2019 International Conference on Internet of Things (iThings) and IEEE Green Computing and Communications (GreenCom) and IEEE Cyber, Physical and Social Computing (CPSCom) and IEEE Smart Data (SmartData)*, pages 937–944. IEEE, 2019.

[91] Mookeun Ji, Juyeon Yoon, Jeongwoo Choo, Minki Jang, and Anthony Smith. Lora-based visual monitoring scheme for agriculture iot. In *2019 IEEE Sensors Applications Symposium (SAS)*, pages 1–6. IEEE, 2019.

[92] Ching-Chung Wei, Shu-Ting Chen, and Pei-Yi Su. Image transmission using lora technology with various spreading factors. In *2019 2nd World Symposium on Communication Engineering (WSCE)*, pages 48–52. IEEE, 2019.

[93] Ruslan Kirichek, Van-Dai Pham, Aleksey Kolechkin, Mahmood Al-Bahri, and Alexander Paramonov. Transfer of multimedia data via lora. In *Internet of Things, Smart Spaces, and Next Generation Networks and Systems*, pages 708–720. Springer, 2017.

[94] Congduc Pham. Robust csma for long-range lora transmissions with image sensing devices. In *2018 Wireless Days (WD)*, pages 116–122. IEEE, 2018.

[95] Chunlei Fan and Qun Ding. A novel wireless visual sensor network protocol based on lora modulation. *International Journal of Distributed Sensor Networks*, 14(3):1550147718765980, 2018.

[96] Oihane Gómez-Carmona, Diego Casado-Mansilla, Frank Alexander Kraemer, Diego López-de Ipiña, and Javier García-Zubia. Exploring the computational cost of machine learning at the edge for human-centric internet of things. *Future Generation Computer Systems*, 112:670–683, 2020.

[97] Yohann Rioual, Johann Laurent, Eric Senn, and Jean-Philippe Diguet. Reinforcement learning strategies for energy management in low power iot. In *2017 International Conference on Computational Science and Computational Intelligence (CSCI)*, pages 1377–1382. IEEE, 2017.

[98] Lei Lei, Huijuan Xu, Xiong Xiong, Kan Zheng, and Wei Xiang. Joint computation offloading and multiuser scheduling using approximate dynamic programming in nb-iot edge computing system. *IEEE Internet of Things Journal*, 6(3):5345–5362, 2019.

[99] Min Chen, Wei Li, Giancarlo Fortino, Yixue Hao, Long Hu, and Iztok Humar. A dynamic service migration mechanism in edge cognitive computing. *ACM Transactions on Internet Technology (TOIT)*, 19(2):1–15, 2019.

[100] Xinchen Lyu, Hui Tian, Li Jiang, Alexey Vinel, Sabita Maharjan, Stein Gjessing, and Yan Zhang. Selective offloading in mobile edge computing for the green internet of things. *IEEE Network*, 32(1):54–60, 2018.

[101] Farzad Samie, Vasileios Tsoutsouras, Lars Bauer, Sotirios Xydis, Dimitrios Soudris, and Jörg Henkel. Oops: Optimizing operation-mode selection for iot edge devices. *ACM Transactions on Internet Technology (TOIT)*, 19(2):1–21, 2019.

[102] Farzad Samie, Lars Bauer, and Jörg Henkel. From cloud down to things: An overview of machine learning in internet of things. *IEEE Internet of Things Journal*, 6(3):4921–4934, 2019.

[103] Imran A Zualkernan, Salam Dhou, Jacky Judas, Ali Reza Sajun, Brylle Ryan Gomez, Lana Alhaj Hussain, and Dara Sakhnini. Towards an iot-based deep learning architecture for camera trap image classification. In *2020 IEEE Global Conference on Artificial Intelligence and Internet of Things (GCAIoT)*, pages 1–6. IEEE, 2020.

[104] Brian H Curtin and Suzanne J Matthews. Deep learning for inexpensive image classification of wildlife on the raspberry pi. In *2019 IEEE 10th Annual Ubiquitous Computing, Electronics & Mobile Communication Conference (UEMCON)*, pages 0082–0087. IEEE, 2019.

[105] Nitis Monburinon, Salahuddin Muhammad Salim Zabir, Natthasak Vechprasit, Satoshi Utsumi, and Norio Shiratori. A novel hierarchical edge computing solution based on deep learning for distributed image recognition in iot systems. In *2019 4th International Conference on Information Technology (InCIT)*, pages 294–299. IEEE, 2019.

[106] Param Popat, Prasham Sheth, and Swati Jain. Animal/object identification using deep learning on raspberry pi. In *Information and Communication Technology for Intelligent Systems*, pages 319–327. Springer, 2019.

[107] Farzad Samie, Lars Bauer, and Jörg Henkel. Hierarchical classification for constrained iot devices: A case study on human activity recognition. *IEEE Internet of Things Journal*, 7(9):8287–8295, 2020.

[108] Hongxu Yin, Zeyu Wang, and Niraj K Jha. A hierarchical inference model for internet-of-things. *IEEE Transactions on Multi-Scale Computing Systems*, 4(3):260–271, 2018.

[109] Baibhab Chatterjee, Dong-Hyun Seo, Shramana Chakraborty, Shitij Avlani, Xiaofan Jiang, Heng Zhang, Mustafa Abdallah, Nithin Raghunathan, Charilaos Mousoulis, Ali Shakouri, et al. Context-aware collaborative intelligence with spatio-temporal in-sensor-analytics for efficient communication in a large-area iot testbed. *IEEE Internet of Things Journal*, 2020.

[110] Ruben M Sandoval, Antonio-Javier Garcia-Sanchez, and Joan Garcia-Haro. Optimizing and updating lora communication parameters: A machine learning approach. *IEEE Transactions on Network and Service Management*, 16(3):884–895, 2019.

[111] Amin Azari and Cicek Cavdar. Self-organized low-power iot networks: A distributed learning approach. In *2018 IEEE Global Communications Conference (GLOBECOM)*, pages 1–7. IEEE, 2018.

[112] Vignesh Mahalingam Suresh, Rishi Sidhu, Prateek Karkare, Aakash Patil, Zhang Lei, and Arindam Basu. Powering the iot through embedded machine learning and lora. In *2018 IEEE 4th World Forum on Internet of Things (WF-IoT)*, pages 349–354. IEEE, 2018.

[113] 3GPP TS 23.401. 3GPP, "TS 23.401 GPRS enhancements for Evolved Universal Terrestrial Radio Access Network access," Rel 16 V16.6.0 (2020-03). 2020.

[114] Jonathan Tournier, François Lesueur, Frédéric Le Mouël, Laurent Guyon, and Hicham Ben-Hassine. A survey of iot protocols and their security issues through the lens of a generic iot stack. *Internet of Things*, page 100264, 2020.

[115] Ivan Ganchev, Zhanlin Ji, and Máirtín O'Droma. A generic iot architecture for smart cities. 2014.

[116] Yulong Shen, Tao Zhang, Yongzhi Wang, Hua Wang, and Xiaohong Jiang. Microthings: A generic iot architecture for flexible data aggregation and scalable service cooperation. *IEEE Communications Magazine*, 55(9):86–93, 2017.

[117] BG96 AT Commands Manual. `https://docs.particle.io/assets/pdfs/Quectel_BG96_AT_Commands_Manual_V2.1.pdf`. Accessed: 2020-01-01.

[118] booktitle=2019 IEEE 17th International Conference on Industrial Informatics (INDIN) Sikora, Axel and Schappacher, Manuel and Amjad, Zubair and others. Test and Measurement of LPWAN and Cellular IoT Networks in a Unified Testbed. volume 1, pages 1521–1527. IEEE, 2019.

[119] Sikora, Axel and others. Performance Measurements of Narrowband-IoT Network in Emulated and Field Testbeds. In *2019 10th IEEE International Conference on Intelligent Data Acquisition and Advanced Computing Systems: Technology and Applications (IDAACS)*, volume 2, pages 780–785. IEEE, 2019.

[120] Mobile Signal Strength Recommendations. `http://www.3gpp.org/specifications/releases`. Accessed: 2021-04-05.

[121] Sigfox: Link Quality Indicator. `https://support.sigfox.com/docs/link-quality:-general-knowledge`. Accessed: 2021-04-05.

[122] Nitin Naik. LPWAN technologies for IoT systems: choice between ultra narrow band and spread spectrum. In *2018 IEEE International Systems Engineering Symposium (ISSE)*, pages 1–8. IEEE, 2018.

[123] Mingjie Liu, Xianhao Wang, Anjian Zhou, Xiuyuan Fu, Yiwei Ma, and Changhao Piao. Uav-yolo: Small object detection on unmanned aerial vehicle perspective. *Sensors*, 20(8):2238, 2020.

[124] Vittorio Mazzia, Aleem Khaliq, Francesco Salvetti, and Marcello Chiaberge. Real-time apple detection system using embedded systems with hardware accelerators: an edge ai application. *IEEE Access*, 8:9102–9114, 2020.

[125] Current/power comparisons of the various RPi Models. `https://www.raspberrypi.org/documentation/hardware/raspberrypi/power/ README.md//` , note = Accessed: 2020-01-01.

[126] Albert S Huang and Larry Rudolph. *Bluetooth essentials for programmers*. Cambridge University Press, 2007.

[127] Joseph Redmon, Santosh Divvala, Ross Girshick, and Ali Farhadi. You only look once: Unified, real-time object detection. In *Proceedings of the IEEE conference on computer vision and pattern recognition*, pages 779–788, 2016.

[128] YOLO: Real-Time Object Detection. `https://pjreddie.com/darknet/yolo/`. Accessed: 2020-01-01.

[129] YOLOv3. `https://github.com/pythonlessons/TensorFlow-2.x-YOLOv3`. Accessed: 2020-01-01.

[130] Jeongyeup Paek and JeongGil Ko. $k$-means clustering-based data compression scheme for wireless imaging sensor networks. *IEEE Systems Journal*, 11(4):2652–2662, 2015.

[131] Binary Encoding Schemes. `https://docs.python.org/3/library/base64.html`. Accessed: 2020-01-01.

[132] Andrew Wessels, Mike Purvis, Jahrain Jackson, and Syed Rahman. Remote data visualization through websockets. In *2011 Eighth International Conference on Information Technology: New Generations*, pages 1050–1051. IEEE, 2011.

[133] Somchai Wen and Wen Dang. Research on base64 encoding algorithm and php implementation. In *2018 26th International Conference on Geoinformatics*, pages 1–5. IEEE, 2018.

[134] MQTT Architecture. `https://mqtt.org/`. Accessed: 2020-01-01.

[135] Gaston C Hillar. *MQTT Essentials-A lightweight IoT protocol*. Packt Publishing Ltd, 2017.

[136] MQTT_Application_Note_Quectel_BG96. `https://sixfab.com/wp-content/uploads/2018/09/Quectel_BG96_MQTT_Application_Note_V1.0.pdf`. Accessed: 2020-01-01.

[137] MQTT Broker. `https://github.com/beerfactory/hbmqtt`. Accessed: 2020-01-01.

[138] AR Muzata, VA Pershina, MS Stepanov, Faurdoir Ndimumahoro, and Juvent Ndayikunda. The modeling of elastic traffic transmisson by the mobile network with nb-iot functionality. In *2021 Systems of Signals Generating and Processing in the Field of on Board Communications*, pages 1–7. IEEE, 2021.

[139] Sergey N Stepanov and Mikhail S Stepanov. Efficient algorithm for evaluating the required volume of resource in wireless communication systems under joint servicing of heterogeneous traffic for the internet of things. *Automation and Remote Control*, 80(11):2017–2032, 2019.

[140] Sergey N Stepanov, Mikhail S Stepanov, Umer Andrabi, and Juvent Ndayikunda. The analysis of resource sharing for heterogenous traffic streams over 3gpp lte with nb-iot functionality. In *International Conference on Distributed Computer and Communication Networks*, pages 422–435. Springer, 2020.

[141] Budi Syihabuddin, Farhan Fathir Lanang, Agus D Prasetyo, and Ratna Mayasari. A bandwidth enhancement of the bowtie antenna using its taper-cut angle optimization for iot applications. In *2021 IEEE 7th International Conference on Smart Instrumentation, Measurement and Applications (ICSIMA)*, pages 1–4. IEEE, 2021.

[142] Daniel Jaramillo-Ramirez and Manuel Perez. Spectrum demand forecasting for iot services. *Future Internet*, 13(9):232, 2021.

[143] Yuan Zheng, Jiabin Wang, Qinghua Chen, and Yihua Zhu. Retransmission number aware channel access scheme for ieee 802.11 ax based wlan. *Chinese Journal of Electronics*, 29(2):351–360, 2020.

[144] Nan Jiang, Yansha Deng, Massimo Condoluci, Weisi Guo, Arumugam Nallanathan, and Mischa Dohler. Rach preamble repetition in nb-iot network. *IEEE Communications Letters*, 22(6):1244–1247, 2018.

[145] Ruki Harwahyu, Ray-Guang Cheng, Wan-Jung Tsai, Jeng-Kuang Hwang, and Giuseppe Bianchi. Repetitions versus retransmissions: Tradeoff in configuring nb-iot random access channels. *IEEE Internet of Things Journal*, 6(2):3796–3805, 2019.

[146] Tahrat Tazrin. *Toward lightweight fusion of AI logic and EEG sensors to enable ultra edge-based EEG analytics on IoT devices*. PhD thesis, 2021.

[147] Claudio Savaglio, Pasquale Pace, Gianluca Aloi, Antonio Liotta, and Giancarlo Fortino. Lightweight reinforcement learning for energy efficient communications in wireless sensor networks. *IEEE Access*, 7:29355–29364, 2019.

[148] Zhihong Tian, Shen Su, Wei Shi, Xiaojiang Du, Mohsen Guizani, and Xiang Yu. A data-driven method for future internet route decision modeling. *Future Generation Computer Systems*, 95:212–220, 2019.

[149] Shunbo Lei, Yunhe Hou, Feng Qiu, and Jie Yan. Identification of critical switches for integrating renewable distributed generation by dynamic network reconfiguration. *IEEE Transactions on Sustainable Energy*, 9(1):420–432, 2017.

[150] Tania Panayiotou, Konstantinos Manousakis, Sotirios P Chatzis, and Georgios Ellinas. A data-driven bandwidth allocation framework with qos considerations for eons. *Journal of Lightwave Technology*, 37(9):1853–1864, 2019.

[151] Mishal Thapa, Bodiuzzaman Jony, Sameer B Mulani, and Samit Roy. Development of intelligent and predictive self-healing composite structures using dynamic data-driven applications systems. In *Handbook of Dynamic Data Driven Applications Systems*, pages 173–191. Springer, 2018.

# Acknowledgements

## Abstract
## Narrowband Internet of Things (NB-IoT): from Radio Network Coverage to Device Energy Consumption Modeling and Energy-Efficient Application

NB-IoT is a 3GPP low-power wide-area network (LPWAN) wireless communication technology that was launched as part of the 4G LTE specifications and that will continue to evolve as part of the 5G specifications. NB-IoT offers attractive features that include lower bandwidth and extended coverage with deep penetrations, power-saving mechanisms for longer device battery-lifetime, appropriate throughput with acceptable latency, and ease of integration into the existing LTE infrastructure, which all make it a strong contender LPWAN technology for implementing massive machine type communications (mMTC). Yet, as a relatively new technology, NB-IoT raises several questions and faces many challenges when it comes to its on-field performances and practical implementations.

While the existing literature on NB-IoT is replete with theoretical and/or analytical models, as well as simulation and emulation based analyses, a comprehensive real-life investigation of the performance of NB-IoT technology from various perspectives is still missing. Regarding its on-field coverage performance, an empirical coverage analysis of the NB-IoT technology in different environments is much needed for gaining a better understanding of its coverage class levels and subsequently achieving better deployment planning. In terms of its device energy consumption, NB-IoT is mostly underestimated for its control and signaling overheads, especially in lower coverage areas. This calls for a thorough investigation of the energy consumption profiling of an NB-IoT radio in different scenarios while in actual operation under a real NB-IoT network. Finally, from the perspective of real-life implementations, there hardly exist practical applications that combine NB-IoT with other state-of-the-art technologies to expand its use-cases that otherwise would be difficult for NB-IoT alone to deliver efficiently.

In line with these challenges, this PhD thesis presents three main contributions:

Firstly, towards a practical NB-IoT network coverage performance, this work proposes an empirical investigation of the NB-IoT network coverage by deploying real devices from one of the main NB-IoT module vendors (i.e., Quectel) and utilizing the test networks of the two mobile network operators (MNOs) that provide NB-IoT service in Estonia. The obtained results from these coverage campaigns show that NB-IoT provides a good network connectivity in an indoor and outdoor environments, whereas its coverage in deep-indoor environments is considerably moderate. Thus, NB-IoT can provide a good network coverage in almost all practical scenarios and can satisfy the IoT needs of today and tomorrow.

Secondly, towards NB-IoT device energy consumption, this work presents a thorough investigation of the energy consumption profiling of the Radio Resource Control (RRC) communication protocol between an NB-IoT radio and a cellular base-station (BS). Using two commercial-off-the-shelf (CoTS) NB-IoT radios operating under the NB-IoT test-networks from two MNOS in Tallin, Estonia, an empirical baseline energy consumption model for an NB-IoT radio is proposed. The validation results for this model indicate that the proposed empirical model accurately depicts the baseline energy consumption of an NB-IoT radio transceiver while operating under a real NB-IoT test-network and at different coverage class levels. The error of the proposed model ranges from as low as 0.33% for longer durations (e.g. when the radio has to activate after several hours or more), and reaches up to approximately 15.38% for shorter durations (e.g. when the radio has to activate after several minutes to hours). Since the majority of NB-IoT applications are intended for longer duration scenarios, the error will lie on the smaller end, as also indicated

by the sensitivity analysis of the model.

Finally, this work builds upon the above gained practical knowledge for combining the NB-IoT technology with Machine Learning (ML) technology to help reduce the communication budget of an NB-IoT radio through edge (local) computations. The detailed computations-communication trade-offs analyses show that local computations can play a pivotal role towards relaxing the channel occupancy from an individual NB-IoT radio, reducing its energy consumption and minimizing the overall transmission time of the data over the NB-IoT network. The on-field results indicate up to 93% reductions in the number of NB-IoT radio transmissions, up to 90.5% reductions in the NB-IoT radio energy consumption, and up to 90% reductions in the data transmission time.

## Kokkuvõte

## Kitsaribaline asjade internet (NB-IoT): raadiovõrgu katvusest seadme energiatarbe modelleerimise ja energiasäästliku rakenduseni

NB-IoT on 3GPP poolt standardiseeritud madala energiatarbe ja suure tegevusraadiusega raadiosidetehnoloogia (LPWAN), mis võeti kasutusse 4G LTE spetsifikatsiooni osana ning areneb edasi 5G standardite osana. NB-IoT evib atraktiivseid omadusi nagu kitsam raadiosignaali ribalaius ja suurem tegevuskaugus ning keskkonnaläbivus, energiasäästumehhanismid seadme patarei pikemaks elueaks, sobiv andmete läbilaskemaht koos vastuvõetava hilistumisega, lihtne integreeritavus olemasolevatesse LTE taristutesse – omadused, mis loovad ühiselt tugeva LPWAN tehnoloogia kandidaadi massiivse masinate vahelise side (mMTC) realisatsioonidele. Siiski, olles suhteliselt uus tehnoloogia, tõstatab NB-IoT mitmeid küsimusi ning seisab silmitsi paljude väljakutsetega, mis on seotud rakendusliku jõudluse ja praktiliste realisatsioonidega.

Ehkki olemasolev kirjandus on märkimisväärselt täidetud NB-IoT teoreetiliste ja/või analüütiliste mudelitega, samuti simulatsioonidel baseeruvate analüüsidega, siis kõikehõlmav reaaleluline uuring NB-IoT tehnoloogia jõudlusest erinevatest aspektidest lähtudes endiselt puudub.Seoses reaalsete paigaldiste leviala kvaliteedi hindamisega on empiiriline NB-IoT tehnoloogia leviala analüüs erinevates keskkondades ülimalt vajalik, et paremini mõista levikvaliteeti ja sellest lähtudes saavutada parem paigaldise planeerimine. Energiatarbe osas on NB-IoT puhul enamasti alahinnatud juhtimise ja signaliseerimisega kaasnevat lisaenergiakulu, seda eriti madalama levikvaliteediga piirkondades. See nõuab NB-IoT raadio energiatarbe põhjalikku profileerimist erinevates stsenaariumites reaalse töö korral NB-IoT võrgus. Lõpuks, lähtudes reaalsetest olukordadest, ei leidu praktilisi rakendusi, mis kombineerivad NB-IoT-d teiste moodsate tehnoloogiatega soovitud kasutusjuhtude laiendamiseks, ilma milleta NB-IoT üksi ei suuda töötada efektiivselt.

Kooskõlas nende väljakutsetega on käesoleval doktoritööl kolm peamist tulemust:

Esmalt, reaalse NB-IoT võrgu leviala hindamise osas, pakub töö välja empiirilise uuringu leviala hindamiseks, mille puhul paigaldatakse reaalsed NB-IoT moodulid, tuntud tootjalt (näiteks Quectelilt) ja kasutatakse testvõrke kahelt mobiilvõrgu operaatorilt, mis pakuvad NB-IoT võrguteenust Eestis. Saadud tulemused leviala uuringutest näitavad, et NB-IoT pakub head võrgu ühenduvust sise- ja välisruumides, samas kui katvus sügaval siseruumides on pigem mõõdukas. Seega, NB-IoT suudab pakkuda head võrgu leviala peaaegu kõigi praktiliste kasutusjuhtude puhul ja katab asjade interneti (IoT) vajadusi nii täna kui ka homme.

Teiseks, NB-IoT seadmete energiatarbe osas, esitab töö põhjaliku uuringu NB-IoT raadio ja baasjaama vahelise raadioressursi juhtimise sideprotokolliga seotud energiatarbe profiilist. Kasutades kahte standardset NB-IoT raadioseadet kahe mobiilioperaatori testvõrkudes Tallinnas, on välja pakutud empiiriline energiatarbe baasmudel NB-IoT raadiole. Valideeritud katsetulemused tõestavad, et välja pakutud empiiriline mudel kirjeldab täpselt NB-IoT raadiotransiiveri baasenergiatarvet reaalses NB-IoT katsevõrgus erinevate levitugevuste korral. Pakutud mudeli viga varieerus madalast 0.33%-st pikematel ajavahemikel (näiteks kui raadio aktiveerub peale mitut või rohkemat tundi) ja jõuab kuni umbes 15.38%-ni lühematel ajavahemikel (näiteks kui raadio peab aktiveeruma peale mõnd minutit kuni tundi). Kuna enamus NB-IoT rakendusi on ette nähtud pikaajaliste stsenaariumide jaoks, siis viga asetseb piirkonna väiksemas otsas, mis samuti nähtus mudeli tundlikkuse analüüsist.

Lõpuks, käesolev töö kasutab ülaltoodud praktilisi teadmisi, et kombineerida NB-IoT

tehnoloogiat masinõppega aitamaks vähendada NB-IoT raadio sidevajadust servaarvutuste rakendamise abil. Detailne arvutuste ja side omavahelise jaotuse optimeerimise analüüs näitab, et kohalikud arvutused võivad mängida kesket rolli vähendades sidekanali hõivatust üksiku NB-IoT seadme poolt, vähendades selle energiatarvet ja üldist andmete saatmise aega üle NB-IoT võrgu. Saadud katsetulemused näitavad kuni 93% vähenemist NB-IoT raadioside seansside arvus, kuni 90.5% vähenemist NB-IoT raadio energiatarbes ja kuni 90% vähenemist andmeedastusajas.

# Appendix 1

**I**

Sikandar Zulqarnain Khan, Hassan Malik, Jeffrey Leonel Redondo Sarmiento, Muhammad Mahtab Alam, and Yannick Le Moullec. Dorm: Narrowband iot development platform and indoor deployment coverage analysis. *Procedia Computer Science*, 151:1084–1091, 2019

The 2nd International Workshop on Recent Advances in Cellular Technologies and 5G for IoT Environments (RACT-5G-IoT 2019)

April 29 – May 2, 2019, Leuven, Belgium

# DORM: Narrowband IoT Development Platform and Indoor Deployment Coverage Analysis

Sikandar Zulqarnain Khan, Hassan Malik, Jeffrey Leonel Redondo Sarmiento, Muhammad Mahtab Alam, Yannick Le Moullec

*Thomas Johann Seebeck Department of Electronics, Tallinn University of Technology, Tallinn, Estonia.*
*Email: {sikandar.khan, hassan.malik, jeredo, muhammad.alam, yannick.lemoullec}@taltech.ee*

## Abstract

The development of DORM (integrateD cOmpact naRrowband platforM) node is presented that combines low cost and low power components in a multi-layer architecture to support versatile NB-IoT applications. In our proposed DORM node, the processing component provides an interface to a variety of sensors and the radio component provides connectivity to the IoT cloud as required by IoT applications. Furthermore, an overview of our NB-IoT test network is presented that is deployed at Tallinn University of Technology (TalTech) campus, Estonia with a detailed description of its various functionality layers. In addition, an in-field investigation of the coverage of our NB-IoT system is made whereby our DORM nodes are deployed across the TalTech campus so as to explore its connectivity performance and possible issues in an indoor scenario. We made empirical measurements on NB-IoT coverage for different elevation levels, a key performance indicator that most of the operators would be interested in. We obtained averaged SNR and RSSI values in the range of 18 dB to 23 dB and -65 dBm to -70 dBm, respectively. Our obtained results show that our NB-IoT system provides an excellent connectivity in indoor environments and can satisfy IoT application requirements. However, small variations in these SNR and RSSI values are observed at different elevation levels possibly due to positioning of the measuring nodes, proximity of the antenna with respect to the base-station, building structure and its construction material and the surrounding environment of the placement of our DORM nodes.

*Keywords:* NB-IoT development platform; NB-IoT coverage; NB-IoT Cloud; Measurement campaign; Cumulocity server.

---

\* Sikandar Zulqarnain Khan. Tel.: +372-5637-1180.
*E-mail address: sikandar.khan@taltech.ee*

## 1. Introduction

LPWAN includes diverse competing technologies such as Sigfox, LoRa, LTE-M, NB-IoT, Ingenu, and Telensa, etc., [1-2], but NB-IoT outperforms all other LPWAN technologies in terms of coverage, energy efficiency, and cost by utilizing the existing cellular infrastructure [3]. NB-IoT is a variant of the long-term evolution (LTE) that uses 180 kHz bandwidth and corresponds to one physical resource block (PRB) of LTE. NB-IoT can be deployed in three different modes, i.e., in-band and guard-band within the existing LTE band, and standalone mode outside the LTE band. The choice of mode selection is critical and has an impact on the overall network coverage, quality of service (QoS) as well as capital expenditure (Capex). To support the flexibility and switching between these modes, NB-IoT extensively uses the LTE design such as OFDM in downlink and single carrier frequency-division multiple access (SC-FDMA) in the uplink. However, many design changes such as retransmission for coverage extensions, scheduling delay for reducing computational complexity, power boosting for downlink transmissions have been introduced to ensure its best coexistence with the existing LTE infrastructure and to fulfil the need of IoT applications. The detailed design changes with a key insight on the technology can be found in the standard in [4].

NB-IoT allows long-range communications at low data rates and is most suitable for delay-tolerant applications. It can provide a data rate of 250 Kbps for multi-tone downlink communication and 20 Kbps for single-tone uplink communications. For data collection at the lowest layer, NB-IoT utilizes end-nodes that are powered by chargeable batteries and are embedded with sensors for gathering data from their surroundings.

The device complexity of NB-IoT nodes is reduced as compared to other unlicensed LPWAN technologies including LTE-Cat M1 devices for addressing the ultralow-power IoT applications. The NB-IoT nodes feature battery saving modes such as PSM and eDRX to achieve higher energy efficiency and longer battery life where the future NB-IoT nodes are expected to have a battery life of more than 10 years as per the standard.

There are already existing NB-IoT deployments around the world, such as NB-IoT at sea in Norway [5], Connected Sheep in Norway [6], Smart metering and tracking in Brazil [7], Smart City in Las Vegas [8], and 346 NB-IoT covered cities in China [9]. These examples illustrate the fast growing interest in and adoption of NB-IoT for practical use-cases. However, the information available about the underlying platforms is focused on the use-cases and do not present details about the implementation at the device and network levels. Thus, so far, publicly available details on NB-IoT real-life performance are scarce.

As part of our ongoing research efforts on NB-IoT, our group has built and deployed a test platform comprising 50 NB-IoT (DORM) nodes, a commercial base-station from Telia Eesti, and a cloud backend server to gain and share an in-depth understanding of NB-IoT. The goal of this paper is two-fold. Firstly, to develop an integrated (DORM) platform using commercial-off-the-shelf (COTS) hardware components to enable seamless multi-interface connectivity that can provide end-to-end solutions for NB-IoT applications. Secondly, we present preliminary experimental results that characterize the real-life performance of NB-IoT in an indoor scenario for different elevation levels by utilizing Telia's commercial base-station that is installed at the premises of TalTech campus. In particular, our results show the impact of different elevation levels on the performance of NB-IoT in an indoor scenario and the corresponding penetration losses that are investigated in details.

The rest of this paper is organized as follows. In Section II, we present our NB-IoT system setup that is installed at TalTech campus and we discuss its various functionality layers in detail. Section III presents the results generated by the NB-IoT system setup at the TalTech campus in terms of its coverage and connectivity. Section IV concludes this work with some future directions.

## 2. NB-IoT System Architecture installed at Tallinn University of Technology (TalTech) campus, Estonia.

A generic IoT system is comprised of a number of blocks to facilitate functionalities such as sensing and monitoring of the surroundings, exchange and communication of data, management and analysis of information, investigation and decision making, and storage and backup of data for future use. In this work, we present the NBIoT system setup that is deployed across TalTech campus and we discuss its various functionality layers as shown in Figure 1. The three layers of this NB-IoT system can be categorized as under:

1. Perception layer (DORM nodes are deployed across TalTech campus for sensing the surroundings.)
2. Network Layer (Telia's commercial Base-station is installed at TalTech campus that supports 5G network.)
3. Cloud Platform (Cumulocity server is setup for supporting and interfacing users' applications.)

DORM nodes are deployed across TalTech campus to collect data from their surroundings through dedicated sensors, packs the collected data into proper format, and transmit it to the next higher layer i-e., "Network Layer". At the "Network Layer", a commercial Base-station (BS) operated by Telia, supports LTE Cat-NB1 network to collect all the transmitted data from the deployed nodes and send it further to the highest layer of the NB-IoT system i-e., "Cloud Platform Server". The "Cloud Platform Server" provides an interface for secure communication between the NB-IoT Network and the users' applications, data analytics for decision making and data storage for backup and future use. In the subsections that follow, each of the layer of our NB-IoT system at TalTech campus is explained in details.
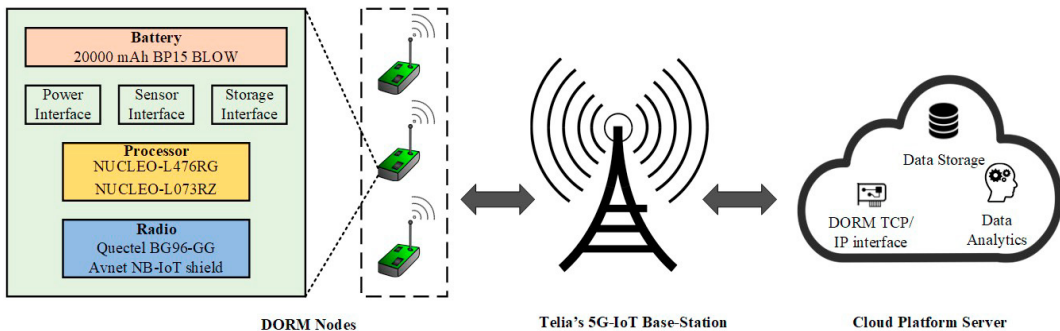


Figure 1: Architecture of NBIoT setup at Tallinn University of Technology (TalTech) campus, Estonia.

### 2.1. Perception Layer (DORM nodes)

Many enabling technologies are used to setup customizable IoT nodes that can collect data from their surroundings and sends it to the cloud for further analysis and investigation. Most developers opt for microcontroller-based boards such as Arduino, Nucleo, etc., that can collect and process the data coming from the sensors and a radio module such as Texas Instruments, Quectel, etc. to provide an Internet connection to the network or cloud. However, the choice of microcontrollers (MCUs) and radio modules is often very complex, due to the fact that a trade-off between costs, performances and functionalities is needed for each particular application.

The two versions of our DORM nodes are shown in Figure 2. They combine ultra-low-power STM32-based Nucleo boards (L476RG (Cortex M4) [10] or L073RZ (Cortex M0+) [11]) with Quectel BG96 chipset-based boards (Avnet Silica NB-IoT shield [12] or Quectel GSM/NB-IoT EVB Kit [13]) and are powered by an external 20000 mAh BP15 BLOW battery. The STM32-based Nucleo boards are used as the processing units as they are highly affordable and can be extended with a large number of hardware add-ons to seamlessly work with a wide range of sensors. The Quectel BG96 radio chipset features ultra-low power consumption and supports LTE Cat NB1 (i.e. 3GPP Release 13 NB-IoT) along with a set of industry-standard interfaces (such as USB/UART/I2C/Status Indicator) suitable for a wide range of IoT applications.
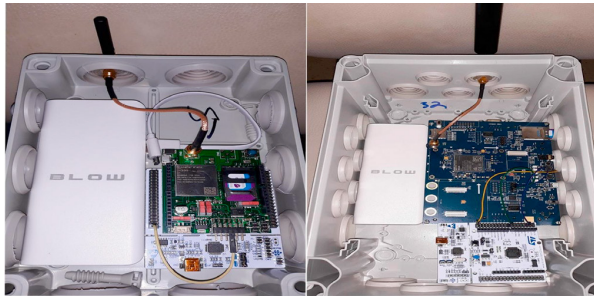
Figure 2: DORM nodes: Left: NUCLEO-L476RG board + Quectel BG96-GG Starter Kit.
Right: NUCLEO-L073RZ board + Avnet Silica NB-IoT Sensor Shield (BG96).

Inside our DORM nodes, the data collected by sensors is transferred to the STM32 microcontroller through dedicated interfaces where it is encapsulated into UDP packets format and sent to the BG96 module through UART interface. The BG96 module first establishes a secure connection with the BS and afterwards sends the data to the NB-IoT network. Figure 3 shows a snapshot of the QCOM interface where the BG96 module establishes an LTE Cat NB1 connection with the BS through the use of AT commands before sending any data to the network.
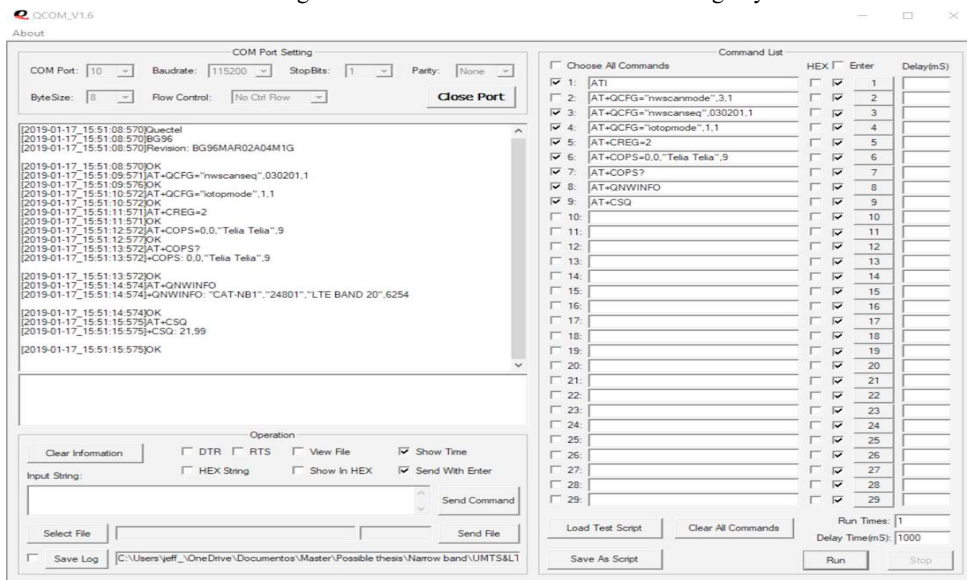


Figure 3: Set of AT commands used by BG96 module to establish connection with the BS.

The first (ATI) command delivers product information to the user which in our case is Quectel BG96 module. The second (AT+QCFG="nwscanmode") command specifies the RATs (Radio Access Technologies) to be searched where we have specified to look for LTE RAT only. The third command (AT+QCFG="nwscanseq") specifies the searching sequence of the available RATs where our search sequence is (e.g.: 030201) LTE Cat NB1, LTE Cat M1 and GSM. The next (AT+QCFG="iotopmode") command configures the Network Category to be searched under LTE RAT and we configure it for LTE Cat NB1. Afterwards, the (AT+CREG) command enables the network registration, and the AT+COPS commnd returns the currently selected network operator which in our case is Telia. Once registered with the network, the (AT+QNINFO) command indicates the network information such as the access technology selected, the operator, and the band selected. Finally, (AT+CSQ) command provides the signal quality in terms of received signal strength (RSSI) of the network. Further information on these and related AT commands can be found in [14].

## 2.2. Cloud Layer (Cumulocity Application)

In a typical IoT system, the cloud analyse all the data traffic that comes from the IoT nodes through the gateway network to give an accurate feedback to the user (application). Predictive analytics in data mining could be used for analysing and predicting the possible outcomes. The cloud services must also guarantee the security and QoS capabilities where the data must be stored in a safe and secure storage for future needs. Our cloud platform in the NB-IoT setup at TalTech campus features a secure communication between the NB-IoT Network and the Cumulocity backend server that provides a user interface for IoT applications. The data that is received from any particular DORM node is securely stored on the Cumulocity backend; where a trace of all the previous data with device ID, location and timings is kept securely. A snapshot of the Cumulocity online dashboard for the SNR and RSSI values received from DORM node 15 (iot_tester 15) at particular date and time is shown in Figure 4.
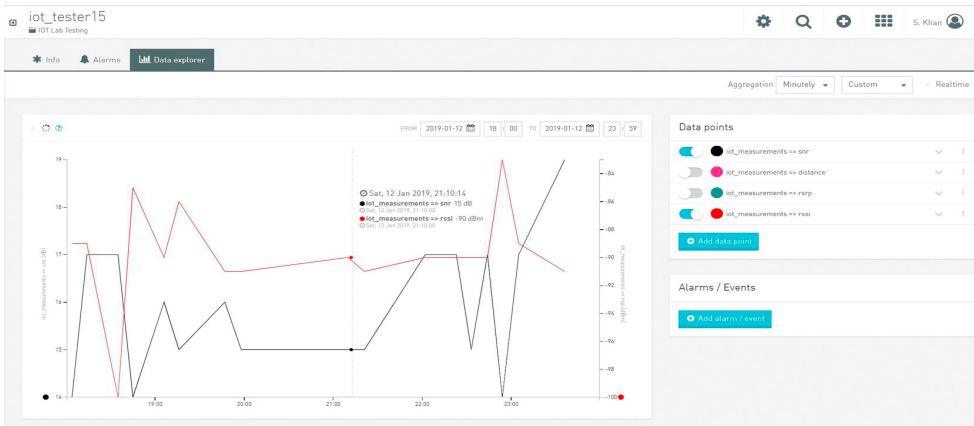


Figure 4: The SNR and RSSI values received at the Cumulocity server from IoT Tester 15 on Sat, 12 Jan 2019 from 18:00-23:59 respectively.

## 3. Results generated by our NB-IoT System at Tallinn University of Technology (TalTech) campus, Estonia.

With an aim to investigate the indoor coverage of our NB-IoT system at TalTech campus, we choose an observation point inside our building, hosting Thomas Johann Seebeck Department that is at a distance of 300 m from the BS, as shown in Figure 5 (left). DORM nodes were deployed at different elevation levels (floors) of this five-story building at almost the same location where the height of these floors from ground are: 1st floor is 0 m, 2nd floor is 03 m, 3rd floor is at 09 m, 4th floor is at 12 m, and 5th floor is at 15 m, respectively. Furthermore, the Baste-station is at a height of around 20 m from the ground as shown in Figure 5 (right).
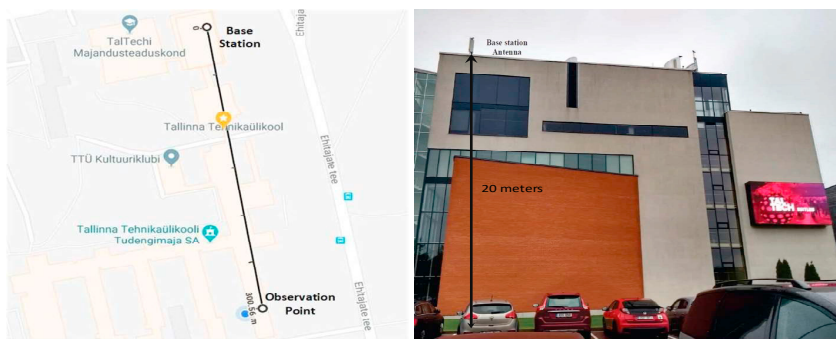


Figure 5: Our observation point is 300m away from the BS as shown by Google Maps (left) where our BS is 20m above the ground (right).

Table 1 presents the average results obtained from DORM nodes at different elevation levels (floors) for a duration of 6 hours in the morning (08:00-13:59) and a duration of 6 hours in the evening (18:00-23:59) at an observation point that is 300 m away from the BS. The columns for Signal Strength in Table 1 are derived and based on the RSSI scale values for NB-IoT presented in [15] and summarized in Table 2. The obtained SNR and RSSI values show that our installed NB-IoT system at TalTech campus provides good connectivity to satisfy the IoT application requirements in indoor environments for different elevation levels.

Table 1: Average SNR and RSSI values obtained at 300m from the Base-station for different elevation levels.

| Floor Number (Elevation from the ground) | Observation point at 300 meters from the BS | | | | | |
| | Morning (08:00-13:59) | | | Evening (18:00-23:59) | | |
| | Avg. SNR (dB) | Avg. RSSI (dBm) | Signal Strength | Avg. SNR (dB) | Avg. RSSI (dBm) | Signal Strength |
| 5th Floor (15 m) | 18.11 | -65.75 | Good | 19.13 | -64.93 | Good |
| 4th Floor (12 m) | 18.68 | -67.50 | Good | 19.74 | -66.61 | Good |
| 3rd Floor (9 m) | 21.12 | -68.04 | Good | 21.33 | -67.71 | Good |
| 2nd Floor (3 m) | 21.28 | -69.48 | Good | 21.75 | -68.92 | Good |
| 1st Floor (0 m) | 23.58 | -70.20 | Good | 23.74 | -69.70 | Good |

Table 2: NB-IoT Signal Strength (RSSI) reference values [15].

| LTE | NB-IoT | Signal Strength |
| --- | --- | --- |
| > −65 dBm | > −60 dBm | Excellent |
| −65 to −75 dBm | −60 to −80 dBm | Good |
| −75 to −85 dBm | −80 to −95 dBm | Fair |
| −85 to −95 dBm | −95 to −110 dBm | Poor |
| < −95 dBm | < −110 dBm | Disconnect |

As evident from the results as shown in Table 1, there is a clear difference between the averaged SNR and RSSI values obtained at different timings of the day. In the morning, the obtained SNR and RSSI values are lower than those obtained in the evening and the reason for this could be an increased human activity during the peak hours of the morning. Conversely, when human activity comes to a cease with the closing of the day (in evening), the obtained SNR and RSSI values are slightly higher. The same phenomena could be observed from the graphs obtained in Figure 6, where a lot of disturbance is seen during the peaks hours in the morning as visible from variations in the SNR and RSSI values. However, these variations smooth out when most of the human activity comes to a cease during the close of the day. Our results also show that there is a higher packet loss ratio at higher elevation levels (top floors) than those at lower elevation levels (down floors). These packet losses are indicated by broken lines of the graphs in Figure 6 where each discontinuity represents a packet loss.

In terms of elevation levels, the SNR and RSSI values are in the range of 18dB to 23dB and -65 dBm to -70 dBm, respectively. This shows that our NB-IoT system setup at TalTech campus provides an excellent coverage in an indoor scenario for all elevation levels. However, little variations in the signal strength are observed at different elevation levels due to the positioning of devices, proximity of antenna with respect to the base-station, building material and its structure and the surrounding environment of each particular location of placement of DORM nodes.
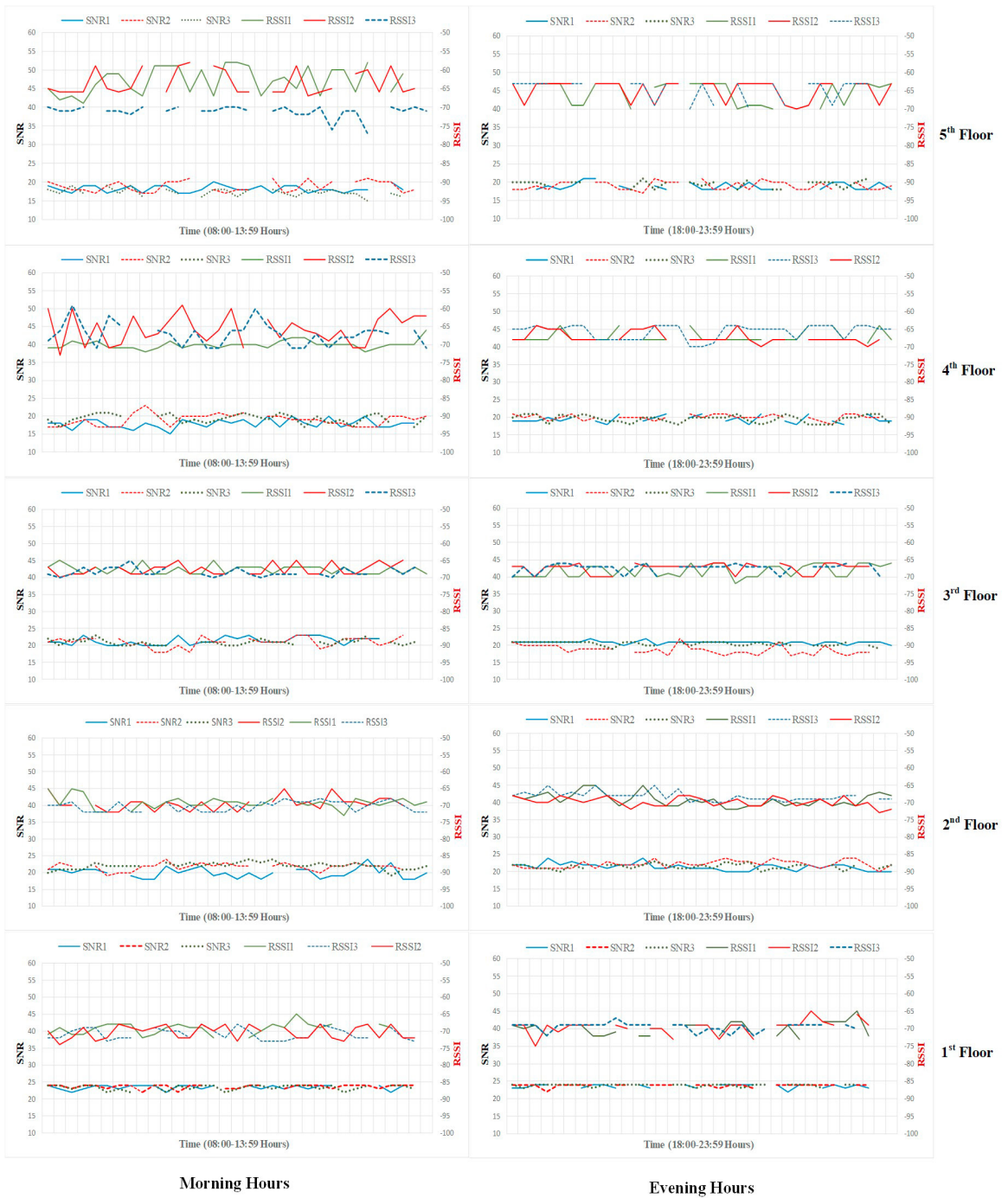
Figure 6: Data collected at different hours of the day for various elevation levels (Floors). The graphs in the left column portrays the SNR and RSSI values collected during morning hours (08:00-13:59) while the graphs in the right column shows the data collected in the evening hours (18:00-23:59).

## 4. Conclusion and Future Directions

The NB-IoT system architecture at Tallinn University of Technology is presented where DORM nodes are deployed across the TalTech campus to collect data from their surroundings within the coverage range of the installed NB-IoT Base-station. The development of our DORM nodes from the available COTS technologies is discussed where they are capable of collecting data from their surroundings through embedded sensors, encapsulating the collected data into a proper format and sending the formatted data to the IoT cloud for further analysis and investigation. Additionally, the NB-IoT system's coverage at TalTech campus is analysed in terms of the received SNR and RSSI values for different elevation levels and the produced results are discussed.

In future, we plan to extend this work with a comprehensive real-life investigation of the energy consumptions of our DORM nodes and further research towards Green IoT solutions.

## Acknowledgements

## References

[1] H. Malik, M. M. Alam, Y. L. Moullec, and A. Kuusik, "NarrowBand-IoT Performance Analysis for Healthcare Applications," Procedia Computer Science, 9th International Conference on Ambient Systems, Networks and Technologies (ANT 2018) Affiliated Workshops, vol. 130, pp. 1077 – 1083, 2018.

[2] Petäjäjärvi, Juha, et al. "Evaluation of LoRa LPWAN technology for indoor remote health and wellbeing monitoring." International Journal of Wireless Information Networks, vol. 24, no. 2, pp. 153–165, Jun 2017.

[3] Alam, Muhammad Mahtab, et al. "A Survey on the Roles of Communication Technologies in IoT-Based Personalized Healthcare Applications." IEEE Access 6 (2018): 36611-36631.

[4] "3GPP TR45.820: Cellular System Support for Ultra Low Complexity and Low Throughput Internet of Things," Tech. Rep., 2015.

[5] Telia. Eesti. AS, "The world's first use of the narrowband IoT at sea," [online] , Available: https://www.telia.no/magasinet/verdens-forste-bruk-av-narrowband-iot-til-sjos/. Access Date: 7th Feb.,2019.

[6] Telia Nordic, "The world's largest IoT pilot," [online] , Available: https://www.telia.no/magasinet/verdens-storste-iot-pilot/. Access Date: 7th Feb.,2019.

[7] u-blox (SIX:UBXN), "U-blox runs NB-IoT lab and field trails in Brazil with Huawei, Vivo, Cas and PinMyPet," [online] , Available: https://www.u-blox.com/en/press-releases/u-blox-runs-nb-iot-lab-and-field-trials-brazil-huawei-vivo-cas-tecnologia-and/. Access Date: 7th Feb.,2019.

[8] T-Mobile, "Smart Cities: Harnessing data to improve the way we live.," [online] , Available: https://iot.t-mobile.com/solutions/smart-cities/. Access Date: 7th Feb.,2019.

[9] China Mobile, "China Mobile Hong Kong NB-IoT Commercial Demo Event.," [online], Available: http://www.hk.chinamobile.com/en/about_us/media_centre/NewsPDF/20170928pr.html /. Access Date: 7th Feb., 2019.

[10] NUCLEO L476, [online] , Available: https://os.mbed.com/platforms/ST-Nucleo-L476RG/

[11] NUCLEO L073RZ, [online] , Available: https://os.mbed.com/platforms/ST-Nucleo-L073RZ/

[12] Avnet Silica NB-IoT Sensor Shield., [On-line], Available: https://www.avnet.com/wps/portal/silica/products/new-products/npi/avnet nb-iot-shield-sensor/

[13] Quectel. "GSM/NB-IoT EVB Kit.," [Online]. Available: https://www.quectel.com/product/gsmevb.htm

[14] BG96 AT commands manual, Ver. 2.1, Quectel Wireless Solutions Co., Ltd., May 2018.

[15] Teltonika. Mobile Signal Strength Recommendations. [Online]. Available: https://wiki.teltonika.lt/

# Appendix 2

**II**

Hassan Malik, Sikandar Zulqarnain Khan, Jeffrey Leonel Redondo Sarmiento, Alar Kuusik, Muhammad Mahtab Alam, Yannick Le Moullec, and Sven Pärand. Nb-iot network field trial: Indoor, outdoor and underground coverage campaign. In *2019 15th International Wireless Communications Mobile Computing Conference (IWCMC)*, pages 537–542, 2019

# NB-IoT Network Field Trial: Indoor, Outdoor and Underground Coverage Campaign

Hassan Malik, Sikandar Zulqarnain Khan, Jeffrey Leonel Redondo Sarmiento,
Alar Kuusik, Muhammad Mahtab Alam, Yannick Le Moullec, Sven Pärand*
Thomas Johann Seebeck Department of Electronics, Tallinn University of Technology, *Telia Estonia Ltd
Tallinn, Estonia
Email: {hassan.malik, sikandar.khan, jeredo, alar.kuusik, muhammad.alam, yannick.lemoullec}@taltech.ee,
*sven.parand@telia.ee

*Abstract*—Recent advancements in cellular technologies allow discrete computing devices embedded with sensors to communicate over long distances with low-cost and low-energy consumption. This could drastically impact the future internet of thing (IoT) ecosystem. In this regard, Third Generation Partnership Project (3GPP) has introduced a new cellular-based technology called Narrowband Internet of Things (NB-IoT) which is one of the potential technologies for enabling IoT application in vehicular, health-care, industry 4.0, etc. However, NB-IoT technology is still in its infancy and so far it is unclear whether it is sufficiently reliable to complement or replace existing short-range and cellular technologies to enable such use-case scenarios. Therefore, this paper presents a preliminary investigation of the coverage of NB-IoT in three different scenarios i.e., outdoor, indoor, and underground with empirical measurements, one of the key performance indicators in which operators are most interested. The measurements were conducted on Tallinn University of Technology (TalTech) campus and nearby residential areas within a range of $700$ m. The obtained results indicate that NB-IoT is able to provide good connectivity to meet the IoT application requirements in outdoor and indoor environments. However, for an underground scenario with the beam enabled for $700$ m, it is only possible to provide connectivity to the devices up to $400$ m. Furthermore, it is also observed that NB-IoT is able to provide connectivity to devices with a received signal strength indicator (RSSI) value as low as $-105$ dBm as compared to $-95$ dBm as in long-term evolution (LTE).

*Index Terms*—NB-IoT, coverage, RSSI, IoT, outdoor, underground, indoor, deployment, measurement campaign, IoT cloud platform, cumulocity

## I. INTRODUCTION

The recent advancements in wireless technologies for enabling low-power and low-cost communication over long-range open a plethora of possibilities to introduce diverse applications (i.e., smart cities, industry automation, logistic, health-care, etc) for the Internet of Things (IoT) ecosystem [1], [2]. Many key industrial players and academics have shown immense interest in enabling recently introduced low-power wide area network (LPWAN) technologies. The landscape of LPWAN is diverse and is constituted of several competing technologies such as SigfoX, LoRa, LTE-M, NB-IoT, Weightless, Ingenu, Telensa, etc [2], [3]. Among these technologies, NB-IoT is considered to be the most promising as it outperforms other LPWAN technologies in terms of coverage, energy efficiency, and cost due to the ease of utilizing the already existing cellular infrastructure.

NB-IoT is a variant of the long-term evolution (LTE) for supporting the diverse requirements of IoT applications. The core of NB-IoT is based on orthogonal frequency-division multiple access (OFDMA), similar to LTE. However, the total system bandwidth support is limited to $180$ kHz which corresponds to one physical resource block (PRB) of LTE. Such a meager bandwidth requirement enables NB-IoT to be deployed in three different modes, namely Standalone, In-band and Guard band. The choice of the mode selection is critical and has an impact on the overall network coverage, quality of service (QoS) as well as capital expenditure (Capex). To support the flexibility and switching between the modes, NB-IoT extensively uses the LTE design such as OFDM in downlink and single carrier frequency-division multiple access (SC-FDMA) in the uplink. However, to meet the requirements set forth by expected IoT applications, some design changes have been introduced such as retransmission for coverage extension, scheduling delay for computational complexity reduction, a power boost for downlink transmission, as well as control channel design. The control channel design changes are primarily due to the limited system bandwidth, as in the case of LTE control channels were span on multiple PRBs. The main target of these changes is to satisfy the need of IoT applications and to ensure the best coexistence with the existing LTE system while reusing the same infrastructure. The detailed design changes along with the key insight on the technology can be found in the standard [4].

### A. Motivation and Related Work

NB-IoT operates within the LTE frequency band in case of in-band and guard band deployments; therefore, it is really important to investigate the expected coverage supported by this technology, particularly from the perspective of telecom operators. This will help them estimate the expected cell sites required to cover a specific area and the number of devices connectivity support. NB-IoT aims to enable IoT applications which are outdoor (i.e., autonomous cars), indoor (i.e., smart home, smart grid) and underground (i.e., smart drainage systems), where each scenario has particular requirements in terms of coverage due to different penetration losses. This calls for detailing the coverage analysis of these scenarios.

537

However, so far, few efforts have been done for NB-IoT coverage analysis. In [5], the evaluation of NB-IoT coverage and outage probability in outdoor, indoor and underground setups is presented through computer simulations with an average inter-site distance of 6.2 km. It is concluded that for the underground scenario the outage probability is significantly higher for practical deployment purposes. In [6], the authors provide a simulation-based comparison of different technologies such as GPRS, LoRa, SigfoX, and NB-IoT in outdoor and indoor setups located in both rural and urban areas. Similarly, in [7], the authors present the simulation based coverage analysis of NB-IoT on different maximum coupling losses (MCL) and compared that with LTE. It is shown that for some scenarios, NB-IoT provides up to 20 dB coverage extension as compared to LTE. A coverage analysis based on link-level simulations for the different control channels of NB-IoT is presented in [8]. Furthermore, a simulation-based comparison of LoRa and NB-IoT coverage for the smart drainage system and smart metering is presented in [9], [10]. Moreover, a detailed analysis of NB-IoT link-level performance in both in-band and standalone deployment for smart grid application is also presented in [11].

As claimed in the standard and in most of the simulation results presented above, NB-IoT provides 20 dB coverage extension as compared to LTE; however, to test this hypothesis, it is important to test the technology with real deployments.

*B. Contribution*

To help deploying NB-IoT for practical applications, this paper presents a practical investigation of NB-IoT coverage in all the possible scenarios i.e., outdoor, indoor, and underground, with an extensive experimental measurement campaign using Telia's base station and TalTech NB-IoT sensor node named as DORM (integrateD cOmpact naRrowband platforM) based on commercially available NB-IoT compliant devices. To the best of our knowledge, this is the first empirical measurement

campaign in the open literature to study the coverage of this technology. We believe that this study facilitates realizing and developing practical IoT applications based on NB-IoT. Furthermore, the results of this study will also help the operators to plan cell deployments and to estimate Capex costs.

The remainder of the paper is structured as follows. Section II presents the measurement and experimental setup that include the detailed area under study, the type of device used for measurement and the base station settings and location. Section III presents the comprehensive results of coverage in terms of received signal strength indicator (RSSI) and packet loss percentage for outdoor, indoor, and underground scenarios. Finally, concluding remarks are drawn in Section IV.

## II. Experimental Setup and Measurement Campaign

The measurement campaign for this paper is done at Tallinn University of Technology (Taltech) and the neighboring residential area. It should be noticed that all the required permissions from the residents have been obtained to place the devices in indoor and underground locations accordingly. The locations of the devices along with the covered area which is approximately 700 m, is shown in Fig. 1. The covered area which includes residential buildings which are mostly three to five storey apartment buildings. However, some of these building have a single storey such as shops, etc; therefore, for indoor scenario, the ground floor is selected for all locations. Furthermore, for the buildings that lack an underground or basement, the nearest possible option is considered. The measurement campaign is carried out with 20 NB-IoT compliant devices. It is worth to note that Telia's base station at TalTech is configured with NB-IoT; however, the neighboring base stations are still operating on LTE and the results in this study are expected to be impacted by the interference from the neighboring cells.
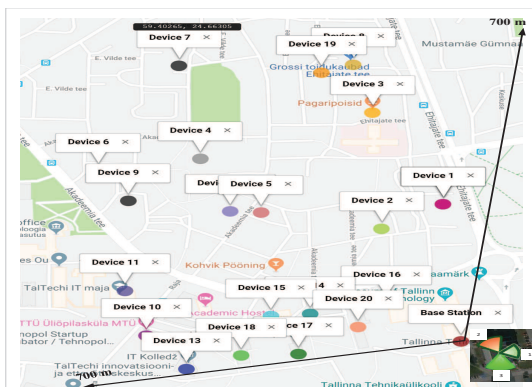


Fig. 1. Area under study. The bottom-right corner presents the available Telia's beams with their respective coverage area. The measurement campaign is conducted with beam 2.
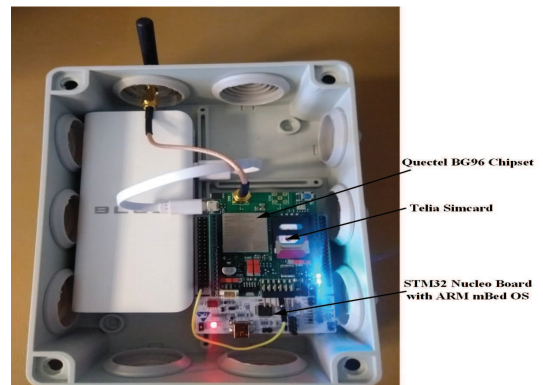


Fig. 2. NB-IoT enabled DORM node.

538

## A. NB-IoT Node

The Avnet Silica NB-IoT shield [12] sensor nodes used in the measurements are built around Quectel BG96 chipset. These are used in conjunction with STM32 Nucleo boards which support mbed OS for quick development and leverage free stacks like SSL, MQTT, COAP etc., as shown in Fig. 2. During the measurements, the NB-IoT nodes are deployed in various locations for more than 12 hours, where each device transmits data packets containing the distance, RSSI and Signal-to-interference-plus-noise ratio (SINR) after every 10 minutes through the base station to the cloud server.

## B. Telia's Base Station

For the base station, we have used Telia's commercially enabled NB-IoT base station with in-band deployment mode, which is installed at the premises of Taltech main building. The antenna of the base station is mounted approximately at a height of 20 m from the sea-level. Moreover, the base station is configured in a tri-sector antenna mode with three beams, each reaching around 700 m. However, for this experiment we have used only one beam; the corresponding selected area is colored in orange, as presented in Fig. 1. We use one beam only due to the lack of buildings in the coverage area of the two other beams (the corresponding areas are mostly made up of forest with no possibility for indoor or underground setups).

## III. PERFORMANCE EVALUATION

This section presents the coverage analysis of NB-IoT in outdoor, indoor, and underground scenarios for one cell sector enabled with the commercial base station and NB-IoT compliant devices. The aim of this investigation is to test the hypothesis set by the simulation results in the literature and the NB-IoT standard that each beam is able to reach at least 700 m and able to support device connectivity with RSSI value below −110 dBm. Therefore, the deployment of NB-IoT by Telia aims to reach 700 m and so far the cell deployment is done accordingly. Moreover, a comparison of LTE and NB-IoT is also presented based on RSSI to test the claim that NB-IoT is able to extend the coverage by 20 dB.

Fig. 3 presents the coverage results for the outdoor scenario in terms of RSSI in the form of a radio signal heat map (created with Excel Power Maps analytic tool) with visual aggregation set as an average. It can be observed that the RSSI values range from −60.5 dBm to −110 dBm and the setup is able to cover almost all of the area. However, it is interesting to highlight that out of 20 devices, 1 device is in outage as shown in Table I. However, before drawing any conclusion,

TABLE I
NUMBER OF DEVICES IN OUTAGE.

| Scenario | Total devices deployed | Devices in Outage |
|---|---|---|
| Outdoor | 20 | 1 |
| Indoor | 20 | 3 |
| Underground | 20 | 8 |
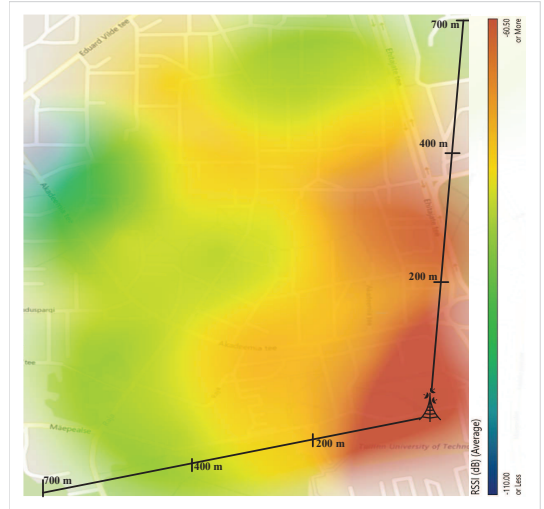


Fig. 3. Coverage of NB-IoT for outdoor scenario in terms of RSSI.

we have done the measurement of the particular device for approximately 1 week and we observed that connectivity in that area is not possible. Therefore, to reflect this in the results, we have assigned the device with an RSSI value of −110 dBm (which is equivalent to no coverage). It can be noted that the distance is measured using Google Maps (i.e., ground-to-ground level); if we consider the antenna height and elevation to the device (as most of the devices are on ground level), it



Fig. 4. Coverage of NB-IoT for indoor scenario in terms of RSSI.

Fig. 5. Temporal link dynamic of Device 4 in an indoor scenario for 6 hours in the morning and evening, respectively, in terms of RSSI



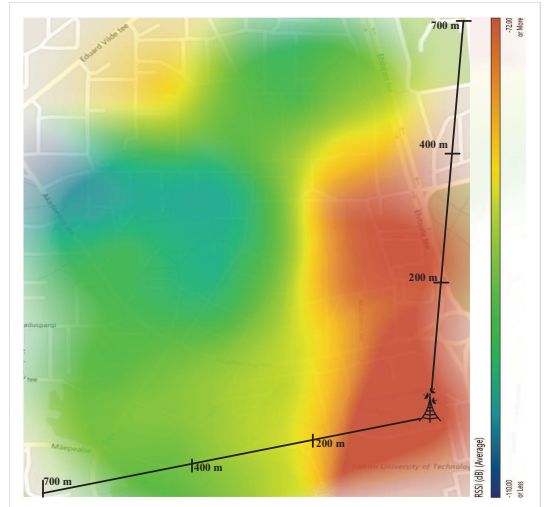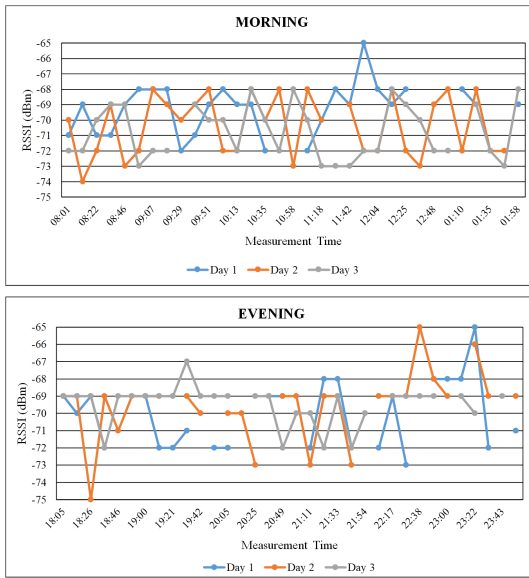Fig. 6. Coverage of NB-IoT for underground scenario in terms of RSSI.

is logical to conclude that NB-IoT is able to cover the devices within 700 m although some portions are with poor signal strength of down to $-92$ dBm.

Fig. 4 shows the NB-IoT coverage in the indoor scenario; the impact of penetration losses due to buildings or other obstacles is obvious as the RSSI ranges from $-72$ dBm to $-110$ dBm and the number of devices in outage increased to 3, as shown in Table I. During the measurement campaign, it has been noticed that a number of factors influence the signal strength and RSSI such as building material and structure, position with respect to beam direction, proximity to antenna, etc. To see the temporal link dynamics and the impact of environment, we have placed Device 4 which is around 400 m from the base station for three consecutive days for 6 hours in the morning and evening, respectively, as presented in Fig.5. It can be noted that the RSSI value varies significantly, particularly in the morning time when there is more activity going on in the neighboring environment, i.e. more abrupt variations in RSSI is observed as compared to the evening. Furthermore, blank points in Fig.5 represents the corresponding packet losses. It can be concluded from Fig.5 that even though the device's RSSI ranges from $-65$ dBm to $-75$ dBm, still significant packet losses are observed.

Fig. 6 presents the underground scenario and it is important to highlight that for the measurements, locations that are one level down from the ground are considered. It can be seen that the coverage of NB-IoT for the underground scenario is worse as compared to the indoor and outdoor scenarios, with an RSSI range from $-78$ dBm to $-110$ dBm and with 8 devices in
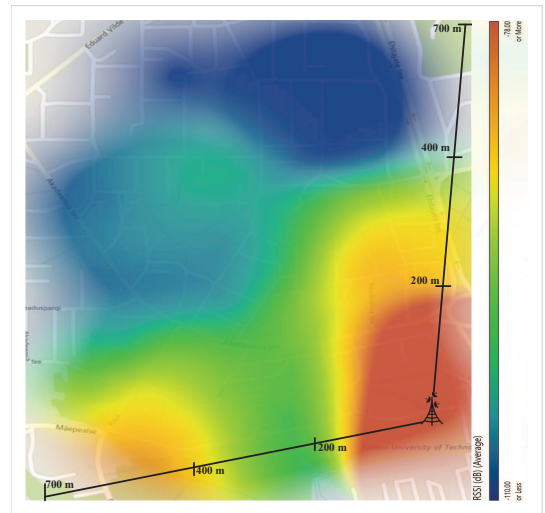
outage as presented in Table I. It is seen from the results that after 400 m, most of the devices are in complete outage.

To further investigate the underground scenario in detail, we have placed 3 devices at a short distance from each other and on different angles or positions within the beam; for these, significant differences in RSSI are observed. The devices are placed in the TalTech underground parking space of around 100 m and located within $350 - 400$ m from the base station. To be accurate, the underground parking located in an area between Device 17 and Device 18, as shown in Fig. 1. Among the three devices, one is still in outage and the other two are in low RSSI region, as shown in Fig. 7. The experiment is carried out in the evening for 6 hours and for 2 consecutive days. It has been observed that the device location within the parking impacts RSSI significantly i.e., depending on whether the device is behind a car, behind a pillar, in a corner, middle of the parking lot, etc.

Fig. 8 highlights the packet losses of the devices in all the three scenarios ( outdoor, indoor and underground). It can be seen that the packet losses are quite high in the indoor and underground scenarios. Even if the RSSI is within the acceptable region, still significant packet losses are seen. The major reason for such behaviours is the placement of the devices, which can be observed by studying all the results collectively. The most important aspects that affect the performance are the building structure, the location of the device and not to forget the interference from the LTE users in the neighboring cells. It is further noted that the performance of NB-IoT is worse in the mornings as compared to the evenings due to more human activity during the day which affects the signal strength, the number of connected users, and the corresponding traffic in the neighboring cell which are all typically higher during the

Fig. 8. Percentage of packet losses per device in outdoor, indoor and underground scenario for Device 1 and Device 2.
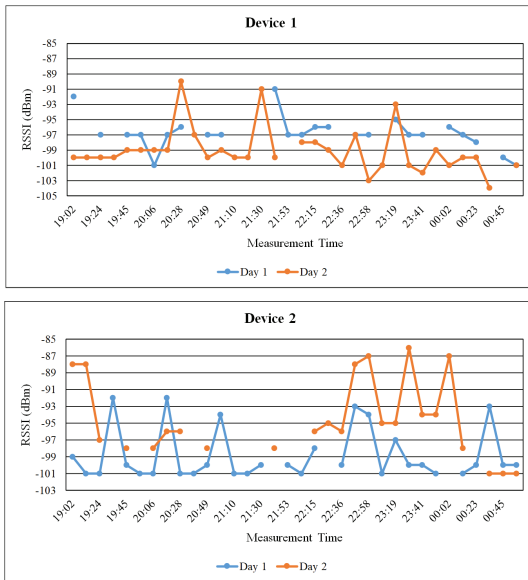
Fig. 7. Temporal link dynamic of Device 1 and Device 2 placed in an underground parking lot in terms of RSSI.

morning hours.

Lastly, Table II presents a comparison of the expected coverage between LTE and NB-IoT in terms of RSSI, as per the standard. In practice, it can be seen from all the results that NB-IoT is able to connect to devices even at an RSSI value of $-105$ dBm, whereas the maximum theoretical RSSI value supported by LTE is $-95$ dBm. On the other hand, observing Fig. 3, the excellent connection establishment in NB-IoT is when the RSSI value is greater than $-60$ dBm. Therefore, it can be noted that, NB-IoT is able to extend the coverage by approximately 10 dB in a real deployment as compared to 20 dB in standard according to our preliminary study. Therefore, for any LPWAN technology including NB-IoT, it is a challenge to provide ideal coverage to a certain geographical area and ensure connectivity in outdoor, indoor and underground scenarios simultaneously. To address this issue, one possible solution for the operators is to move to small cells which will potentially increase the Capex. The results presented in this paper are based on preliminary investigation based on a single type of hardware and using more sophisticated antennas or hardware may impact the results. However, the results presented in this work provide a holistic overview of the expected coverage in all these scenarios and can be used by operators as a reference point.

## IV. CONCLUSION

To the best of authors' knowledge, this paper presents one of the first efforts to practically evaluate the feasibility of using a newly introduced LPWAN technology i.e., NB-IoT,
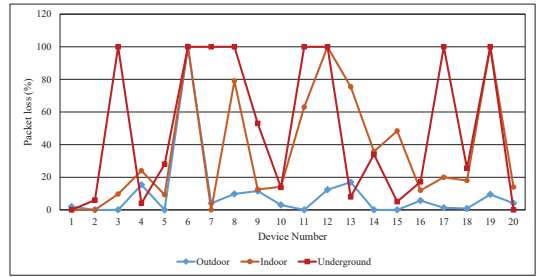
in outdoor, indoor, and underground setups. In this regards, we have presented the results of the empirical measurement campaign carried out at Taltech University, Estonia, to provide a comprehensive overview on the coverage of NB-IoT in an in-band deployment mode. Based on the results, it can be concluded that in practice NB-IoT extends the coverage as compared to LTE and is able to meet the IoT application requirements in outdoor and indoor scenarios. However, so far, the results for underground scenarios are not promising enough to support future IoT applications in such setups. Furthermore, it is also observed that by reducing the radius of the beam from 700 m to 400 m, NB-IoT is able to fully satisfy the requirements of any IoT application in outdoor, indoor, and also underground in a real-life environment. Further investigations with different hardware, environment conditions, and performance indicators such as energy efficiency and data rate are needed to fully evaluate the practical potential of this technology, which we aim at performing as future work.

TABLE II
COMPARISON OF RECEIVED SIGNAL STRENGTH BETWEEN LTE AND NB-IoT [13].

| LTE | NB-IoT | Signal Strength |
|---|---|---|
| $> -65$ dBm | $> -60$ dBm | Excellent |
| $-65$ to $-75$ dBm | $-60$ to $-80$ dBm | Good |
| $-75$ to $-85$ dBm | $-80$ to $-95$ dBm | Fair |
| $-85$ to $-95$ dBm | $-95$ to $-110$ dBm | Poor |
| $\leq -95$ dBm | $\leq -110$ dBm | Disconnect |

541

REFERENCES

[1] H. Malik, M. M. Alam, Y. L. Moullec, and A. Kuusik, "NarrowBand-IoT Performance Analysis for Healthcare Applications," *Procedia Computer Science, 9th International Conference on Ambient Systems, Networks and Technologies (ANT 2018) Affiliated Workshops*, vol. 130, pp. 1077 – 1083, 2018.

[2] J. Petäjäjärvi, K. Mikhaylov, R. Yasmin, M. Hämäläinen, and J. Iinatti, "Evaluation of LoRa LPWAN Technology for Indoor Remote Health and Wellbeing Monitoring," *International Journal of Wireless Information Networks*, vol. 24, no. 2, pp. 153–165, Jun 2017.

[3] M. M. Alam, H. Malik, M. I. Khan, T. Pardy, A. Kuusik, and Y. L. Moullec, "A Survey on the Roles of Communication Technologies in IoT-Based Personalized Healthcare Applications," *IEEE Access*, vol. 6, pp. 36 611–36 631, 2018.

[4] "3GPP TR45.820: Cellular System Support for Ultra Low Complexity and Low Throughput Internet of Things," Tech. Rep., 2015.

[5] I. Z. Kovcs, P. Mogensen, M. Lauridsen, T. Jacobsen, K. Bakowski, P. Larsen, N. Mangalvedhe, and R. Ratasuk, "LTE IoT link budget and coverage performance in practical deployments," in *IEEE 28th Annual International Symposium on Personal, Indoor, and Mobile Radio Communications (PIMRC)*, 2017, pp. 1–6.

[6] M. Lauridsen, H. Nguyen, B. Vejlgaard, I. Z. Kovacs, P. Mogensen, and M. Sorensen, "Coverage Comparison of GPRS, NB-IoT, LoRa, and SigFox in a 7800 km Area," in *IEEE 85th Vehicular Technology Conference (VTC Spring)*, 2017, pp. 1–5.

[7] A. Adhikary, X. Lin, and Y. . E. Wang, "Performance Evaluation of NB-IoT Coverage," in *IEEE 84th Vehicular Technology Conference (VTC-Fall)*, 2016, pp. 1–5.

[8] R. Ratasuk, B. Vejlgaard, N. Mangalvedhe, and A. Ghosh, "NB-IoT system for M2M communication," in *IEEE Wireless Communications and Networking Conference*, 2016, pp. 1–5.

[9] H. Malik, N. Kandler, M. M. Alam, I. Annus, Y. L. Moullec, and A. Kuusik, "Evaluation of low power wide area network technologies for smart urban drainage systems," in *IEEE International Conference on Environmental Engineering (EE)*, 2018, pp. 1–5.

[10] M. Pennacchioni, M. D. Benedette, T. Pecorella, C. Carlini, and P. Obino, "NB-IoT system deployment for smart metering: Evaluation of coverage and capacity performances," in *2017 AEIT International Annual Conference*, 2017, pp. 1–6.

[11] Y. Li, X. Cheng, Y. Cao, D. Wang, and L. Yang, "Smart Choice for the Smart Grid: Narrowband Internet of Things (NB-IoT)," *IEEE Internet of Things Journal*, vol. 5, no. 3, pp. 1505–1515, 2018.

[12] Avnet. Avnet Silica NB-IoT Sensor Shield. [Online]. Available: https://www.avnet.com/wps/portal/silica/products/new-products/npi/avnet-nb-iot-shield-sensor/

[13] Teltonika. Mobile Signal Strength Recommendations. [Online]. Available: https://wiki.teltonika.lt/

# Appendix 3

**III**

Nishant Poddar, Sikandar Zulqarnain Khan, Jakob Mass, and Satish Narayana Srirama. Coverage analysis of nb-iot and sigfox: Two estonian university campuses as a case study. In *2020 International Wireless Communications and Mobile Computing (IWCMC)*, pages 1491–1497. IEEE, 2020

# Coverage Analysis of NB-IoT and Sigfox:
# Two Estonian University Campuses as a Case Study

Nishant Poddar[*], Sikandar Zulqarnain Khan[**], Jakob Mass[*], Satish Narayana Srirama[*]
[*]University of Tartu, Institute of Computer Science, Tartu, Estonia
[**]Thomas Johann Seebeck Department of Electronics, Tallinn University of Technology, Tallinn, Estonia
poddar@ut.ee, sikandar.khan@taltech.ee, jakob.mass@ut.ee, satish.srirama@ut.ee

*Abstract*—**This paper presents the empirical results of the coverage analysis of two LPWAN technologies i.e. NB-IoT and Sigfox, conducted on university campuses in the two main cities of Estonia, i.e. Tartu and Tallinn, using the two commercially available NB-IoT operators and the single Sigfox operator in Estonia. Most of the existing literature on NB-IoT coverage is replete with RSSI-based coverage analyses. However, RSSI is most of the time not sufficient for evaluating LTE-based technologies including NB-IoT. Thus, our investigation of NB-IoT coverage considers three parameters: RSSI, RSRP, and RSRQ such that in situations where RSSI values are unavailable, the coverage analysis is based on RSRP and RSRQ. For Sigfox coverage, we base our analysis only on the RSSI factor, as Sigfox being a Non-LTE technology. Both technologies are evaluated in indoor, outdoor and deep-indoor/underground environments to provide an understanding of their coverage in various propagation and penetration conditions. Our results indicate that in outdoor scenarios, both Sigfox and NB-IoT achieve good to excellent coverage with almost 0% packet losses. However, in indoor scenarios, few packet losses were observed in Sigfox while no packet losses were observed in NB-IoT, even with a weaker coverage, and possibly due to re-transmissions that is a salient feature of NB-IoT, making it more reliable than its competitive LPWAN technologies. However, in deep-indoor or underground scenarios, coverage outages were recorded for NB-IoT, especially in Tartu area, indicating its weaker coverage in that city.**

*Index Terms*—**LPWAN, NB-IoT, Sigfox, LoRaWAN, coverage, network-testing, RSRP**

## I. INTRODUCTION

Low Power Wide Area Networks (LPWANs) provide long range transmissions allowing for a communication range of up to 40 km in rural zones and up to 10 km in urban zones [1], low development cost with device price as low as $5, low energy profiles with battery life of up to 10 years or more [2], and low operator subscription costs [3]. The basic motivation behind LPWAN technologies is transmitting a few short-length messages per day or weeks and even months in the long and mid radio range for supporting Internet of Things (IoT) applications. It is for these various reasons that many LPWAN technologies have been introduced, both in the licensed and unlicensed frequency spectra, to fulfil the various needs of diverse IoT applications. Among the available LPWAN technologies, Sigfox, LoRaWAN, and NB-IoT are the most prevalent and emerging technologies, with technical differences though, that are selected as per the individual application requirements [4].

Sigfox provides promising results in terms of long range, low power and low cost and has been deployed in more than 70 countries[1] around the globe. A typical Sigfox device powered by a 2400 mAh battery can achieve a theoretical lifetime of 2.5 years while sending one message every 10 min at 100 or 600 bits/s depending on the region, and an asymptotic lifetime of 14.6 years if the message transmission rate decreases [5].

In 2015, LoRaWAN was standardized by the LoRa-Alliance and is currently deployed across 42 countries. It is still under roll-out in many countries due to the interests of various mobile operators, industrial partners and academic researchers. As per the current specification it supports data rate up to 50 kbps in both uplink and downlink, depending on the spreading factors [4].

NB-IoT allows long-range communications at low data rates and is most suitable for delay-tolerant applications. It can provide a data rate of 250 kbps for multi-tone downlink communication and 20 kbps for single-tone uplink communications. For data collection at the lowest layer, NB-IoT utilizes end-nodes that are powered by chargeable batteries and are embedded with sensors for gathering data from their surroundings. The device complexity of NB-IoT nodes is reduced as compared to other unlicensed LPWAN technologies, including LTE-Cat M1 devices, for addressing the ultralow-power IoT applications. The NB-IoT nodes feature battery saving modes such as PSM and eDRX to achieve higher energy efficiency and longer battery life where the future NB-IoT nodes are expected to have a battery life of more than 10 years as per the standard.

### A. Motivation and Related Work

Although many efforts have been put to compare the various performance parameters of the available LPWAN technologies, they are limited in the sense that most conclusions are based on very few or restricted number of parameters. For example, the authors in [6] produced empirical results for NB-IoT network trial, but their conclusions were based on only one performance indicator i.e., RSSI. Based on their one-factor conclusions they claimed that NB-IoT provides good connectivity in an indoor and outdoor scenario but do not provide any good performance in deep-indoor/underground scenarios. The same authors in [7] claimed good performance of NB-IoT coverage in an indoor scenario at different elevation levels, but

[1]https://www.sigfox.com/en/coverage

their conclusions were based on only two factors i.e. RSSI and SNR. Similarly, the authors in [8] produced simulation-based coverage analysis of GPRS, Sigfox, LoRa and NB-IoT for indoor and outdoor scenarios but provided no details on how these simulation-based results could be related to real-world scenarios. However, the same authors in their work [9] compared the coverage and capacity analysis of SigFox, LoRa, GPRS, and NB-IoT using a real site deployment covering 8000 km$^2$ in Northern Denmark. Similarly, in [10], authors produced the empirical results for NB-IoT using the commercial Orange network in Belgium, their conclusions were based on three network parameters i.e., RSSI, RSRP, and SINR. Based on their observations, NB-IoT is quite robust in terms of low interference, coverage (both outdoor and deep indoor), high reliability with no packet loss even in low signal strength. In [11], the authors conducted an experiment in Ireland that showed Sigfox end devices were able to communicate as far as 25 km with base stations at RSSI as high as -145 dBm.
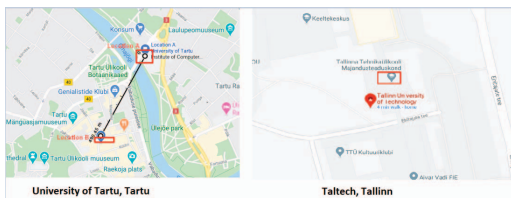


Figure 1: Location of measuring points in Tartu (Location A and Location B at University of Tartu, left) and Tallinn (TalTech, right)

In this work, we propose to advance the understanding of choosing among the available LPWAN operators based on their network performance (connectivity), reliability, scalability, and provided services within two Estonian cities (Tartu and Tallinn) as a use case. Our goal is to give a comparison of the LPWAN technologies in Tartu and Tallinn university campuses, however, due to limited availability of LoRaWAN network it has been excluded, and we focus on analysing the coverage performance of NB-IoT and Sigfox only. Furthermore, we consider only the uplink data for our analysis. The locations chosen for our observations include *Delta* and *Paabel* buildings located at the University of Tartu (UT), and Thomas Johann Seebeck Department of Electronics located at Tallinn University of Technology (TalTech), as shown on the maps in Figure 1. We base our conclusions on three parameters analysis i.e., RSSI, RSRP, and RSRQ where RSRP and RSRQ are important indicators to be considered for analysing the LTE technologies [10], [12].

The remainder of the paper is organized as follows. Section II presents the overview of the current LPWAN technologies that are publicly available in Estonia. Section III presents our experimental setup providing details of the NB-IoT and Sigfox nodes that were deployed at the above mentioned locations for data collection. Analysis and results are provided in Section IV. Section V concludes this work with future directions.

## II. OVERVIEW OF THE PUBLICLY AVAILABLE LPWAN TECHNOLOGIES ACROSS ESTONIA

There are four main public LPWAN service providers in Estonia i.e. Telia Eesti AS, Elisa Eesti AS, Connected Baltics OÜ, and Levikom Eesti OÜ; each providing a different LPWAN technology across Estonia. Telia and Elisa operate the NB-IoT technology and cover around 90% of the whole territory of Estonia by providing service to the entire population of Estonia. This covered geography is indicated by the large shaded ellipsoid in Figure 2. Connected Baltics[2] is the exclusive Sigfox operator in Estonia and covers the major cities of Estonia: Tallinn, Tartu, Pärnu and Narva by covering around 70% of the Estonian population. The geographic coverage of Sigfox across the major cities of Estonia from the Connected Baltics is indicated by small heated circles (red, blue and green) as shown in Figure 2. LEVIKOM [3] provides LoRaWAN services but no details about their coverage in Estonia and thus we have omitted showing their coverage in Figure 2.
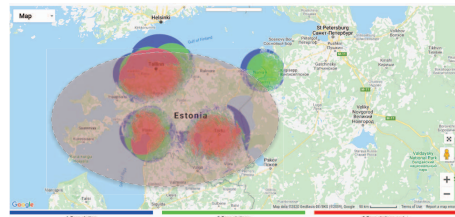


Figure 2: Sigfox (red, blue, green smaller circles) and NB-IoT (large shaded ellipsoid) coverage in Estonia

## III. EXPERIMENTAL SETUP

To measure the RF values, we have used the below hardware in shorter time-span (half-day/day) and single cloud platform Ubidots[4] for data collection and analysis.

### A. NB-IoT Node

We used NB-IoT DORM nodes [7] for deployment and data collection; these devices were deployed at various locations inside and outside the main buildings of the two campuses at TalTech and University of Tartu to cover up the area. These devices were inserted with NB-IoT SIM cards from the two different NB-IoT operators (referred to as Operator A and Operator B in the rest of this paper). The DORM nodes were programmed to transmit data packets every 30 minutes. These included RSSI, RSRP, and RSRQ values. The transmitted data packets were received and collected at a freely-available cloud platform i.e., Ubidots for further analysis and investigation.

[2]https://www.connectedbaltics.com/coverage/
[3]https://www.levikom.ee/iot/
[4]https://ubidots.com/

1492

Figure 3: Some of the NB-IoT (uncased) and Sigfox nodes, and batteries



(a) Outdoor     (b) Indoor     (c) Deep-Indoor

Figure 4: Examples of deployment scenarios (a) outdoor, (b) indoor, and (c) deep-indoor

### B. Sigfox Node

The proprietary Sigfox Airwits[5] devices have been used for analysing the Sigfox network in Tartu and Tallinn in the specified locations. Each Sigfox device is programmed to transmit data to the base station every 30 minutes. These messages upon receiving at Sigfox backend are forwarded to Ubidots in JSON format which contains the RSSI values along with time stamps.

The deployment has been carried out in two campuses with the devices as shown in Figure 3.

## IV. RESULTS

This section presents the RF results of NB-IoT and Sigfox in three different scenarios i) Outdoor ii) Indoor iii) Deep Indoor/Basement as illustrated in Figure 4 in University of Tartu and TalTech as aforementioned. The radio coverage depends on link budget and other radio parameters for e.g., transmission power, connector loss, antenna gain, the height of antenna that directly affects the overall coverage. Factors like free space path loss, fading reflection, refraction, building structure, and Fresnel zone also affects the coverage [13], [14]. We based our conclusions on a 3-factor analysis by considering i) RSSI ii) RSRP and iii) RSRQ of the received signal as explained briefly below. Further, we divide the RSSI, RSRP and RSRQ into four distinct classes of link quality: POOR, FAIR, GOOD and EXCELLENT. The exact corresponding values differ for

NB-IoT and Sigfox in the results; the respective values have been detailed in Tables I for RSSI; and Table II for RSRP and RSRQ in case of NB-IoT.

*1) RSSI:* Received Signal Strength Indicator (RSSI) or "Total Power", is the radio signal strength within the receive bandwidth. It is usually the power received by antenna calculated in dBm [15].

| > −65 dBm | EXCELLENT |
|---|---|
| −65 to −75 dBm | GOOD |
| −75 to −85 dBm | FAIR |
| < -85 dBm | POOR |

(a) NB-IoT [14], [15]

| > -122dBm | | EXCELLENT |
|---|---|---|
| -135dBm < RSSI ≤ -122dBm | | GOOD |
| -122dBm < RSSI | | GOOD |
| -135dBm < RSSI ≤ -122dBm if the n | | FAIR |
| RSSI ≤ -135dBm | | POOR |

(b) Sigfox [16]

Table I: RSSI reference values NB-IoT and Sigfox

*2) RSRP:* Reference Signal Received Power (RSRP) is similar to RSSI and refers to the average received power of LTE over the resource elements that carry cell-specific reference signals within certain frequency bandwidth. RSRP is applicable to *RRC_idle* and *RRC_connected* states. Additionally, RSRP does the better job than RSSI for LTE since it measures the signal power from the specific sector while excluding the noise and interference from other sectors. Therefore, RSRP is a more suitable parameter to be considered. Nevertheless, we have tried to analyse the corresponding RSSI measurement as well whenever possible.

It should be noted in the below results that at higher values of RSRP, the BG96 has not calculated the RSSI, it should not be interpreted as packet loss; the same characteristics have been observed in other radio modules e.g., SARA-N210 [10], therefore the graphs below have breaks in RSSI values.

*3) RSRQ:* Reference Signal Received Quality (RSRQ) indicates the quality of the received reference signal and is applicable only in *RRC_connected* state of LTE. It is calculated in dB as:

$$RSRQ = N \times RSRP/RSSI$$

Where, N defines the number of physical resource blocks.

| > −84 dBm | EXCELLENT |
|---|---|
| −85 to −102 dBm | GOOD |
| −103 to −111 dBm | FAIR |
| < -112 | POOR |

| >−5 dB | EXCELLENT |
|---|---|
| -5 to -8 dB | GOOD |
| -8 to -11 dB | FAIR |
| < -11 dB | POOR |

(a) RSRP        (b) RSRQ

Table II: Reference values of NB-IoT as per 3GPP standards [14], [15]

Furthermore, the results have been categorised below into three subsections based on three deployment scenarios.

### A. Outdoor

Figure 5 presents the RF coverage results in *University of Tartu* in Locations A and B shown in Fig. 1. In our measurements, it was observed that *operator B* had slightly better outdoor coverage than *operator A* with average RSRP -91.2 dBm compared to -97.4 dBm, as

shown in Figure 7. For RSSI, *operator B* has shown good performance with average RSSI of -77 dBm at location A and -69 dBm RSSI recorded at location B, compared to -90 dBm and -87 dBm, respectively, in case of *operator A*. On the other hand, for Sigfox the average RSSI values recorded at Locations A and B were -114 dBm and -103 dBm respectively, which reflects excellent coverage as per [16]. For RSRQ, which is defined as quality of received signal [15], *Operator A* has showed lower RSRQ index at location B compared to *operator B* which shows the weak coverage of *operator A* at this location.

In addition to the above, in *Taltech* Figure 6, *operator A* has good coverage with average RSSI value -64 dBM whereas *operator B* has fair coverage with average RSSI value -87 dBm. Similar to RSSI, other parameters RSRP and RSRQ showed similar patterns for *operator A* having median RSRP value -64 dBm compared to -97 dBm in case of *operator B* Figure 7, and Sigfox on the other hand had good RSSI strength with -101 dBm which reflects excellent coverage as per Table I.

(a) NB-IoT Operator A

(b) NB-IoT Operator B
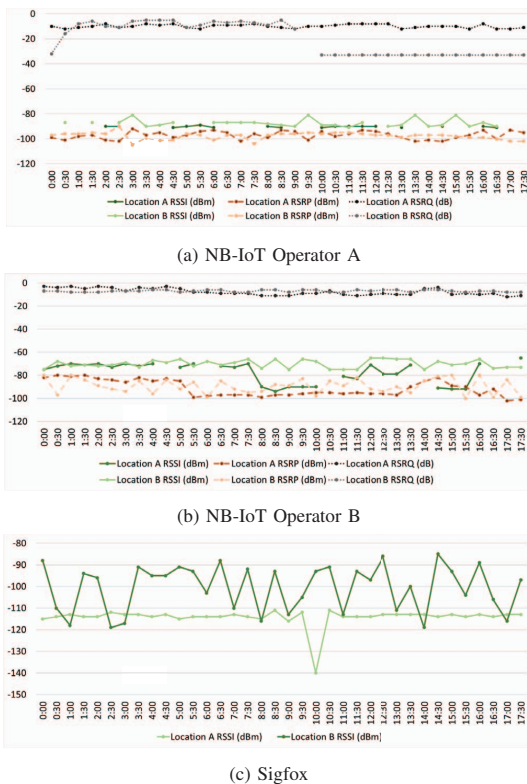
(c) Sigfox

Figure 5: RF coverage and signal quality: outdoor scenario at University of Tartu

It is important to highlight NB-IoT and Sigfox both had 0% packet loss for the outdoor scenario.

(a) NB-IoT Operator A

(b) NB-IoT Operator B

(c) Sigfox
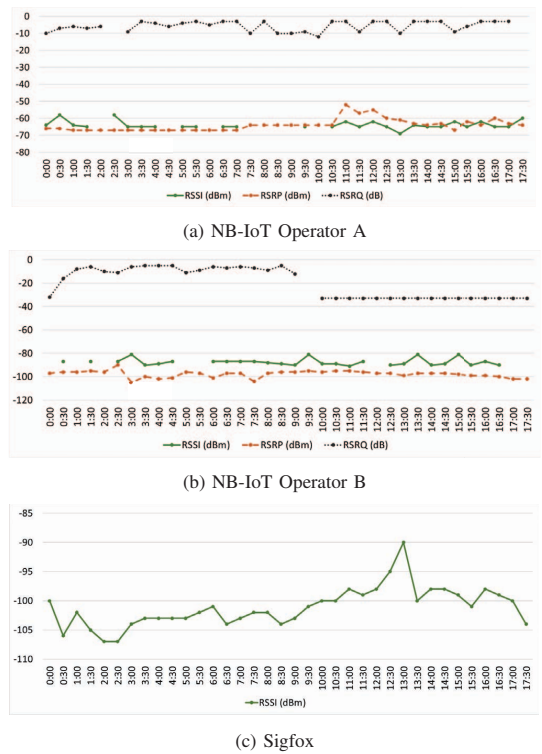
Figure 6: RF coverage and signal quality: outdoor scenario at TalTech



Figure 7: NB-IoT RSRP distribution in Tallinn and Tartu

### B. Indoor

Figure 8 illustrates the RSSI, RSRP and RSRQ values in indoor scenarios in both campuses. In our measurement, at *University of Tartu* Location A, for NB-IoT *operator A*, our nodes did not measured any RSSI strength, which is result of RSRP above the threshold value. The average RSRP and
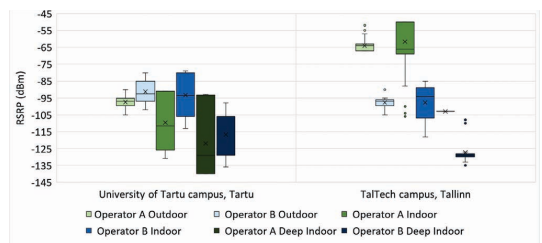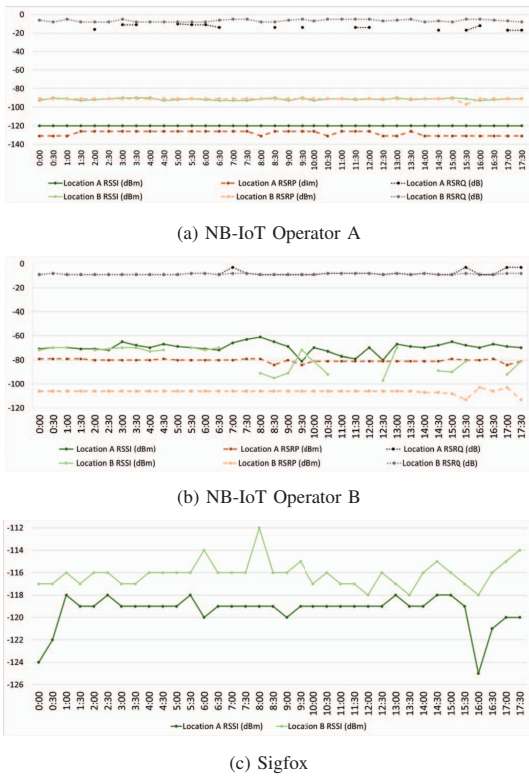
1494

(a) NB-IoT Operator A



(b) NB-IoT Operator B



(c) Sigfox

Figure 8: RF coverage and signal quality: indoor scenario at University of Tartu



(a) NB-IoT Operator A



(b) NB-IoT Operator B



(c) Sigfox

Figure 9: RF coverage and signal quality: indoor scenario at in TalTech

RSRQ index measured were -128 dBm and -14 dB, which reflects poor coverage as per Table II. However, interestingly, even with weaker coverage strength there were no packet loss which shows NB-IoT reliability and robustness which is due to the fact that a packet can be re-transmitted (up to 128 repetitions in uplink), which increases the success probability at the price of energy consumption.

It was also observed in Location A that with the increase in human occupancy in the building, which is directly proportional to active mobile users, there were fluctuations in the RSSI in both NB-IoT operators; however, the same was not observed with Sigfox, which shows that Sigfox is unaffected by neighboring LTE interference and noises which is due to its ultra narrow band modulation [17].

Furthermore, at TalTech campus, see Figure 9, it was observed that NB-IoT *operator A* had better coverage compared to *Operator B*. During the measurement cycle, the average RSRP calculated was -68 dBm for *Operator A* with respect -88 dBm at level 1 for *operator B*. For the same settings at level 2 the average RSRP value for *operator B* increased to

-107 dBM compared to -54 dBm in case of *operator A*.

For both campuses in indoor scenario, we observed few packet losses in Sigfox compared to NB-IoT, which shows that even with weaker signal strength NB-IoT is reliable and resilient.

### C. Deep Indoor

Figures 10-11 present the RF coverage of NB-IoT and Sigfox in deep-indoor. It is interesting to note that NB-IoT *operator A* had NB outage in *University of Tartu* location A. Therefore, it has been assigned value 0 for all corresponding RF parameters. However, on the other hand *operator B* had maximum packet loss of 61%, followed by Sigfox for same location that had 9% packet loss. The average RSRP observed, see Figure 7, at this site was -133 dBm for *operator B* which quantifies to poor coverage. In addition

1495
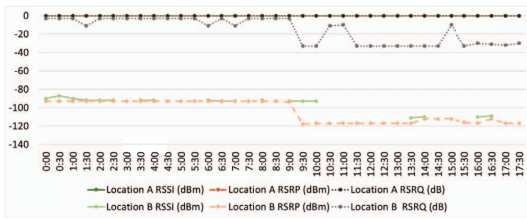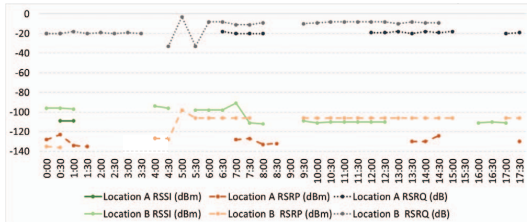
(a) NB-IoT Operator A
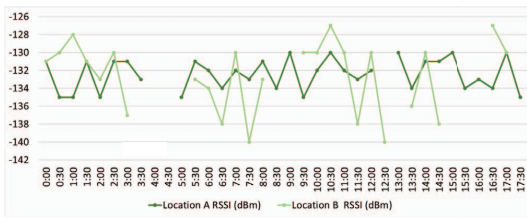


(b) NB-IoT Operator B



(c) Sigfox

Figure 10: RF coverage and signal quality: deep indoor scenario in University of Tartu

to the above, at location B of *University of Tartu* there were 33% of packet loss in case of NB-IoT *Operator B*, followed by 0% packet loss in case of *operator A*, which confirms that *operator B* has weaker deep indoor coverage penetration at this location. This observation also confirms, NB-IoT performances are affected by building structure and material used.

Furthermore, the same outage and high packet loss was not observed in TalTech campus for NB-IoT which shows both operators *operator A* and *operator B* have dense narrow band network in that area at the time of writing this paper.

## V. CONCLUSION

In this paper we provided an evaluation of real-time coverage of NB-IoT and Sigfox in two university campuses in the two main cities of Estonia (Tartu and Tallinn). These results provide a comprehensive overview of coverage recorded in different scenarios and can be further used by operators as a reference point. The coverage and signal quality results show promising performance for Outdoor and Indoor scenarios.
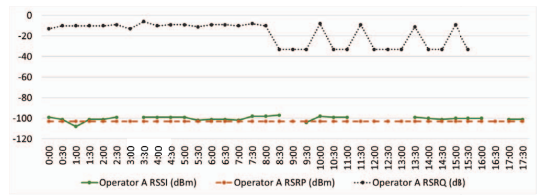


(a) NB-IoT Operator A
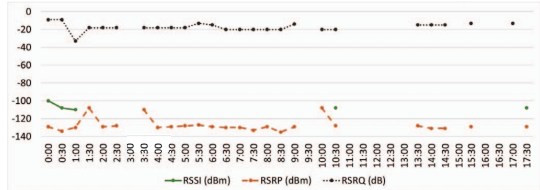


(b) NB-IoT Operator B
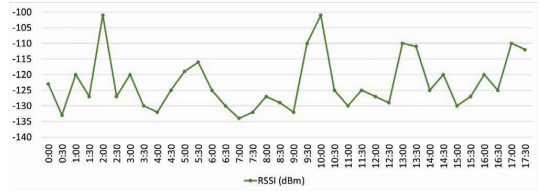


(c) Sigfox

Figure 11: RF coverage and signal quality: deep indoor scenario in TalTech

However, for NB-IoT Deep Indoor scenario, the results were better in TalTech as compared to University of Tartu. Sigfox, on the other hand, achieved a good coverage in both campuses in Outdoor, Indoor and Deep-Indoor scenarios with very minimum packet losses (pack losses which were observed in Indoor and Deep-Indoor with NB-IoT).

In future work, we would extend our research with different radio modems, environment conditions and would analyse the data rate and energy efficiency of LPWAN technologies.

## VI. ACKNOWLEDGMENT

REFERENCES

[1] M. Centenaro, L. Vangelista, A. Zanella, and M. Zorzi, "Long-range communications in unlicensed bands: The rising stars in the IoT and smart city scenarios," *IEEE Wireless Communications*, vol. 23, no. 5, pp. 60–67, 2016.

[2] D. Patel and M. Won, "Experimental study on low power wide area networks (LPWAN) for mobile Internet of Things," in *2017 IEEE 85th Vehicular Technology Conference (VTC Spring)*. IEEE, 2017, pp. 1–5.

[3] U. Raza, P. Kulkarni, and M. Sooriyabandara, "Low power wide area networks: An overview," *IEEE Communications Surveys & Tutorials*, vol. 19, no. 2, pp. 855–873, 2017.

[4] Mekki, Kais and Bajic, Eddy and Chaxel, Frederic and Meyer, Fernand, "Overview of cellular LPWAN technologies for IoT deployment: Sigfox, LoRaWAN, and NB-IoT," in *2018 IEEE International Conference on Pervasive Computing and Communications Workshops (PerCom Workshops)*. IEEE, 2018, pp. 197–202.

[5] C. Gomez, J. C. Veras, R. Vidal, L. Casals, and J. Paradells, "A sigfox energy consumption model," *Sensors*, vol. 19, no. 3, p. 681, 2019.

[6] H. Malik, S. Z. Khan, J. L. R. Sarmiento, A. Kuusik, M. M. Alam, Y. Le Moullec, and S. Pärand, "NB-IoT Network Field Trial: Indoor, Outdoor and Underground Coverage Campaign," in *2019 15th International Wireless Communications & Mobile Computing Conference (IWCMC)*. IEEE, 2019, pp. 537–542.

[7] S. Khan, H. Malik, M. Alam, and Y. Le Moullec, "Dorm: Narrowband iot development platform and indoor deployment coverage analysis," in *Proceedings of the 2nd International Workshop on Recent Advances in Cellular Technologies and 5G for IoT Environments (RACT-5G-IoT 2019), Leuven, Belgium*, vol. 29, 2019.

[8] M. Lauridsen, H. Nguyen, B. Vejlgaard, I. Z. Kovács, P. Mogensen, and M. Sorensen, "Coverage comparison of GPRS, NB-IoT, LoRa, and SigFox in a 7800 km$^2$ area," in *2017 IEEE 85th Vehicular Technology Conference (VTC Spring)*. IEEE, 2017, pp. 1–5.

[9] B. Vejlgaard, M. Lauridsen, H. Nguyen, I. Z. Kovács, P. Mogensen, and M. Sorensen, "Coverage and capacity analysis of Sigfox, LoRa, GPRS, and NB-IoT," in *2017 IEEE 85th vehicular technology conference (VTC Spring)*. IEEE, 2017, pp. 1–5.

[10] S. S. Basu, A. K. Sultania, J. Famaey, and J. Hoebeke, "Experimental Performance Evaluation of NB-IoT," in *2019 International Conference on Wireless and Mobile Computing, Networking and Communications (WiMob)*. IEEE, 2019, pp. 1–6.

[11] K. E. Nolan, W. Guibene, and M. Y. Kelly, "An evaluation of low power wide area network technologies for the internet of things," in *2016 international wireless communications and mobile computing conference (IWCMC)*. IEEE, 2016, pp. 439–444.

[12] F. Afroz, R. Subramanian, R. Heidary, K. Sandrasegaran, and S. Ahmed, "SINR, RSRP, RSSI and RSRQ measurements in long term evolution networks," *International Journal of Wireless & Mobile Networks*, 2015.

[13] b. Sikora, Axel and Schappacher, Manuel and Amjad, Zubair and others, "Test and Measurement of LPWAN and Cellular IoT Networks in a Unified Testbed," vol. 1. IEEE, 2019, pp. 1521–1527.

[14] Sikora, Axel and others, "Performance Measurements of Narrowband-IoT Network in Emulated and Field Testbeds," in *2019 10th IEEE International Conference on Intelligent Data Acquisition and Advanced Computing Systems: Technology and Applications (IDAACS)*, vol. 2. IEEE, 2019, pp. 780–785.

[15] 3GPP, "Mobile Signal Strength Recommendations." [Online]. Available: http://www.3gpp.org/specifications/releases

[16] Sigfox, "Link Quality: general knowledge." [Online]. Available: https://support.sigfox.com/docs/link-quality:-general-knowledge

[17] N. Naik, "LPWAN technologies for IoT systems: choice between ultra narrow band and spread spectrum," in *2018 IEEE International Systems Engineering Symposium (ISSE)*. IEEE, 2018, pp. 1–8.

1497

# Appendix 4

 IV
Sikandar M. Zulqarnain Khan, Muhammad Mahtab Alam, Yannick Le Moul-
lec, Alar Kuusik, Sven Pärand, and Christos Verikoukis. An empirical mod-
eling for the baseline energy consumption of an nb-iot radio transceiver.
*IEEE Internet of Things Journal*, 8(19):14756–14772, 2021

# An Empirical Modeling for the Baseline Energy Consumption of an NB-IoT Radio Transceiver

Sikandar M. Zulqarnain Khan, Muhammad Mahtab Alam, *Senior Member, IEEE*,
Yannick Le Moullec, *Senior Member, IEEE*, Alar Kuusik, *Member, IEEE*, Sven Pärand,
and Christos Verikoukis, *Senior Member, IEEE*

*Abstract*—NarrowBand Internet of Things (NB-IoT) is an emerging cellular IoT technology that offers attractive features for deploying low-power wide-area networks suitable for implementing massive machine-type communications. NB-IoT features include, e.g., extended coverage and deep penetration for massive connectivity, longer battery-life, appropriate throughput, and desired latency at lower bandwidth. Regarding the device energy consumption, NB-IoT is mostly underestimated for its control and signaling overheads, which calls for a better understanding of the energy consumption profiling of an NB-IoT radio transceiver. With this aim, this work presents a thorough investigation of the energy consumption profiling of the radio resource control (RRC) communication protocol between an NB-IoT radio transceiver and a cellular base station. Using two different commercial off the shelf NB-IoT boards and two mobile network operators (MNOs) NB-IoT test networks operational at Tallinn University of Technology, Estonia, we propose an empirical baseline energy consumption model. Based on comprehensive analyses of the profile traces from the widely used BG96 NB-IoT module operating in various states of the RRC protocol, our results indicate that the proposed model accurately depicts the baseline energy consumption of an NB-IoT radio transceiver while operating at different coverage class levels. The evaluation errors of our proposed model vary between 0.33% and 15.38%.

*Index Terms*—BG96 chip, empirical energy consumption model, LPWAN, narrowband Internet of Things (NB-IoT), NB-IoT networks, power consumption.

## I. INTRODUCTION

THE THIRD-GENERATION partnership project (3GPP) has introduced new cellular technologies to enable a wide range of cellular communications specifically for machine-to-machine and Internet-of-Things applications. These include LTE-M (Long-Term Evolution for Machines) and NB-IoT (NarrowBand-IoT) technologies. On one end, LTE-M includes

LC-LTE/MTCe (LTE Cat 0) and eMTC (enhanced machine-type communication) technologies (wherein, eMTC includes LTE Cat M1 and LTE Cat M2), particularly targeted at applications that require mobility and higher data rates [1]. On the other hand, NB-IoT includes LTE CAT-NB1 and LTE CAT-NB2 technologies, particularly targeted at applications that require lower complexity and lower data rates [2], [3]. Furthermore, both eMTC and NB-IoT are built upon the existing and already deployed 4G LTE infrastructure to support energy-constrained, mostly battery-powered IoT devices [4].

To reduce the power consumption of an end device, also called a user equipment (UE), both eMTC and NB-IoT provide extended versions of the existing power saving features of the legacy LTE technology, i.e., extended discontinuous reception (eDRX) and power saving mode (PSM), to help prolong the UE's battery lifetime [5], [6]. Utilizing these features in the UE requires a radio resource control (RRC) connection setup between the UE and the network; a detailed overview of this RRC protocol is provided in Section II of this article.

The eDRX feature enables the device to switch off parts of its radio circuitry, thereby operating with limited functionality and, thus, reduced power consumption [7], making it a useful feature for network-oriented applications, where the device can be woken up remotely by the network as needed, e.g., in smart-grid applications. The PSM feature, on the other hand, enables the device to switch off its radio circuity, thereby operating with the lowest possible power consumption [7], making it a useful feature for device-oriented applications, where the device is not accessible to the network but is woken up locally as scheduled (time triggered) by the application, e.g., in smart-metering and public-bike-sharing applications, etc.

A typical NB-IoT device include a radio transceiver, a microcontroller, and additional peripherals as its main components; among them, the radio transceiver has significantly higher energy consumption. Thus, understanding the details of the energy consumption of the radio transceiver is an important research topic in order to better estimate the lifetime of NB-IoT devices.

### A. State of the Art

Several works have evaluated the NB-IoT technology in terms of UE's power consumption analysis and battery life-time estimations [6]–[22]; these works can be categorized into analytical, simulations, and experimental measurement-based

analyses. Most of these works provide analytical models with simulation-based energy estimations [8]–[16]. For example, the work in [8] focuses on finding the optimum length of an eDRX cycle to help mitigate the signaling cost in an LTE network with simulation-based analysis. Sultania *et al.* [10] have presented an NB-IoT energy consumption model with uplink and downlink data transmissions as defined by the Poisson processes. Tsoukaneri *et al.* [11] and Yeoh *et al.* [12] have tried to estimate the NB-IoT device battery lifetime by using some simplified energy consumption equations, whereas Andres-Maldonado *et al.* [14] have proposed an NB-IoT UE energy consumption analytical model based on the Markov chains. Similarly, the work in [16] presents an analytical model for evaluating the latency and maximum number of devices in any network. Overall, most of the analytical models as presented in these works have been validated through network simulators. Such validations have higher uncertainty as the models' estimates and the validations do not use accurate actual measurements.

Several works have also provided experimental power consumption analysis of the NB-IoT technology, such as [17]–[24]. For example, the work in [17] focuses on the design of an NB-IoT prototype for delay-tolerant applications while operating in different Coverage Levels (CEL) of the network. Although this work provides power consumption measurements of the NB-IoT UE as a whole, the individual power consumption details for each state of the operating mode of radio/node are missing. The work in [18] focuses on the latency issues of NB-IoT while making use of a commercial NB-IoT network in Belgium. Although this work provides empirical results for analyzing the network performance in terms of setup times, throughput, and latency, it does not present the power consumption details of the UE. The work in [19] provides empirical results for the current traces of the CoTS NB-IoT platform, i.e., Ublox SARA-N211 when operating on Vodafone's network in Barcelona, Spain. While this work provides coarse-grained current traces for the various states of the radio, i.e., active waiting (C-DRX mode), Idle waiting (eDRX), and PSM; the underneath fine-grained details for their respective C-DRX cycles, eDRX cycles including paging time windows (PTW) and their underneath I-DRX cycles with sleep periods (SP) and paging occasions (POs) are missing.

Lauridsen *et al.* [21] claim to provide the first publicly available empirical power consumption measurements for the NB-IoT devices but their measurement setup is emulated using a Keysight UXM, a standard-compliant NB-IoT BS emulator. That is why it is unclear as to what extent their results would map onto a real network. Similarly, the work in [23] proposes a Dual-RAT LPWAN node combining an NB-IoT and LoRaWAN radio into one node with all the necessary power regulator circuitry. Here too, the power consumption numbers are given for the whole node only, and the individual power graphs for the radio modes and their internal state details are missing.

Considering the above sate-of-the-art and to the best of our knowledge, the following research gaps exist in the literature. First, no detailed baseline power consumption assessment of the NB-IoT radio has yet been provided. Second, an accurate energy consumption model that truly depicts the empirical energy consumption of an NB-IoT radio across its various stages of RRC operation (i.e., attach, active waiting, idle waiting, and resume) is missing. Third, recently published works on the NB-IoT UE's power consumption present only a coarse-grain analysis of the NB-IoT node(s), mostly providing the aggregated power consumption of the whole node, where the individual power consumption details of the underneath activities remain mostly obscured. In other words, the detailed energy-consumption profiling of the various states of the CoTS NB-IoT radio module(s) and its underneath activities remain unexplored to date. Fourth, most of the existing analyses are based on emulated NB-IoT networks [in particular, the base-station (BS)] and not on actual network operating BS. Similarly, the detailed energy consumption profiling of the commercially available (CoTS) NB-IoT devices under real mobile network operators (MNOs) networks are yet to be explored.

### B. Contributions

This work provides a modeling methodology for profiling the baseline energy consumption of an NB-IoT radio transceiver based on detailed empirical measurements. The modeling methodology considers all the states of the RRC protocol standardized by 3GPP and, hence, is applicable to general NB-IoT radio chips that are standard compliant.

The main contributions of our article and its positioning with reference to the state of the art can be summarized as follows.

1) Decomposition of the LTE RRC protocol with precise details and experimental demonstrations: while the 3GPP standard documentation ([6], [25]–[27]) and a number of papers in the literature (among others [19]) present the key concepts of the LTE RRC protocol, to the best of our knowledge, this work is the first one to delve into a fine-grained analysis of the LTE RRC protocol while mapping its different stages and modes with equally detailed experimental results in terms of energy consumption, thereby providing details and an understanding of the baseline energy consumption at a level not available so far.

2) Empirical and detailed power consumption measurements of CoTS NB-IoT radio transceiver while operating under real networks: in contrast to most existing works (e.g., [19], [21], and [23]) that are limited to the aggregated power or energy consumption of the whole NB-IOT UE and/or rely on either simulations or emulated networks, this work analyzes the energy consumption of the radio transceiver in detail (i.e., for each state of the RRC protocol) while operating under two MNOs-deployed NB-IoT test networks; this provides not only a more detailed analysis but also more realistic, empirical-based results as compared to the state of the art.

3) The derivation of an accurate energy consumption model for an NB-IoT radio transceiver: existing models are
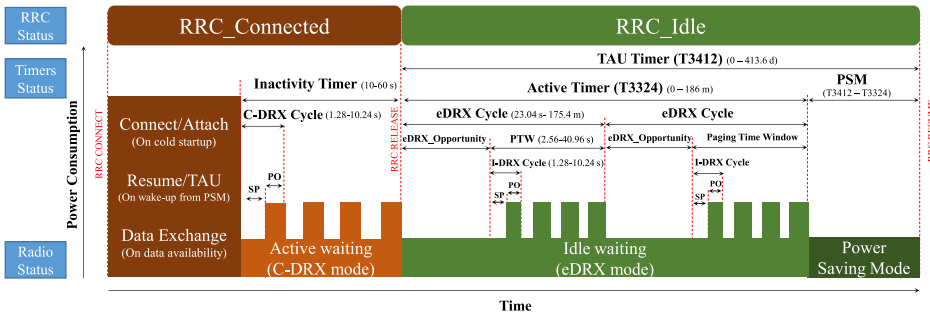
Fig. 1. RRC protocol reference model for the NB-IoT radio. It is composed of two complementary states, i.e., RRC_Connected and RRC_Idle and exploits Active waiting, Idle waiting, and Power Saving Mode (PSM) after establishing a connection with the network. From top to bottom: (top) RRC connection status, (middle) timers with their minimum and maximum limits, and (bottom) radio status with associated power consumption, as depicted schematically.

analytical only and/or not detailed enough to reflect all the inner mechanisms at play in the NB-IoT radio. To overcome this gap, and to the best of our knowledge, this article is the first one to propose a detailed and realistic NB-IoT radio transceiver energy consumption model, thanks to the detailed analysis and real-life empirical experiments mentioned above.

4) The proposed model is evaluated under real life conditions and we calculate the difference between the energy consumption obtained from the real-life deployment versus the energy consumption predicted by using our proposed model. Our results show that the error of the proposed model ranges between 0.33% and 15.38%, with the largest deviations occurring in the attach and resume procedures.

The remainder of this article is organized as follows. Section II provides an overview of the RRC protocol, whereas Section III presents our proposed NB-IoT radio energy consumption model. Section IV presents the empirical measurement results of the NB-IoT radio energy consumption at its various states of operation and Section V presents the evaluation of the proposed model. Section VI summarizes our conclusions and future works.

## II. OVERVIEW OF RADIO RESOURCE CONTROL (RRC) PROTOCOL

The RRC is a communication protocol between an end device/UE and the BS [also termed evolved Node-B (eNB)] through which network services, such as connection establishment, connection maintenance, data exchange, sleep and notification patterns, security and Quality of Service (QoS), etc., take place. The RRC protocol model has only two complementary states , i.e., 1) RRC_Connected and 2) RRC_Idle, as shown in the RRC protocol reference model in Fig. 1; the radio alternates between these two states during operation.

As shown in Fig. 1, the UE, on power up (or cold start), requests a network connection from the BS which upon acknowledgement is granted network resources and it thus enters into the RRC_Connected state. The connection establishment takes place in the "Attach" procedure and is always initiated by the UE. Once connected, the exchange of [uplink(Tx)/downlink(Rx)] data between the UE and the network takes place in the allocated transmission and reception slots that have been previously allocated to the UE during the "Attach" procedure. After a secure exchange of data, the UE listens to the broadcast information from the eNB for a certain period of time that is termed as "Active waiting" and whose period is set by the network operator. If any data arrive during this period, the RRC connection is resumed for the exchange of data between the UE and the network such that active waiting period restarts at the end of the data exchange. However, if no data arrive during active waiting, the eNB releases the connection and the UE switches to the RRC_Idle state, thereby saving all the context of the network in local memory.

Transiting into RRC_Idle state, the UE may enter either into eDRX or into PSM as per its configuration. The UE can also alternate between these two states, with eDRX first and PSM next, incase if both states are enabled. In the eDRX mode, the UE listens to the broadcast information from the eNB in cyclic patterns known as eDRX cycles; hence, this phase is termed the eDRX mode. When the eDRX mode expires or when it is forced to expire, the UE switches to the PSM mode during which it turns off its radio and is, therefore, not reachable by the network. This mechanism facilitates the device to enter deeper hardware sleep modes and thus contribute toward maximum power savings of the UE's battery, but at the cost of increased latency.

To summarize, the NB-IoT radio goes through the following states as it operates under the RRC protocol , i.e., 1) *Attach*—Registration to the network on a cold start or power up; 2) *Data Exchange (Tx/Rx)*—transmission and reception of data to/from the network; 3) *Active Waiting (C-DRX Mode)*—continuous listen to the broadcast information from the eNB for a period as permitted by the network operator and as configured by the UE; 4) *Idle Waiting (eDRX mode)*—partly listens to the broadcast information from eNB for a period as permitted by the operator and as configured by the UE; 5) *Power Saving Mode (PSM)*—shutdown of the radio activity for a period as requested by the UE and that as acknowledged by the network; and 6) *Tracking Area Update (TAU)*—resuming the connection with eNB on wake up from PSM.

All these radio states are shown in the RRC reference model in Fig. 1.

Details of these radio states are discussed in what follows.

### A. Attach—RRC_Connected State

On powering up, the radio scans the air for a suitable network interface through a contention-based random access (RA) preamble to which the eNB responds with a random access response (RAR) message. The UE then sends an RRC connection request to which the eNB responds with an RRC connection setup and the UE thus gets connected to the eNB. Afterward, the UE establishes a connection with the core network and generates an access stratum (AS) security context for secure exchange of data. After a successful AS security setup, the eNB reconfigures the RRC connection to finally establish a data radio bearer for the UE to uplink its data packets in the allocated transmission (Tx) slots. Further details on the attach procedure can be found in [26] and [27].

### B. Data Exchange (Tx/Rx)—RRC_Connected State

When the UE wants to transmit some data to the network, it first establishes an RRC connection with the network through an Attach procedure (on powering up) or TAU procedure (on waking up from PSM) and transits to the RRC Connected state. It then transmits its data packets to the network in its allocated transmission (Tx) slots using some transmission protocols (such as UDP, HTTPS, MQTT, etc). On the other hand, when the network wants to transmit some data to the UE (i.e., the UE will now receive data), there are two possibilities for the network to reach the UE in its RRC_Idle state, depending on whether it is in eDRX or PSM mode. If the UE is in eDRX mode, it periodically listens to the broadcast messages from the network during the paging occasion (PO) of each I-DRX cycle. In this case, the network sends a paging message to the UE and notifies it of the pending downlink traffic. As the UE interprets the paging message, it initiates a connection resume/reconnect procedure to get connected to the network and, thus, the exchange of downlink data between the UE and network occurs in the allocated reception (Rx) slots. However, if the UE is in PSM mode, it is not reachable by the network until the expiration of its PSM period (i.e., T3412-T3324). As the PSM expires, the UE initiates the TAU procedure to resume connection with the network, after which the data exchange occur. More details on data exchange can be found in [13] and [28].

### C. Active Waiting—RRC_Connected State

Discontinuous reception (DRX) is a legacy LTE feature that enables the UE to discontinuously receive the physical downlink control channel (PDCCH) to maintain network synchronization and determine if there is any pending downlink data. In the LTE RRC protocol, the DRX feature can be enabled both in the RRC_Connected state, i.e., Connected-DRX (C-DRX), and in the RRC_Idle state, i.e., Idle-DRX (I-DRX). In the RRC_Connected state, when there is no data traffic, the UE alternates between a sleep period (SP) during which the radio remains quiet and a paging occasion (PO), also called the paging event (PE), during which the radio monitors the PDCCH such that SP and PO alternates in a cyclic pattern that is termed the C-DRX cycle (where *C* stands for the connected state of the radio). These SPs and POs patterns (i.e., C-DRX cycles) repeat for the entire duration of "Active waiting" phase and whose length is controlled by the value of the inactivity timer. The value of the inactivity timer is operator specific (10–60 s in most commercial networks) and the UE cannot override its value as set by the operator. Furthermore, the inactivity timer starts running automatically; either at the end of data exchange between the UE and the network or when no data are available after the Attach procedure, where upon its expiration, the network releases the connection and the device switches to RRC_Idle state [25]. If some data arrive while the UE is still active waiting (i.e., Inactivity Timer is running), the connection is resumed for the exchange of data between the UE and the network; the inactivity timer restarts at the end of this data exchange and the UE enters into its active waiting phase again.

### D. Idle Waiting (eDRX Mode)—RRC_Idle State

In the RRC_Idle state, new resources cannot be requested from the network. However, the UE is still reachable by the network, where it periodically monitors the physical downlink control channel (PDCCH) in cyclic patterns. The NPDCCH monitoring takes place during the on-phase of an I-DRX cycle (where I stands for Idle state of the radio), i.e., PO or PE, whereas during the next off-phase of the I-DRX cycle, i.e., SP, the radio does not perform any activity. These I-DRX cycles repeat for the entire duration of a paging time window (PTW). A PTW itself forms the active phase of an eDRX Cycle such that each PTW is followed by an inactive phase that is termed an eDRX_Opportunity and during which the radio remains inoperative for until the beginning of the next PTW. These cyclic patterns of eDRX_Opportunity and PTW, i.e., eDRX Cycles occur repeatedly during the entire span of the idle waiting state of the radio. Since idle waiting involves repeated eDRX cycles, this phase is also termed the eDRX mode. All these nested cycles of activity and inactivity periods occurring during the eDRX mode are shown in the RRC protocol reference model in Fig. 1.

The eDRX mode is controlled by a set of timers where the active timer (i.e., T3324) primarily controls the time lapse of the entire duration of the eDRX mode and can have an extended range from 0 to 186 min for NB-IoT, with a maximum period of 175.4 min for its eDRX cycle and a maximum period of 40.96 s for its PTW. The maximum I-DRX cycle can be of 10.24 s for NB-IoT. The minimum and maximum limits of these cycles for NB-IoT technology are also indicated in the RRC protocol reference model in Fig. 1. Further details on their minimum and maximum ranges can be found in [6] and [7]. It is worth mentioning here that the UE can configure the length of its eDRX mode, the length of its eDRX cycle, and the duration of its PTW, only if permitted by the network.

### E. PSM—RRC_Idle State

On expiration of the active (T3324) timer, the UE exits idle waiting (eDRX mode) and enters into a power saving mode (PSM). While in PSM, the UE turns its radio off for as

long as the TAU timer is running and its energy consumption approaches to almost that of its power-off state. It is worth noting that though the radio or UE is not reachable by the network, it is still registered with the network, so that when the UE wakes up from PSM, it does not have to go through the registration process all over again; this adds to a significant amount of energy savings in reducing the signaling overhead. Further details on the resume procedure can be found in [15], [26], [27], and [28].

As the TAU (T3412) timer expires, the PSM is exited and the UE wakes up to perform the "Tracking Area Update (TAU)" procedure when the already registered UE reconnects with the network to check for any pending uplink/downlink data. Once this data exchange has occurred, the active waiting period restarts; when it ends, the UE enters into the RRC_Idle state and the cycle repeats. It should be noted here that the PSM mechanism implies a low power consumption at the cost of higher latency. Because the network has to wait until the UE is up again from its PSM and reachable by the network. As NB-IoT is designed for latency-tolerant applications, the UE may (deep) sleep for an extended range of up to 413 days and still be registered with the network. More details on the PSM state can be found in [6] and [19].

### F. Tracking Area Update (TAU)—RRC_Connected State

On expiration of the TAU (T3412) timer, the device wakes up from its PSM and reconnects to the network to indicate its availability in the TAU procedure. During the TAU procedure, the UE listens to any scheduled DL data that, if exist, are downloaded in the allocated reception (Rx) slots. Similarly, if the UE has any UL data, it is transferred to the network in the allocated transmission (Tx) slots. If no data exist for exchange, the inactivity timer starts so that the device enters into the active waiting phase. As it finishes, the device enters into idle waiting and the cycle continues. Further details on the TAU procedure can be found in [6], [26], and [27].

This section has presented an in-depth analysis of the NB-IoT RRC protocol phases; thanks to this knowledge, we can now proceed with building an empirical NB-IoT UE energy consumption model, which we describe in the next sections.

### III. Proposed Model for Profiling the Baseline Energy Consumption of NB-IoT Radio Transceiver

In addition to the detailed analysis of the RRC protocol presented in the previous section, an empirical model that provides a detailed baseline energy consumption of the RRC protocol is presented in this section.

Since the RRC protocol has only two states, i.e., 1) RRC_Connected and 2) RRC_Idle, the total energy consumed by an RRC radio can be given as

$$E_{\text{TOTAL}} = E_{\text{RRC\_CONNECTED}} + E_{\text{RRC\_IDLE}}. \quad (1)$$

In the RRC_Connected state, the radio goes through the four following states, i.e., Attach, Data Exchange (Tx/Rx), Active waiting (C-DRX), and TAU. The Attach procedure occurs only after a cold start; whereas, the TAU procedure occurs each

time the radio wakes up from PSM. Thus, the total energy consumed during the RRC_Connected state can be written as

$$E_{\text{RRC\_CONNECTED}} = E_{\text{ATTACH}} + E_{\text{Tx/Rx}} \\ + E_{\text{C-DRX}} + E_{\text{TAU}}. \quad (2)$$

As the inactivity timer finishes, the RRC connection is released and the radio goes into the RRC_Idle state where the radio first enters into Idle waiting state or eDRX mode, followed by PSM. Thus, the total energy consumed during the RRC_Idle state can be written as

$$E_{\text{RRC\_IDLE}} = E_{\text{eDRX}} + E_{\text{PSM}}. \quad (3)$$

Since Energy = Power × Time, the average energy consumption during the RRC_Connected state can be written as

$$E_{\text{RRC\_CONNECTED}} = \{P_{\text{ATTACH(avg)}} \times T_{\text{ATTACH}}\} \\ + \{(P_{\text{Tx(avg)}} \times T_{\text{Tx}}) + (P_{\text{Rx(avg)}} \times T_{\text{Rx}})\} \\ + \{P_{\text{C-DRX(avg)}} \times T_{\text{InactivityTimer}}\} \\ + \{P_{\text{TAU(avg)}} \times T_{\text{TAU}}\}. \quad (4)$$

Since the ActiveWaiting (C-DRX mode) period is a series of repeated C-DRX cycles, the above equation can be rewritten as

$$E_{\text{RRC\_CONNECTED}} = \{P_{\text{ATTACH(avg)}} \times T_{\text{ATTACH}}\} \\ + \{(P_{\text{Tx(avg)}} \times T_{\text{Tx}}) + (P_{\text{Rx(avg)}} \times T_{\text{Rx}})\} \\ + \{P_{\text{C-DRX(avg)}} \times (T_{\text{CDRX\_Cycle}} \\ \times N_{\text{CDRX\_Cycles}})\} \\ + \{P_{\text{TAU(avg)}} \times T_{\text{TAU}}\} \quad (5)$$

where $T_{\text{CDRX\_Cycle}}$ is the time period of each C-DRX cycle, and $N_{\text{CDRX\_Cycle}}$ is the total number of C-DRX cycles that occur during the ActiveWaiting period.

Similarly, the average energy consumption of the radio during the RRC_Idle state is

$$E_{\text{RRC\_IDLE}} = E_{\text{eDRX}} + E_{\text{PSM}} \quad (6)$$

and can be rewritten as

$$E_{\text{RRC\_IDLE}} = \{P_{\text{eDRX(avg)}} \times T_{\text{eDRX}}\} + \{(P_{\text{PSM(avg)}} \times T_{\text{PSM}}\}. \quad (7)$$

The duration of the entire Idle state of the radio, and its eDRX and PSM durations, can be set by the values of 3GPP-specified timers, such that

$$T_{\text{RRC\_IDLE}} = T_{3412} \quad (8)$$
$$T_{\text{eDRX}} = T_{3324} \quad (9)$$
$$T_{\text{PSM}} = T_{3412} - T_{3324}. \quad (10)$$

Thus, the average energy consumption of the radio during the RRC_Idle state can be rewritten as

$$E_{\text{RRC\_IDLE}} = \{P_{\text{eDRX(avg)}} \times T_{3324}\} \\ + \{P_{\text{PSM(avg)}} \times (T_{3412} - T_{3324})\}. \quad (11)$$

Since, the eDRX mode is composed of repeated eDRX cycles, thus

$$
\begin{aligned}
E_{\text{RRC\_IDLE}} = {} & \left\{ P_{\text{eDRX(avg)}} \times \left( T_{\text{eDRX\_Cycle}} \times N_{\text{eDRX\_Cycles}} \right) \right\} \\
& + \left\{ \left( P_{\text{PSM(avg)}} \times (T_{3412} - T_{3324}) \right) \right\} \quad (12)
\end{aligned}
$$

where $T_{\text{eDRX\_Cycle}}$ is the time period of each eDRX cycle and $N_{\text{eDRX\_Cycles}}$ is the total number of eDRX cycles that occur during the IdleWaiting period.

Since each eDRX cycle is composed of a PTW (active phase of an eDRX cycle) and eDRX_opportunity (inactive phase of an eDRX cycle), the above equation can be expanded to

$$
\begin{aligned}
E_{\text{RRC\_IDLE}} = {} & \left\{ P_{\text{eDRX(avg)}} \times \left( T_{\text{eDRX\_PTW}} + sT_{\text{eDRX\_OPP}} \right) \right. \\
& \left. \times N_{\text{eDRX\_Cycles}} \right\} \\
& + \left\{ \left( P_{\text{PSM(avg)}} \times (T_{3412} - T_{3324}) \right) \right\}. \quad (13)
\end{aligned}
$$

Moreover, since the power consumption of PTW and eDRX_opportunity during each eDRXcycle is different, the above equation can be written as

$$
\begin{aligned}
E_{\text{RRC\_IDLE}} = {} & \left\{ \left( P_{\text{eDRX\_PTW(avg)}} \times T_{\text{eDRX\_PTW}} \right) \right. \\
& + \left( P_{\text{eDRX\_OPP(avg)}} \times T_{\text{eDRX\_OPP}} \right) \\
& \left. \times N_{\text{eDRX\_Cycles}} \right\} \\
& + \left\{ \left( P_{\text{PSM(avg)}} \times (T_{3412} - T_{3324}) \right) \right\}. \quad (14)
\end{aligned}
$$

As PTW is a repeated sequence of I-DRX cycles, the above becomes

$$
\begin{aligned}
E_{\text{RRC\_IDLE}} = {} & \left\{ \left( P_{\text{eDRX\_PTW(avg)}} \right. \right. \\
& \left. \times \left( T_{\text{I--DRX\_Cycle}} \times N_{\text{I--DRX\_Cycles}} \right) \right. \\
& + \left( P_{\text{eDRX\_OPP(avg)}} \times T_{\text{eDRX\_OPP}} \right) \\
& \left. \times N_{\text{eDRX\_Cycles}} \right\} \\
& + \left\{ \left( P_{\text{PSM(avg)}} \times (T_{3412} - T_{3324}) \right) \right\} \quad (15)
\end{aligned}
$$

where $T_{\text{I--DRX\_Cycle}}$ is the time period of each $\text{I--DRX}$ cycle and $N_{\text{I--DRX\_Cycles}}$ is the total number of $\text{I--DRX}$ cycles occurring during the PTW of each eDRXcycle.

Next, since each $\text{I--DRX}$ cycle has an on phase (i.e., PO) during which the NPDSCCH signal is monitored and an off phase with no activity, the above equation can be expanded to

$$
\begin{aligned}
E_{\text{RRC\_IDLE}} = {} & \left\{ \left( P_{\text{I--DRX\_on(avg)}} \times T_{\text{I--DRX\_on}} \right) \right. \\
& + \left( P_{\text{I--DRX\_off(avg)}} \times T_{\text{I--DRX\_off}} \right) \\
& \left. \times N_{\text{I--DRX\_Cycles}} \right) \\
& + \left( P_{\text{eDRX\_OPP(avg)}} \times T_{\text{eDRX\_OPP}} \right) \\
& \left. \times N_{\text{eDRX\_Cycles}} \right\} \\
& + \left\{ \left( P_{\text{PSM(avg)}} \times (T_{3412} - T_{3324}) \right) \right\}. \quad (16)
\end{aligned}
$$

Finally, given that

$$
E_{\text{TOTAL}} = E_{\text{RRC\_CONNECTED}} + E_{\text{RRC\_RELEASED}} \quad (17)
$$

we obtain

$$
\begin{aligned}
E_{\text{TOTAL}} = {} & \left\{ \left\{ P_{\text{ATTACH(avg)}} \times T_{\text{ATTACH}} \right\} \right. \\
& + \left\{ \left( P_{\text{Tx(avg)}} \times T_{Tx} \right) + \left( P_{\text{Rx(avg)}} \times T_{Rx} \right) \right\} \\
& + \left\{ P_{\text{C--DRX(avg)}} \times \left( T_{\text{CDRX\_Cycle}} \times N_{\text{CDRX\_Cycles}} \right) \right\} \\
& \left. + \left\{ P_{\text{TAU(avg)}} \times T_{\text{TAU}} \right\} \right\} \\
& + \left\{ \left\{ \left\{ \left( P_{\text{I--DRX\_on(avg)}} \times T_{\text{I--DRX\_on}} \right) \right. \right. \right.
\end{aligned}
$$

$$
\begin{aligned}
& \left. + \left( P_{\text{I--DRX\_off(avg)}} \times T_{\text{I--DRX\_off}} \right) \times N_{\text{I--DRX\_Cycles}} \right\} \\
& + \left\{ \left( P_{\text{eDRX\_OPP(avg)}} \times T_{\text{eDRX\_OPP}} \right) \times N_{\text{eDRX\_Cycles}} \right\} \\
& + \left\{ P_{\text{PSM(avg)}} \times (T_{3412} - T_{3324}) \right\} \right\}.
\end{aligned}
$$

$$(18)$$

For simplicity, the above equation can be rearranged in terms of the 3GPP-specified timers such that each row in the following equation represents the energy consumption of each separate state of the radio, i.e., Attach, Data Exchange [Transmit (Tx) and Receive (Rx)] , Active waiting (C-DRX mode), Idle waiting (eDRX mode), deep sleep mode (PSM) and Resume (TAU), i.e.,

$$
E_{\text{TOTAL}} = \left( \begin{array}{c} \left\{ P_{\text{ATTACH(avg)}} \times T_{ATTACH} \right\} \\ + \left\{ \left( P_{\text{Tx(avg)}} \times T_{\text{Tx}} \right) + \left( P_{\text{Rx(avg)}} \times T_{\text{Rx}} \right) \right\} \\ + \left\{ P_{\text{C--DRX(avg)}} \times \left( T_{\text{InactivityTimer}} \right) \right\} \\ + \left\{ P_{\text{TAU(avg)}} \times T_{\text{TAU}} \right\} \end{array} \right)
$$

$$
+ \left( \begin{array}{c} \left\{ \left( P_{\text{eDRX(avg)}} \times T_{3324} \right) \right\} \\ + \left\{ P_{\text{PSM(avg)}} \times (T_{3412} - T_{3324}) \right\}. \end{array} \right) \quad (19)
$$

This section has presented the proposed NB-IoT UE energy consumption model. The next sections detail the corresponding results and corresponding evaluations.

## IV. EMPIRICAL MEASUREMENTS

As explained in Section I-A, works on experimental energy consumption profiling of NB-IoT radio transceivers are limited. To overcome the limitations of the state of the art, a comprehensive model for profiling the empirical energy consumption of an NB-IoT radio transceiver using the RRC protocol has been proposed in the previous section. The proposed model relies on empirical measurements; this section presents our experimental setup and measurement results obtained with two widely used CoTS NB-IoT radio boards (both equipped with BG96 module) with network configurations from two MNOs (referred to as Operator 1 and Operator 2) operating NB-IoT test networks at Tallinn University of Technology.

### A. Experimental Setup

The two CoTS NB-IoT radio modules, i.e., Avnet Silica NB-IoT sensor shield [29] and Quectel UMTS & LTE EVB Kit [30], are based on the 3GPP Rel-13 compliant Quectel BG96 LPWAN module [31]. They are used for conducting the current and power consumption measurements, while in actual operation, under the two publicly available test networks provided by Operator 1 and Operator 2.

A Keysight Technologies N6705C DC Power Analyzer (PA) [32] is used for collecting the current and power traces during these measurement campaigns. Our test-bed setup, composed of an Avnet shield as our device under test (DUT) DUT1 and Quectel EVB Kit as our DUT2, along with the Keysight's PA, is shown in Fig. 2. A constant voltage of 3.3 V is supplied to DUT1 and 3.8 V to DUT2 by the PA. AT commands are sent from the QCOM software running on the PC through the USB-PMOD interface for DUT1 and through the USB interface, configured accordingly, for DUT2. SIM cards for both the
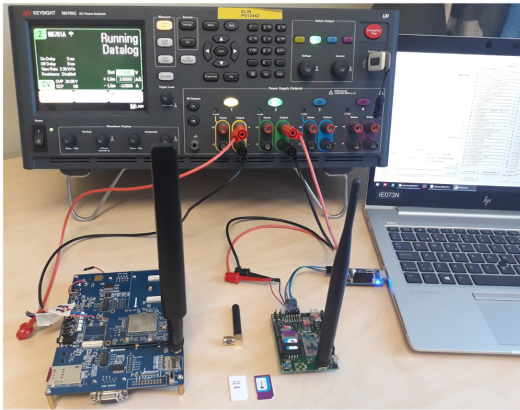
Fig. 2.  Testbed Setup with Quectel BG96 and Avnet Silica BG96 NB-IoT radio modules, Keysight N6705C DC Power Analyzer, and SIM cards from Operator 1 and Operator 2.

TABLE I
DETAILS OF THE PUBLICLY AVAILABLE NB-IoT NETWORKS THAT HAVE BEEN USED DURING OUR MEASUREMENT CAMPAIGNS ON TEST LOCATION

| Details | Operator 1 | Operator 2 |
|---|---|---|
| Operator numeric code | 24801 | 24802 |
| Selected Access Technology | CAT-NB1 | CAT-NB1 |
| Selected Band | LTE BAND 20 | LTE BAND 20 |
| Selected Channel ID | 6254 | 6152 |
| CE level (at test locations) | 0 , 1 | 0 , 1 |
| SNR {0(bad) to 31(good)}(dB) | 28 , 6   (avg) | 21 , 5   (avg) |
| SINR{0(bad) to 250 (good)}(dB) | 185, 178  (avg) | 153, 142 (avg) |
| RSSI{-110(bad) to -60(good)}(dBm) | -67, -101 (avg) | -72, -110 (avg) |
| RSRP{-140(bad) to -44(good)}(dBm) | -67, -111 (avg) | -74, -117 (avg) |
| RSRQ{-19.5(bad) to -3(good)}(dB) | -3 , -9   (avg) | -3 , -10  (avg) |

networks under test are also visible in our setup, as shown in Fig. 2.

From a practical perspective, it should be mentioned that though the BG96 module of both DUTs were flashed with the latest firmware (FW) version, setting up the (T3324/T3412) timers to our desired values was a cumbersome procedure. Upon contacting Quectel, it turned out that even the latest FW (i.e., BG96MAR02A07M1G) has updates in the form of subversions; installing the latest subversion (i.e., BG96MAR02A07M1G_01.016.01.016) solved most of the Timers' related issues. Similarly, the built-in USB-USB interface on DUT1 that is provided to receive power and AT commands from a PC disrupted the power measurements from the PA. To avoid these disruptions, we used an FTDI chip-based serial communication interface to utilize its built-in USB-UART PMOD interface [33] and bypassed its USB-USB port. We also disabled all the functional LEDs [34] of DUT1 to get accurate power consumption measurements from the PA. As for testing DUT2, we also modified it as per the documents provided to us by the Quectel Team. Finally, the details of the two MNOs NB-IoT test networks that have been considered for carrying out this research are summarized in Table I.

During our measurement campaign, the NB-IoT devices were placed at different locations inside Thomas Johann

TABLE II
OPERATOR SPECIFIC AND UE CONFIGURABLE PARAMETERS

| Network Params | Symbol | Value |
|---|---|---|
| Attach | *T_ATTACH* | Network_conditions |
| Inactivity Timer | *InactivityTimer* | Operator_defined |
| C-DRX Cycle | *CDRX_Cycle* | Operator_defined |
| RRC_Idle | *RRC_Idle* | UE defined = T3412 Timer value |
| Active Timer | *T3324 Timer* | UE defined = T3324 Timer value |
| eDRX Cycle | *eDRX_Cycle* | Network defined; UE configurable |
| PagingTimeWindow | *PTW* | Network defined; UE configurable |
| eDRX_Opportuity | *eDRX_Opp* | (eDRX_Cycle - PTW) |
| I-DRX Cycle | *I-DRX_Cyc* | Operator_defined |
| PowerSavingMode | *PSM* | UE defined = (T3412-T3324) value |

Seebeck Department of Electronics building and students' dormitory building that are located on TalTech campus. For triggering the different CEL, the devices were deployed on the second basement (B2) floor of Thomas Johann Seebeck Department of Electronics building, where the received signal strength is lower than on the upper floors. On each test location, the current value of the CE level was queried using the adequate AT commands and when the required CE levels were achieved, i.e., CE Level 0 and CE Level 1, the measurements were made accordingly.

Small differences between the two operators in terms of their SNR, SINR, RSSI, RSRP, and RSRQ for the same CE levels could be observed from their respective values as given in Table I. However, to smooth out the minor variations of the individual results for SNR, SINR, RSSI, RSRP, and RSRQ; their experiments were repeated in the order of 100 times on each test location and the obtained results were averaged into their final values, under their respective CE levels, as summarized in Table I. Table II summarizes the network parameters that are operator specific and/or UE configurable with a short description of their control and possible values.

### B. Measurements Approach

The Data Logger function of the Keysight PA records the output (voltage, current, and power) data logs of the arbitrary waveform at a sampling rate of 50 kHz. The display of the PA can be configured to examine these waveforms with a precision of up to 20 $\mu$s. For example, in Fig. 3, the waveform of the power consumption of BG96 radio under real network is recorded as a data log file from the Keysight PA. This data log file is displayed in the "Maker View" of the data logger screen where the power trace P1 (Label 3 in Fig. 3) is displayed with 100 mW/Div (Label 1 in Fig. 3) on vertical/power scale and 20.0 s/d (Label 4 in Fig. 3) on the horizontal/time scale of the PA screen. The voltage (V1) and current (I1) (under Label 1 in Fig. 3) are not selected for readability. The markers m1 and m2 (Label 2 in Fig. 3) are set to positions, where they intersect the P1 trace of the BG96 radio at the beginning and end of its C-DRX mode (Active waiting); thus, the information available under Labels 5 to 10 presents the data available between m1 and m2 markers and can be read as summarized in Table III.

All the measurement results presented in rest of this article are recorded as data log files and displayed in the Marker view of the PA, similar to the one as shown in Fig. 3. This approach is used to produce actual power traces of the BG96 radio under

TABLE III
READING DATA FROM THE MARKER VIEW OF THE POWER ANALYZER

| Symbol/Field | Description |
|---|---|
| 1 Trace Controls | Identifies the voltage/div. or current/div. settings. Tick ($\sqrt{}$) indicates the trace is on. Dots ($\cdots$) indicate the trace is off. *In current setup, we only select the power trace.* |
| 2 m1/m2 markers | Shows where the measurement markers intersect the selected waveform. Data values at the bottom of the display (i.e. labelled **5**-**10**) are referenced to the intersect locations of the markers. Calculations are based on the data points in between the intersect locations. |
| 3 Data Trace | Voltage, Current, Power trace as selected in Label 1. |
| 4 Time/Div. | Identifies the horizontal time-base setting , i.e. the scale of each horizontal square on the screen. |
| 5 m1 | Indicates the m1 marker value in volts, amps, or watts at the intersection point. Also indicates the distance in time of the m1 marker in relation to the present trigger position. |
| 6 m2 | Indicates the m2 marker value in volts, amps, or watts at the intersection point. Also indicates the distance in time that the m2 marker is in relation to the present trigger position. |
| 7 Delta | Indicates the absolute difference ($\Delta$) between the markers in units (volts, amps, or watts) and in time (s). |
| 8 Min. | Indicates the minimum data value (in volts, amps, or watts) between the marker locations of the selected waveform. Also indicates the distance in time of the minimum value in relation to the present trigger position. |
| 9 Avg. | Calculates the average data value (in volts, amps, or watts) between the marker locations of the selected waveform. Time indicates the time between markers over which the average value is calculated. *For all the measurements in rest of this work, we only consider the average values of power consumption and elapsed time for the power trace in between the m1 and m2 markers that are indicated by the current 'Avg.' field.* |
| 10 Max. | Indicates the maximum data value (in volts, amps, or watts) between the marker locations of the selected waveform. Also indicates the distance in time of the maximum value in relation to the present trigger position. |
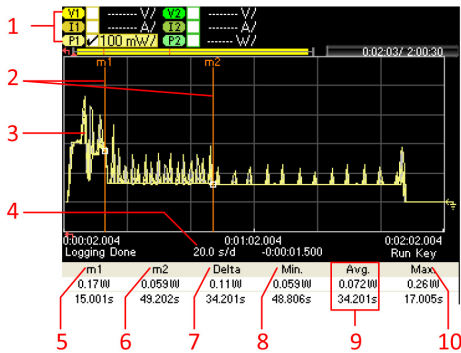


Fig. 3. Measurement Setup with Keysight N6705C DC Power Analyzer: Example of an NB-IoT waveform and measurement information available in the marker view.

real network with on-field measurements from the PA. For all the power measurements and energy calculations for rest of the waveforms/traces in this article, Label 9 provides an average power consumption and average timings between the m1 and m2 markers. These markers are set to various positions on the respective power traces of the BG96 radio transceiver, so as to obtain the adequate power consumption and timings details for the various states of its RRC operation.

*C. Empirical Results*

A number of experiments were conducted using two CoTS NB-IoT radio modules operating under two MNOs operating NB-IoT test networks in Tallinn, Estonia. To verify and evaluate the correctness of our proposed model, various timings for the different states of the NB-IoT radio modules were tried and tested for different power saving schemes. The generated results were tested for various versions of the FWs of these radio modules to verify their impact on the performance of the NB-IoT radio as they are continuously updated and to see to

what extent they are compliant with the 3GPP defined NB-IoT standards. Our obtained results from these tests are explained in the subsections that follow.

*1) Testing Active Waiting (C-DRX) Mode of the Avnet BG96 Radio Under Operator1 Network:* To evaluate the detailed energy consumption of the C-DRX mode of the BG96 radio, we set the network parameters as C-DRX = 1, eDRX = 0, and PSM = 0 and obtained our empirical results for Operator1 network, as shown in Fig. 4. It could be observed that Operator1 had no limitations on the duration of its C-DRX mode as the radio remains in its active waiting state for as long as it was powered on. This is shown in Fig. 4(b), where the average power consumption for the entire C-DRX mode is measured to be 0.082 W. Fig. 4(c) details that each C-DRX cycle of 2.56 s with an average power consumption of 0.082 W. Fig. 4(a) details the attach procedure of the BG96 radio with the Operator1 network with an average power consumption of 0.18 W over 18.6 s.

During the second phase of the same experiment, the C-DRX mode of the BG96 radio was limited to a duration of 1 m, after which the radio was forced to switch to its PSM state, as shown in Fig. 5. The respective average power consumption for the C-DRX mode and C-DRX cycle, as shown in Fig. 5(a) and (c), was found to be the same as previously. However, the average power consumption of the PSM of the BG96 radio was found to be 0.19 mW, as shown in Fig. 5(b).

*2) Testing Idle Waiting (eDRX) Mode of Avnet BG96 Radio Under Operator1 Network:* To evaluate the fine-grained energy consumption of the eDRX mode of the BG96 radio with the underneath details of its eDRX cycle(s) that includes an eDRX_Opportunity and a PTW, and the underneath I-DRX cycles of each PTW, we carried out a second series of experiments, where we set the network parameters as C-DRX = 0, eDRX = 1, and PSM = 1 with T3324 timer = 4 m; such that the eDRX mode runs for 4 min and then switches to its PSM state. Our results from these experiments are summarized in Fig. 6. The average power consumption for the entire eDRX mode was found to be 0.071 W, as shown in Fig. 6(a), 0.070 W
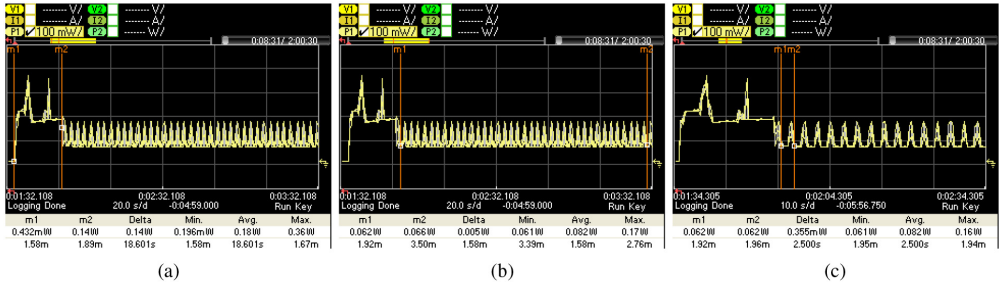
Fig. 4. Continuous CDRX Mode with BG96/Avnet shield under Operator 1. (a) Power trace of UE's Attach procedure with an average power consumption of 0.18 W. (b) Power trace of C-DRX mode with an average power consumption of 0.082 W. (c) Power trace of UE's C-DRX cycle with an average power consumption of 0.082 W.
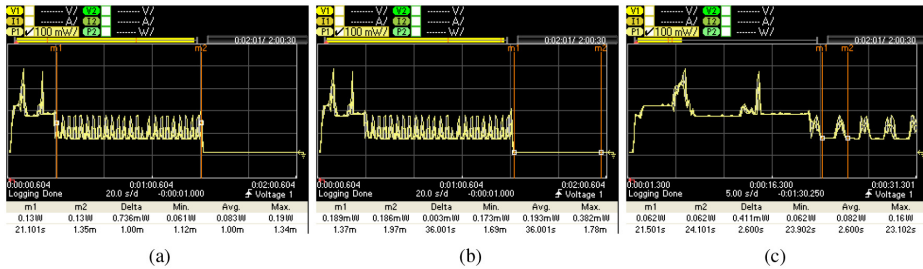


Fig. 5. Controlled C-DRX Mode with BG96/Avnet shield under Operator1. (a) Power trace of UE's C-DRX mode with an average power consumption of 0.083 W. (b) Power trace of UE's PSM with an average power consumption of 0.19 mW. (c) Power trace of UE's C-DRX cycle with an average power consumption of 0.082 W.
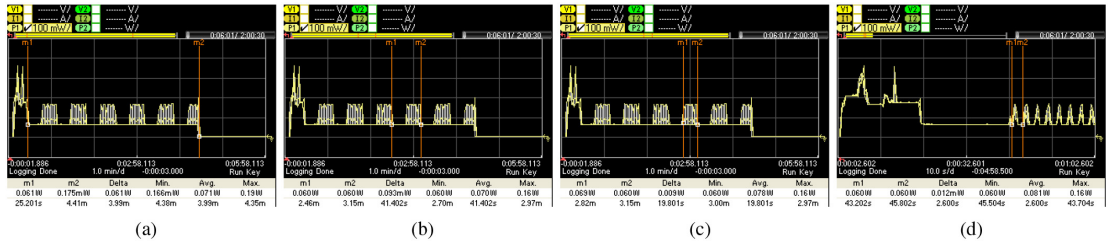


Fig. 6. eDRX Mode (i.e., C-DRX = 0, PSM = 1, and T3324 = 4 m) with BG96/Avnet shield under Operator1. (a) Power trace of UE's eDRX mode with an average power consumption of 0.071 W. (b) Power trace of UE's eDRX cycle with an overall average power consumption of 0.070 W. (c) Power trace of UE's PTW with an average power consumption of 0.078 W. (d) Power trace of I-eDRX cycle with an average power consumption of 0.081 W.

for each eDRX cycle of 41.40 s, as shown in Fig. 6(b), and 0.078 W for the PTW of 19.80 s each, as shown in Fig. 6(c). The I-DRX cycle was found to be 2.56 s with an average power consumption of 0.081 W, as shown in Fig. 6(d).

*3) Testing Power Cycle (a Repeated Sequence of C-DRX, eDRX, and PSM) of the Avnet BG96 Radio Under Operator1 Network:* In these set of experiments, we evaluated the fine-grained energy consumption of the BG96 radio in a power cycle consisting of the C-DRX mode, eDRX-Mode, and PSM with the T3324 timer set to 4 min and T3412 timer set to 1 h; the results are shown in Fig. 7. All the obtained results were found to be the same as in the previous Experiment 1 and Experiment 2. Furthermore, it was observed that the radio automatically woke up from its PSM to reattach with the network and repeat its power cycle with its previous settings. The power traces for the C-DRX, eDRX, and PSM states during these experiments are shown in Fig. 7(a)–(c), respectively.

Furthermore, we transmitted 10 bytes of data from the BG96 radio on Operator1 network using UDP protocol at different CEL, as shown in Fig. 8(a) and (b). It was observed that the radio consumed 0.000372 Wh to transmit data at CEL = 0; whereas, it consumed 0.000816 Wh to transmit the same data at CEL = 1, i.e., an increase of 124.09%.

*4) Testing Power Cycle of the Avnet BG96 Radio Under Operator2 Network:* All the above experiments were repeated with the Avnet BG96 shield under similar conditions but this time with Operator 2's network. The obtained results from these tests are summarized in Fig. 9. During these tests, it was observed that Operator 2's network had more restrictions on
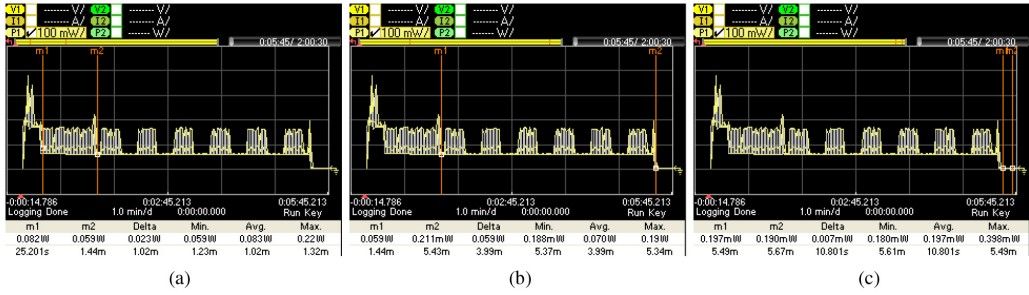
Fig. 7. Power cycle with BG96/Avnet shield under Operator1 network. (a) C-DRX mode runs for 1.0 min (UE configured). (b) eDRX mode runs for 4 min (UE-configured). (c) PSM runs for 60 min (UE-configured), not shown in full for readability.

TABLE IV
SUMMARY OF THE POWER CONSUMPTION OF VARIOUS STATES OF THE AVNET SILICA BG96 SHIELD UNDER THE OPERATOR1 NETWORK

| Avnet Silica BG96 shield current and power consumption details with a constant 3.3V power supply | | |
|---|---|---|
| **Operational Modes** | *Avg Current* | *Avg Power* |
| **Attach/Resume Procedure ( ≈ 18s)** | **56.8 mA** | **180 mW** |
| **C-DRX Mode(Not fixed to any value)** | **25.1 mA** | **82 mW** |
| C-DRX Cycle = 2.56 s | 25.1 mA | 82 mW |
| On duration (PO) = 1.28 s | 32 mA | 110 mW |
| Off duration (SP) = 1.28 s | 18.1 mA | 59 mW |
| **eDRX Mode (as defined by T3324 = 4 m)** | **21.8 mA** | **71 mW** |
| eDRX Cycle= 40.96 s | 21.8 mA | 70 mW |
| PTW = 20.48 s | 25.5 mA | 78 mW |
| I-eDRX Cycle = 2.56 s | 24.47 mA | 81 mW |
| On duration (PO) = 1.28 s | 31 mA | 110 mW |
| Off duration (SP) = 1.28 s | 17.98 mA | 59 mW |
| eDRX Opportunity = 20.48 s | 17.97 mA | 59 mW |
| **PSM Mode (as defined by (T3412-T3324) value)** | **0.05 mA** | **0.19 mW** |

their network parameters as compared to Operator 1, i.e., the UE/radio had little provisions to configure the network parameters. For example, the C-DRX mode was fixed to 34 s (during all our tests); whereas, the eDRX mode and PSM could be configured by the UE as desired. However, the eDRX cycle and its underneath PTW in the C-DRX mode could not be configured (contrary to the case with Operator 1). It was also noted that the radio took 12.6 s on average to get connected to Operator 2's network, as compared to an average of 18 s on Operator 1's network.

Furthermore, we transmitted 10 bytes of data from the BG96 radio on Operator 2's network using the UDP protocol at different CEL, as shown in Fig. 10(a) and (b). It was observed that the radio consumed 0.00011 Wh at CEL = 0; whereas, it consumed 0.00016 Wh to transmit the same data at CEL = 1, i.e., an increase of 45.45%. Similarly, a comparison between the effects of overheads involved in the two data transmission protocols (i.e., UDP and HTTPs) on the energy consumption of the radio was also made, where the desired data of 10 bytes (that were required to be sent from the radio) were transmitted from the BG96 radio on Operator 2's network at different CEL, with additional 61 bytes of data that were the requirement of the HTTPs protocol for its server setup. The obtained power traces from these experiments are shown in Fig. 11(a) and (b). It was observed that the radio consumed 0.00052 Wh at CEL = 0 and 0.00080 Wh at CEL = 1 for the transmission of the same 71 Bytes of data through the HTTPS protocol, i.e., an increase of 53.8% in the energy
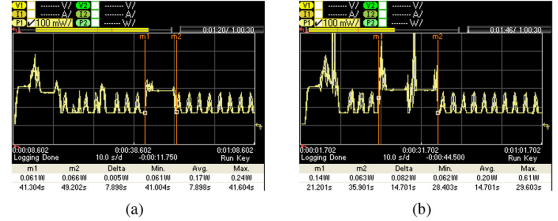


Fig. 8. Transmitting ten bytes of data using UDP protocol on Operator1 network. (a) Data Transmission at CEL = 0 consumes 0.17 W for 7.898 s (0.000372 Wh). (b) Data Transmission at CEL = 1 consumes 0.20 W for 14.701 s (0.000816 Wh), i.e., an increase of 119.35%.

consumption when the CEL changed, i.e., the radio transmits for longer time because of the lower signal strength. In comparison to the UDP transmission protocol, this was an increase of 372% and 400% at CEL = 0 and CEL = 1, respectively, because of transmitting the extra 61 bytes of data overhead.

Tables IV and V summarize the power consumption of various states of the Avnet Silica BG96 shield under Operator1 and Operator2 test networks, respectively.

*5) Verifying Our Results for Operator1 and Operator2 Networks With Quectel BG96 EVB Kit:* All the above experiments were repeated for both the operators on the same location and under similar conditions using the Quectel BG96 EVB kit [30]. Since similar power graphs for C-DRX, eDRX,

Fig. 9.　Power cycle of the Avnet BG96 shield under Operator2 network: (a) C-DRX mode runs for 34.2 s, (b) eDRX mode runs for 1.0 min (UE configured), and (c) PSM runs for 1.0 h (UE configured), not shown in full for readability. In the Operator 2 network, the C-DRX Cycle is 2.1 s while the I-DRX Cycle is 5.12 s.

TABLE V
SUMMARY OF THE POWER CONSUMPTION OF VARIOUS STATES OF THE AVNET SILICA BG96 SHIELD UNDER THE OPERATOR2 NETWORK

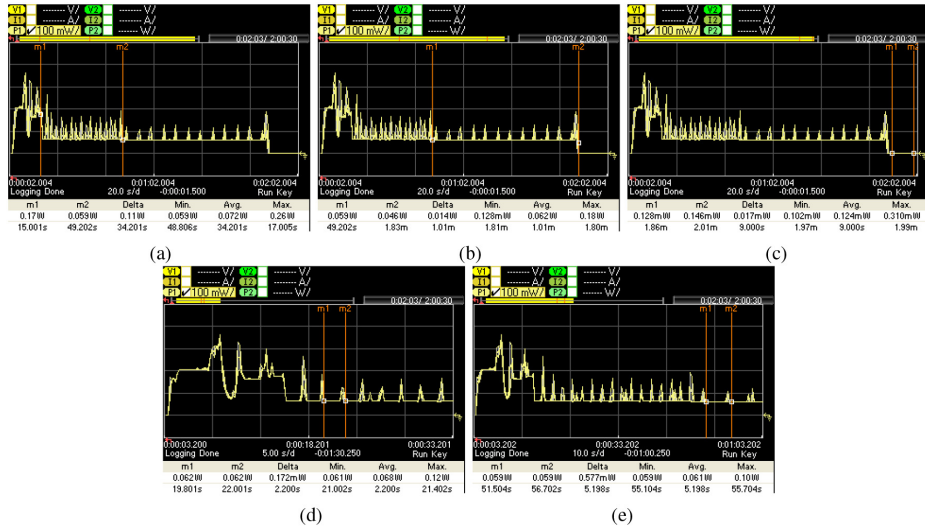| Avnet Silica BG96 shield current and power consumption details with a constant 3.3V power supply | | |
|---|---|---|
| Operational Modes | *Avg Current* | *Avg Power* |
| **Attach/Resume Procedure ( ≈ 12 s)** | **40.1 mA** | **190 mW** |
| **C-DRX Mode (Fixed to 34 s)** | **21.3 mA** | **72 mW** |
| C-DRX Cycle = 2.1 s | 21.2 mA | 70 mW |
| On duration (PO) = 0.5 s | 28 mA | 98 mW |
| Off duration (SP) = 1.6 s | 18.6 mA | 62 mW |
| **eDRX Mode (as defined by T3324)** | **19.2 mA** | **63 mW** |
| eDRX Cycle = 5.12 s (Fixed) | 18.8 mA | 62 mW |
| On duration (PO) = 0.3 s | 26.2 mA | 87 mW |
| Off duration (SP) = 4.7 s | 18.2 mA | 60 mW |
| **PSM Mode (as defined by (T3412-T3324) value)** | **0.03 mA** | **0.12 mW** |
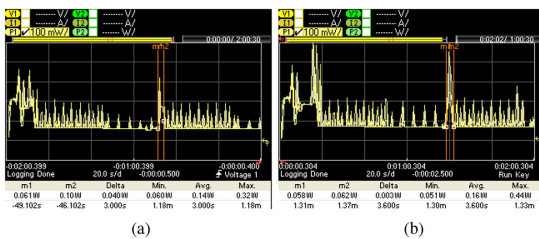


Fig. 10.　Transmitting ten byte of data using UDP protocol on Operator2 network. (a) Data Transmission at CEL = 0 consumes 0.14 W for 3 s (0.00011 Wh). (b) Data Transmission at CEL = 1 consumes 0.16 W for 3.6 s (0.00016 Wh), i.e., an increase of 45.45%.
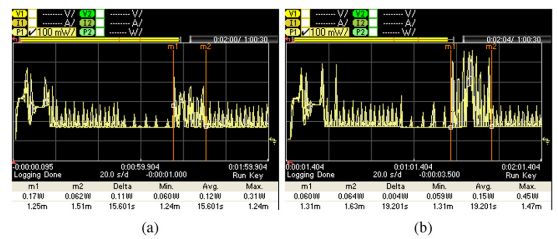


Fig. 11.　Transmitting 71 bytes of data to ThingSpeak server [35] using HTTPS protocol on Operator2 network. (a) Data Transmission at CEL = 0 consumes 0.12 W for 15.6 s (0.00052 Wh). (b) Data Transmission at CEL = 1 consumes 0.15 W for 19.2 s (0.0008 Wh), i.e., an increase of 53.84%.

and PSM modes of the BG96 radio were obtained from the PA, these graphs are not included in this article for conciseness. Nevertheless, the results obtained for all these tests are summarized in Tables VI and VII, respectively.

Finally, a side-by-side comparison of the current and power consumption of the two boards, i.e., Avnet BG96 shield and

Quectel BG96 EVB kit, for both the networks, i.e., Operator 1 and Operator 2, are summarized in Tables VIII and IX.

### D. Summary and Discussion of the Measurement Results

In the remainder of this section, we summarize our main observations of the experimental results and present a discussion thereof.

TABLE VI
SUMMARY OF THE POWER CONSUMPTION OF VARIOUS STATES OF QUECTEL BG96 EVB KIT UNDER THE OPERATOR1 NETWORK

| QUECTEL BG96 Kit current and power consumption details with a constant 3.8V power supply | | |
|---|---|---|
| **Operational Modes** | ***Avg Current*** | ***Avg Power*** |
| **Attach/Resume Procedure ( ≈ 18 s)** | **51.8 mA** | **200 mW** |
| **C-DRX Mode(Not fixed by the operator)** | **26.1 mA** | **100 mW** |
| C-DRX Cycle = 2.56 s | 25.6 mA | 97 mW |
| On duration (PO) = 1.28 s | 30.6 mA | 120 mW |
| Off duration (SP) = 1.28 s | 20.1 mA | 78 mW |
| **eDRX Mode (as defined by T3324 = 4 m)** | **20.22 mA** | **77 mW** |
| eDRX Cycle= 40.96 s | 20.22 mA | 77 mW |
| PTW = 20.48 s | 22.77 mA | 87 mW |
| I-eDRX Cycle = 2.56 s | 22.57 mA | 86 mW |
| On duration (PO) = 1.28 s | 27.6 mA | 100 mW |
| Off duration (SP) = 1.28 s | 16.9 mA | 66 mW |
| eDRX Opportunity = 20.48 s | 17.1 mA | 66 mW |
| **PSM Mode (value of (T3412-T3324))** | **0.05 mA** | **0.20 mW** |

TABLE VII
SUMMARY OF THE POWER CONSUMPTION OF VARIOUS STATES OF QUECTEL BG96 EVB KIT UNDER THE OPERATOR2 NETWORK

| QUECTEL BG96 kit current and power consumption details with a constant 3.8V power supply | | |
|---|---|---|
| **Operational Modes** | ***Avg Current*** | ***Avg Power*** |
| **Attach/Resume Procedure ( ≈ 12s)** | **59.3 mA** | **190 mW** |
| **C-DRX Mode (Fixed to 34 s)** | **25.3 mA** | **86 mW** |
| C-DRX Cycle = 2.1 s | 25.2 mA | 85 mW |
| On duration (PO) = 0.5 s | 28 mA | 170 mW |
| Off duration (SP) = 1.6 s | 18.6 mA | 78 mW |
| **eDRX Mode (as defined by T3324)** | **19.2 mA** | **63 mW** |
| eDRX Cycle = 5.12 s (Fixed) | 30.8 mA | 100 mW |
| On duration (PO) = 0.4 s | 29.8 mA | 98 mW |
| Off duration (SP) = 4.7 s | 22.9 mA | 76 mW |
| **PSM Mode (value of (T3412-T3324))** | **0.05 mA** | **0.19 mW** |

TABLE VIII
SIDE BY SIDE COMPARISON OF THE AVERAGE POWER MEASUREMENTS OF AVNET BG96 SHIELD AND QUECTEL BG96 EVB KIT UNDER OPERATOR1 AND OPERATOR2 NETWORKS

| Power Consumption of the Avnet BG96 shield and Quectel BG96 EVB Kit | | | | |
|---|---|---|---|---|
| Quectel / Avnet | **Attach (mW)** | **CDRX (mW)** | **eDRX (mW)** | **PSM (mW)** |
| **Operator 1** | 200 / 180.0 | 100 / 82.0 | 77.0 / 71.0 | 0.20 / 0.19 |
| **Operator 2** | 190 / 190.0 | 86.0 / 72.0 | 63.0 / 63.0 | 0.19 / 0.12 |

TABLE IX
SIDE BY SIDE COMPARISON OF THE AVERAGE CURRENT MEASUREMENTS OF AVNET BG96 SHIELD AND QUECTEL BG96 EVB KIT UNDER OPERATOR1 AND OPERATOR2 NETWORKS

| Current consumption of the Avnet BG96 shield and Quectel BG96 EVB Kit | | | | |
|---|---|---|---|---|
| Quectel / Avnet | **Attach (mA)** | **CDRX (mA)** | **eDRX (mA)** | **PSM (mA)** |
| **Operator 1** | 51.8 / 56.8 | 26.1 / 25.1 | 20.22 / 21.8 | 0.05 / 0.05 |
| **Operator 2** | 59.3 / 40.1 | 25.3 / 21.3 | 19.2 / 19.2 | 0.05 / 0.03 |

For the results shown in Tables IV–IX, the experiments were repeated in the order of 100 times and the values were averaged accordingly. As indicated previously, Table IV summarizes the current and power consumption details of the Avnet shield under Operator1's network; whereas, Table V summarizes the current and power consumption details of the Avnet board under Operator2's network. Comparing the current and power data from both of these tables, it can be noted that with Operator1's network, the BG96 radio consumes more power on average for most of its operational modes as compared to when operating under Operator2' network. It can also

be noted that contrary to the other radio modes, the power and current data values for the PSM are the same with both networks.[1]

The same observations stand true when comparing the current and power consumption data in Tables VI and VII

---

[1]It is also noted that the average current consumption for PSM = 0.05 mA, which is higher than the 0.01 mA value indicated in the datasheet [31]. Such a difference can be due to the additional components needed to implement a BG96 minimum system on the Avnet shield (e.g., power regulator, USB interface, etc.). Such a difference is also in line with our observation that, in a practical system, the energy consumption of NB-IoT radio transceivers is often under-estimated.

obtained for the Quectel BG96 EVB kit for both of these networks. It is clear that the BG96 radio consumes more power on average for most of its operational modes when connected to Operator1's network as compared to Operator2.

However, comparing the current and power consumption data as obtained for both of these boards , i.e., Avnet Silica and Quectel EVB kit, it is also clear that the latter consumes more for the same network parameters and under the same network conditions.

To have a better overview of all the data from the above-mentioned tables, we have further summarized them in Tables VIII and IX. All in all, it can be said that from the network side Operator1 has a higher energy consumption, while from the device side, the Quectel EVB Kit consumes more than the AVNET shield.

While the current and power consumption differences between the two boards can be explained by the fact the Quectel EVB kit features more active components than the Avnet Silica board, the differences between the two networks call for a more detailed discussion, as presented in what follows.

An essential point to keep in mind is that the UE settings affect its energy consumption to a great extent, in particular in terms of active waiting, idle waiting and PSM. At the same time, these also have a notable impact on the application QoS. In parallel, the network settings also have a significant impact on the energy consumption of the UE. In more details:

1) the inactivity timer is operator specific; thus, depending on the network configuration, this can be a major energy-saving factor on the UE side. Our results have shown that Operator2 provides greater flexibility in terms of control and configurability of the C-DRX (within the inactivity timer) mode as compared to Operator1. On the other hand, Operator1 does not limit the length of its active waiting period (within the inactivity timer). This explains why Operator1 consumes more as compared to Operator 2 since the latter has a controlled active waiting period. Moreover, since the inactivity timer is reset after each downlink data exchange, the longer its span the larger its impact on the UE energy consumption. Similarly, if downlink data are received in fragments, the energy consumption due to the inactivity timer will add up;

2) the activity timer is UE configurable, but its underneath eDRX cycles with its PTW and its underneath I-DRX cycles are network specific; thus, their settings affect the overall energy consumption of the UE. Operator2 also provides a greater flexibility in terms of control and configurability of its eDRX settings as compared to Operator1; since the former supports more robust settings for these parameters, it is thus more energy friendly from the UE perspective. However, the effects of such parameters on the QoS of application are still unknown and beyond the scope of this article. Though Operator 1 provides more flexibility in these settings, the overall energy consumption of the radio is higher;

3) the power consumption of the PSM of the radio is nearly identical with both operators. This can be explained by the fact that when in the PSM mode, most parts of the radio module are turned off and no operator-specific parameter affects the current drawn by the chip. However, a general comment is that while the longer the radio stays in PSM, the larger its energy savings, this translates in increased latency cost and, thus, possibly reduced QoS for the application. This important tradeoff in NB-IoT is not yet fully explored in the literature;

4) our experiments have also shown that the transmission power varies with the signal strength of the radio and, thus, affects the UE energy consumption. The transmit power can be ramped-up to a maximum of 23 dBm, whether when connecting to the BS or while transmitting data. For example, in Fig. 11(a), it can be seen that the power for data transmission is 0.12 W (i.e., 20.79 dBm) and 0.15 W (i.e., 21.76 dBm) in Fig. 11(b). Since the UE has no provision to control its transmit power, the energy consumption from the UE transmit power point of view is not an exclusive UE feature;

5) the data transmission protocol varies in terms of their control overheads, data payloads, CEL, and security/guarantees. These various aspects yield different energy consumption as seen in our experimental results when transmitting data with the UDP and HTTPs protocols in two different coverage classes. For example, Figs. 8 and 10 show that transiting from the CEL = 0 to CEL = 1 with UDP leads to energy consumption increases between 45% and 119%, i.e., up to more than a factor 2. Fig. 11(a) and (b) shows that the same transition with HTTPs leads to an increase of 53.84%, i.e., slightly more than a factor 1.5. Also, as mentioned earlier, the increase between UDS and HTTPs ranges from 372% and 400%.

Moreover, from the results obtained through these experiments, it is clear that almost all of the 3GPP defined UE states are attainable on both MNO's test networks, and thus by extension on commercial networks; this is in stark contrast to what has been reported in most of the existing literature so far. The results also indicates that all the power saving features of the NB-IoT technology are included in the considered CoTS NB-IoT radio chips and could be utilized as per the application requirements. However, as the hardware and software developments of NB-IoT are ongoing, special care must be taken to choose the right firmware for the right hardware that is being used for the specific application. Our results also show that all the timers are flexible and can be set as per the 3GPP standards provided the network operators allow any such provisions from the network side and this should be kept in mind by application developers to obtain network access.

## V. EVALUATION OF OUR PROPOSED MODEL

Section IV has presented individual empirical measurement results for various timings for the different states of the NB-IoT radio module for different power saving schemes. Next, in this section we: 1) evaluate the error of our proposed model by calculating the difference between the energy consumption obtained from the real-life deployment versus that predicted by
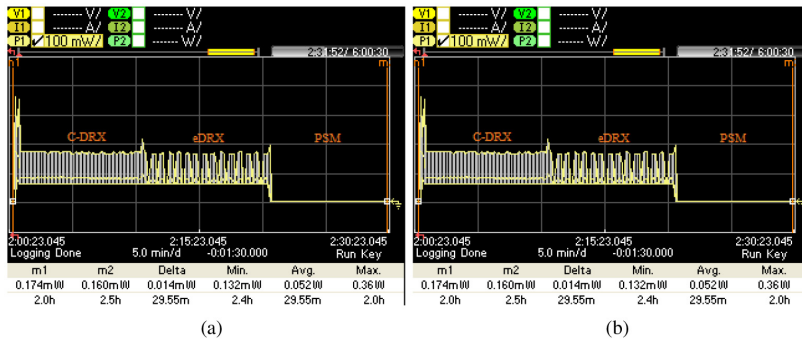
Fig. 12. Power traces of the first evaluation test with the Avnet BG96 shield operating on Operator1 network. (a) Power cycle of 30 min ("29.55 m" displayed between m1 and m2 markers) that includes an Attach procedure of 18 s, C-DRX, e-DRX, and PSM of a bit less than 10 min each. (b) Power cycle of (a) is repeated two times in an observation window of 60 min ("59.53 m" displayed between m1 and m2 markers).
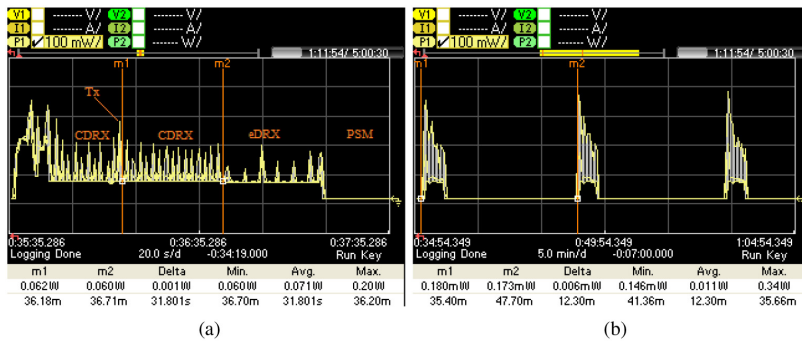


Fig. 13. Power traces of the second evaluation test with Avnet BG96 shield on Operator2 network. (a) Power cycle of 12.3 min that includes an Attach procedure of 12.1 s, C-DRX mode of 20 s, Tx (10 bytes data over UDP) of 3 s, repeated C-DRX of 32 s ("31.801 s" displayed between m1 and m2 markers), eDRX of 34 s and PSM of a bit more than 10 min (not shown in full for readability). (b) Power cycle of (a) 12.3 min ("12.30 m" displayed between m1 and m2 markers) is repeated 3 times (the last PSM phase is not shown in full for readability).

the model and 2) we summarize the sensitivity analysis conducted to evaluate which parameters have the largest impact on the total energy consumption in our proposed model.

### A. Model Evaluation Tests

We have conducted three sets of experiments of which the base cycle lasts from 12.3 min to 1.2 h and is repeated from 2 to 10 times during the observation window. Doing so forces the NB-IoT radio in various operational conditions and allows characterizing the average differences between the energy consumption predicted by the model and the real-life values. The three sets of experiments use the Avnet BG96 shield operating on the Operator1 or Operator2 network, as described in what follows.

The first evaluation test was executed with an Avnet BG96 shield board operating on the Operator1 network. The test consisted of a base power cycle of 30 min as captured between m1 and m2 (29.55 min shown) in Fig. 12(a) and repeated twice in an observation window of 1 h (59.53 min shown) between m1 and m2, as shown in Fig. 12(b). As can be seen in Fig. 12(a), the base power cycle includes an attach procedure of 18 s, and C-DRX, e-DRX, and PSM states of a bit less than 10 min each where the average power consumption for the base power

cycle is 0.052 W. As can be seen in Fig. 12(b), it is repeated twice over a period of 60 min captured between m1 and m2 (59.53 min shown), where the average power consumption is found to be 0.052 W. The energy consumed per each power cycle as per (19) is 0.022 Wh; whereas, that measured with the PA is 0.026 Wh. The energy consumed for the entire observation window as per (19) is 0.044 Wh; whereas, that measured with the PA is 0.052 Wh, i.e., an error of 15.38%, as indicated in Table X.

The second evaluation test was also conducted with an Avnet BG96 shield, but this time operating on Operator2 network. The test consisted of the base power cycle shown in Fig. 13(a) (m1 and m2 in this figure are used to record the repeated C-DRX cycle of the radio after a data transmission (Tx)); this power cycle is repeated three times as shown in Fig. 13(b). The base power cycle lasts 12.3 min and includes an Attach procedure of 12.1 s, C-DRX mode of 20 s, Tx through UDP protocol of 3 s, repeated C-DRX of 32 s, eDRX of 34 s, and PSM of a bit more than 10 m. The base power cycle consumes on average 0.011 W during the 12.3-min duration, i.e., an average energy consumption of 0.0022 Wh. As indicated in Table X, the energy consumed per power cycle as per (19) is 0.0024 Wh, i.e., an error of 9.09%.

TABLE X
NB-IoT RADIO ENERGY CONSUMPTION ERROR: PROPOSED MODEL VERSUS REAL-LIFE EVALUATION TESTS

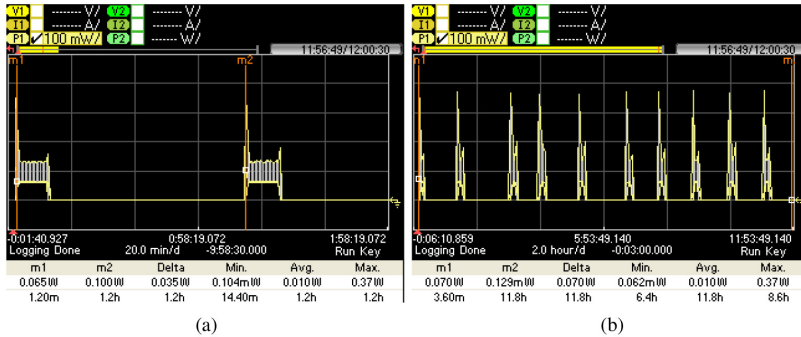| Test setup | Energy as per model (Wh) | Energy as per measurement (Wh) | Relative Error (%) |
|---|---|---|---|
| Avnet BG96 shield, Operator1 | 0.052 | 0.044 | 15.38 |
| Avnet BG96 shield, Operator2 | 0.0024 | 0.0022 | 9.09 |
| Avnet BG96 shield, Operator2 | 0.01204 | 0.01200 | 0.33 |



Fig. 14. Power traces of the third evaluation test with Avnet BG96 shield under Operator2 network. (a) Power cycle of 1.2 h ("1.2 h" between m1 and m2 markers) including an Attach procedure of 12.1 s, C-DRX of 32 s, e-DRX of 10 min, and PSM of 64 min. (b) Power cycle of (a) is repeated ten times in an observation window of 11.8 h ("11.8 h" between m1 and m2 markers). (Note that some of the PSM durations are shorter than others.)

Like the second one, the third evaluation test was conducted with the Avnet BG96 shield operating under the Operator2 network, but this time for a longer duration. The base cycle lasts 1.2 h, including an Attach procedure of 12 s, CDRX of 32 s, e-DRX of 10 min, and PSM of 64 min, as shown in Fig. 14(a). This power cycle of 1.2 h has an average power consumption of 0.010 W. It is then repeated ten times in an observation window of 11.8 h, as shown in Fig. 14(b) (note that some of the PSM durations are shorter than others). In this case, the energy consumed per power cycle measured with the PA is 0.01200 Wh; whereas, as per (19), it is found to be 0.01204 Wh, i.e., an error of 0.33% only, as indicated in Table X.

The error of the proposed model ranges from as low as 0.33% for longer durations (e.g., when the radio has to activate after several hours or more), and reaches up to approximately 15.38% for shorter durations (e.g., when the radio has to activate after several minutes to hours). Since the majority of NB-IoT applications are intended for longer duration scenarios, the error will lie on the smaller end; as also indicated by the sensitivity analysis of the model.

Regarding system noise and environmental noise, we have used CoTS NB-IoT devices in order to create a realistic energy consumption model that reflects the practical performance of such devices, including possible inherent system noises. Furthermore, precautions (grounding of measurement equipment, etc.) were taken when carrying out our experiments, and no environmental noises were observed during our measurement campaign. Regarding interference, although there could be an impact due to intercell and intracell interferences, we have not experienced such interferences due to the limited number of devices connected to our test networks (the issue of intercell interference has been investigated in our previous work [36], [37], i.e., 10%–15% throughput can be improved while exploiting inference minimization schemes).

TABLE XI
SENSITIVITY ANALYSIS OF THE POWER CONSUMPTION
PARAMETERS OF BG96 RADIO

| BG96 Power Parameters | | | | | | |
|---|---|---|---|---|---|---|
| $P_{TAU}$ | $P_{ATTACH}$ | $P_{TX}$ | $P_{RX}$ | $P_{CDRX}$ | $P_{eDRX}$ | $P_{PSM}$ |
| 0.18W | 0.18W | 0.17W | 0.16W | 0.083W | 0.070W | 0.0002W |

### B. Summary of the Sensitivity Analysis of the Model

The sensitivity analysis (SA) was carried out on both the power consumption parameters and timings parameters of the proposed model.

The SA of the power consumption parameters, i.e., $P_{ATTACH}$, $P_{TX}$, $P_{RX}$, $P_{CDRX}$, $P_{eDRX}$, $P_{PSM}$, and $P_{TAU}$, of our proposed model indicates that they are technology-dependent and may vary for various chipsets. For example, typical values for the power consumption parameters of the BC95 chipset (an advanced IoT chipset from Quectel) are slightly lower than those for the BG96 chipset from the same vendor. Similarly, the values for these power parameters may also differ slightly from vendor to vendor. That is why these power parameters affect the overall energy consumption of the radio but only to a smaller extent. Since we have used BG96 chipset-based modules for all our experiments in this work, we thus decided to use the values for the power consumption parameters of BG96 chipset; with a possible impact on the overall energy consumption of the radio in a descending order as shown in Table XI.

On the other hand, the timing parameters of the proposed model, i.e., $T_{ATTACH}$, $T_{TX}$, $T_{RX}$, $T_{CDRX}$, $T_{eDRX}$, $T_{PSM}$, and $T_{TAU}$ have their minimum and maximum values (as standardized by 3GPP) as given in Table XII.

The sensitivity analysis of these timing parameters indicates that they have an impact on the total energy consumption of the radio, in a descending order, as explained as follows.

TABLE XII
SENSITIVITY ANALYSIS OF THE TIMINGS PARAMETERS
OF NB-IoT RADIO

| Minimum and Maximum values for the Timing Parameters | | | | |
|---|---|---|---|---|
| $T_{TAU}$ / $T_{ATTACH}$ | $T_{TX}$ / $T_{RX}$ | $T_{CDRX}$ | $T_{eDRX}$ | $T_{PSM}$ |
| 18.6s - # of attempts | 0s–# of transmissions | 10s–60s | 0s–186m | 0s–413d |

1) $T_{ATTACH}$ has the most impact on the overall energy consumption of the radio, especially when the radio wakes up frequently (e.g., in patterns of a few minutes). However, in less frequent scenarios (e.g., once per day or weeks), its impact is negligible. Furthermore, the TAU procedure has almost the same effect as that of the ATTACH procedure (especially from the practical perspective).

2) The active waiting period, i.e., $T_{CDRX}$ and the idle waiting period, i.e., $T_{eDRX}$ have almost an equal impact on the total energy consumption of the radio. However, since the Inactivity timer is limited by the operator (usually set to lower than 60 s), its impact on the total energy consumption is lower as compared to $T_{CDRX}$ of relatively longer durations.

3) Similarly, the impact of the payload size both in ($T_{TX}$, $T_{RX}$) is not significant on the total energy consumption of the radio while the radio is operating in good coverage. However, as the coverage worsens, its impact adds up as a function of the number of repetitions that an NB-IoT radio has to perform in that CEL.

4) Finally, the effect of PSM and its benefits in terms of the total energy consumption of the radio becomes substantial only when enabled for longer durations.

## VI. CONCLUSION

NB-IoT is an emerging technology, which is expected to dominate the IoT landscape in terms of wireless communication technology for massive machine-type communication. Understanding the energy budget of NB-IoT is important; however, this is weakly addressed in the state of the art. The motivation of this work was thus to provide a modeling methodology for profiling the baseline energy consumption of an NB-IoT radio transceiver based on the RRC protocol standardized by 3GPP. The proposed energy consumption model provides a detailed and realistic NB-IoT radio transceiver energy consumption model; the detailed analysis of the RRC protocol and empirical measurements illustrates the fine-grained energy consumption of the RRC protocol for two development boards operating on two MNOs test networks. Finally, the real-life empirical evaluation results showed that the error of the proposed model ranges between 0.33% and 15.38%. The proposed model and its evaluation ensure that it is viable to be used as a reference benchmark for NB-IoT radio communication. In the future, we will explore energy consumption optimization strategies depending on the lifetime requirement of a given application; the proposed baseline energy consumption model will be used to evaluate the impact of such optimization strategies.

## REFERENCES

[1] A. Rico-Alvarino *et al.*, "An overview of 3GPP enhancements on machine to machine communications," *IEEE Commun. Mag.*, vol. 54, no. 6, pp. 14–21, Jun. 2016.

[2] Y.-P. E. Wang *et al.*, "A primer on 3GPP narrowband Internet of Things," *IEEE Commun. Mag.*, vol. 55, no. 3, pp. 117–123, Mar. 2017.

[3] P. Mekikis *et al.*, "NFV-enabled experimental platform for 5G tactile Internet support in industrial environments," *IEEE Trans. Ind. Informat.*, vol. 16, no. 3, pp. 1895–1903, Mar. 2020.

[4] J. Serra, L. Sanabria-Russo, D. Pubill, and C. Verikoukis, "Scalable and flexible IoT data analytics: When machine learning meets SDN and virtualization," in *Proc. IEEE 23rd Int. Workshop Comput. Aided Model. Design Commun. Links Netw. (CAMAD)*, 2018, pp. 1–6.

[5] *Medium Access Control (MAC) Protocol Specification (Release 8), Version 8.0.0*, 3GPP Standard TS 36.321, 2008.

[6] *Evolved Universal Terrestrial Radio Access (E-UTRA); Radio Resource Control (RRC); Protocol Specification (Release 10)*, 3GPP Standard TS 36.331, 2012.

[7] *Radio Resource Control (RRC)*, 3GPP Standard TS 36.331, 2012.

[8] C.-W. Chang and J.-C. Chen, "Adjustable extended discontinuous reception cycle for idle-state users in LTE-A," *IEEE Commun. Lett.*, vol. 20, no. 11, pp. 2288–2291, Nov. 2016.

[9] A. K. Sultania, C. Delgado, and J. Famaey, "Implementation of NB-IoT power saving schemes in ns-3," in *Proc. Workshop Next-Gener. Wireless NS-3*, 2019, pp. 5–8.

[10] A. K. Sultania, P. Zand, C. Blondia, and J. Famaey, "Energy modeling and evaluation of NB-IoT with PSM and EDRX," in *Proc. IEEE Globecom Workshops (GC Wkshps)*, 2018, pp. 1–7.

[11] G. Tsoukaneri, F. Garcia, and M. K. Marina, "Narrowband IoT device energy consumption characterization and optimizations," in *Proc. EWSN*, 2020, pp. 1–12.

[12] C. Y. Yeoh, A. B. Man, Q. M. Ashraf, and A. K. Samingan, "Experimental assessment of battery lifetime for commercial off-the-shelf NB-IoT module," in *Proc. 20th Int. Conf. Adv. Commun. Technol. (ICACT)*, 2018, pp. 223–228.

[13] P. Andres-Maldonado, P. Ameigeiras, J. Prados-Garzon, J. Navarro-Ortiz, and J. M. Lopez-Soler, "Narrowband IoT data transmission procedures for massive machine-type communications," *IEEE Netw.*, vol. 31, no. 6, pp. 8–15, Nov./Dec. 2017.

[14] P. Andres-Maldonado, M. Lauridsen, P. Ameigeiras, and J. M. Lopez-Soler, "Analytical modeling and experimental validation of NB-IoT device energy consumption," *IEEE Internet Things J.*, vol. 6, no. 3, pp. 5691–5701, Jun. 2019.

[15] P. Andres-Maldonado, P. Ameigeiras, J. Prados-Garzon, J. J. Ramos-Munoz, and J. M. Lopez-Soler, "Optimized LTE data transmission procedures for IoT: Device side energy consumption analysis," in *Proc. IEEE Int. Conf. Commun. Workshops (ICC Workshops)*, 2017, pp. 540–545.

[16] M. El Soussi, P. Zand, F. Pasveer, and G. Dolmans, "Evaluating the performance of EMTC and NB-IoT for smart city applications," in *Proc. IEEE Int. Conf. Commun. (ICC)*, 2018, pp. 1–7.

[17] R. Mozny, P. Masek, M. Stusek, K. Zeman, A. Ometov, and J. Hosek, "On the performance of narrow-band Internet of Things (NB-IoT) for delay-tolerant services," in *Proc. 42nd Int. Conf. Telecommun. Signal Process. (TSP)*, 2019, pp. 637–642.

[18] S. S. Basu, A. K. Sultania, J. Famaey, and J. Hoebeke, "Experimental performance evaluation of NB-IoT," in *Proc. Int. Conf. Wireless Mobile Comput. Netw. Commun. (WiMob)*, 2019, pp. 1–6.

[19] B. Martinez, F. Adelantado, A. Bartoli, and X. Vilajosana, "Exploring the performance boundaries of NB-IoT," *IEEE Internet Things J.*, vol. 6, no. 3, pp. 5702–5712, Jun. 2019.

[20] S. Duhovnikov, A. Baltaci, D. Gera, and D. A. Schupke, "Power consumption analysis of NB-IoT technology for low-power aircraft applications," in *Proc. IEEE 5th World Forum Internet Thin. (WF-IoT)*, 2019, pp. 719–723.

[21] M. Lauridsen, R. Krigslund, M. Rohr, and G. Madueno, "An empirical NB-IoT power consumption model for battery lifetime estimation," in *Proc. IEEE 87th Veh. Technol. Conf. (VTC Spring)*, 2018, pp. 1–5.

[22] P. Jörke, R. Falkenberg, and C. Wietfeld, "Power consumption analysis of NB-IoT and EMTC in challenging smart city environments," in *Proc. IEEE Globecom Workshops (GC Wkshps)*, 2018, pp. 1–6.

[23] K. Mikhaylov *et al.*, "Multi-RAT LPWAN in smart cities: Trial of LoRaWAN and NB-IoT integration," in *Proc. IEEE Int. Conf. Commun. (ICC)*, 2018, pp. 1–6.

[24] M. Lukic, S. Sobot, I. Mezei, D. Danilovic, and D. Vukobratovic, "In-depth real-world evaluation of NB-IoT module energy consumption," 2020. [Online]. Available: arXiv:2005.13648.

[25] *GPRS Enhancements for Evolved Universal Terrestrial Radio Access Network (E-UTRAN) Access*, 3GPP Standard TS 23.401, 2013.

[26] *GPRS Enhancements for Evolved Universal Terrestrial Radio Access Network Access, Release 14, V14.1.0*, 3GPP Standard TS 23.401, 2016.

[27] *GPRS Enhancements for Evolved Universal Terrestrial Radio Access Network Access, Release 16, V16.6.0*, 3GPP Standard TS 23.401, 2020.

[28] *LTE; General Packet Radio Service (GPRS) Enhancements for Evolved Universal Terrestrial Radio Access Network (E-UTRAN) Access, Version 14.3.0 Release 14*, ETSI Standard TS 123 401, 2017.

[29] Avnet:Silica. *Avnet: Quality Electronic Components Services*. Accessed: Apr. 29, 2021. [Online]. Available: https://www.avnet.com/wps/portal/silica/products/new-products/npi/2018/avnet-nb-iot-shield-sensor/

[30] Quectel UMTS LTE EVB Kit. *Quectel*. Accessed: Apr. 29, 2021. [Online]. Available: https://www.quectel.com/product/umts-lte-evb-kit/

[31] Quectel LPWA IoT Module. *BG96 LTE Cat M1/NB1/EGPRS Module*. Accessed: Apr. 29, 2021. [Online]. Available: https://www.quectel.com/product/lte-bg96-cat-m1-nb1-egprs/

[32] Keysight Technologies. *N6705C DC Power Analyzer*. Accessed: Apr. 19, 2021. [Online]. Available: https://www.keysight.com/en/pd-2747858-pn-N6705C/dc-power-analyzer-modular-600-w-4-slots?cc=EE&lc=eng

[33] Digilent. *Pmod-USB-to-UART-Interface*. Accessed: Apr. 19, 2021. [Online]. Available: https://store.digilentinc.com/pmod-usbuart-usb-to-uart-interface/

[34] Avnet-Silica-team. *NBIOTBG96SHIELD-HW-Schematic*. Accessed: Apr. 19, 2021. [Online]. Available: https://github.com/Avnet-Silica-team/NBIoTBG96-HW/blob/master/BAENBIOTBG96SHIELD_RSR1157C-SCHEMA.pdf/

[35] ThingSpeak Server. *ThingSpeak for IoT Projects*. Accessed: Apr. 19, 2021. [Online]. Available: https://thingspeak.com/channels/1085017/

[36] H. Malik, H. Pervaiz, M. M. Alam, Y. Le Moullec, A. Kuusik, and M. A. Imran, "Radio resource management scheme in NB-Iot systems," *IEEE Access*, vol. 6, pp. 15051–15064, 2018.

[37] H. Malik *et al.*, "Radio resource management in NB-IoT systems: Empowered by interference prediction and flexible duplexing," *IEEE Netw.*, vol. 34, no. 1, pp. 144–151, Jan./Feb. 2020.

**Sikandar M. Zulqarnain Khan** received the M.Sc. degree in electronics, electrical, control and instrumentation engineering from Hanyang University, Seoul, South Korea, in 2010.

He joined the COMSATs Institute of Information Technology, Islamabad, Pakistan, as a Faculty Member. In 2014, he joined the Instituto de Telecomunicaes of Aveiro, Aveiro, Portugal, as a Researcher. He joined Scuola Superiore Sant'Anna, Pisa, Italy, as a Researcher. In 2017, he joined the School of ECE, Technical University of Crete, Chania, Greece, as a Visiting Researcher. Since 2018, he has been with Thomas Johann Seebeck Department of Electronics, TalTech, Tallinn, Estonia. He has authored several conference and journal research papers. His research interests include embedded systems, control systems, wireless communications, and embedded artificial intelligence.

**Muhammad Mahtab Alam** (Senior Member, IEEE) received the M.Sc. degree in electrical engineering from Aalborg University, Aalborg, Denmark, in 2007, and the Ph.D. degree in signal processing and telecommunication from the INRIA Research Center, University of Rennes 1, Rennes, France, in 2013.

In 2013, he joined the Swedish College of Engineering and Technology, Wah Cantonment, Pakistan, as an Assistant Professor. He did his postdoctoral research with Qatar Mobility Innovation Center, Doha, Qatar, from 2014 to 2016. In 2016, he joined as the European Research Area Chair holder and an Associate Professor with the Thomas Johann Seebeck Department of Electronics, Tallinn University of Technology, Tallinn, Estonia, where he was elected as a Professor, in 2018. In 2019, he become the Head of Communication Systems Research Group and leading number of National and International projects. His research interests include the fields of wireless communications and connectivity, NB-IoT 5G/B5G smart networks and services, and low-power wearable networks for SmartHealth.

**Yannick Le Moullec** (Senior Member, IEEE) received the M.Sc. degree from the Université de Rennes I, Rennes, France, in 1999, and the Ph.D. and HDR (accreditation to supervise research) degrees from the Université de Bretagne Sud, Lorient, France, in 2003 and 2016, respectively.

From 2003 to 2013, he successively held a Postdoctoral Researcher, an Assistant Professor, and an Associate Professor positions with the Department of Electronic Systems, Aalborg University, Aalborg, Denmark. He then joined the Thomas Johann Seebeck Department of Electronics, Tallinn University of Technology, Tallinn, Estonia: Senior Researcher from 2013 to 2016 and professorship since 2017. His research interests include embedded systems, reconfigurable systems, IoT, and application thereof. He has supervised or co-supervised more than 50 M.Sc. students and 11 Ph.D. students. He has been involved in more than 20 projects, including five as PI, co-PI, or co-main applicant; one such notable project was the H2020 COEL ERA-Chair project from 2015 to 2019. He is a member of the IEEE Sustainable ICT Technical Community and the IEEE Circuits and Systems Society.

**Alar Kuusik** (Member, IEEE) received the Ph.D. degree in IT from the Tallinn University of Technology (TalTech), Tallinn, Estonia, in 2001; followed by Postdoctoral program with Tokyo Denki University, Tokyo, Japan.

He currently serves the position of Estonian C/COM/IT joint Chapter Chair. He also serves the position of a Senior Researcher and a Lecturer with TalTech, focusing on IoT, biomedical sensorics, and body area networking. He has been developing commercial embedded electronic devices for U.S. and European customers and involved with several international research and innovation projects related to smart environment, telecare, and m-health. He has been consulting Estonian government and hospitals in telemedicine topics. He has published over 50 peer-reviewed articles and owns several patents.

**Sven Pärand** received the M.Sc. degree in telecommunications and the Ph.D. degree in electronics and telecommunication from the Tallinn University of Technology, Tallinn, Estonia, in 2006 and 2018, respectively.

He has been an Engineer with Telia Estonia Ltd., Tallinn, since 2012, initially working on IMS and migration toward the Next Generation Network. Starting form 2018, he moved on to work as a 5G development manager with the aim of deploying the 5G network with Telia Estonia. He is currently the mobile services owner at the same company, responsible for the management and development of all mobile services across all of all the mobile generations.

**Christos Verikoukis** (Senior Member, IEEE) received the Ph.D. degree in broadband indoor wireless communications from UPC, Barcelona, Spain, in 2000.

He is currently a Fellow Researcher Research Director (R4) with the Telecommunications Technological Centre of Catalonia, Castelldefels, Spain, and an Adjunct Professor with the University of Barcelona, Barcelona. He has authored over 140 journal articles, over 200 conference articles, three books, 14 book chapters, and three patents. He has participated in more than 30 competitive research projects, while he has supervised 19 Ph.D. students and ten Postdoctoral Researchers.

Dr. Verikoukis received the Best Paper Award at the IEEE ICC 2011 2020, the IEEE GLOBECOM 2014 and 2015, the EuCNC 2016, and the EURASIP 2013 Best Paper Award of the Journal on Advances in Signal Processing. He is currently the IEEE ComSoc EMEA Director and a Member-at-Large of IEEE ComSoc GITC.

# Appendix 5

**V**

Sikandar Zulqarnain Khan, Yannick Le Moullec, and Muhammad Mahtab Alam. An NB-IoT-Based Edge-of-Things Framework for Energy-Efficient Image Transfer. *MDPI Sensors*, 17(21):5929–5949, 2021

*Article*

# An NB-IoT-Based Edge-of-Things Framework for Energy-Efficient Image Transfer

**Sikandar Zulqarnain Khan** *[ID], **Yannick Le Moullec** [ID] **and Muhammad Mahtab Alam** [ID]

Thomas Johann Seebeck Department of Electronics, Tallinn University of Technology, 19086 Tallinn , Estonia; yannick.lemoullec@taltech.ee (Y.L.M.); muhammad.alam@taltech.ee (M.M.A.)
* Correspondence: sikandar.khan@taltech.ee

**Abstract:** Machine Learning (ML) techniques can play a pivotal role in energy efficient IoT networks by reducing the unnecessary data from transmission. With such an aim, this work combines a low-power, yet computationally capable processing unit, with an NB-IoT radio into a smart gateway that can run ML algorithms to smart transmit visual data over the NB-IoT network. The proposed smart gateway utilizes supervised and unsupervised ML algorithms to optimize the visual data in terms of their size and quality before being transmitted over the air. This relaxes the channel occupancy from an individual NB-IoT radio, reduces its energy consumption and also minimizes the transmission time of data. Our on-field results indicate up to 93% reductions in the number of NB-IoT radio transmissions, up to 90.5% reductions in the NB-IoT radio energy consumption and up to 90% reductions in the data transmission time.

**Keywords:** NB-IoT development platform; NB-IoT network; NB-IoT cloud; NB-IoT-based Edge-of-Things; image transmission

## 1. Introduction

Visual IoT is a paradigm where the environment is meant to be observed by camera-equipped IoT sensor nodes. The collected visual data from these nodes are transmitted to the cloud by means of adequate wireless communication technology. Several IoT communication technologies could be utilized for transmitting the collected visual data to the cloud and may include NB-IoT, LTE Cat-M1, LoRAWAN, Sigfox, etc. However, choosing a communication technology depends on the many factors that the particular technology has to offer in terms of its uplink/downlink data rates, transmission latency, device power consumption, as well as network availability and network coverage. Since visual IoT deals with transmitting a large amount of data to the cloud, it faces crucial challenges in terms of device power consumption, desired and achievable data rates, desired and achievable latency and the associated device and network cost.

In this work, we explore the suitability of NB-IoT technology for visual data transfer over the air with a focus on the channel occupancy, power consumption and time needed to transmit visual data from an individual NB-IoT radio. For illustration purposes, the power and time needed when using a naive implementation of visual data transfer from an NB-IoT radio is shown in Figure 1. The figure shows the power graph when transmitting a color image (1600 × 1200 pixels, 357.17 kB) over a Quectel BG96 radio module (in NB-IoT mode). Between markers m1 and m2, 239 transmissions are needed (corresponding to 12.60 m of channel occupancy) with an average power consumption of 0.17 W, which translates to an energy consumption of 0.0357 Wh.

While the transmit power of the NB-IoT module cannot be reduced, it is desirable to reduce the time and energy key performance indicators.

This raises several questions that to date have not been explored from a research point of view, which encompasses the following intertwined aspects:

- How should the overall NB-IoT architecture be organized for an efficient visual data transfer over the air? That is, how many hierarchical layers are needed and what could be their respective roles for collecting, processing, and transmitting data to the cloud?
- What are the suitable wireless communication technologies for transmitting visual data between the several layers of this architecture?
- What type of data processing is needed at what particular layer, taking into consideration the strength and limitation of each layer, and what could be the associated benefits in terms of the bandwidth utilization, channel flexibility and congestion alleviation?
- Lastly, what could be energy-latency trade-offs from the device and network perspective?

We address these questions by demonstrating a hierarchical smart-gateway-based visual NB-IoT testbed, as shown in Figure 2, where several heterogeneous IoT devices are connected to the gateway through short-range wireless communication technologies such as Bluetooth and Bluetooth low energy (BLE), and ZigBee, etc. The gateway is connected to the cloud by means of Low Power Wide Area Networking (LPWAN), specifically NB-IoT. The benefits of having a gateway-based system are many-fold. First, since IoT devices typically have low power budgets and limited computational and storage capabilities, the gateway-based setup allows these nodes to transmit their (visual) data to the gateway without any heavy computations. The compute-intensive gateway node thus performs all the heavy computations including running ML algorithms on the data that are to be transmitted over the air. Secondly, since only the gateway node provides access to the cloud through its LPWAN radio (i.e., NB-IoT in our case), the other nodes are only equipped with short-range communication radios i.e., BT, BLE. This minimizes the number of radios in the core (NB-IoT) network. Thirdly, since the gateway node is computationally capable, it carries out a substantial amount of local data processing, i.e., "Edge computing" for more control of data over the air. This can compensate for the limited bandwidth and lower data rates of LPWAN technologies, NB-IoT in particular [1]. We thus illustrate all these aspects through an edge-of-things computing-based NB-IoT framework for an efficient visual data transfer over the air and produce the associated on-field empirical results.



**Figure 1.** Power graph of the BG96 NB-IoT module when transmitting an image (1600 × 1200 pixels, 357.17 kB). A total of 239 transmissions are needed (12.60 m) with an average power of 0.17 W, which translates to an energy consumption of 0.0357 Wh.
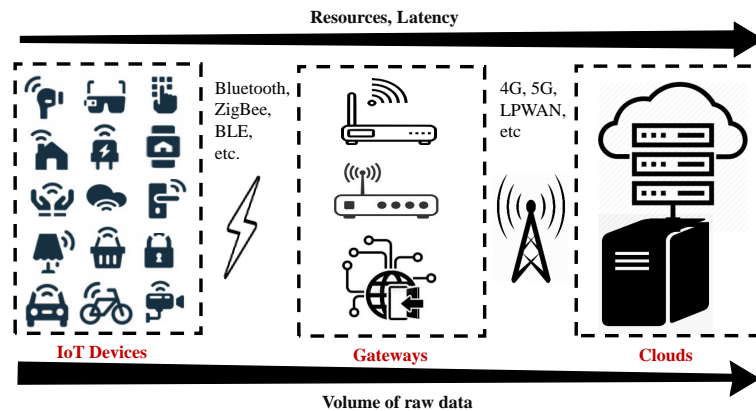
**Figure 2.** Hierarchical architecture of a generic gateway-based IoT testbed.

*1.1. State-of-the-Art*

C. Pham in 2016 (a year after the introduction of the LoRaWAN framework) used a LoRa network for the first time for image data transfer in a visual surveillance application [2]. He successfully transmitted an image of about 2.4 Kb up to 1.8 km using LoRa. Jebril et al. [3] proposed an approach for mangrove forest monitoring in Malaysia, wherein they transferred image sensor data over the LoRa physical layer (PHY) in a node-to-node network model. In their work, they also proposed a novel scheme for overcoming the bandwidth limitations of LoRa. Chen et al. [4] suggested a light trustworthy communication protocol called MPLR for image dispatching in LoRa to facilitate image monitoring in an agricultural IoT platform. Ji et al. [5] proposed a method for farming application wherein an image is transmitted into a tiny grid of patches such that any grid patch is only dispatched when a change in it is noticed. They showed that this approach reserves a lot of link budget during the surveillance of static agriculture sites and provides better performance. Wei et al. [6] proposed a methodology for transmission of JPEG compressed image data in a multiplexing mode with different spreading factors to reduce the transmission time of image data by keeping the quality of the images at the receiver side to high PSNR values. Other similar works that use LoRA for image transmission include [7–9].

From the perspective of utilizing edge computing for increasing the efficiency of IoT, several works have proposed and evaluated ML techniques for higher energy efficiency, bandwidth saving, lower latency, and collaborative intelligence of the network [1,10–15]. However, most of these works provide analytical models with simulation-based results that cannot be entirely relied upon for the real deployed networks because simulation-based validations do not accurately portray the empirical measurements of real-life systems. Other works such as [16–19] proposed deep learning for image recognition and classifications in IoT-based architectures. However, the focus of most of these works is mostly the obtained accuracy and precision of the models used for sending the final inferences to the cloud rather than original images. These works also lack the details on the amount of energy that is being consumed for ML computations with respect to the energy gains in terms of the device and network perspective. Nevertheless, some works proposed and utilized ML for increasing the energy efficiency of IoT nodes. For example the work in [20] uses an ML technique to determine whether to offload the classification of the current input data to the higher processing gateway layer or to perform it locally on the node and thereby achieve energy savings. However, they used the CC1350 IoT platform (a short range radio device) and lack details on larger families of networks such as LPWAN technologies. The work in [21] presented a hierarchical inference model to cut down the amount of data that are to be transmitted, and produced interesting energy-related results. However, they made use of BLE and ZigBee transmission protocols, lacking any correlation with LPWAN technologies. Though the work in [22] presented a real-time context-aware

and collaborative intelligence among nodes in a large-area IoT testbed, they showcased their results using LoRa and BLE only. Other works that consider the use of ML for energy efficiency in LoRa networks include [23–25].

### 1.2. Contributions

The main contributions of this work and its positioning with reference to the state of the art and the aforementioned questions can be summarized as follows:

- We showcase a practical edge-of-things computing-based framework for dispatching optimized images over an NB-IoT test network wherein computations at the edge help reduce the number of NB-IoT radio transmissions over the core network.
- We practically show how the reductions in the communication budget of the radio can in turn contribute to relaxing the channel occupancy, minimizing the network load and reducing the transmission latency.
- We provide in-depth in-sensor analytics of the communication and computational cost of the gateway node along with mapping its energy-latency trade-offs.

The remainder of this paper is organized as follows. Section 2 provides an overview of the hardware architecture of our proposed three-layer hierarchical model and Section 3 presents the algorithmic structure at each layer. Section 4 presents in-field experimental results and energy evaluation of the proposed system. Finally, Section 5 concludes the paper.

## 2. Hardware Architecture of Our Proposed Three Layers Hierarchical Model

Our proposed system as shown in Figure 3 includes the following nodes at three hierarchical layers.

A—Detection and Vision Node (DVN) at the Perception (Monitor) Layer;
B—Smart Transmit Node (STN) at the Gateway Layer;
C—Server node (SN) at the Cloud Layer.
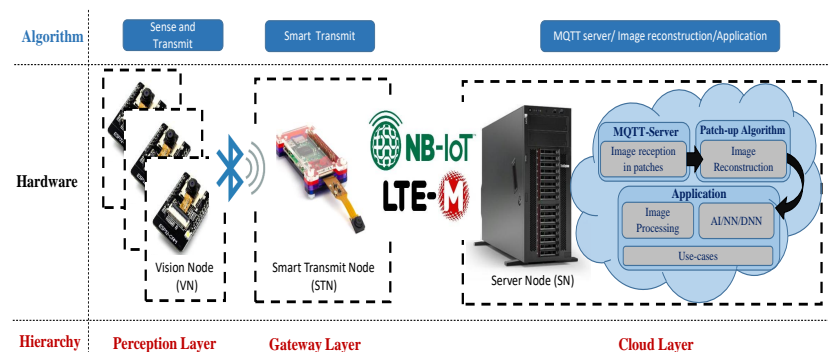


**Figure 3.** Proposed three-layer hierarchical model for energy-efficient image transfer via NB-IoT

### 2.1. Detection and Vision Node (DVN) at Perception Layer

An ESP32-CAM AI-Thinker module [26] is integrated with an HC-SR501 Passive InfraRed (PIR) sensor [27] into a Detection and Vision Node (DVN) that is mounted over the automatic gate barrier of Tallinn University of Technology (TalTech)'s main entrance as shown in Figure 4. The ESP32-CAM module is-based on an ESP32 SoC chipset [28] with Bluetooth/WIFI connectivity, a 2MP OV2640 image sensor, a built-in hardware JPEG encoder [29], and a support for power saving features. The HC-SR501 PIR motion sensor [27] can detect any motion within an adjustable range between 3 m and 7 m [30]. As any vehicle enters into the DVN's sensitivity field, the PIR sensor detects its presence and wakes up the ESP-32 CAM module from its deep sleep mode. The ESP32-CAM module captures an image of the entering vehicle and sends it to the STN at the gateway layer through

Bluetooth connectivity. As the image transmission ends, the DVN enters its deep sleep mode once again.
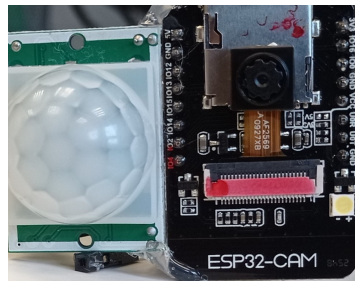


(**a**) Integrating the ESP-32 AI CAM module with HC-SR501 PIR sensor into a DVN



(**b**) The DVN is mounted at the entrance barrier of the TalTech campus.

**Figure 4.** Detection and Vision Node at the perception layer.

### 2.2. Smart Transmit Node (STN) at Gateway Layer

A Raspberry Pi (RPi) 3B module [31] is attached to an IoT cellular HAT [32] into a Smart Transmit Node (STN) and is deployed at the gateway layer of our proposed 3-layer hierarchical model as shown in Figure 5. The STN receives images from the DVN through a Bluetooth connectivity, processes it locally and smart transmits these images to the Server Node (SN) at the cloud layer through NB-IoT connectivity. The RPi 3B is preferred over its latest counterparts, i.e., RPi 3B+ and RPi 4B, as it has lower power consumption [33] and sufficient computational capability to safely run our ML algorithms. The attached Sixfab's cellular IoT HAT is an add-on for Raspberry Pi that is based on Quectel's BG96 chipset adding Cat NB1 (NB-IoT)/Cat M features to Raspberry Pi modules. More details on the module can be found in [34].
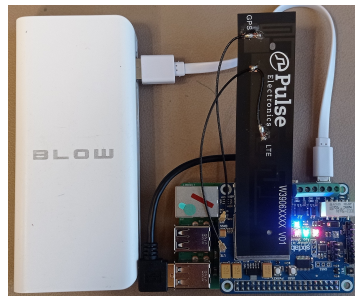


(**a**) Integrating the RPi 3B with the Cellular IoT HAT into STN
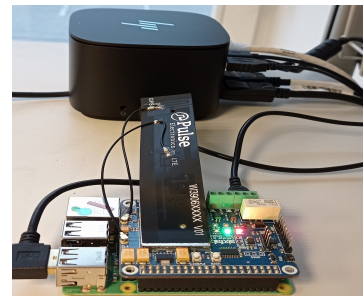


(**b**) The STN can be powered by battery as shown in (**a**) or a DC power supply as shown in (**b**).

**Figure 5.** Smart Transmit Node at the gateway layer.

### 2.3. Server Node (SN) at Cloud Layer

Our physical server is based on an Intel Core-i7 platform that operates at 2.2 GHz, and is equipped with 8GB SRAM, 512GB HDD and runs Windows 10 as its Operating System (OS). Python (version 3.8) with all the required libraries runs on top of Windows 10. A Python-based HBMQTT broker (an open source MQTT broker and client implementation) is accessible to all its clients, both physical and virtual, through an internet connection via a dedicated IP address and a port.

## 3. Algorithmic Structure at Each Hierarchical Layer

The algorithms running across the various nodes of our three-layer hierarchical model include:

- A—A Sense a Transmit algorithm running over DVN
- B—A Smart Transmit algorithm running over STN
- C—An MQTT broker, Image reconstruction and an Application running over the SN

### 3.1. Sense and Transmit Algorithm over the DVN

The algorithm running over the DVN works in a sense-and-transmit fashion where, upon any motion detection from the PIR sensor, the node wakes-up to capture an image of the approaching vehicle and sends it to the STN through a BT connectivity. As the transmission end, the DVN goes back into its deep sleep until triggered again by the PIR motion sensor. This is shown in Figure 6. The corresponding algorithm running over the DVN is given in Algorithm 1.

---

**Algorithm 1:** Sense and transmit algorithm: vehicle detection, image capture, and image transmission algorithm running inside the Detection and Vision Node (DVN).

---

System initialization **begin**
 | Threshold distance = *hardware_set*;
 | Activate deep sleep mode = *True*;
 | Motion monitoring = *True*;
**end**
Motion detection **begin**
 | **if** (*motion_detected*)*:* == *True* **then**
  | Activate deep sleep mode = *False*;
  | Capture image = *True*;
  | Connect with BT server (RPi) = *True*;
  | Transfer image via BT = *True*;
  | Activate deep sleep mode = *True*;
 | **else**
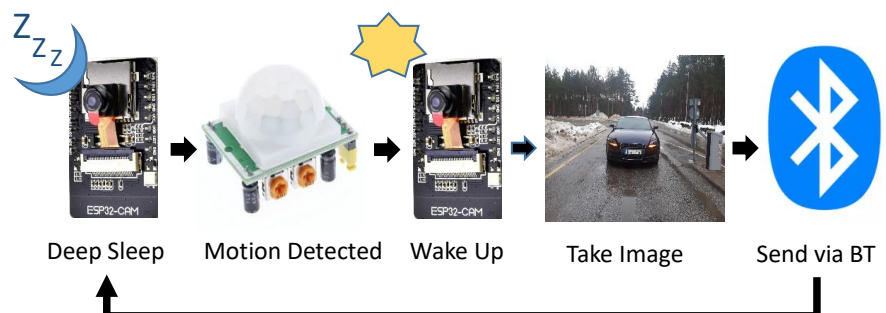  | Motion monitoring = *True*;
 | **end**
**end**

---



**Figure 6.** Sense and transmit procedure.

### 3.2. Smart Transmit Algorithm Running over the STN

The STN runs a series of algorithms in a sequential order as shown in Figure 7. They are discussed in their order of execution in the subsections to follow.
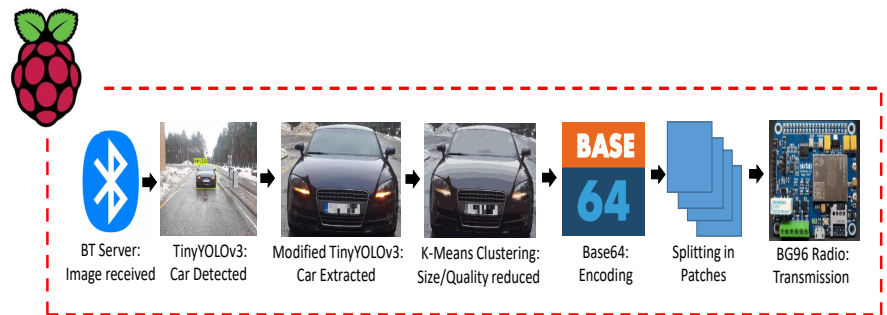
**Figure 7.** Smart transmit procedure.

1—Bluetooth Server:

Bluetooth (BT) is capable of transmitting data wirelessly, in short range, at nearly 1 MB/s. Traditional BT works in a client–server architecture, such that the device that initiates the connection is called a BT-client (VDN in our case), and the one that accepts the connection is called a BT-server (STN in our case) [35]. As the BT-client attempts to initiate an outbound connection with the BT-server on the specified port, the BT-server establishes a two-way socket-connection if the connecting device is found to be authentic. Furthermore, the BT-server could connect to a maximum of 8 clients simultaneously at any particular time [35]. However, for test purposes, our BT-server connects to only one BT-client, i.e., the VDN that is installed at the entrance barrier of the TalTech campus and is situated at a distance of approximately 50 m from the BT-server. Upon connection establishment, the BT-server receives an image of the entering vehicle from the DVN and passes it to Tiny-YOLOv3 for vehicle detection and extraction as discussed below.

2—Tiny-YOLOv3 for vehicle detection and extraction:

"You Only Look Once" (YOLO) is a state-of-the-art, real-time object detection algorithm proposed by Redmon et al. in their work in [36]. Since, traditional YOLO [37] is not suitable to run on embedded devices such as Raspberry Pi, due to its large memory size and high computational demands, a variation of the traditional YOLO called tiny YOLO-v3 [38] is installed to run on RPi 3B for vehicle detection in the received image. By modifying the code of tiny YOLO-v3, the detected vehicle in the image is extracted and saved as a separate JPG image file in the memory. Thus our modified tiny YOLO-v3 discards the unnecessary information from the received image that could produce significantly high costs both in terms of the RPi processing and NB-IoT radio transmissions (to be discussed later in the Results section). The output image from Tiny-YOLOv3 is then fed into K-means clustering for size reduction as discussed below.

3—K-MEANS Clustering algorithm:

Since an image comprises a large data-set of pixels, such that each pixel is represented by 3 bytes that contain its RGB (Red–Blue–Green) intensity value in the range 0–255. Thus, K-means clustering could be exploited to cluster all the pixels of an image into similar RGB values and could be exploited for image compression [39], image segmentation [40] and color quantization [41,42].

For our particular use-case, we exploit the existing technique of [39] to use K-means clustering for image compression, i.e., by reducing the number of colors of an image to the most commonly occurring colors of an image. The number of k colors could be set as desired by the programmer or it could also be optimised to a minimum K that would output an image to a reasonable quality. It should be noted here that this method of compression gives significant reductions in terms of size of an image and leads to significant reductions in the number of radio transmissions.

4—BASE-64 Encoding of the compressed image:

Binary to text encoding schemes [43] become essential for transferring image data to web-sockets, so that the image data do not interfere with the many internet protocols in its way to its destination [44]. Moreover, Quectel's BG96 module requires the use of the special character 'CTRL+Z' (by convention often described as $\wedge \mathbb{Z}$ that is equivalent to the number 26 in decimals or 0x1A in hex) at the end of the data to be transmitted over the radio [45]. Thus, without using any encoding scheme, the radio cannot differentiate between the number 26 that might occur as part of the image data that are to be transmitted and the end of the image data [46]. Thus, the use of an encoding scheme becomes a necessity, especially when utilizing the BG96 module. Altogether, this is why we make use of the Base64 encoding scheme, the most commonly used encoding scheme, to transmit our image over the internet.

5—Transmission of the encoded image over the air through an MQTT protocol:

The encoded image is sent over the air (NB-IoT network) by the BG96 radio utilizing an MQTT protocol [47]. Owing to its lightweight, low complexity, and easy implementation, the message queue telemetry transport (MQTT) protocol has become one of the most popular communication protocols for Machine-to-Machine (M2M) connectivity in the Internet-of-Things (IoT) paradigm [47]. The MQTT protocol works in a publish–subscribe fashion and runs on top of the Transmission Control Protocol/Internet Protocol (TCP/IP). The publish–subscribe mechanism requires a broker, also known as server, to which all the clients connect and share their information. A client that sends a message, through the broker, is called a publisher while a client that receives a message, through the broker, is called a subscriber. The broker filters all the incoming messages from all the publishers and distributes them accordingly to the subscribers. More details on the MQTT protocol architecture an its working can be found in [48]. Since the MQTT protocol supports sending a maximum payload of 1548 bytes [45], images of larger size cannot be transmitted in a single communication transaction. To overcome this, an algorithm running inside the STN breaks down each image into a grid of patches, each of 1500 bytes, such that these patches are dispatched separately with a header indicating its order in the source image. This is shown on the left side of Figure 8. The number of communication transactions that are required to send an image that is larger than the minimum transaction of ca. 1500 bytes size is given as Equation (1). Furthermore, the re-transmissions in NB-IoT (where up to 128 repetitions are possible in the uplink communication) ensures the successful reception of each segment at the receiver end, even in low coverage areas [49].

$$\#\_communication\_transactions = \left\lceil \frac{image\_size \, (\text{kB})}{1.5} \right\rceil \tag{1}$$
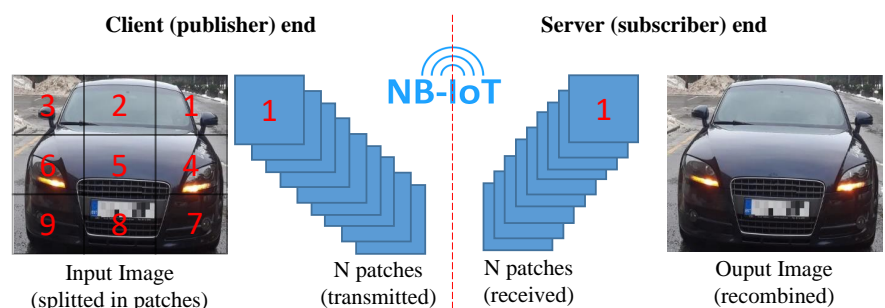


**Figure 8.** Splitting of an image into patches (at the publisher end) and its reconstruction (at the server end) procedure.

*3.3. MQTT Broker, Image Reconstruction and an Application Running over the SN*

A python-based HBMQTT broker [50] supporting a full set of MQTT 3.1.1 protocol specifications, runs over the SN and is accessible to any physical/virtual client through an

IP address and a port. Since the image from STN is received in patches, a -Python-based image-reconstruction algorithm combines all these received patches in proper order to re-construct the encoded image as sent from STN.

The application, used as an example, monitors a parking lot in terms of the authorized vehicles. The collected images contain detailed information of the entering vehicles such as their type, color and more specifically their license plate numbers. These images are compared against a database of authorized vehicles. When an unknown vehicle is detected, the security services are notified with the visual description of the front of the vehicle. The image processing performed at the edge node (more specifically, the smart gateway) reduces the size of the images by (i) extracting the region of interest (front of the vehicle) and (ii) decreasing the number of colors. While (i) is bound by the contours of the front of the vehicles, (ii) is more flexible and we have explored various numbers of colors (K value in the K-Means algorithm) and identified that K = 12 is a good trade-off between reducing the image size while keeping sufficient quality regarding the license plate number and visual description of the front of the vehicle. In general, there could be a number of use-cases where image transmission would be required by applications such as [16,51,52], etc.

## 4. On-Field Experimental Trials with Energy/Time Consumption Evaluations

The field-deployed DVN is installed at the entrance barrier of Tallinn University of Technology (TalTech) campus and is configured to generate images of an approaching vehicle with different resolutions, i.e., (i) $1600 \times 1200$ full-resolution image, (ii) $800 \times 600$ medium-resolution image, (iii) $640 \times 480$, and (iv) $320 \times 240$ low-resolution images. Examples of these on-field images are shown in Figure 9 with their details given in Table 1.



(**a**) Resolution type (4:3 aspect ratio): UXGA ($1600 \times 1200$), size: 360 kB approx.



(**b**) Resolution type (4:3 aspect ratio): SVGA ($800 \times 600$), size: 120 kB approx.



(**c**) Resolution type (4:3 aspect ratio): VGA ($640 \times 480$), size: 88 kB approx.



(**d**) Resolution type (4:3 aspect ratio): QVGA ($320 \times 240$), size: 45 kB approx.

**Figure 9.** Images of different resolutions and sizes as generated by the field-deployed DVN at the entrance barrier of the TalTech Campus.

**Table 1.** Image details with their resolution, aspect ratio, total number of pixels and their sizes in (kB) when stored in JPG format.

| Resolution Type | Resolution (W × H) | Aspect Ratio | Max. No of Pixels (Max. 2MP) | Total Size (kB) |
|---|---|---|---|---|
| UXGA | 1600 × 1200 | 4:3 | 1920,000 | 357.17 |
| SVGA | 800 × 600 | 4:3 | 480,000 | 118.89 |
| VGA | 640 × 480 | 4:3 | 307,200 | 87.18 |
| QVGA | 320 × 240 | 4:3 | 76,800 | 44.79 |

The DVN after capturing an image of the vehicle transmits it to the GN through its Bluetooth connectivity. The received image at the GN is fed as an input image to the modified Tiny-YOLOv3 that extracts the detected vehicle and discards the rest of the unwanted information, i.e., bytes that could cause significant costs in terms of the communication and energy cost of the radio. Although this cropped-out image has a lower resolution as compared to its source image, its quality in terms of the number of associated colors remains the same. For example, for an input UXGA image (i.e., Figure 9a), the corresponding detected and extracted images are shown in Figure 10a,b, respectively. Since the output images from Tiny-YOLOv3 for the rest of images as shown in Figure 9b–d look the same, they are omitted from the display. However, their details are summarized in Table 2. For example, the first row in Table 2 indicates that an input image of 1600 × 1200 resolution and 357.17 kB size is reduced to an image of 513 × 355 resolution and 66.97 kB size, i.e., 81% reduction in the size of the source image thanks to TINY-YOLOv3 extraction.
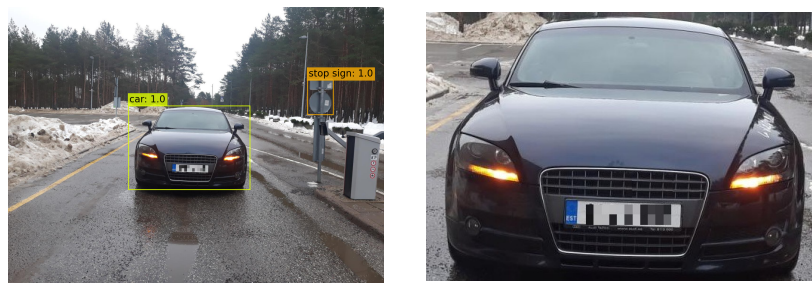


(**a**) Detected Vehicle: original Image Resolution (1600 × 1200), size: 360 kB approx.

(**b**) Cropped out vehicle: cropped image resolution (513 × 355), size: 66.97 kB approx.

**Figure 10.** Output images from TINY-YOLOv3 algorithm: (**a**) detected vehicle and (**b**) cropped-out vehicle.

**Table 2.** Images with their input/output properties (resolution, size in kB) and percent reduction in size when processed in JPG format before and after the application of TINY-YOLOv3.

| Input Image (JPG) Resolution | Detected Vehicle (JPG) Resolution | Input Image Size (kB) | Extracted Image Size (kB) | Percent Reduction in Size Thanks to Cropping |
|---|---|---|---|---|
| 1600 × 1200 | 513 × 355 | 357.17 | 66.97 | 81% |
| 800 × 600 | 260 × 175 | 118.89 | 20.51 | 82% |
| 640 × 480 | 206 × 138 | 87.18 | 14.35 | 83% |
| 320 × 240 | 105 × 67 | 44.79 | 4.60 | 89% |

The cropped-out image from Tiny YOLO-v3 is fed as an input to the K-means clustering algorithm for compression based on the reduction in its number of colors into K number of colors (i.e., K clusters). The output images from the K-means clustering algorithm for K = 5, 10, 12, and 20 with an input image of 513x355 resolution are shown in Figure 11a–d, respectively. For input images of other resolutions, the details in terms of their total number

of colors, sizes and the corresponding output images from K-means clustering algorithm in terms of K number of colors and their resulting size(s) are summarized in Table 3. For example, the second column in Table 3 details the output images from the K-means clustering algorithm for an input image of $513 \times 355$ resolution for different K values. So, when it is in all of its 25,512 colors (output from Tiny YOLO-v3), it occupies 66.97 kB (as indicated by the third row and third column). However, when it is reproduced in only 12 colors (as indicated by the fifth row and third column), its size is reduced to 32.0 kB, almost half the original size. Thus, as the number of colors in the source image decreased (down the rows in first column), the corresponding size of the output images from K-means clustering algorithm decreases (in the corresponding size column).



(**a**) Output image from the K_Means algorithm for K (colors) = 5, Size: 27.1 kB approx.

(**b**) Output image from the K_Means algorithm for K (colors) = 10: Size: 31.6 kB approx.

(**c**) Output image from the K_Means algorithm for K (colors) = 12: Size: 32 approx.

(**d**) Output image from the K_Means algorithm for K (colors) = 20: Size: 34 kB approx.

**Figure 11.** Output of the K_Means algorithm for an input image with a resolution of $513 \times 355$ pixels, total number of pixels = 182,115, total number of unique colors = 25,512 and an input size = 66.97 kB. (**a**) K = 5, (**b**) K = 10, (**c**) K = 12, and (**d**) K = 20. Note: the number plate in each output image from K_Means algorithm is mosaicked for display in this work for security reasons. However, the real application demands a visible number plate of the entering vehicle for identification.

The output image from the K-means clustering algorithm is then encoded into Base64 format for the reasons discussed in the previous section. After encoding, the image is split up into chunks, each of 1500 bytes, for possible transmission over the NB-IoT radio as a single transmission. The number of these chunks and their corresponding number of transmissions depend upon the total size of the image that is to be transmitted and can be derived from Equation (1).

**Table 3.** K-means clustering on images of various resolutions, colors and sizes and the resulting images with K number of colors (clusters) and their output sizes in kB.

| Images from T-YOLOv3 | Resolution 1 (513 × 355) | | Resolution 2 (260 × 175) | | Resolution3 (206 × 138) | | Resolution 4 (105 × 67) | |
|---|---|---|---|---|---|---|---|---|
| **K Clusters** | **Color** | **Size** | **Color** | **Size** | **Color** | **Size** | **Color** | **Size** |
| **K = all colors** | 25,512 | 66.97 | 14,503 | 20.51 | 11,340 | 14.35 | 4830 | 4.60 |
| K = 20 | 20 | 34.1 | 20 | 11.1 | 20 | 8.0 | 20 | 3.1 |
| **K = 12** | 12 | **32.0** | 12 | **10.2** | 12 | **7.2** | 12 | **2.5** |
| K = 10 | 10 | 31.6 | 10 | 10.1 | 10 | 7.0 | 10 | 2.3 |
| K = 5 | 5 | 27.1 | 5 | 8.2 | 5 | 5.8 | 5 | 2.1 |

**color:** No. of colors in the image, **Size:** given in kB. K = 12 (in bold font) corresponds to the best trade-off between the number of colors and achieved size reductions.

### 4.1. Computation Cost

To assess the energy consumption of the proposed computations, i.e., execution of TINY-YOLOv3 followed by the execution of the K-means clustering algorithm, the power consumption of RPi 3B and its corresponding execution times for these algorithms were measured. It was found that the mean %CPU utilization of RPi was <10.0% in idle state, i.e., when no code was being executed while the mean %CPU utilization remained almost constant during the stress condition, i.e., above 90% during the execution of each individual implementation, i.e., TinyYOLOv3 and the K-Means clustering algorithmsIt was found that the mean %CPU utilization of RPi was <10.0% in idle state, i.e., when no code was being executed while its %CPU utilization reaches to a maximum of 93% in stress condition, i.e, when the code was being executed. It was also observed that the RPi's CPU was never starved out even while processing the highest resolution image on a single core (note: for experimental purposes we disabled all but one of the cores to assess if it can handle the code with only one core). As for the current and power consumption, the Raspberry Pi 3B consumed, on average, a mean current of 260 mA at 5.0 V (which is about 1.3 W) in its idle state and it consumed, on average, a mean current of 350 mA at 5.0 V (which is about 1.75 W) under stress conditions. Table 4 summarizes the energy consumed by Raspberry Pi 3B for processing original images to create their optimized versions.

**Table 4.** Energy consumed by Raspberry Pi 3B for processing an original image to create an optimized version.

| Per Image Energy Consumption of Raspberry Pi 3B | | | |
|---|---|---|---|
| **Resolution** | **Computing Power (W)** | **Execution Time (s)** | **Energy Consumed (Wh)** |
| 1600× 1200 | 1.75 | 22 | 0.0107 |
| 800 × 600 | 1.75 | 18 | 0.0072 |
| 640 × 480 | 1.75 | 13 | 0.0063 |
| 320 × 240 | 1.75 | 6 | 0.0029 |

W:Watt, s: seconds, Wh: Watthour.

For processing an image, the RPi took, on average, 22 s to process a 2 MP full-resolution image (1600 × 1200) while it took, on average, 5 s to process the low-resolution (320 × 240) image. The RPi thus consumed, on average, 0.010 Wh of energy to process the high-resolution image while it consumed, on average, 0.0024 Wh of energy to process the low-resolution image. The per image energy consumption of RPi (i.e., computation energy) for processing of these images of various resolutions is summarized in Table 4.

### 4.2. Reducing the Communication Budget of an NB-IoT (BG96) Radio

Thanks to local computations (application of ML algorithms on images), the sizes of the (source) images are significantly reduced, as summarized in Table 3. These reductions

in size contribute greatly towards minimizing the communication budget of an NB-IoT radio, both in terms of its number of transmissions and its energy consumption. Table 5 summarizes the total number of NB-IoT radio transmissions that are required to send images in their full resolution and colors (with no local computations) in comparison to sending their optimized versions with reduced resolutions and a reduced number of colors. For example, an input image of $1600 \times 1200$ resolution requires a total of 239 transmissions (3rd column) to be transmitted over the radio, while its optimized version image of $513 \times 355$ resolution 12 colors requires only 22 transmissions (6th column) to be transmitted over the radio, i.e., 90% reductions in the total number of NB-IoT radio transmissions.

**Table 5.** Reduced numbers of transmissions for transmitting an optimized image with K = 12 colors in contrast to transmitting an original with K = all colors given in kB.

| Original Image (Full Resolution, and All Colors) | | | Optimized Image (Cropped and K= 12 Colors) | | | $R_{ed}$_Tr (%) |
|---|---|---|---|---|---|---|
| Resolution | Size | $R_{eq}T$ | Resolution | Size | $R_{eq}T$ | |
| $1600 \times 1200$ | 357.17 | 239 | $513 \times 355$ | 32.0 | 22 | −90 |
| $800 \times 600$ | 118.90 | 80 | $260 \times 175$ | 10.2 | 7 | −91 |
| $640 \times 480$ | 87.18 | 58 | $206 \times 138$ | 7.2 | 5 | −91.3 |
| $320 \times 240$ | 44.7 | 30 | $105 \times 67$ | 2.5 | 2 | −93.3 |

$R_{eq}T$: required number of transmissions, $R_{ed}Tr$: reduced number of transmissions, $R_{eq}T$: is obtained by dividing the size of an image in kB by 1.5 as given in Equation (1).

To calculate the energy consumption of the BG96 radio (in NB-IoT mode) for the involved transmissions, the baseline energy consumption model for an NB-IoT radio as detailed in [53] is used, as represented by Equation (2). According to this equation, the total energy consumption of an NB-IoT radio is the sum of all of its energy states, i.e., Attach, Tx, Rx, TAU, eDRX and PSM where the energy consumption of each state is obtained by multiplying its power consumption parameter $P_{STATE}$ by its timing parameter ($T_{STATE}$) such that:

$$
\begin{aligned}
E_{TOTAL} = \\
\begin{pmatrix}
\{P_{ATTACH(avg)} \times T_{ATTACH}\} + \\
\{(P_{Tx(avg)} \times T_{Tx}) + (P_{Rx(avg)} \times T_{Rx})\} + \\
\{P_{C-DRX(avg)} \times (T_{InactivityTimer})\} + \\
\{P_{TAU(avg)} T_{TAU}\}
\end{pmatrix} \\
+ \begin{pmatrix}
\{(P_{eDRX(avg)} \times T_{3324})\} + \\
\{P_{PSM(avg)} \times (T_{3412} - T_{3324})\}
\end{pmatrix}
\end{aligned}
\tag{2}
$$

The sensitivity analysis (SA) of this model [53] is briefly discussed in what follows. First, Table 6 summarizes the power consumption parameters of this model in descending order and Table 7 summarizes the minimum and maximum values for the timing parameters of this model as standardized by 3GPP.

**Table 6.** Power consumption parameters of the BG96 radio.

| BG96 Power Consumption Parameters | | | | | | |
|---|---|---|---|---|---|---|
| $P_{TAU}$ | $P_{ATTACH}$ | $P_{TX}$ | $P_{RX}$ | $P_{CDRX}$ | $P_{eDRX}$ | $P_{PSM}$ |
| 0.18 W | 0.18 W | 0.17 W | 0.16 W | 0.083 W | 0.070 W | 0.0002 W |

**Table 7.** Timings parameters of the BG96 radio.

| Minimum and Maximum Values for the Timing Parameters | | | | |
|---|---|---|---|---|
| $T_{TAU}/T_{ATTACH}$ | $T_{TX}/T_{RX}$ | $T_{CDRX}$ | $T_{eDRX}$ | $T_{PSM}$ |
| 18.6 s (on avg.) | 0 s–# of transmissions | 10 s–60 s | 0 s–186 m | 0 s–413 d |

Then, since the power consumption parameters (Table 6) remain fixed for each state of the BG96 chipset, the timing parameters (durations) of these states (Table 7) affect the overall energy consumption of the radio to a greater extent. Considering the short periods of the Attach, and TAU states of the NB-IoT radio, their impact on the total energy consumption of the radio is not very significant. However, the transmission time ($T_{TX}$) and the reception time ($T_{RX}$) of the radio affect the overall energy consumption of the NB-IoT radio to a much greater extent as their duration prolongs. Thus, from the perspective of the sensitivity analysis of the NB-IoT radio, shortening the duration of its Transmission state ($T_{TX}$) reduces its energy consumption to a greater extent and this is what we achieve through utilizing the ML algorithms at the STN node at the gateway layer, i.e., reducing the number of transmissions.

Communication Cost

To measure the energy consumption of the BG96 radio (in NB-IoT mode) for transmitting these images (original and optimized) over the publicly available NB-IoT test network, their associated power graphs were measured using a Keysight Technologies N6705C DC Power Analyzer (PA) [54]. These power graphs are shown in Figures 12–15 and display the average power consumption measurements of an NB-IoT (BG96) radio along with the associated transmission periods for the images, i.e., (a) when transmitted as original and (b) when transmitted as optimized. For example, Figure 12 shows that the BG96 radio consumed 0.0357 Wh of energy in transmitting the original image of $1600 \times 1200$ resolution while it consumed only 0.0034 Wh for transmitting its optimized version (with K = 12 colors). Figure 13 shows that the BG96 radio consumed 0.0102 Wh energy for transmitting an image of resolution $800 \times 600$ while it consumed only 0.0014 Wh of energy in transmitting its optimized version. Similarly, for Figure 14 the consumption of BG96 radio for transmitting an original image of resolution $640 \times 480$ is 0.0085 Wh where it consumes only 0.0015 Wh in transmitting its optimized version. Lastly, for Figure 15, the difference in the energy consumption of the BG96 radio for transmitting an original image of resolution $320 \times 240$ and transmitting its optimized version is 0.0008 Wh. Table 8 shows the transmission times of original images in contrast to the transmission times of optimized images. For example an original image of $1600 \times 1200$ resolution takes 12.6 min to be transmitted over the radio while its optimized version image of $513 \times 355$ resolution in 12 colors only take 1.20 min to be transmitted over the radio, a 90% in its transmission time as indicted by the third row of Table 8. Table 9 summarizes the energy consumption measurements for BG96 radio for transmitting original images in comparison to transmitting their optimized versions with K = 12 colors. The energy measurement calculation for each image is obtained by multiplying its average total transmission time (Figures 11–14) with the transmission power of the radio, i.e, 0.17 W.
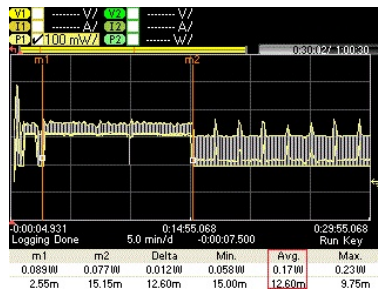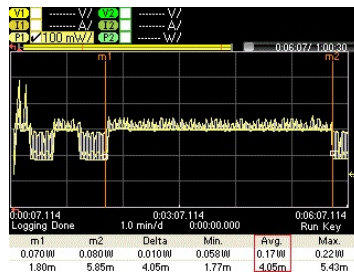
(**a**) Power graph of the BG96 NB-IoT module when transmitting an image (1600 × 1200 pixels, 357.17 kB). A total of 239 transmissions are needed (12.60 m) with an average power of 0.17 W, which translates to an energy consumption of 0.0357 Wh
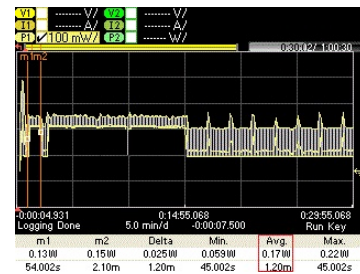
(**b**) Power graph of the BG96 NB-IoT module when transmitting an image (513 × 355 pixels, 32 kB). A total of 22 transmissions are needed (12.60 m) with an average power of 0.17 W, which translates to an energy consumption of 0.0034 Wh

**Figure 12.** The energy consumed for transmitting an original image is (**a**) 0.0357 Wh and for transmitting its optimized version it is (**b**) 0.0034 Wh, i.e., 90.5% energy savings.



(**a**) Power graph of the BG96 NB-IoT module when transmitting an image (800 × 600 pixels, 118.9 kB). A total of 80 transmissions are needed (4.05 m) with an average power of 0.17 W, which translates to an energy consumption of 0.0102 Wh

(**b**) Power graph of the BG96 NB-IoT module when transmitting an image (260 × 175 pixels, 10.2 kB). A total of 7 transmissions are needed (34.20 s) with an average power of 0.17 W, which translates to an energy consumption of 0.0.0016 Wh

**Figure 13.** The energy consumed for transmitting an original image is (**a**) 0.012 Wh and for transmitting its optimized image it is (**b**) 0.0016 Wh, i.e., 84.3% energy savings.

(**a**) Power graph of the BG96 NB-IoT module when transmitting an image (640 × 480 pixels, 87.18 kB). A total of 58 transmissions are needed (3.00 m) with an average power of 0.17 W, which translates to an energy consumption of 0.0085 Wh



(**b**) Power graph of the BG96 NB-IoT module when transmitting an image (206 × 138 pixels, 7.2 kB). A total of 5 transmissions are needed (32.40 s) with an average power of 0.17 W, which translates to an energy consumption of 0.0015 Wh
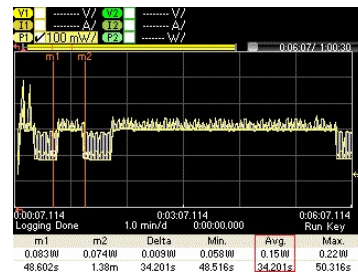
**Figure 14.** The energy consumed for transmitting an original image is (**a**) 0.0085 Wh and for transmitting its optimized version it is (**b**) 0.0015 Wh, i.e., 82.3% energy savings.



(**a**) Power graph of the BG96 NB-IoT module when transmitting an image (320 × 240 pixels, 44.79 kB). A total of 30 transmissions are needed (1.6 m) with an average power of 0.17 W, which translates to an energy consumption of 0.0034 Wh



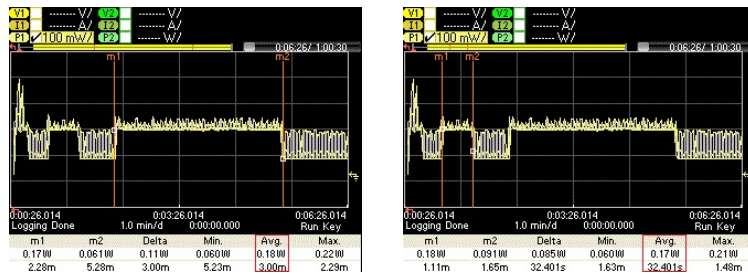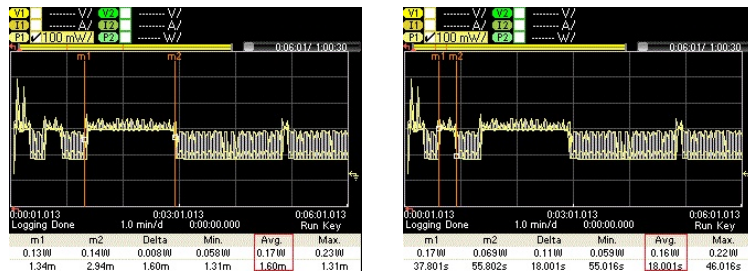(**b**) Power graph of the BG96 NB-IoT module when transmitting an image (105 × 67 pixels, 2.5 kB). A total of 2 transmissions are needed (18.00 s) with an average power of 0.17 W, which translates to an energy consumption of 0.0008 Wh

**Figure 15.** The energy consumed for transmitting an Original image is (**a**) 0.0034 Wh and for transmitting its Optimized image it is (**b**) 0.0008 Wh; 76.5% energy savings.

**Table 8.** The reduced transmission period for transmitting an optimized image with K = 12 colors in contrast to transmitting an original image with K = all colors.

| Reduction in the Transmission Period of NB-IoT Radio | | | | | | |
|---|---|---|---|---|---|---|
| Original Image (All Colors) | | | Optimized Image (K= 12 Colors) | | | Red_TrTime (%) |
| Resolution | Size | TrTime | Resolution | Size | TrTime | |
| 1600 × 1200 | 357.17 | 12.60 m | 513 × 355 | 32.0 | 1.20 m | −90 |
| 800 × 600 | 118.90 | 4.05 m | 260 × 175 | 10.2 | 34.20 s | −82 |
| 640 × 480 | 87.18 | 3.0 m | 206 × 138 | 7.2 | 32.4 s | −82 |
| 320 × 240 | 44.7 | 1.6 m | 105 × 67 | 2.5 | 18.0 s | −81 |

**TrTime:** transmission time (m: minutes, s: seconds), **Red_TrTime:** percent reductions in transmission time.

**Table 9.** The reduced energy consumption for transmitting an optimized image with K = 12 colors in contrast to transmitting an original image with K = all colors.

| Reduction in the Energy Consumption of the NB-IoT Radio | | | | | |
|---|---|---|---|---|---|
| Original Image (in All Colors) | | Optimized Image (in K = 12 Colors) | | $E_{Red}$ (Wh) | $E_{Red}$ (%) |
| Resolution | $E_{con}$ (Wh) * | Resolution | $E_{con}$ (Wh) | | |
| 1600 × 1200 | 0.0357 | 513 × 355 | 0.0034 | −0.0323 | −90.5 |
| 800 × 600 | 0.0102 | 260 × 175 | 0.0016 | −0.0086 | −84.3 |
| 640 × 480 | 0.0085 | 206 × 138 | 0.0015 | −0.0070 | −82.3 |
| 320 × 240 | 0.0034 | 105 × 67 | 0.0008 | −0.0026 | −76.5 |

$E_{con}$: energy consumed, $E_{Red}$: energy reduction, $E_{Red}$ (%): energy reduction in percentage, *: $E_{con}$ is obtained by multiplying $P_{Tx}$ with $T_{Tx}$ (For reference see Tables 6 and 7).

*4.3. Trade-Offs in the Computation vs. Communication Costs*

Table 10 summarizes the overall energy savings per image considering both their computation and communication cost. For example, when an original image of 1600 × 1200 resolution is transmitted from an NB-IoT radio (without any local computation) it consumes 0.0357 Wh (as indicated by the third row of Table 10). On the other hand, when it is processed locally by the RPi, it consumes 0.0107 Wh in computations (Table 4) and 0.0034 Wh in transmissions (Table 9), i.e., a total of 0.0141 Wh; this is a 0.0216 Wh energy difference, i.e., a total of 60% energy savings for a single image. Since Table 10 shows the energy savings per image; these individual energy savings scale-up as a multiple of the number of images that are processed by the RPi. For example, the RPi processed, on average, six images of 1600 × 1200 resolution in an hour, i.e., a total of 144 cars entered the campus in 24 h, and it thus saved on an average 0.20 Wh of energy in 24 h. With this rate, it can save on average 1.41 Wh of energy in a week and so on. It should also be noted that these energy savings are the outcome from a single STN at the gateway layer and these savings could further scale-up as a function of the increasing number of smart nodes in the network. As a side-note, since a single 100 W PVC solar panel generates around 400 Wh/24 h, a 15/20 W solar panel could also be utilized to power such a system [16].

**Table 10.** Overall energy savings in transmitting an optimized image (considering both its computing and communication energy) as compared to transmitting an original image (communication energy only since no computation needed).

| Energy Consumption per Original Image vs. Energy Consumption per Optimized Image | | | | | |
|---|---|---|---|---|---|
| Original Image | | Optimized Image | | E_Savings (Wh) (a–b) | ES (%) |
| Resolution | $E_{COMM}$ (Wh) (a) | Resolution | $E_{COMP} + E_{COMM}$ (Wh) (b) | | |
| 1600 × 1200 | 0.0357 | 513 × 355 | 0.0107 + 0.0034 | 0.0216 | −60.50 |
| 800 × 600 | 0.0102 | 260 × 175 | 0.0072 + 0.0016 | 0.0014 | −13.72 |
| 640 × 480 | 0.0085 | 206 × 138 | 0.0063 + 0.0015 | 0.007 | −8.23 |
| 320 × 240 | 0.0034 | 105 × 67 | 0.0029 + 0.0008 | 0.002 | −5.88 |

$E_{COMM}$: communication energy, $E_{COMP}$: computation energy, E_Savings: total energy savings per image, ES (%): percent reduction in energy consumption.

Finally, Table 11 summarizes the reductions in the transmission times for original images vs. the transmission times for optimized images. For example, an original image of 1600 × 1200 resolution takes 12.6 min to be transmitted over the air by a BG96 (in NB-IoT mode) radio while its optimized version (513 × 355 resolution in 12 colors) needs 22 s in computations and 1.20 min in transmission. This reduces the transmission time of this single image by 11.3 m, an 89% decrease in transmission time (i.e., 89% faster delivery) of the image. Figure 16 summarizes the energy and time savings in transmitting optimized

images of $513 \times 355$, $206 \times 175$ and $105 \times 67$ resolutions as compared to transmitting their original counterparts of resolution $1600 \times 1200$, $800 \times 600$ and $640 \times 480$, respectively.

**Table 11.** Overall time savings in transmitting an optimized image (considering both its computing and transmitting time) as compared to transmitting an original image (transmitting time only since no computation needed).
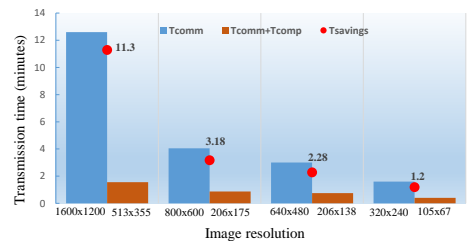
| Transmission Time per Original Image vs. Transmission Time per Optimized Image | | | | | |
|---|---|---|---|---|---|
| Original Image | | Optimized Image | | T_Savings (a–b) | TS (%) |
| Resolution | $T_{COMM}$ (a) | Resolution | $T_{COMP} + T_{COMM}$ (b) | | |
| $1600 \times 1200$ | 12.6 min | $513 \times 355$ | 22 s + 1.20 min | 11.3 min | −89.68 |
| $800 \times 600$ | 4.05 min | $260 \times 175$ | 18 s + 34.2 s | 3.18 min | −78.51 |
| $640 \times 480$ | 3.0 min | $206 \times 138$ | 13 s + 32.4 s | 2.28 min | −76.00 |
| $320 \times 240$ | 1.6 min | $105 \times 67$ | 6 s + 18 s | 1.20 min | −75.00 |

$T_{COMM}$: transmission time, $T_{COMP}$: computation Time(min: minutes, s: seconds), **ES (%)**: percent reduction in transmission time.
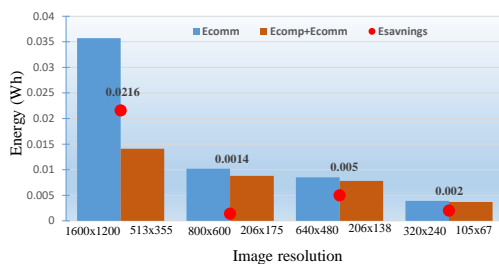


(**a**) Energy saved in transmitting an optimized image (considering both its computing and communication energy (orange block)) as compared to transmitting an original image (considering its communication energy only since no computation is needed (blue block)). The red dots represents the total energy saved in Wh during transmission.

(**b**) Time saved in transmitting an optimized image (orange block) as compared to transmitting an original image (blue block). The red dots show the total time saved in minutes during transmission.

**Figure 16.** The energy and time saved in transmitting an optimized image of resolution $513 \times 355$ is 0.0216 Wh and 11.3 min. Similarly, energy and time saved in transmitting an image of resolution $206 \times 175$ is 0.0014 Wh and 3.18 min, and energy and time saved in transmitting an image of resolution $105 \times 67$ is 0.002 Wh and 1.2 min, respectively.

## 5. Conclusions

Our application verifies our proposed scheme for image transmission via NB-IoT, and this supports the industrial and academic trend which promotes NB-IoT as the future solution for IoT infrastructure.

Our on-field investigation showed promising results in terms of green Internet of Things, particularly ML for green and smart communications. Our results showed that potentially significant energy gains can be achieved by eliminating the unwanted data from transmitting over the IoT networks. We showcased this with our present setup operating on a publicly available NB-IoT network. We also showed that smart transmissions pays in terms of the increased responsiveness of the system.

Consequently, machine learning techniques running over the edge of any IoT infrastructure can potentially revolutionize the future IoT technologies that may include LoRAWAN, Sigfox, NB-IoT, CatM etc. The inference being done on the edge would save sending a huge amount of data over the IoT networks and would save significantly in terms of power, energy and timings of the over all IoT infrastructure.

In the future, we plan to optimize the operation of an NB-IoT radio in terms of its various operating states to improve its energy consumption, depending on the required latency and battery lifetime of a given application.

**Author Contributions:** Conceptualization, S.Z.K. and Y.L.M.; methodology, S.Z.K.; implementation, S.Z.K.; validation, S.Z.K., Y.L.M. and M.M.A.; writing—original draft preparation, S.Z.K.; writing—review and editing, S.Z.K., Y.L.M. and M.M.A.; supervision, Y.L.M. and M.M.A.; project administration, Y.L.M. and M.M.A.; funding acquisition, M.M.A. All authors have read and agreed to the published version of the manuscript.

**Conflicts of Interest:** The authors declare no conflict of interest.

## References

1. Chen, M.; Li, W.; Fortino, G.; Hao, Y.; Hu, L.; Humar, I. A dynamic service migration mechanism in edge cognitive computing. *ACM Trans. Internet Technol. (TOIT)* **2019**, *19*, 1–15.
2. Pham, C. Low-cost, low-power and long-range image sensor for visual surveillance. In Proceedings of the 2nd Workshop on Experiences in the Design and Implementation of Smart Objects, New York, NY, USA, 3–7 October 2016; pp. 35–40.
3. Jebril, A.H.; Sali, A.; Ismail, A.; Rasid, M.F.A. Overcoming limitations of LoRa physical layer in image transmission. *Sensors* **2018**, *18*, 3257.
4. Chen, T.; Eager, D.; Makaroff, D. Efficient image transmission using lora technology in agricultural monitoring iot systems. In Proceedings of the 2019 International Conference on Internet of Things (iThings) and IEEE Green Computing and Communications (GreenCom) and IEEE Cyber, Physical and Social Computing (CPSCom) and IEEE Smart Data (SmartData), Atlanta, GA, USA, 14–17 July 2019; pp. 937–944.
5. Ji, M.; Yoon, J.; Choo, J.; Jang, M.; Smith, A. Lora-based visual monitoring scheme for agriculture iot. In Proceedings of the 2019 IEEE Sensors Applications Symposium (SAS), Sophia Antipolis, France, 11–13 March 2019; pp. 1–6.
6. Wei, C.C.; Chen, S.T.; Su, P.Y. Image Transmission Using LoRa Technology with Various Spreading Factors. In Proceedings of the 2019 2nd World Symposium on Communication Engineering (WSCE), Nagoya, Japan, 20–23 December 2019; pp. 48–52.
7. Kirichek, R.; Pham, V.D.; Kolechkin, A.; Al-Bahri, M.; Paramonov, A. Transfer of multimedia data via LoRa. In *Internet of Things, Smart Spaces, and Next Generation Networks and Systems*; Springer: Cham, Switzerland, 2017; pp. 708–720.
8. Pham, C. Robust CSMA for long-range LoRa transmissions with image sensing devices. In Proceedings of the IEEE 2018 Wireless Days (WD), Dubai, United Arab Emirates, 3–5 April 2018; pp. 116–122.
9. Fan, C.; Ding, Q. A novel wireless visual sensor network protocol based on LoRa modulation. *Int. J. Distrib. Sens. Netw.* **2018**, *14*, 1550147718765980.
10. Gómez-Carmona, O.; Casado-Mansilla, D.; Kraemer, F.A.; López-de Ipiña, D.; García-Zubia, J. Exploring the computational cost of machine learning at the edge for human-centric Internet of Things. *Future Gener. Comput. Syst.* **2020**, *112*, 670–683.
11. Rioual, Y.; Laurent, J.; Senn, E.; Diguet, J.P. Reinforcement learning strategies for energy management in low power iot. In Proceedings of the IEEE 2017 International Conference on Computational Science and Computational Intelligence (CSCI), Las Vegas, NV, USA, 14–16 December 2017; pp. 1377–1382.
12. Lei, L.; Xu, H.; Xiong, X.; Zheng, K.; Xiang, W. Joint computation offloading and multiuser scheduling using approximate dynamic programming in NB-IoT edge computing system. *IEEE Internet Things J.* **2019**, *6*, 5345–5362.
13. Lyu, X.; Tian, H.; Jiang, L.; Vinel, A.; Maharjan, S.; Gjessing, S.; Zhang, Y. Selective offloading in mobile edge computing for the green internet of things. *IEEE Netw.* **2018**, *32*, 54–60.
14. Samie, F.; Tsoutsouras, V.; Bauer, L.; Xydis, S.; Soudris, D.; Henkel, J. Oops: Optimizing operation-mode selection for IoT edge devices. *ACM Trans. Internet Technol. (TOIT)* **2019**, *19*, 1–21.
15. Samie, F.; Bauer, L.; Henkel, J. From cloud down to things: An overview of machine learning in internet of things. *IEEE Internet Things J.* **2019**, *6*, 4921–4934.
16. Zualkernan, I.A.; Dhou, S.; Judas, J.; Sajun, A.R.; Gomez, B.R.; Hussain, L.A.; Sakhnini, D. Towards an IoT-based Deep Learning Architecture for Camera Trap Image Classification. In Proceedings of the 2020 IEEE Global Conference on Artificial Intelligence and Internet of Things (GCAIoT), Dubai, United Arab Emirates, 12–16 December 2020; pp. 1–6.
17. Curtin, B.H.; Matthews, S.J. Deep Learning for Inexpensive Image Classification of Wildlife on the Raspberry Pi. In Proceedings of the 2019 IEEE 10th Annual Ubiquitous Computing, Electronics & Mobile Communication Conference (UEMCON), New York, NY, USA, 10–12 October 2019; pp. 0082–0087.

18. Monburinon, N.; Zabir, S.M.S.; Vechprasit, N.; Utsumi, S.; Shiratori, N. A Novel Hierarchical Edge Computing Solution Based on Deep Learning for Distributed Image Recognition in IoT Systems. In Proceedings of the IEEE 2019 4th International Conference on Information Technology (InCIT), Bangkok, Thailand, 24–25 October 2019; pp. 294–299.
19. Popat, P.; Sheth, P.; Jain, S. Animal/object identification using deep learning on raspberry pi. In *Information and Communication Technology for Intelligent Systems*; Springer: Singapore, 2019; pp. 319–327.
20. Samie, F.; Bauer, L.; Henkel, J. Hierarchical classification for constrained IoT devices: A case study on human activity recognition. *IEEE Internet Things J.* **2020**, *7*, 8287–8295.
21. Yin, H.; Wang, Z.; Jha, N.K. A hierarchical inference model for Internet-of-Things. *IEEE Trans. Multi-Scale Comput. Syst.* **2018**, *4*, 260–271.
22. Chatterjee, B.; Seo, D.H.; Chakraborty, S.; Avlani, S.; Jiang, X.; Zhang, H.; Abdallah, M.; Raghunathan, N.; Mousoulis, C.; Shakouri, A.; et al. Context-Aware Collaborative Intelligence with Spatio-Temporal In-Sensor-Analytics for Efficient Communication in a Large-Area IoT Testbed. *IEEE Internet Things J.* **2020**, *8*, 6800–6814.
23. Sandoval, R.M.; Garcia-Sanchez, A.J.; Garcia-Haro, J. Optimizing and updating lora communication parameters: A machine learning approach. *IEEE Trans. Netw. Serv. Manag.* **2019**, *16*, 884–895.
24. Azari, A.; Cavdar, C. Self-organized low-power iot networks: A distributed learning approach. In Proceedings of the 2018 IEEE Global Communications Conference (GLOBECOM), Abu Dhabi, United Arab Emirates, 9–13 December 2018; pp. 1–7.
25. Suresh, V.M.; Sidhu, R.; Karkare, P.; Patil, A.; Lei, Z.; Basu, A. Powering the IoT through embedded machine learning and LoRa. In Proceedings of the 2018 IEEE 4th World Forum on Internet of Things (WF-IoT), Singapore, 5–8 February 2018; pp. 349–354.
26. ESP32 DataSheet. Available online: https://www.espressif.com/sites/default/files/documentation/esp32_datasheet_en.pdf (accessed on 1 January 2020).
27. HC SR501 Passive Infrared Sensor. Available online: Available online: https://www.componentsinfo.com/hc-sr501-module-pinout-datasheet/ (accessed on 1 January 2020).
28. Espressif ESP32. Available online: http://esp32.net/ (accessed on 1 January 2020).
29. OV2640 DataSheet. Available online: https://www.arducam.com/ov2640/ (accessed on 1 January 2020).
30. HC SR501 Range: Adjustable Sensitivity. Available online: https://www.epitran.it/ebayDrive/datasheet/44.pdf/ (accessed on 1 January 2020).
31. Raspberry Pi 3 Model B. Available online: https://www.raspberrypi.org/products/raspberry-pi-3-model-b// (accessed on 1 January 2020).
32. Raspberry Pi LTE Cellular Modem Kit. Available online: https://sixfab.com/ (accessed on 1 January 2020).
33. Current/Power Comparisons of the Various RPi Models. Available online: https://www.raspberrypi.org/documentation/hardware/raspberrypi/power/README.md// (accessed on 1 January 2020).
34. Raspberry Pi Connects with Sixfab. Available online: https://docs.sixfab.com/docs/raspberry-pi-cellular-iot-application-shield-technical-details (accessed on 1 January 2020).
35. Huang, A.S.; Rudolph, L. *Bluetooth Essentials for Programmers*; Cambridge University Press: Cambridge, UK, 2007.
36. Redmon, J.; Divvala, S.; Girshick, R.; Farhadi, A. You only look once: Unified, real-time object detection. In Proceedings of the IEEE Conference on Computer Vision and Pattern Recognition, Las Vegas, NV, USA, 27–30 June 2016; pp. 779–788.
37. YOLO: Real-Time Object Detection. Available online: https://pjreddie.com/darknet/yolo/ (accessed on 1 January 2020).
38. YOLOv3 Github. Available online: https://github.com/pythonlessons/TensorFlow-2.x-YOLOv3 (accessed on 1 January 2020).
39. Paek, J.; Ko, J. *K*-Means clustering-based data compression scheme for wireless imaging sensor networks. *IEEE Syst. J.* **2015**, *11*, 2652–2662.
40. Kanungo, T.; Mount, D.M.; Netanyahu, N.S.; Piatko, C.D.; Silverman, R.; Wu, A.Y. An efficient k-means clustering algorithm: Analysis and implementation. *IEEE Trans. Pattern Anal. Mach. Intell.* **2002**, *24*, 881–892.
41. Dehariya, V.K.; Shrivastava, S.K.; Jain, R. Clustering of image data set using k-means and fuzzy k-means algorithms. In Proceedings of the IEEE 2010 International Conference on Computational Intelligence and Communication Networks, Bhopal, India, 26–28 November 2010; pp. 386–391.
42. Hu, Y.; Su, B. Accelerated k-means clustering algorithm for colour image quantization. *Imaging Sci. J.* **2008**, *56*, 29–40.
43. Binary Encoding Schemes. Available online: https://docs.python.org/3/library/base64.html (accessed on 1 January 2020).
44. Wessels, A.; Purvis, M.; Jackson, J.; Rahman, S. Remote data visualization through websockets. In Proceedings of the IEEE 2011 Eighth International Conference on Information Technology: New Generations, Las Vegas, NV, USA, 11–13 April 2011; pp. 1050–1051.
45. MQTT_Application_Note_Quectel_BG96. Available online: https://sixfab.com/wp-content/uploads/2018/09/Quectel_BG96_MQTT_Application_Note_V1.0.pdf (accessed on 1 January 2020).
46. Wen, S.; Dang, W. Research on Base64 Encoding Algorithm and PHP Implementation. In Proceedings of the IEEE 2018 26th International Conference on Geoinformatics, Kunming, China, 28–30 June 2018; pp. 1–5.
47. MQTT Architecture. Available online: https://mqtt.org/ (accessed on 1 January 2020).
48. Hillar, G.C. *MQTT Essentials—A Lightweight IoT Protocol*; Packt Publishing Ltd.: Birmingham, UK, 2017.
49. Poddar, N.; Khan, S.Z.; Mass, J.; Srirama, S.N. Coverage Analysis of NB-IoT and Sigfox: Two Estonian University Campuses as a Case Study. In Proceedings of the IEEE 2020 International Wireless Communications and Mobile Computing (IWCMC), Limassol, Cyprus, 15–19 June 2020; pp. 1491–1497.

50. MQTT Broker. Available online: https://github.com/beerfactory/hbmqtt (accessed on 1 January 2020).
51. Liu, M.; Wang, X.; Zhou, A.; Fu, X.; Ma, Y.; Piao, C. UAV-YOLO: Small Object Detection on Unmanned Aerial Vehicle Perspective. *Sensors* **2020**, *20*, 2238.
52. Mazzia, V.; Khaliq, A.; Salvetti, F.; Chiaberge, M. Real-time apple detection system using embedded systems with hardware accelerators: An edge AI application. *IEEE Access* **2020**, *8*, 9102–9114.
53. Khan, S.Z.; Alam, M.M.; Le Moullec, Y.; Kuusik, A.; Pärand, S.; Verikoukis, C. An Empirical Modelling for the Baseline Energy Consumption of an NB-IoT Radio Transceiver. *IEEE Internet Things J.* **2021**, doi:10.1109/JIOT.2021.3072769.
54. Keysight Technologies. *N6705C DC Power Analyzer*; Keysight Technologies: Santa Rosa, CA, USA, 2014.

# Curriculum Vitae

**1. Personal data**

Name                              Sikandar Muhammad Zulqarnain Khan
Date and place of birth           1 January 1982, Pakistan

**2. Contact information**

Address                           Tallinn University of Technology, TalTech,
                                  Thomas Johann Seebeck Department of Electronics,
                                  Ehitajate tee 5, 19086 Tallinn, Estonia
Phone                             +372 535 033 52
E-mail                            sikandar.khan@taltech.ee

**3. Education**

2018–2022      T. J. S. Department of Electronics,
               Tallinn University of Technology, TalTech, Estonia.
               *PhD studies*
2008–2010      Department of Electronic, Electrical, Control & Instrumentation Engineering,
               Hanyang University, South Korea.
               *MS studies*
2008–2011      Department of Computer Systems Engineering,
               University of Engineering and Technology (U.E.T), Pakistan.
               *BS studies*

**4. Language competence**

Pushto         Mother Tongue
Urdu           fluent
English        fluent
Italian        basic
Estonian       basic

**5. Professional employment**

09.2018–01.2022      Researcher, T. J. S. Department of Electronics, TalTech, Estonia.
02.2017–09.2017      Researcher, ECRELS Lab, Technical University of Crete, Greece.
01.2015–09.2017      Researcher, TeCIP Institute, CNR, Italy.
05.2014–12.2014      Researcher, Instituto de Telecomunicacoes, Aveiro, Portugal.
09.2010–04.2014      Faculty, COMSATs University Islamabad, Abbottabad Campus, Pakistan.
09.2008–08.2010      Research Assistant, RSC Lab, Hanyang University, South Korea.
04.2005–08.2008      Lecturer, DCSE, University of Engg. & Technology, Pakistan.

**6. Expert Domains**

Electronics Systems       Embedded Systems       Control Systems       Mechatronic Systems
Real-time Systems         Reconfigurable Systems   Adaptive Systems      Green IoT Systems

## 7. Computer skills

- Operating systems: Windows, Linux, Raspbian.

- Document preparation: MS Word, MS Excel, MS Power Point, Latex.

- Programming languages: C, C++ ,TCL ,Python, Assembly, Verilog HDL, AT commands.

- Protocols: UDP, HTTP , MQTT, TCP/IP.

- Hardware Instruments: DMM, Frequency Generator, Oscilloscope, Power Analyzer, Network Analyzer, Logic Analyzer etc.

- Hands on Experience: Time to Digital Converters, Laser Range Finders, PID/Fuzzy Logic Controllers, BG96/BC95 transcievers, MicroControllers (8051, Arduino, STM32, MSP430, ESP32), FPGA boards (Xilinx, Altera, Zynq7000/Zybo), NB-IoT/CatM transceivers (BG96, BC95).

- Electronic components: Resistors, Capacitors, Inductors, Transformers, Diodes, Zener diodes, BJTs, FETs, OpAmps,etc.

- Software IDEs: Xilinx ISE, Vivado IDE, Arduino IDE, Supervised/Unsupervised Machine Learning softwares.

## 8. Defended theses

- 2010, Development of a pulse Time of Flight (ToF) LASER Range Finder (LRF) System, MSc, supervisor Prof. Sanghyeom Baeg, Department of Electronic, Electrical, Control and Instrumentation Engineering, Hanyang University, South Korea.

- 2005, Development of a preemptive OS for an 8051 micro-controller, supervisor Dr. Umar Sheikh, University of Engineering and Technology (UET), Pakistan.

## 9. Field of research

- Green IoT Technologies

- Re-configurable Systems

- Control Systems

- Communication Systems

- Embedded Systems

- Real-time Systems

## 10. Scientific work
### Papers

1. Sikandar Zulqarnain Khan, Yannick Le Moullec, and Muhammad Mahtab Alam. An NB-IoT-Based Edge-of-Things Framework for Energy-Efficient Image Transfer. *MDPI Sensors*, 17(21):5929–5949, 2021.

2. Sikandar M. Zulqarnain Khan, Muhammad Mahtab Alam, Yannick Le Moullec, Alar Kuusik, Sven Pärand, and Christos Verikoukis. An empirical modeling for the baseline energy consumption of an nb-iot radio transceiver. *IEEE Internet of Things Journal*, 8(19):14756–14772, 2021.

3. Nishant Poddar, Sikandar Zulqarnain Khan, Jakob Mass, and Satish Narayana Srirama. Coverage analysis of nb-iot and sigfox: Two estonian university campuses as a case study. In *2020 International Wireless Communications and Mobile Computing (IWCMC)*, pages 1491–1497. IEEE, 2020.

4. Hassan Malik, Sikandar Zulqarnain Khan, Jeffrey Leonel Redondo Sarmiento, Alar Kuusik, Muhammad Mahtab Alam, Yannick Le Moullec, and Sven Pärand. Nb-iot network field trial: Indoor, outdoor and underground coverage campaign. In *2019 15th International Wireless Communications Mobile Computing Conference (IWCMC)*, pages 537–542, 2019.

5. Sikandar Zulqarnain Khan, Hassan Malik, Jeffrey Leonel Redondo Sarmiento, Muhammad Mahtab Alam, and Yannick Le Moullec. Dorm: Narrowband iot development platform and indoor deployment coverage analysis. *Procedia Computer Science*, 151:1084–1091, 2019.

6. Sikandar Zulqarnain Khan; Rashiduddin Kakar; Muhammad Mahtab Alam; Yannick Le Moullec; Haris Pervaiz. *A Green IoT Node Incorporating Transient Computing, Approximate Computing and Energy/Data Prediction*, IEEE 17th Annual Consumer Communications and Networking Conference, Las Vegas, United States, 10th Jan., 2020.

7. Sikandar Khan, Kyprianos Papadimitriou, Giorgio Buttazzo, Kostas Kalaitzakis. *A Reconfigurable PID Controller*, International Symposium on Applied Reconfigurable Computing (ARC), pp 392–403, Santorini, Greece, May 2-4, 2018.

8. Sikandar Khan, Giorgio Buttazzo. *Increasing the resolution of laser rangefinders using low frequency pulses*, International Journal of Embedded Systems, Volume 9, Issue 2 > 2017.

9. Sikandar Khan, Daniel Dinis, Rinato Lopes, Paulo Pedreiras, Joaquim Ferreira. *Improved real-time communication infrastructure for ITS*, Simpósio de Informática INFORUM (2014). Portugal: University of Aveiro, Portugal.

10. Sikandar Zulqarnain Khan, Daniel Dinis, Renato Lopes, Paulo Pedreiras, Joaquim Ferreira. *A Matlab-based Scheduling Simulator for Deterministic Real-time Communications in ITS*, International Symposium on Ambient Intelligence and Embedded Systems: AmiEs-2014, 2-4 October, 2014 Aveiro, Portugal.

# Elulookirjeldus

## 1. Isikuandmed

| | |
|---|---|
| Nimi | Sikandar Muhammad Zulqarnain Khan |
| Sünniaeg ja -koht | 1 January 1982, Pakistan |

## 2. Kontaktandmed

| | |
|---|---|
| Aadress | Tallinn University of Technology, TalTech, |
| | Thomas Johann Seebeck Department of Electronics, |
| | Ehitajate tee 5, 19086 Tallinn, Estonia |
| Phone | +372 535 033 52 |
| E-mail | sikandar.khan@taltech.ee |

## 3. Haridus

| | |
|---|---|
| 2018–2022 | T. J. S. Department of Electronics, Tallinn University of Technology, TalTech, Estonia. *PhD studies* |
| 2008–2010 | Department of Electronic, Electrical, Control & Instrumentation Engineering, Hanyang University, South Korea. *MS studies* |
| 2008–2011 | Department of Computer Systems Engineering, University of Engineering and Technology (U.E.T), Pakistan. *BS studies* |

## 4. Keelteoskus

| | |
|---|---|
| Pushto keel | emakeel |
| Urdu keel | kõrgtase |
| inglise keel | kõrgtase |
| Italian keel | algtase |
| Eesti keel | algtase |

## 5. Teenistuskäik

| | |
|---|---|
| 09.2018–01.2022 | Researcher, T. J. S. Department of Electronics, TalTech, Estonia. |
| 02.2017–09.2017 | Researcher, ECRELS Lab, Technical University of Crete, Greece. |
| 01.2015–09.2017 | Researcher, TeCIP Institute, CNR, Italy. |
| 05.2014–12.2014 | Researcher, Instituto de Telecomunicacoes, Aveiro, Portugal. |
| 09.2010–04.2014 | Faculty, COMSATs University Islamabad, Abbottabad Campus, Pakistan. |
| 09.2008–08.2010 | Research Assistant, RSC Lab, Hanyang University, South Korea. |
| 04.2005–08.2008 | Lecturer, DCSE, University of Engg. & Technology, Pakistan. |

## 6. Ekspertdomeenid

| | | | |
|---|---|---|---|
| Electronics Systems | Embedded Systems | Control Systems | Mechatronic Systems |
| Real-time Systems | Reconfigurable Systems | Adaptive Systems | Green IoT Systems |

### 7. Arvuti oskused

- Operating systems: Windows, Linux, Raspbian.

- Document preparation: MS Word, MS Excel, MS Power Point, Latex.

- Programming languages: C, C++ ,TCL ,Python, Assembly, Verilog HDL, AT commands.

- Protocols: UDP, HTTP , MQTT, TCP/IP.

- Hardware Instruments: DMM, Frequency Generator, Oscilloscope, Power Analyzer, Network Analyzer, Logic Analyzer etc.

- Hands on Experience: Time to Digital Converters, Laser Range Finders, PID/Fuzzy Logic Controllers, BG96/BC95 transcievers, MicroControllers (8051, Arduino, STM32, MSP430, ESP32), FPGA boards (Xilinx, Altera, Zynq7000/Zybo), NB-IoT/CatM transceivers (BG96, BC95).

- Electronic components: Resistors, Capacitors, Inductors, Transformers, Diodes, Zener diodes, BJTs, FETs, OpAmps,etc.

- Software IDEs: Xilinx ISE, Vivado IDE, Arduino IDE, Supervised/Unsupervised Machine Learning softwares.

### 8. Kaitstud lõputööd

- 2010, Development of a pulse Time of Flight (ToF) LASER Range Finder (LRF) System, MSc, supervisor Prof. Sanghyeom Baeg, Department of Electronic, Electrical, Control and Instrumentation Engineering, Hanyang University, South Korea.

- 2005, Development of a preemptive OS for an 8051 micro-controller, supervisor Dr. Umar Sheikh, University of Engineering and Technology (UET), Pakistan.

### 9. Teadustöö põhisuunad

- Green IoT Technologies

- Re-configurable Systems

- Control Systems

- Communication Systems

- Embedded Systems

- Real-time Systems

### 10. Teadustegevus

1. Sikandar M. Zulqarnain Khan, Muhammad Mahtab Alam, Yannick Le Moullec, Alar Kuusik, Sven Pärand, and Christos Verikoukis. An empirical modeling for the baseline energy consumption of an nb-iot radio transceiver. *IEEE Internet of Things Journal*, 8(19):14756–14772, 2021.

2. Sikandar Zulqarnain Khan, Rashiduddin Kakar, Muhammad Mahtab Alam, Yannick Le Moullec, and Haris Pervaiz. A green iot node incorporating transient computing, approximate computing and energy/data prediction. In *2020 IEEE 17th Annual Consumer Communications Networking Conference (CCNC)*, pages 1–6, 2020.

3. Nishant Poddar, Sikandar Zulqarnain Khan, Jakob Mass, and Satish Narayana Srirama. Coverage analysis of nb-iot and sigfox: Two estonian university campuses as a case study. In *2020 International Wireless Communications and Mobile Computing (IWCMC)*, pages 1491–1497. IEEE, 2020.

4. Hassan Malik, Sikandar Zulqarnain Khan, Jeffrey Leonel Redondo Sarmiento, Alar Kuusik, Muhammad Mahtab Alam, Yannick Le Moullec, and Sven Pärand. Nb-iot network field trial: Indoor, outdoor and underground coverage campaign. In *2019 15th International Wireless Communications Mobile Computing Conference (IWCMC)*, pages 537–542, 2019.

5. Sikandar Zulqarnain Khan, Hassan Malik, Jeffrey Leonel Redondo Sarmiento, Muhammad Mahtab Alam, and Yannick Le Moullec. Dorm: Narrowband iot development platform and indoor deployment coverage analysis. *Procedia Computer Science*, 151:1084–1091, 2019.

6. Sikandar Zulqarnain Khan; Rashiduddin Kakar; Muhammad Mahtab Alam; Yannick Le Moullec; Haris Pervaiz. *A Green IoT Node Incorporating Transient Computing, Approximate Computing and Energy/Data Prediction*, IEEE 17th Annual Consumer Communications and Networking Conference, Las Vegas, United States, 10th Jan., 2020.

7. Sikandar Khan, Kyprianos Papadimitriou, Giorgio Buttazzo, Kostas Kalaitzakis. *A Reconfigurable PID Controller*, International Symposium on Applied Reconfigurable Computing (ARC), pp 392–403, Santorini, Greece, May 2-4, 2018.

8. Sikandar Khan, Giorgio Buttazzo. *Increasing the resolution of laser rangefinders using low frequency pulses*, International Journal of Embedded Systems, Volume 9, Issue 2 > 2017.

9. Sikandar Khan, Daniel Dinis, Rinato Lopes, Paulo Pedreiras, Joaquim Ferreira. *Improved real-time communication infrastructure for ITS*, Simpósio de Informática INFORUM (2014). Portugal: University of Aveiro, Portugal.

10. Sikandar Zulqarnain Khan, Daniel Dinis, Renato Lopes, Paulo Pedreiras, Joaquim Ferreira. *A Matlab-based Scheduling Simulator for Deterministic Real-time Communications in ITS*, International Symposium on Ambient Intelligence and Embedded Systems: AmiEs-2014, 2-4 October, 2014 Aveiro, Portugal.